

AD-A034 995

TRW DEFENSE AND SPACE SYSTEMS GROUP REDONDO BEACH CALIF F/G 20/5
INVESTIGATION OF BEAMED ENERGY CONCEPTS FOR PROPULSION. SYSTEMS--ETC(U)
OCT 76 M HUBERMAN, J M SELLEN, R BENSON F04611-76-C-0003
AFRPL-TR-76-66-VOL-1 NL

UNCLASSIFIED

1 of 3

AD
A034995



ADA 034995

AFRPL-TR-76-66

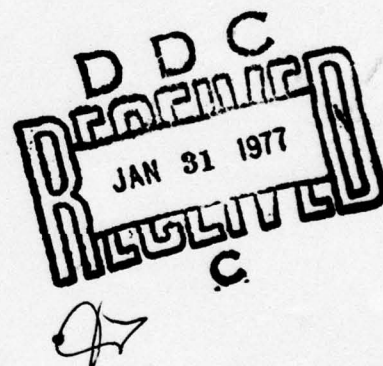
12
NW

INVESTIGATION OF BEAMED ENERGY CONCEPTS FOR PROPULSION

SYSTEMS STUDIES - VOLUME I

TRW DEFENSE AND SPACE SYSTEMS GROUP
ONE SPACE PARK
REDONDO BEACH, CALIFORNIA 90278

AUTHORS: M. HUBERMAN
J. M. SELLEN
R. BENSON
W. DAVENPORT
R. DAVIDHEISER
P. MOLMUD
L. GLATT



OCTOBER 1976

APPROVED FOR PUBLIC RELEASE;
DISTRIBUTION UNLIMITED

AIR FORCE ROCKET PROPULSION LABORATORY
DIRECTOR OF SCIENCE AND TECHNOLOGY
AIR FORCE SYSTEMS COMMAND
EDWARDS AFB, CALIFORNIA 93523

NOTICES

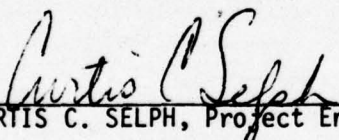
When U.S. Government drawings, specifications, or other data are used for any purpose other than a definitely related government procurement operation, the Government thereby incurs no responsibility nor any obligation whatsoever, and the fact that the Government may have formulated, furnished, or in any way supplied the said drawings, specifications or other data, is not to be regarded by implication or otherwise, or in any manner licensing the holder or any other person or corporation or conveying any rights or permission to manufacture use, or sell any patented invention that may in any way be related thereto.

FOREWORD

This document was prepared by the Applied Technology Division of TRW Defense and Space Systems Group, One Space Park, Redondo Beach, California 90278. It describes work performed under Contract F04611-76-C-0003, Job Order No. 010000PP with the Air Force Rocket Propulsion Laboratory, Edwards AFB, CA 93523. The period of performance represented by the report extended from 2 September 1975 to 1 July 1976.

This work was sponsored and directed by the Air Force Rocket Propulsion Laboratory (AFRPL). Curtis Selph provided program management and technical guidance for the AFRPL. Program management at TRW was provided by M. N. Huberman.

This report has been reviewed by the Information Office/DOZ and is releaseable to the National Technical Information Service (NTIS). At NTIS it will be available to the general public, including foreign nations. This report is unclassified and suitable for general public release.


CURTIS C. SELPH, Project Engineer


CLARK W. HAWK, Chief
Propulsion Applications Branch

FOR THE COMMANDER


E. E. STEIN, Deputy Chief
Liquid Rocket Division

11

ACCESSION TO	White Section	<input checked="checked" type="checkbox"/>
NTIS	Blue Section	<input type="checkbox"/>
DDC		
UNANNOUNCED		
JUSTIFICATION		
BY	DISTRIBUTION/AVAILABILITY CODES	
Dist.	AVAIL. and SPECIAL	

UNCLASSIFIED

SECURITY CLASSIFICATION OF THIS PAGE (When Data Entered)

19 REPORT DOCUMENTATION PAGE		READ INSTRUCTIONS BEFORE COMPLETING FORM	
18 1. REPORT NUMBER AFRPL-TR-76-66-Vol-1	2. GOVT ACCESSION NO.	3. RECIPIENT'S CATALOG NUMBER 9	
6 4. TITLE (and Subtitle) INVESTIGATION OF BEAMED ENERGY CONCEPTS FOR PROPULSION. Systems studies. Volume I.		5. TYPE OF REPORT & PERIOD COVERED FINAL Rept. 2 Sep 75 - 1 Jul 76	
10 7. AUTHOR(s) M. Huberman, J. M. Sellen, R. Benson, W. Davenport R. Davidheiser P. Molmud, L. Glatt		8. PERFORMING ORG. REPORT NUMBER	
9. PERFORMING ORGANIZATION NAME AND ADDRESS TRW Defense and Space Systems Group ✓ One Space Park Redondo Beach, CA 90278		15 CONTRACT OR GRANT NUMBER(s) F04611-76-C-0003 new	
11 CONTROLLING OFFICE NAME AND ADDRESS Air Force Rocket Propulsion Laboratory Director of Science and Technology Air Force Systems Command Edwards AFB, CA 93523		10. PROGRAM ELEMENT, PROJECT, TASK AREA & WORK UNIT NUMBERS	
14. MONITORING AGENCY NAME & ADDRESS (if different from Controlling Office) 12 261 p.		11 12. REPORT DATE Oct 76	
		13. NUMBER OF PAGES 262	
		15. SECURITY CLASS. (of this report) Unclassified	
		15a. DECLASSIFICATION/DOWNGRADING SCHEDULE	
16. DISTRIBUTION STATEMENT (of this Report) This report has been reviewed by the Information Office/DOZ and is releaseable to the National Technical Information Service (NTIS). At NTIS it will be available to the general public, including foreign nations. This report is unclassified and suitable for general public release.			
17. DISTRIBUTION STATEMENT (of the abstract entered in Block 20, if different from Report)			
18. SUPPLEMENTARY NOTES			
19. KEY WORDS (Continue on reverse side if necessary and identify by block number) Beamed energy propulsion Spacecraft propulsion Laser propulsion			
20. ABSTRACT (Continue on reverse side if necessary and identify by block number) The objective of this program is to assess the feasibility of the beamed energy propulsion concept for Air Force missions. The work is divided into three major tasks: 1) system studies; 2) theoretical analyses of the coupling mechanisms between the beamed energy and propellant working fluid and 3) preparation of a test plan for the experimental investigation of the coupling processes for various laser/propellant combinations. The results of the study indicate that beamed energy propulsion is technically feasible. No fundamental obstacles have been identified. However considerable			

DD FORM 1 JAN 73 1473

EDITION OF 1 NOV 65 IS OBSOLETE

UNCLASSIFIED

111

SECURITY CLASSIFICATION OF THIS PAGE (When Data Entered)

409637

JB

UNCLASSIFIED

SECURITY CLASSIFICATION OF THIS PAGE(When Data Entered)

technical development is needed in many areas before the concept can be operationally implemented.

In order to minimize the required collector area, laser concepts are preferred over microwaves. Large diameter microwave receivers will have to be of the rectenna (rectifying antenna) type since conventional receiving reflectors cannot be fabricated to the precision required for efficient large scale collection. Thus microwaves will require electrically powered propulsion. This results in additional thousands of pounds of power conditioning equipment and radiation structure for heat rejection from the electrical subsystem.

→ If space based laser transmitter concepts are to be cost effective they will require the availability of megawatt level space nuclear or solar power stations. Reactant powered space based laser can not be cost effective because of the expense of transporting the reactants to orbit.

→ In view of the large total energy required for each mission, ground based transmitters will be most cost effective when they are operated closed cycle from central station electric power.

Laser transmitting ranges greater than several hundred nautical miles will result in excessive collector sizes. Therefore, ground based transmitters applications will be restricted to orbital functions which can be performed at low orbital altitudes. Thus, synchronous altitude functions such as circularization and repositioning in orbit will not be feasible with ground based transmitting stations, fly-by range considerations will limit thrust periods to 50 seconds (40° of orbital arc).

→ Three promising applications have been identified. The laser powered tug can be cost effective compared to an advanced cryogenic tug. Apsidal rotation correction and drag make-up are two other missions where significant advantages may be realized for the laser powered concept. ←

Extensive hardware development is required. Critical areas include the lasers, thrusters, thruster reaction chamber windows and the collection and coupling subsystems.

UNCLASSIFIED

SECURITY CLASSIFICATION OF THIS PAGE(When Data Entered)

CONTENTS

	<u>Page</u>
1. INTRODUCTION AND SUMMARY	1
1.1 Conclusions and Recommendations	6
2. MISSION SELECTION AND TRADEOFFS	9
2.1 Space Based Transmitters	9
2.2 Ground Based Transmitters	14
2.2.1 Power Scheduling for Ground Transmitters	14
2.2.2 Orbit Raising	18
2.2.3 Apsidal Rotation and Nodal Regression Correction	20
2.2.4 Drag Make-Up	22
2.2.5 Circularization, Change-Of-Plane and Repositioning in Synchronous Orbit	22
2.3 Aircraft and Mountaintop-Based Transmitters	23
2.4 Reusable Tug	23
2.4.1 Weight Breakdown	24
2.4.2 Energy and Power Requirement	28
2.4.3 Thermal Considerations	28
2.4.4 Cost Comparisons	31
2.5 Summary	37
3. MISSION REQUIREMENTS	38
3.1 Probable Air Force Missions	38
3.2 Velocity Increment Determination	40
3.2.1 Atmospheric Mission Velocity Increment Determination	40
3.2.2 Geocentric Circular Orbit Velocity Increment	40
3.2.3 Eccentric Orbit Velocity Increments	42
3.2.4 Repositioning in Synchronous Orbit Velocity Increment Determination	45
3.2.5 Stationkeeping in Synchronous Orbit Velocity Increment Determination	46
3.2.6 Drag Make-Up Velocity Increment Determination	49
3.2.7 Nodal Regression and Apsidal Rotation Velocity Increment Determination	54
3.3 Power Required to Perform Representative AF Missions	54
3.3.1 Power Required for Space Missions	58
3.3.2 Atmospheric Missions	81
3.4 Summary of Mission Requirements	84

CONTENTS (Continued)

	<u>Page</u>
4. LASER GENERATING DEVICES	88
4.1 Laser Types	88
4.1.1 Gas Dynamic Lasers	88
4.1.2 Electric Discharge Laser	90
4.1.3 Chemical Lasers	91
4.2 Operating Efficiency and Reactant Utilization	93
4.3 Summary	99
5. MICROWAVE BEAMED ENERGY	100
5.1 Microwave Concepts and Limitations	102
5.2 Technology of Beamed Microwave Energy	112
5.3 Summary	124
6. LASER BEAM PROPAGATION	125
6.1 General Considerations	125
6.2 Optical Diffraction and Beam Quality Effects	126
6.3 Laser-to-Target Range Effects and Required Collector Size	129
6.4 Transmitter Jitter Beam Broadening	129
6.5 Laser Beam Propagation Including Atmospheric Effects	132
6.5.1 General Considerations	132
6.5.2 Range and Slue Rate Calculations	135
6.5.3 Propagation Calculations	138
6.6 Summary	146
7. LASER RECEIVER SYSTEM	149
7.1 System Components	149
7.2 General Scale Size	149
7.3 Laser Radiation Concentrator	152
7.3.1 Phase Coherence	152
7.3.2 Circle of Confusion	153
7.3.3 Concentrator Weight	155
7.3.4 Required Window Diameter	158
7.4 Laser Receiver Attitude Control Systems	176
7.4.1 Mirror Attitude Control System	176
7.4.2 Concentrator Attitude Control System	180
7.5 Thruster Chamber Windows	181
7.5.1 General Considerations	181
7.5.2 Required Window Thickness	181
7.5.3 Power Transmission Capability	182
7.5.4 Surface and Bulk Absorption	187
7.5.5 Window Defocus of Transmitted Light	192
7.5.6 Additional Window Materials	194

CONTENTS (Continued)

	<u>Page</u>
7.6 Systems Problems	196
7.7 Baseline Test System	198
7.8 Mirror-Concentrator Configurations for a Laser Aided Thruster	200
7.9 Summary	205
8. LASER POWERED THRUSTER	209
8.1 Introduction	209
8.2 Thruster Start-Up Problems	210
8.2.1 Inadvertent Laser Beam Deposition on Thruster End Walls	210
8.2.2 Required Start-Up Flow Condition	213
8.3 Thruster Steady State Operation Problems	215
8.3.1 Heat Input to Thruster Chamber Walls and Rear Face Window	215
8.3.2 Laser Radiation/Propellant Coupling Problems	220
8.4 Thruster Close-Down Problems	224
8.4.1 Inadvertent Laser Beam Deposition on Thruster End Walls	224
8.4.2 Final State Wall, Window, and Propellant Condition	224
8.5 Summary	225
References	226
Appendix A	227
Appendix B	231

LIST OF FIGURES

<u>Figure</u>		<u>Page</u>
1	Initial Total Spacecraft Weight Per Pound of Delivered Payload as a Function of Required ΔV and Propellant Specific Impulse	11
2	Total Energy Required Per Pound of Payload as a Function of ΔV for 100% Efficient Coupling	12
3	Ideal Total Energy Required at 100% Efficient System Coupling to Save 1 lb. of Propellant Weight as a Function ΔV .	13
4	Beamed Laser Propulsion Spacecraft	15
5	Observer From Vertical Versus Orbital for 100 NM Altitude Satellite	17
6	Thrusting Schedule for Apsidal Rotation Correction	21
7	Allowable Daily ΔV for Apsidal Rotation as Function of Initial Total Spacecraft Mass	21
8	Laser Powered Tug: Total Laser Energy and Power Requirement as Functions of System Coupling Efficiency	29
9	Total Mission Energy Cost as a Function of Reactant Cost and Efficiency for 24.5% Laser Propagation and Coupling Efficiency (5.06×10^{11} Joules Total Laser Output).	30
10	Cost Advantage Per Mission as a Function of Shuttle Launch Cost	36
11	Velocity Increment to Achieve Circular Orbit	41
12	Plane Change Velocity for Circular Orbits	43
13	Performance for Any Plane Change	43
14	Synchronous Orbit Velocity Increments for Repositioning	47
15	Atmospheric Density	50
16	Drag Coefficient	52
17	Drag	53
18	Nodal Regression ΔV	55

LIST OF FIGURES (Continued)

<u>Figure</u>		<u>Page</u>
19	Apsidal Rotation Rate	55
20	Velocity Increment for Correcting Apsidal Rotation	56
21	Orbit Transfer Concept	63
22	Plane Change Nomenclature	76
23	Gas Dynamic Laser Schematic	89
24	Electric Discharge Laser Schematic	91
25	Chemical Laser Schematic, HF/DF	92
26	Components of a Beamed Power System	101
27	Gain of Large Antennas	104
28	Theoretical Microwave Antenna-to-Antenna Transmission Efficiency as a Function of Wavelength and Transmission Distance	106
29	Necessary Rectenna Diameter for Total Beam Collection as a Function of Orbit Altitude and Transmission Wavelength	108
30	DC Power Density Converted by a Rectenna as a Function of Transmission Distance, Propagated Wavelength, and Total Power Transmitted	108
31	Power Lost to Drag for a Minimally Sized Rectenna vs Altitude of Rectenna	110
32	Conceptual View of Amplitron Device	114
33	Efficiency of Microwave Generation vs the Normalized Magnetic Field, B/B_0	119
34	VKS-7773	120
35	Far Field Half Angle Versus Aperture Size for Various Wavelengths (corresponding to the Wavelengths Produced by Various Common Lasers) and for Two Levels of Beam Quality	128
36	Target Half Angle Versus Range for Various Sized Target Diameters	130

LIST OF FIGURES (Continued)

<u>Figure</u>		<u>Page</u>
37	Diameter Increase Due to Jitter Versus Range for Various Levels of 2σ Jitter	131
38	Instantaneous Range for Collector Altitude of 75 nm	134
39	Instantaneous Range for Collector Altitude of 100 nm	135
40	Slue Rates for 75 nm Collector Altitude	136
41	Slue Rates for 100 nm Collector Altitude	137
42	Power Variation for 75 nm Collector Altitude	142
43	Power Variation for 100 nm Collector Altitude	143
44	Power Variation for 75 nm Collector Altitude	147
45	Power Variation for 100 nm Collector Altitude	148
46	Laser Receiver System with Mirror, Concentrator, and Thruster for f1 System	150
47	Laser Receiver System with Mirror, Concentrator, and Thruster for f2 System	151
48	Lightweight Concentrator Construction Detail	156
49	Angle θ Relative to the Zenith for Direct Fly Over at 200 Kilometers Perigee, Circular Orbit, and 200 Kilometers Perigee, Highly Eccentric Orbit	161
50	Time Rate of Change of Angle θ with Respect to Zenith for Direct Fly over at 200 Kilometers Perigee, Circular Orbit, and 200 Kilometers Perigee, Highly Eccentric Orbit	162
51	Angular Acceleration, $\ddot{\theta}$ for Direct Fly Over at 200 Kilometers, Perigee, Circular Orbit, and 200 Kilometers, Perigee, Highly Eccentric Orbit	163
52	Aerodynamic Drag per Frontal Area as a Function of Altitude (Mean CIRA Atmosphere), (Spacecraft Orbit Velocity of 7.7 Kilometers per Second).	169
53	Energy Loss per Unit Frontal Area to Aerodynamic Drag as a Function of Altitude (Mean CIRA Atmosphere) for Circular Orbit (Spacecraft Velocity of 7.7 Kilometers per Second)	170

LIST OF FIGURES (Continued)

Figure		Page
54	Required Thrust for Thrust Period During $\pm 30^\circ$ Angular Motion with Respect to Zenith, per Unit Frontal Area, as a Function of Altitude for a Circular Orbit	172
55	Required Laser Beam Power Conversion to Thrust (at $I_{sp} = 770$ seconds) to Sustain Orbital Altitude from Aerodynamic Drag for Thrust Period $\pm 30^\circ$ with Respect to Zenith, as a Function of Altitude, for Frontal Area Sufficient to Intercept Laser Beam at Indicated Half Angles	173
56	Required Laser Beam Power Conversion to Thrust (at $I_{sp} = 1000$ seconds) to Sustain Orbital Altitude from Aerodynamic Drag for Thrust Period $\pm 30^\circ$ with Respect to Zenith, as a Function of Altitude, for Frontal Area Sufficient to Intercept Laser Beam at Indicated Half Angles	174
57	Moments of Inertia of Mirror as a Function of Concentrator Radius, and Assumed Levels of Surface Mass Density, σ	178
58	Required Torque to Move Mirror at Indicated Angular Acceleration Levels as a Function of Concentrator Radius	179
59	Required Window Thickness (Relative to Window Diameter) to Prevent Fracture as a Function of Pressure and Safety Factor for BaF_2 , CaF_2 , and SrF_2	183
60	Characteristic Time, τ_E , for Edge Cooling of CaF_2 , SrF_2 , and BaF_2 Windows as a Function of Window Diameter	186
61	Allowable Power Transmission as a Function of Burst Length for Various Window Diameters for SrF_2 for $t < \tau_E$	188
62	Allowable Power Transmission as a Function of Burst Length for Various Window Diameters for BaF_2 for $t < \tau_E$	189
63	Allowable Power Transmission as a Function of Burst Length for Various Window Diameters for CaF_2 for $t < \tau_E$	190
64	State-of-the-Art Bulk Absorption Coefficients for Laser Window Materials (from Miles)	191

LIST OF FIGURES (Continued)

<u>Figure</u>		<u>Page</u>
65	Laser Beam Shape for Planar Thruster Chamber Windows and Shaped Thruster Chamber Windows	193
66	Strength and Hardness Characteristics of Potential Laser Window Materials (from Miles)	195
67	Beamed Laser Propulsion Spacecraft	201
68	Reorientation of Concentrator, Mirror, and Concentrator-Mirror Axis During Direct Flyover of Laser Aided Thruster System	203
69	Laser Aided Thruster with H ₂ Gas Cooling of Rear Face Window Face and Edges, and Methanol Vapor Propellant Injection	211
70	Laser Aided Thruster with H ₂ Gas Bypass for Throat and Chamber Wall Cooling	221
71	Asymmetric Laser Beam/Propellant Coupling Resulting from Off-Axis Laser Beam Injection into Thrust Chamber	223

LIST OF TABLES

<u>Table</u>		<u>Page</u>
1	Tug Mission Requirements	3
2	Laser Powered Tug (LPT) and Advanced Cryogenic Tug (ACT) Comparison	4
3	Detailed Weight Breakdown	25
4	Tug Propellant Costs per Mission	33
5	Per Mission Cost Differential of LPT Compared to ACT (76 dollars)	35
6	Velocity Increments to Achieve Eccentric Orbits	44
7	Stationkeeping Velocity Increment Requirements	49
8	Power for Circular Orbit Without Plane Change	59
9	Power for Circular Orbits with Plane Change*	59
10	Power for Eccentric Orbit Without Plane Change	59
11	Power for Eccentric Orbits with Plane Change	60
12	Power for Repositioning in Synchronous Orbit	60
13	1 lb Drag Make-Up Power	61
14	Firing Time Available for 40° Arc	62
15	Orbital Periods	63
16	Apogee Altitudes of Transfer Ellipses	66
17	Velocity at Perigee	68
18	Allowable Beam On-Times	69
19	Velocity Increments for Transfer Orbits from Initial 100 NM Parking Orbit	70
20	Additional Candidate Transfer Orbits for Initial 100 NM Parking Orbit	71
21	Additional Candidate Transfer Orbit Velocities at Perigee - for 100 NM Initial Parking Orbit	72

LIST OF TABLES (Continued)

<u>Tables</u>		<u>Page</u>
22	Available Beam On-Time at Perigee for Additional Candidate Transfer Orbits	72
23	Velocity Increments with Additional Candidates for 1st Transfer	73
24	Sequential Transfer Orbits that have a Required Beam Power Level of About 10 MW for 100 NM Initial Parking Orbit	74
25	Plane Changing Thrust Application Efficiency	77
26	Power for Synchronous Orbit Plane Change*	78
27	Power to Daily Correct Nodal Regression for Various Orbital Altitudes for a 4000 lb Vehicle with an $I_{sp} = 1000$ sec	79
28	Power per Day to Correct Apsidal Rotation for a 4000 lb Vehicle with a Specific Impulse of 1000 sec	80
29	747 Class Future Aircraft Power Requirements	81
30	Power Required for Ground Launched Vehicles*	82
31	Power Required for Air to Air Missiles	83
32	Power Required for Ballistic Missiles	83
33	Summary of Power for Atmospheric Missions	85
34	Summary of Power for Space Missions*	86
35	Theoretical Efficiency Limits	94
36	Selected Candidate Energy Sources	95
37	Microwave Power Transmission Efficiencies	113
38	Distribution of Power in the CW Amplitron	116
39	VKS-7773 Klystron CW Amplifier Operating Characteristics	121
40	High Efficiency Klystron CW Amplifier for Space Applications	121
41	Proposed High Efficiency Klystron CW Amplifier Operating Characteristics	122

LIST OF TABLES (Continued)

<u>Tables</u>		<u>Page</u>
42	High-Efficiency Klystron CW Amplifier for Space Applications	123
43	Parametric Results for Ground Base (Sea Level) Transmitter Directed at Overhead Collector	139
44	Parametric Results for Aircraft Based Transmitter Directed at Overhead Collector	145
45	Allowable Temperature Rise, ΔT_f , in Degrees Kelvin, without Window Fracture for Safety Factors of 2 and 4.	185
46	Performance Parameters of a 30 cm Diameter Sapphire Thruster Window (HF, 2.8 μ M Incident)	196
47	Problem Areas in the Laser Receiver System and Possible Approaches to Solution	197
48	Baseline Test System with Initial Systems Tests	199
49	Principal Design Factors in Mirror/Concentrator/Thruster and Concentrator/Mirror/Thruster Configurations	204
50	Estimated Thrust Chamber Throat Diameter for Assumed 125 PSI Methanol Injection and $I_{sp} = 800$ Seconds Output Flow	212
51	Propellant and Thruster Wall Conditions Required Prior to Laser Beam Entry	214

1. INTRODUCTION AND SUMMARY

The objective of this program is to assess the feasibility of the beamed energy propulsion concept for Air Force missions. The work is divided into three major tasks: 1) system studies, 2) theoretical analyses of the coupling mechanisms between the beamed energy and propellant working fluid, and 3) preparation of a test plan for the experimental investigation of the coupling processes for various laser/propellant combinations.

The basis of the beamed energy concept is for an orbiting vehicle to convert an incoming energy beam into propulsive energy. The major system payoff is increased specific impulse and concomitant weight savings. Achieving this goal will depend on the emergence of several new technologies: 1) beamed energy generation and transmission to the receiving vehicle, 2) energy reception and coupling into the propulsion system, and 3) generation of high specific impulse at relatively high thrust levels.

In principal, either microwave or laser energy beams are capable of providing the propulsive power. However, fairly early in this study it was determined that microwave concepts result in excessive weight and size penalties for the target vehicle. Consequently, later portions of the study dealt solely with laser beams.

A prime concern has been to identify meaningful missions which do not require gigawatt power levels. As shown in Section 3 of this volume, satellite propulsion applications appear more promising than atmospheric missions in that they offer several opportunities where excessive laser power is not required and where propellant weight reductions will result in significant cost savings.

For orbiting satellites there are still several constraints which drive the mission requirements toward high power levels. They include:

- Short thrusting periods due to range and line-of-sight geometry constraints
- Heavy payloads in order to off-set the cost and weight of the laser receiver system

- High total impulse in order to achieve propellant weight savings sufficient to offset the system fixed weight penalties.

As a result of the above considerations, the most promising missions utilize thousands of pounds of propellant at approximately 800 to 1000 seconds specific impulse. The total energy requirements are $\sim 10^{11}$ joules.

The laser source for energy transmission to a given orbiting vehicle can be based either in space, on an aircraft or on the ground. Reactant powered space-based lasers are uneconomical because the weight of the laser reactants transported to space exceeds the propellant weight savings for the target vehicle. Therefore, to be cost effective, a space-based laser transmitter has to be either nuclear-electric or solar-electric powered. Since megawatt-level space nuclear- or solar-powered sources will not be available for several decades, ground based transmitter concepts have been selected as offering the opportunity for earliest implementation.

When suitable power sources become available, space-based transmitters will have the lowest operating power requirements of the three siting options. Atmospheric absorption and refraction losses will be eliminated. Thrust duration constraints due to atmospheric slant-angle absorption and horizon limiting effects will be relaxed. The allowable thrusting periods can be significantly extended and the laser range shortened when the transmitter satellite track parallels the receiving satellite track. More frequent thrusting will be possible since there will no longer be a need to synchronize thrust periods with an earth-bound 24-hour period of rotation. As a result of these potential mission advantages the low power space-based transmitter has received considerable emphasis in many parts of this report. However, the discussions also provide considerable insight into the ground-based transmitter concept.

Section 2 of this volume summarizes the various mission concepts which were initially considered and then provides more detailed analyses of those ground-based transmitter concepts which offer the opportunity for earliest implementation. These are:

- Apsidal Rotation and Nodal Regression Correction
- Drag Make-up
- Reusable Laser Powered Tug for Orbit Raising to Synchronous Altitude and Return

The first two missions can be performed with a 10 MW laser. The reusable tug requires a 500 MW laser. The apsidal rotation correction mission requires one year of 49 feet per second per day correction for an 8,000 pound inert weight. This mission can be performed with 8,000 pounds of 800 second specific impulse space storable propellant. For a "conventional" 220 second specific impulse hydrazine system, 93,600 pounds would be needed, clearly an impossible requirement. Using similar assumptions for the drag make-up application, a propellant weight advantage of approximately 3300 pounds/year can be achieved for an average drag force of ~ 0.03 pound.

A complete systems weight and cost comparison has been made between the laser powered tug (LPT) and an equivalent advanced cryogenic propellant tug (ACT). The costs of the two mission concepts were found to be approximately equal. However a \$1 million cost would result for the LPT if shuttle costs escalate significantly. The tug mission requirements are summarized in Table 1.

Table 1. Tug Mission Requirements

Initial Orbit Altitude	100 NM Circular
Final Orbit Altitude	100 NM by 19,323 NM Elliptical
One-Way ΔV	8128 fps
Payload to Synchronous Altitude	6000 lb
Retrieval Payload	1350 lb*

* Payload reduction results from propellant expenditures of 3,000 pounds for circularization and station acquisition, 300 pounds for AVCS and 1350 pounds for decircularization and rendezvous.

The mission parameters for the competing tug concepts are summarized in Table 2. The LPT uses 1000-second specific impulse hydrogen propellant. The ACT uses LO_2/LH_2 propellant at 470 seconds specific impulse.

The ACT requires a 7-day round trip duration; the LPT a 28-day duration. The 28-day round trip is a compromise between longer mission durations which minimize laser power requirements and shorter durations

Table 2. Laser Powered Tug (LPT) and Advanced Cryogenic Tug (ACT) Comparison

	LPT	ACT
Thrust (lbf)	5609	15,000
Specific Impulse (seconds)	1000	470
Round Trip Duration (days)	28	7
First Ignition Weight (lbs)	11,735	17,321
Burn-out Weight (lbs)	4,361	3,514

which (1) allow for a sufficient number of reuse opportunities during a reasonable calendar time and (2) minimize LH_2 boil-off and fuel cell consumption. An alternative means of reducing laser power would be to decrease the payload. However, significant reductions below 6000 pounds orbit-raising capability would seriously compromise the number of available applications.

The first ignition weights are 11,735 pounds for the LPT and 17,321 pounds for the ACT. Thus the shuttle payload weight saving for a launch-to-parking orbit is 5586 pounds. The burn-out weights for shuttle transport back to earth are 4361 and 3514 pounds for the LPT and ACT respectively, resulting in a 847 pound weight saving for the ACT return trip. However this differential is of second order in comparison to the ascent weight advantage for the LPT.

The high specific impulses postulated for candidate missions are predicated on the laser's ability to directly heat a hot gas core while the chamber walls are cooled by incoming propellant so that the average gas temperature exceeds that of the thruster structural materials. This is the same principle that arc jets have been based on and its success for the present application will depend on the ability of the laser beam to be absorbed directly into the propellant.

For short term applications such as orbit raising, hydrogen is the preferred propellant. Its low molecular weight should make specific impulses in excess of 1000 seconds easily attainable as has been demonstrated with arc jets. However, it will have to be seeded with other

substances to provide sufficient coupling to the laser beam. For long term orbit applications, space storable propellants are preferred. As discussed in Volume 2 of this report, methyl alcohol is an interesting propellant for this application because of its ability to form CO molecules and carbon particles, both of which aid in the laser absorption process. Other potential laser/propellant combinations are also discussed in Volume 2.

The use of electric propulsion in conjunction with the conversion of beamed laser power into electrical power has been ruled out. The additional efficiency loss in converting the laser beam into electrical energy and the higher power requirement of an electric propulsion system increase the laser power requirement by almost one order of magnitude. Since the power requirements already exceed present laser system capabilities, any further increase would be highly undesirable. An additional negative factor is that the required thrust levels are several orders of magnitude greater than presently planned electric propulsion capabilities. The weight and thermal integration requirements of the power conversion and conditioning system pose further potential problems.

In addition to development of the propulsion device itself, the laser powered propulsion concept will depend to a great extent on the future parallel development of several non-propulsive technologies, i.e., high powered lasers, pointing, tracking and collecting subsystems, and spacecraft attitude control technology. Fortunately, the required parallel development is being pursued for other applications and need not be charged directly to the propulsion task. Similarly, although a separate transmitting station is required, such stations will probably be used for other military purposes and thus may not be a direct charge to the propulsion task.

Several system and mission planning considerations require more detailed future study. These include further definition of the range of allowable spacecraft trajectories and orbits, attitude control and pointing requirements during thrusting, and the operational spacecraft configuration implications for accommodating the laser receiver to provide unobstructed optical paths from the transmitter and to the

thruster. Specifications need to be developed for coordinating propellant flow with ground-based laser initiation and shut-off. A preferred throttling philosophy (propellant flow and/or laser power) will have to be defined to maintain optimum thruster performance as the range varies during thrusting.

Volume 1 of this report contains the systems study portion of the program. Section 2 of this volume summarizes the analyses of the recommended systems concepts. Section 3 presents the more detailed mission requirements. Sections 4 through 8 then discuss the major subsystem aspects of a beamed energy propulsion system, namely, beam transmitting station, propagation, pointing and tracking, beam collection and coupling, and finally the thruster subsystem.

Volume 2 of this report is a theoretical treatment of the coupling mechanisms for various laser/propellant combinations. The main emphasis has been on particulate and molecular absorption mechanisms which do not require the high electron densities associated with efficient inverse bremsstrahlung absorption. Relatively large thruster chamber dimensions have been assumed in order to minimize the risk of laser damage to the chamber walls. This has the added advantage of relaxing dimensional tolerances and ultimately producing weight and cost savings in the form of a lighter, less dimensionally rigid, concentrator system.

Volume 3 contains additional classified data related to laser systems.

1.1 CONCLUSIONS AND RECOMMENDATIONS

The following paragraphs are major conclusions and recommendations of this study.

Beamed energy propulsion is technically feasible. No fundamental obstacles have been identified. However, considerable additional study and technical development are needed in many areas before the concept can be operationally implemented.

In order to minimize the required collector area, laser concepts are preferred over microwaves. Large diameter microwave receivers will have to be of the rectenna (rectifying antenna) type since conventional receiving reflectors cannot be fabricated to the precision required for efficient

large scale collection. Thus microwaves will require electrically powered propulsion. This results in additional thousands of pounds of power conditioning equipment and radiation structure for heat rejection from the electrical subsystem.

Ground based transmitter concepts offer the opportunity for earliest implementation. Space based laser transmitter concepts can potentially lower the power requirements but to be cost effective they will require the availability of megawatt-level space nuclear or solar power stations. A reactant powered space based laser will not be cost effective because of the expense of transporting the reactants to orbit.

In view of the large total energy required for each mission, ground based transmitters will be most cost effective when they are operated closed cycle from central station electric power.

Laser transmitting ranges greater than several hundred nautical miles will result in excessive collector sizes. Therefore, ground based transmitters applications will be restricted to orbital functions which can be performed at low orbital altitudes. Thus, synchronous altitude functions such as circularization and repositioning in orbit will not be feasible with ground based transmitters. When high altitude space based transmitter concepts do become feasible the range of potential applications will be correspondingly enlarged. For stationary transmitting stations, fly-by range considerations will limit thrust periods to 50 seconds (4° of orbital arc).

Three promising applications have been identified. A laser powered tug has been shown to be potentially cost competitive with an advanced cryogenic tug. Apsidal rotation correction and drag make-up are two other missions where significant advantages may be realized for the laser powered concept.

Considerable additional study and technical development are needed before the beamed energy propulsion concept can be operationally implemented. Critical hardware areas include the lasers, thrusters, thruster reaction chamber windows and the collection and coupling subsystems.

Additional systems studies needed to more firmly evaluate the potential payoffs include the following:

- Detailed mission planning and optimization for each of the three candidate missions. Drag make-up and apsidal rotation correction should be combined into one mission.
- Detailed tradeoffs of the benefits of thrusting at higher altitudes in order to achieve less drag and longer available thrusting periods at the cost of larger required collector areas.
- Detailed thrust scheduling tradeoffs for the reusable laser powered tug.
- A separate laser collection and coupling system design study to fully assess the impact of this massive and complex subsystem.
- Careful assessment of the impact of start and stop losses on total propellant consumption for short thrusting periods.
- Additional iteration of the present study results at the several hundred megawatts laser power level. The greatest needs are in the areas of atmospheric propagation, collection and coupling, and thruster design. Greater emphasis should also be placed on thermal integration.

2. MISSION SELECTION AND TRADEOFFS

This section discusses the selection and analysis of various missions for beamed energy propulsion. The beamed energy is assumed to be provided by a laser since, as discussed in Section 5, microwave beams do not appear practical for this application. A major emphasis has been to determine those mission concepts which have the chance for earliest implementation, i.e., those which do not require either gigawatt laser power levels or space-based solar or nuclear megawatt power sources. As the result of an extensive selection process based on the above considerations, the following missions, which utilize ground based laser transmitters, have been chosen as offering the greatest promise:

1. Apsidal Rotation and Nodal Regression Correction
2. Drag Make-Up
3. Reusable Tug for Orbit Raising to Synchronous Altitude

It will be shown that 8,000 pounds of laser powered 800 second specific impulse propellant will perform an apsidal rotation correction mission that would otherwise require 93,600 pounds of conventional 220-second specific impulse propellant. For the second mission, above, a laser powered propellant weight savings of approximately 7,500 lbs/year for compensating an average drag force of ~ 0.07 pounds will be shown.

The section concludes with a detailed weight and cost comparison of a laser powered space tug (LPT) and an advanced cryogenic tug (ACT). It will be shown that the LPT is cost competitive with the ACT. Furthermore, a \$1 million advantage may result for the LPT if shuttle costs escalate in the future.

2.1 SPACE BASED TRANSMITTERS

A major consideration for beamed energy propulsion is that the added cost of providing laser power must be less than the cost savings achieved by having to boost less propellant to orbit. This section shows that this consideration leads to the conclusion that the space based transmitter concept must use either solar or nuclear power in order to avoid excessive reactant transport costs.

The propellant weight (W_p) required per pound of delivered inert weight is given by:

$$W_p = W_o - 1$$

where:

$$W_o = \exp \Delta V / g I_{sp} = \text{initial total spacecraft weight}$$

ΔV = velocity increment, ft/sec

$$g = 32.2 \text{ ft/sec}$$

I_{sp} = specific impulse, seconds

The present study assumes specific impulses of the order of 800 to 1000 seconds for beamed energy systems. These replace specific impulses of 300 seconds for conventional upper stages, 470 seconds for advanced cryogenic upper stages and 220 seconds for hydrazine auxiliary propulsion.

Figure 1 shows initial total spacecraft weight per pound of final payload versus ΔV for the specific impulses of interest. As would be expected, the advantages of high I_{sp} increase dramatically with ΔV . For laser systems of limited power, the implication is that low total mass, high ΔV missions are favored for beamed energy propulsion.

The total propulsive energy (at 100% system efficiency) required per pound of delivered inert mass is:

$$E_o = 21.8 W_p I_{sp}^2 \quad \text{Joules/pound of payload}$$

Figure 2 shows the total energy requirements as a function of ΔV . Thus, neglecting inefficiencies, total laser energies in the range of 3 to 100 megajoules are required per pound of delivered inert mass. Therefore, high ΔV missions with thousands of pounds of payload will require of the order of 10^{11} joules.

The total laser energy required per pound of propellant weight saving is equal to:

$$\frac{E_o}{W_p, \text{ Conventional} - W_p, \text{ Beamed}}$$

and is plotted in Figure 3. These results show that even at $\Delta V = 50,000$ ft/

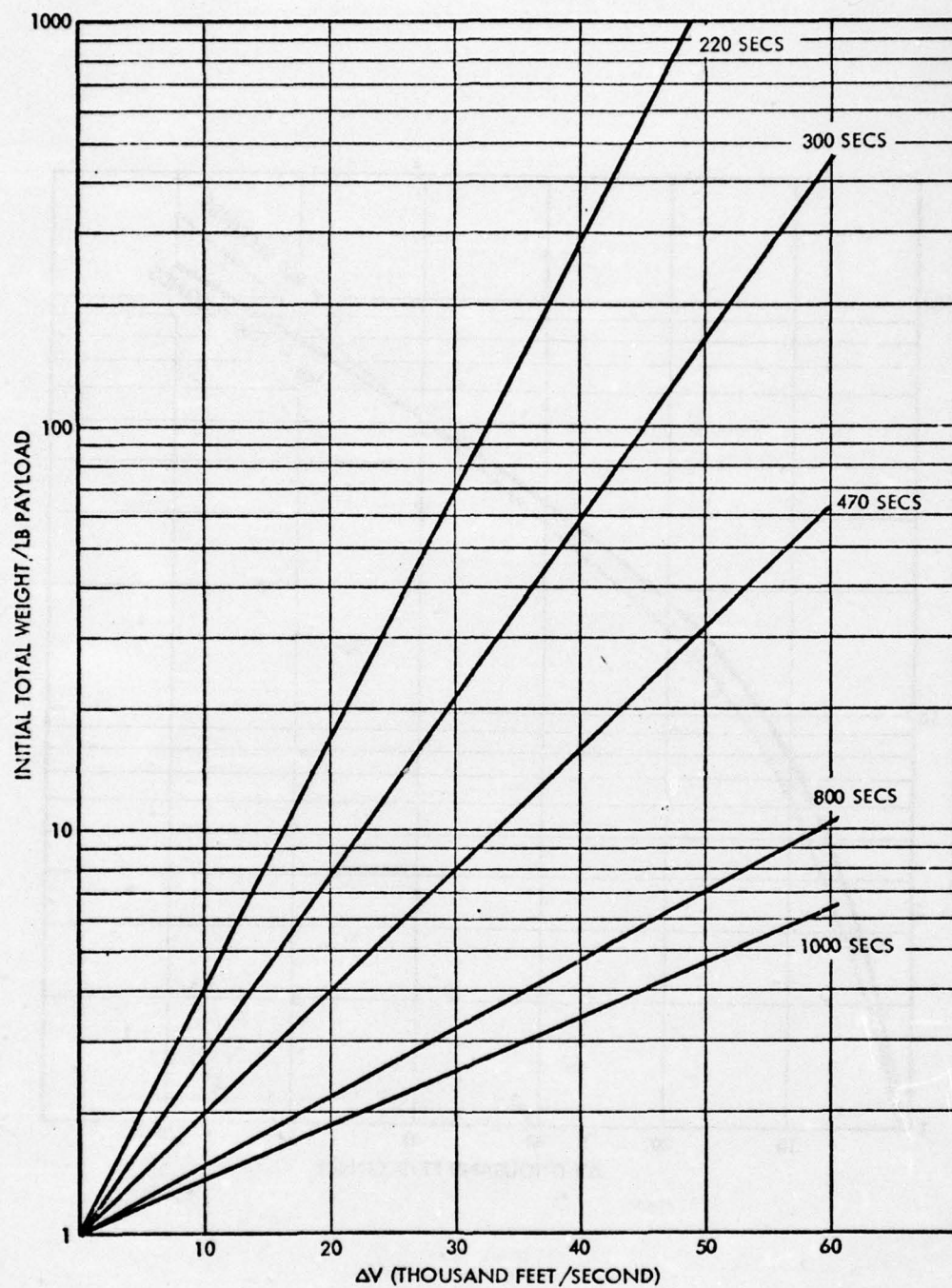


Figure 1. Initial Total Spacecraft Weight Per Pound of Delivered Payload as a Function of Required ΔV and Propellant Specific Impulse.

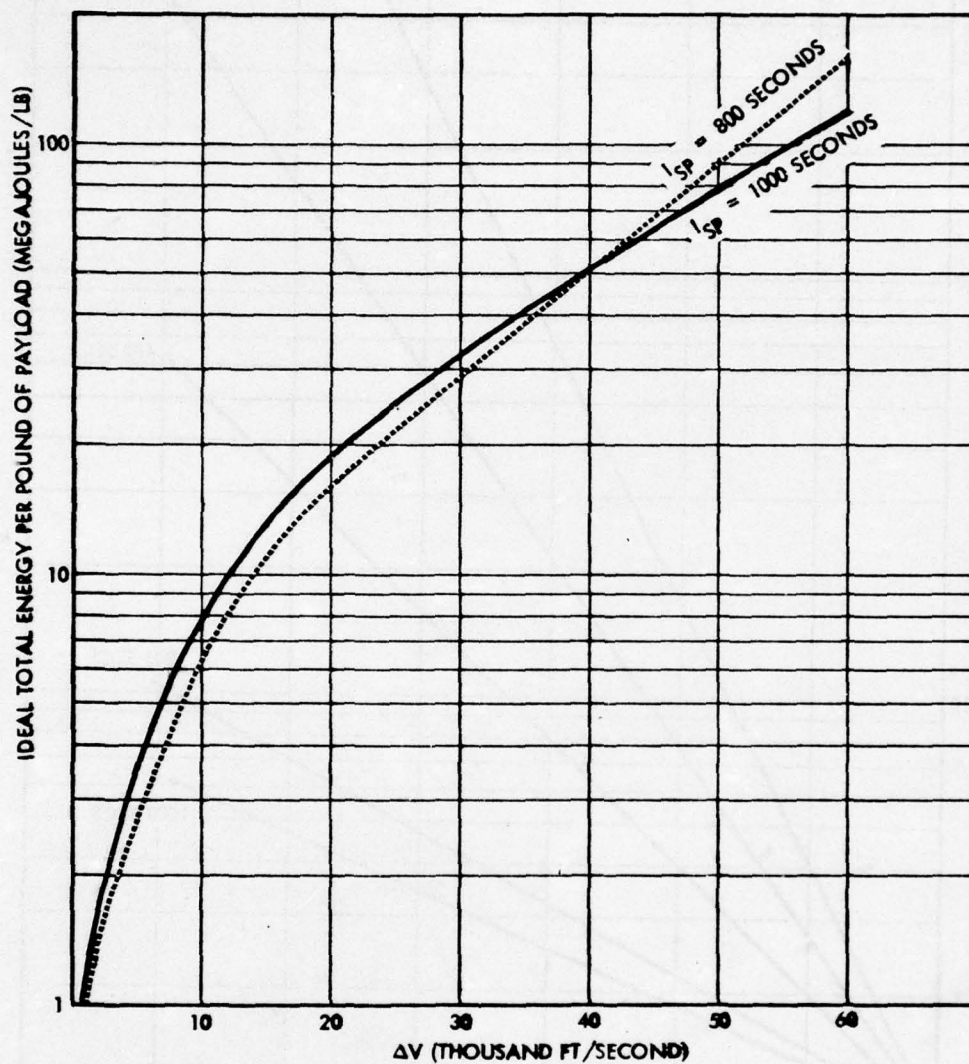


Figure 2. Total Energy Required Per Pound of Payload as a Function of ΔV for 100% Efficient Coupling.

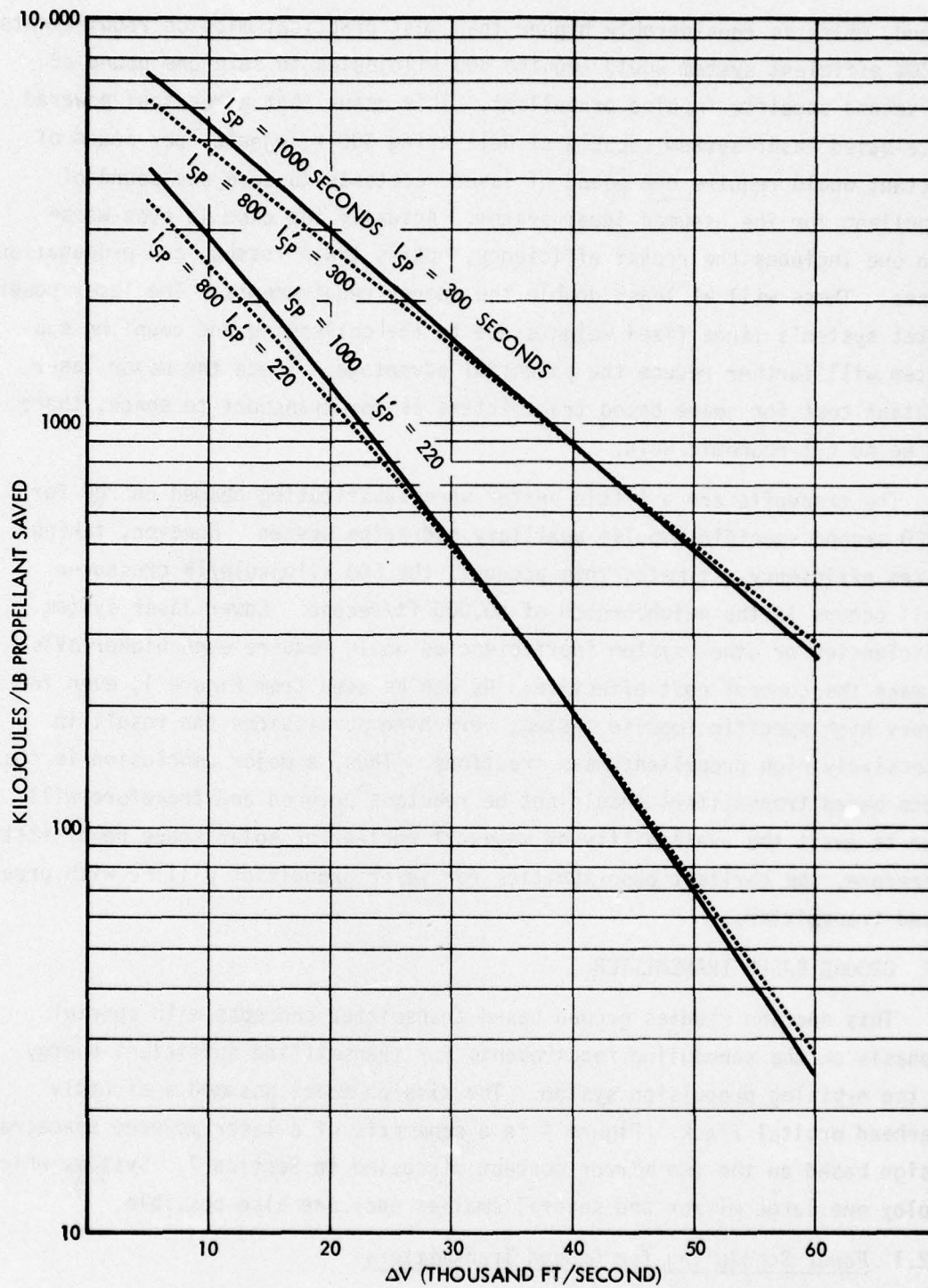


Figure 3. Ideal Total Energy Required at 100% Efficient System Coupling to Save 1 lb. of Propellant Weight as a Function ΔV .

second, which is considerably higher than most practical mission requirements, a 100% efficient system would require 500 kilojoules to save one pound of 300 second specific impulse propellant. This means that a reactant powered space-based laser system capable of delivering 500 kilojoules per pound of reactant would require one pound of laser reactants to save one pound of propellant for the assumed ideal system. Actually the case is even worse when one includes the rocket efficiency, optics train losses, and propagation losses. These will at least double the energy requirements. The laser powered rocket system's large fixed weights due to the collecting and coupling subsystem will further reduce the potential advantage. Since the major laser reactant cost for space based transmitters is for transport to space, there can be no net economic gain.

The tradeoffs are a little better when substituting beamed energy for a 220 second specific impulse auxiliary hydrazine system. However, taking system efficiency estimates into account, the 500 kilojoule/lb crossover still occurs in the neighborhood of 50,000 ft/second. Lower laser system efficiencies or other system inefficiencies would require even higher ΔV 's to make the concept cost effective. As can be seen from Figure 1, even for a very high specific impulse system, very high ΔV missions can result in excessively high propellant mass fractions. Thus, a major conclusion is that space based transmitters should not be reactant powered and therefore will have to await the availability of megawatt nuclear or solar space power stations. Therefore, the earliest opportunities for laser propulsion will be with ground based transmitters.

2.2 GROUND BASED TRANSMITTER

This section studies ground based transmitter concepts with special emphasis on the scheduling requirements for transmitting sufficient energy to the orbiting propulsion system. The mission model assumed a directly overhead orbital track. Figure 4 is a schematic of a laser powered spacecraft design based on the two mirror concept discussed in Section 7. Systems which employ one large mirror and several smaller ones are also possible. ⁽¹⁾

2.2.1 Power Scheduling for Ground Transmitters

The calculations will assume the following efficiency estimates for coupling to a 100 nm altitude satellite:

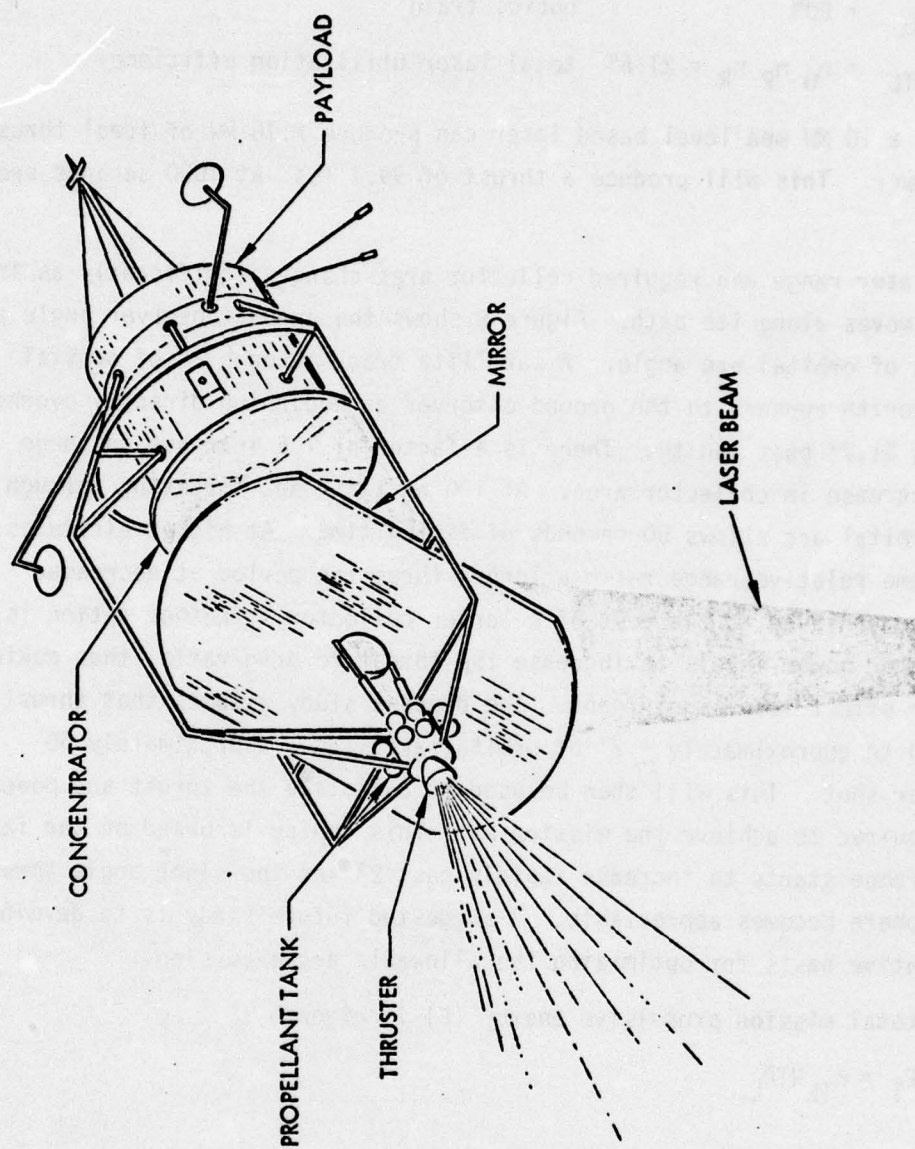


Figure 4. Beamed Laser Propulsion Spacecraft.

η_R	= 50%	rocket efficiency*
η_P	= 54%	propagation efficiency
η_O	= 80%	optics train
η_{TL}	$= \eta_O \eta_P \eta_R = 21.6\%$ total laser utilization efficiency	

Thus, a 10 MW sea level based laser can produce 2.16 MW of ideal thruster kinetic power. This will produce a thrust of 99.1 lbs. at 1000 seconds specific impulse.

The laser range and required collector area change significantly as the satellite moves along its path. Figure 5 shows the ground observer angle as a function of orbital arc angle. A satellite track through 2° of orbital arc past zenith appears to the ground observer as beginning directly overhead and ending 51.7° past zenith. There is a factor of 1.6 increase in range and 2.6 increase in collector area. At 100 nm altitude, thrusting through $\pm 2^\circ$ of orbital arc allows 50 seconds of firing time. At higher altitudes and the same relative range ratio a longer thrusting period at decreased drag can be achieved at the cost of a larger collector. Another option is to use higher power levels to increase the thrust to drag ratio, thus making the latter effect less significant. The present study assumes that thrusting is limited to approximately $\pm 2^\circ$ of orbital arc, i.e., approximately 50 seconds per shot. This will then be used to calculate the thrust and power levels required to achieve the mission ΔV . This choice is based on the fact that the range starts to increase rapidly past 2° and the slant angle through the atmosphere becomes appreciable. A suggested future study is to develop a quantitative basis for optimizing the allowable arc excursion.

The total mission propulsive energy (E) is given by:

$$E_T = \eta_{TL} NTP_L$$

* η_R is the net result of all efficiency factors involved in the conversion of laser power incident on the spacecraft into propulsive power. This definition allows for regenerative heat recovery due to the routing of propellant flow through coolant loops. Thus, the rocket efficiency is equal to the ideal propulsive power divided by the incident laser power.

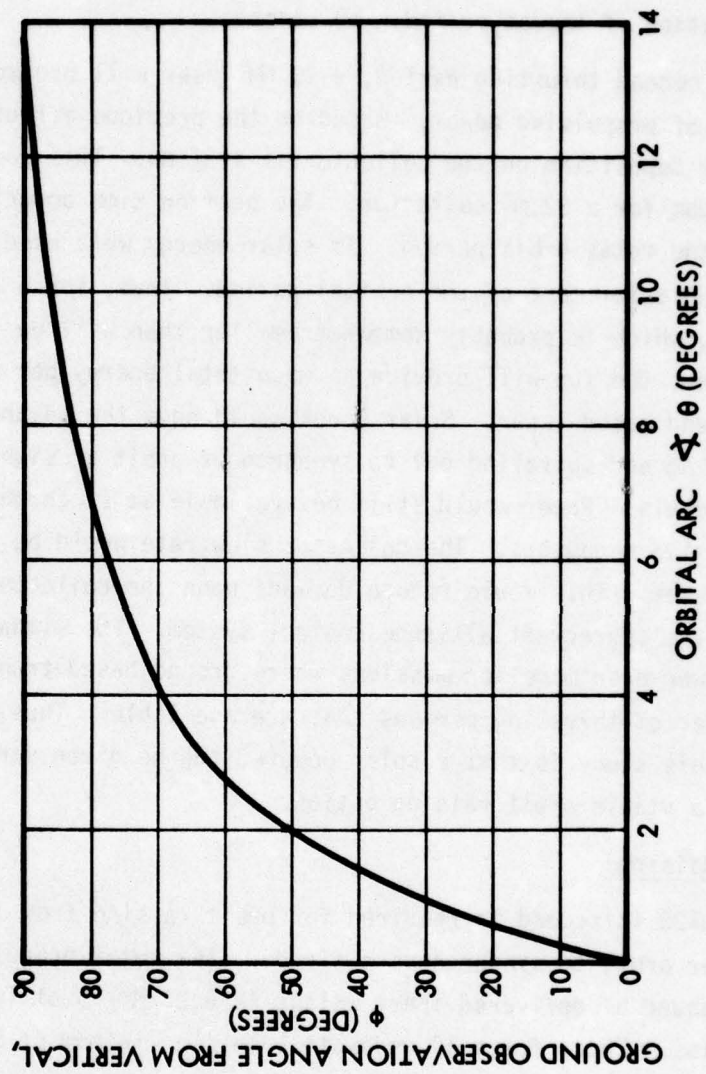


Figure 5. Observer ϕ From Vertical Versus Orbital θ for 100 NM Altitude Satellite.

where

P_L = Laser Power

η_{TL} = Total Efficiency = 0.216

N = Number of thrust periods/mission

T = Duration of thrust period = 50 seconds

In one 50 second thrusting period, a 10 MW laser will produce roughly 100 megajoules of propulsive power. Based on the previous efficiency assumptions the power deposition on the collector is 4.32 MW. This would be equivalent to 100 suns for a 32 m² collector. The beam on time amounts to approximately 1% of the total orbit period. If solar energy were used, the sun would be available for most of the orbital period. Thus, for a 32 m² collector area, which is probably somewhat smaller than will be required by the laser system, the sun will provide as much total energy per orbital period as a 10 MW ground based laser. Solar power would have the advantage of allowing continuous firing and spiraling out to synchronous orbit at significantly lower thrust levels. Power would still be available at synchronous orbit for further propulsive maneuvers. The collector slew rate would be lower than for a laser system. This would reduce demands upon the collector drive mechanism and the spacecraft altitude control system. The situation would favor solar power even more for missions where ground based transmitters limit the number of thrusting periods that are available. Thus, one recommendation of this study is that a solar powered tug be given serious consideration as a viable orbit raising option.

2.2.2 Orbit Raising

A ΔV of 8128 ft/second is required for orbit raising from 100 nautical miles circular orbit to synchronous altitude. The total propulsive energy required per pound of delivered inert weight is 6.26 MJ/lb at 1000 seconds specific impulse. Thus, for a 10 megawatt laser, a minimum of 50 or 60 shots are required to orbit raise 1000 lbs inert weight. With one earth station it would in principle be possible to provide one thrusting period per day if the orbit raising impulses are controlled to synchronize perigee arrival with the earth's rotation. Since the 100 NM circular orbit is only 16.3 periods/day while a 100 NM perigee x synchronous altitude apogee orbit is 2.3 periods/day; only 14 successive harmonics are available for daily synchronization.

Thus, 50 or 60 consecutive thrusting days would not be possible. Furthermore, harmonic synchronization would mean firing at less than full capability for most thrust periods, thus further increasing the total number of periods required. The total orbit raising operation could then take up a significant fraction of a year.

An alternative strategy is to position several launch stations at equal latitude and different optimally selected longitudes. Another alternative is an aircraft based transmitter to provide launch station mobility.

Conventional transfer orbits are usually at approximately 25° inclination. A polar based transmitter station combined with a polar transfer orbit would allow firing once every orbit. However, the additional ΔV required for plane changing (1) to achieve the initial polar parking orbit ($\sim 30,000$ fps) and (2) to change to the equatorial plane after orbit raising ($\sim 15,000$ fps at synchronous altitude) would result in excessive weight penalties.

An additional consideration for mission planning is that unless the transfer orbit is at 63.4° inclination the perigee altitude will continually drift due to apsidal rotation of the elliptical orbit. At 25° inclination, apsidal rotation can be as high as $13^\circ/\text{day}$ for low apogee altitude. Since the magnitude of this effect decreases rapidly with increasing apogee altitude, the degree to which the inclination can deviate from 63.4° will depend on the magnitude of the initial ΔV increments. It may be possible to correct the apsidal rotation by firing nonsymmetrically around perigee. Another possible solution is to use equatorial transfer orbits in conjunction with an equatorial ground station. However, this would increase the total mission ΔV .

The discussion till now has assumed a 1000 pound inert weight delivered into eccentric synchronous transfer orbit. The collection system mass will be at least of the order of 500 pounds. This could be jettisoned before circularization if a retrieval descent is not planned; however, half the remaining weight would still be required for a conventional apogee kick motor system. In either case the remaining synchronous payload is too small by an order of magnitude to be practical. It thus becomes apparent that powers in the 100 MW range will be required to deliver meaningful payloads in a reasonably short time period.

As a result of the preceding discussions, two sharply conflicting desires emerge: (1) a desire to utilize low power laser transmitters to minimize the required development lead time and (2) the need to deliver meaningful payload masses. Arbitrary mission compromises will have to be made on a case-by-case basis. A detailed analysis of a reusable tug for orbit raising is given in Section 2.4.

2.2.3 Apsidal Rotation and Nodal Regression Correction

Apsidal rotation correction is an operation calling for a wide range of daily velocity increments depending on the orbit inclination, eccentricity, and apogee height. The instantaneous power and total propellant requirements depend upon the payload mass, choice of orbit and the total mission duration. The required thrust level varies over the life of the mission as a consequence of propellant mass depletion.

In order to achieve the desired correction without perturbing other orbital parameters, thrusting is required not at perigee but instead at least at two other locations. Figure 6 illustrates a possible thrusting strategy for apsidal rotation correction. The thrust is applied at symmetric points with respect to perigee. For a spacecraft orientation fixed in inertial space one thruster will do. However, provision must then be made for changing the collector orientation relative to the spacecraft (and thruster) for the two points. A more common mission is for the satellite to maintain constant orientation relative to the earth. This simplifies the collector orientation problem, but requires two thruster orientations. For a 100 x 300 nautical mile altitude orbit, the average firing altitude is approximately 200 miles, resulting in a factor of 4 greater collector area than for a 100 mile perigee altitude. The 200-mile altitude allows firing periods of 100 seconds/shot. Long-term space storable propellant with a maximum 800 seconds specific impulse capability will be required. The total delivered daily impulse for two firings per day at a nominal 125 lb thrust level for the 10 MW transmitter is 2.5×10^4 lb secs/day. Figure 7 shows the resultant daily ΔV as a function of initial total satellite mass.

The assumed initial mission requirements are a one year life and 50% of the total initial weight dedicated to propellant. From Figure 1 we can see that the 50% weight factor for 800 seconds specific impulse occurs at



Figure 6. Thrusting Schedule for Apsidal Rotation Correction.

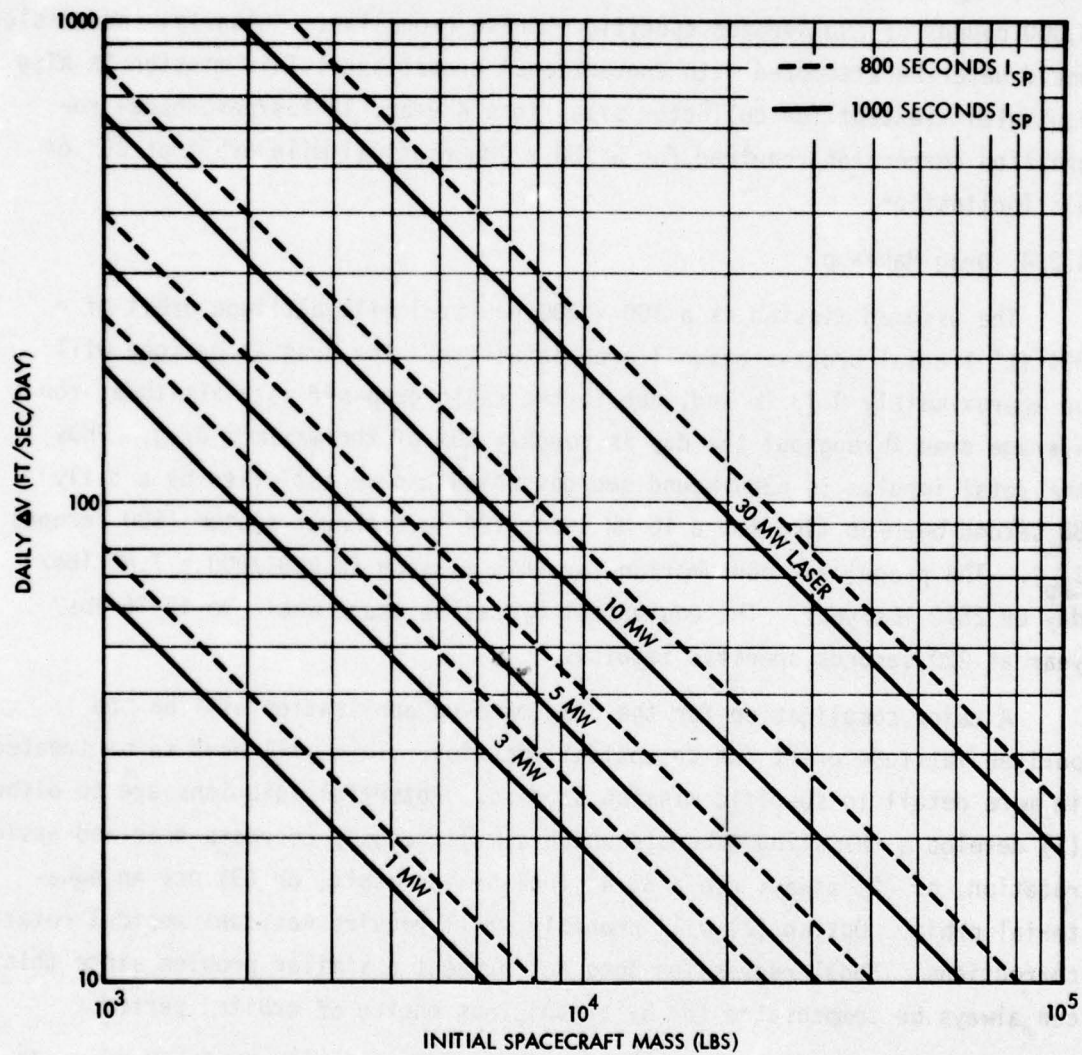


Figure 7. Allowable Daily ΔV for Apsidal Rotation as Function of Initial Total Spacecraft Mass.

$\Delta V = 18,000$ fps. This averages out to 49 fps per day over the year. This is equal to the required apsidal rotation correction for a 100 x 300 nautical mile altitude orbit at either 55° or 90° inclination. The resultant initial spacecraft mass from Figure 7 is 4800 pounds initial weight for a 3 MW laser firing twice daily or a 16,000 pound capability for a 10 MW laser. Thus, at 800 seconds specific impulse a 10 MW laser propulsion system will provide apsidal rotation correction for one year of an 8,000 pound inert weight payload. By comparison, performing the same mission with 220 second specific impulse hydrazine would require 93,600 pounds of propellant as compared to 8,000 pounds of 800 seconds specific impulse propellant. Clearly, the mission would never be attempted with conventional propellant. This mission is also equivalent (except for collector size) to a 4 year, 12 fps/day, nodal regression correction required for a 100 x 300 nautical mile orbit at 25° or 63° inclination.

2.2.4 Drag Make-Up

The assumed mission is a 100 x 300 nautical mile altitude orbit of a 364 ft^2 frontal cross-sectional area satellite. The drag at perigee will be approximately 0.73 lb and, due to the rapid drop-off with altitude, the average drag throughout the day is roughly 10% of the maximum drag. Thus the total impulse is 6284 pound sec/day which can be satisfied by a daily 50 second beam-on time for a 10 MW laser 124 lb.F thrust system (800 seconds I_{sp}). The propellant consumption for this mission is $6284/800 = 7.86$ lbs/day or 2870 lbs/year. The equivalent hydrazine usage would be 10436 lbs/year at 220 seconds specific impulse.

A major complication for the drag make-up application will be the perigee latitude drift due to apsidal rotation. This will have to be treated in more detail in specific mission studies. Potential solutions are to either (1) develop a thrusting schedule which simultaneously corrects drag and apsidal rotation, or (2) always use a 63.4° inclination orbit, or (3) use an equatorial orbit. Option (2) will probably still require residual apsidal rotation corrections. Nodal regression does not present a similar problem since this can always be compensated for by a judicious choice of orbital period.

2.2.5 Circularization, Change-Of-Plane and Repositioning in Synchronous Orbit

The propagation studies have shown that impractically large collector areas, in excess of 10^5 m^2 , are needed for beaming to synchronous altitude.

Thus the missions of interest must be confined to low altitude firings, i.e., orbit raising and low altitude orbital control applications. This consideration eliminates orbit circularization, change-of-plane and repositioning at synchronous altitude as potential missions.

2.3 AIRCRAFT AND MOUNTAINTOP-BASED TRANSMITTERS

These are essentially variations of the ground based transmitter concept. The propagation calculations for the DF laser showed that for an aircraft based laser approximately 20% more power can be delivered into 23% less collector area. Transmitter mobility would be another advantage. The major disadvantage would be the unavailability of low cost ground based electrical power. The mountaintop based transmitter would have a propagation capability intermediate to the aircraft and sea level transmitter. This would be achieved at the cost of restricting the number of available locations.

2.4 REUSABLE TUG

An interesting potential application of beamed laser propulsion is a reusable laser powered tug to provide round trip transport of a satellite between a 100 nautical mile altitude parking orbit and a 100 nautical mile by synchronous altitude elliptical orbit. The one-way ΔV is 8128 feet per second. A 6000 lb payload is delivered to synchronous altitude. A 1350 pound payload is retrieved. This is compatible with a mission profile where the initial 6000 pound payload is reduced to 3000 pounds at start of life on-station as a consequence of post-deployment orbit circularization, plane changing and station acquisition maneuvers. Further payload weight reductions prior to retrieval include ~ 300 pounds for on-station auxiliary propulsion and 1350 pounds for plane-changing and decircularization prior to recovery by the tug.

The laser powered tug (LPT) uses 1000 second specific impulse hydrogen propellant. The advanced cryogenic tug (ACT) uses LO_2/LH_2 propellant at 470 seconds specific impulse. The NASA Baseline Space Tug Configuration Definition ⁽¹⁾ has been used to provide initial subsystem weight estimates as a basis for design iteration. For example, it was possible to immediately determine that the tug burn-out weight would be in the 3000 to 4000 pound range. This item provided the inputs needed for initial propellant weight estimates which in turn modified the burn-out weight estimate. The calcu-

lations were then iterated until self-consistent weight breakdowns were achieved.

The ACT requires a 7-day round trip duration; the LPT a 28-day duration. The 28-day round trip is a compromise between a longer mission duration which minimizes laser power requirements and a shorter duration which (1) allows for a sufficient number of reuse opportunities during a reasonable calendar time and (2) minimizes LH_2 boil-off and fuel cell consumption. An alternative means of reducing laser power would be to decrease the payload. However, significant reductions below 6000 pounds orbit raising capability would seriously compromise the number of available applications.

2.4.1 Weight Breakdown

Detailed weight breakdowns for the cryogenic and laser tugs are given in Table 3.

The first ignition weights are 11,735 pounds for the LPT and 17,321 pounds for the ACT. Thus the weight saving for a shuttle launch to parking orbit is 5586 pounds. The burn-out weights for shuttle transport back to earth are 4361 and 3514 pounds for the LPT and ACT respectively resulting in a 847 pound weight saving for the ACT return trip. This penalty is of second order in comparison to the ascent weight advantage for the LPT.

Most weights were scaled directly from the MSFC Baseline Tug. The body shell and mounting structure were assumed proportional to first ignition weight. Tankage and insulation were assumed proportional to propellant weight in order to obtain the same fractional boil-off rate as calculated for the MSFC study. Weights for the payload and umbilical interface, active and passive thermal controls and avionics, have been taken directly from the MSFC study. The 15,000/lb.F thrust main engine from the MSFC study has been retained for the present advanced cryogenic tug. An average 470 second specific impulse has been assumed. The laser powered thrust is 5609 pounds, which is what would be required for the ascent to be achieved with 14 equal firings of 50 seconds duration each. Thruster weight has been assumed to scale less than linearly to allow for fixed weights and the laser powered device's greater complexity. The ideal thruster exhaust power is 122.3 megawatts for the LPT.

Only one feed, fill, drain and vent system and one propellant loading

Table 3
Detailed Weight Breakdown

	Weight (lb.)	
	Laser Tug	Advanced Cryogenics Tug
STRUCTURE		
Body Shell	190	280
Fuel Tank & Supports	367	113
Oxidizer Tank & Supports	---	65
Thrust Structure	11	29
Mounting Structure	31	31
Payload & Umbilical Interface	<u>263</u>	<u>263</u>
	862	781
PROPULSION		
Engine	200	442
Feed, Fill, Drain & Vent	128	256
Pneumatic & Press	135	61
Hydraulic	29	63
Propellant Loading & Measuring	25	50
APS	<u>293</u>	<u>265</u>
	810	1137
THERMAL CONTROL		
Active Thermal Control	70	70
Fuel Tank Insulation	78	24
Oxidizer Tank Insulation	--	11
Insulation Purge	100	53
Passive Thermal Control	<u>41</u>	<u>41</u>
	304	199
AVIONICS		
Navigation Guidance & Control	154	154
Data Management	158	158
Communications	72	72
Measuring System	92	92
Electrical Power and Distribution	560	410
Rendezvous & Docking	<u>35</u>	<u>35</u>
	1071	921

Table 3 (Continued)

	Weight (lb.)	
	Laser Tug	Advanced Cryogenics Tug
LASER COLLECTION AND COUPLING		
First Mirror (94.6 m ²)	522	
Concentrator (31 m ²)	171	
Structure & Drive Motors	100	
Sensors & Drive Electronics	<u>25</u>	
	818	---
10% GROWTH CONTINGENCY INCLUDING FASTENERS	387	304
TOTAL DRY WEIGHT	4252	3342
UNUSABLE RESIDUALS		
Trapped Propellant	19	40
Trapped Gases	41	88
Fuel Bias	--	17
Hydraulic Fluid	1	5
APS Reserve	25	9
APS Trapped	16	6
Trapped Water	<u>7</u>	<u>7</u>
	109	172
BURN OUT WEIGHT	4361	3514
EXPENDABLES		
LOX Boiloff	---	35
Fuel Boiloff	571	44
Start/Stop	114	77
Fuel Cell Reactant	<u>700</u>	<u>175</u>
	1385	331
PROPELLANT RESERVES	63	134
USABLE PROPELLANTS		
LH ₂	5679	1893
LOX	---	11358
APS	<u>247</u>	<u>90</u>
	5926	13341
FIRST IGNITION WEIGHT	11735	17321

and measuring system are needed for the monopropellant laser tug. The pneumatic and pressurant systems were scaled to total propellant volume. The hydraulic system for thruster gimbaling is scaled to thruster weight. Apart from the difference in propellant and tankage requirements, identical auxiliary propulsion systems were postulated for the two missions.

The APS propellant is a small fraction of the total tug weight. Based on the MSFC numbers, the APS propellant requirements were scaled as approximately 7.35×10^{-4} pounds per day per pound of first ignition weight. The APS propellant tankage weight fraction was assumed to be 20%. The main weight impacts of the thermal control are the weight variations with volume of the fuel tank insulation, oxidizer tank insulation and insulation purge.

The avionics systems weight for the two tug concepts was assumed to be constant with the exception of the fuel cell reactant and tankage requirements. The main factor here is the four times longer operational period for the LPT. Additional fuel cell reactants for the laser collection system will be relatively negligible because of the short total thrusting time.

The laser collector system weight is dominated by the mirror and collector. The propagation studies indicated that a 50 to 100 m² collection aperture area would be required for a 2.5 m diameter transmitter. For the system weight calculated here, it has been assumed that at a total of 125.6 m² of collection area are required. This is a conservative assumption if a workable one mirror system can be devised. For a two mirror system the assumption is optimistic since it requires a 31 m² concentrator area preceded by a 94.6 m² first mirror. The mirror area ratio is what would be required for a 100 nm altitude flyover through $\pm 2^\circ$ of orbital arc around perigee centered directly over the transmitter. It may be possible to reduce the required mirror size by locating the ground station further down track but this would require further study. The reflector specific weights are 2.5 Kg/m².

The unusable residuals have been scaled in proportion to the relevant reactants volumes. Fractional hydrogen boil-off was scaled to mission duration. The ACT start/stop and fuel cell reactants were taken directly from the MSFC study. The LPT start/stop was based on an equivalent one second propellant usage per firing. This is highly optimistic and future detailed thruster design studies should give high priority to estimating start/stop consumption.

As previously stated, fuel cell reactant requirements were assumed proportional to total mission duration.

2.4.2 Energy and Power Requirement

Total ideal propulsive energy for the mission is 1.24×10^{11} joules (8.56×10^{10} joules up, 3.82×10^{10} down). For fourteen equal ascent firings of 50 seconds each the average propulsive power is 122 megawatts. The same propulsive power would be applied during descent. However the total descent firing time would be only 313 seconds as compared to 700 seconds for ascent. The laser power requirements will depend on the various propagation and coupling efficiencies. Figure 8 shows the total laser power requirements as a function of system efficiency. A conservative goal is 24.5% total system efficiency which requires 500 megawatts laser power and 5.06×10^{11} joules for the entire mission. This would be compatible with 80% optics train efficiency, 54% propagation efficiency and 57% rocket efficiency. The 57% rocket efficiency may be optimistic for a space storable propellant such as methanol but be conservative for seeded hydrogen.

A rough estimate to the energy cost lower limit can be obtained by assuming a 30% electrical-to-laser conversion efficiency and an electrical power cost of 2.5¢ per kilowatt-hour ($\$6.94 \times 10^{-9}$ per joule) which is the present cost of commercial electric power. The total energy cost per mission would then be \$11.7K, which would be negligible. Reactant powered lasers would cost appreciably more. For example, for a laser efficiency of 100 kilojoules/pound and a reactant cost of 10¢ per pound; i.e., a laser energy cost of $\$10^{-6}$ /joule; the total mission energy cost is \$506,000. Figure 9 shows total mission energy costs for various combinations of laser efficiencies and reactant costs. It can be seen that total reactant costs will probably always exceed \$100,000 and may easily reach \$1,000,000; thus providing a powerful argument for the cost benefits of central station power in conjunction with a closed cycle. The closed cycle would also circumvent the logistic problem of supplying 10^6 pounds of reactants per mission.

2.4.3 Thermal Considerations

The laser power incident on the reflecting system is 216 megawatts. The highest power density occurs for a cross-sectional area of the order of 31m^2 . For a reflector absorptivity of 0.002, a reflector specific weight of 2.5 Kg/m^2

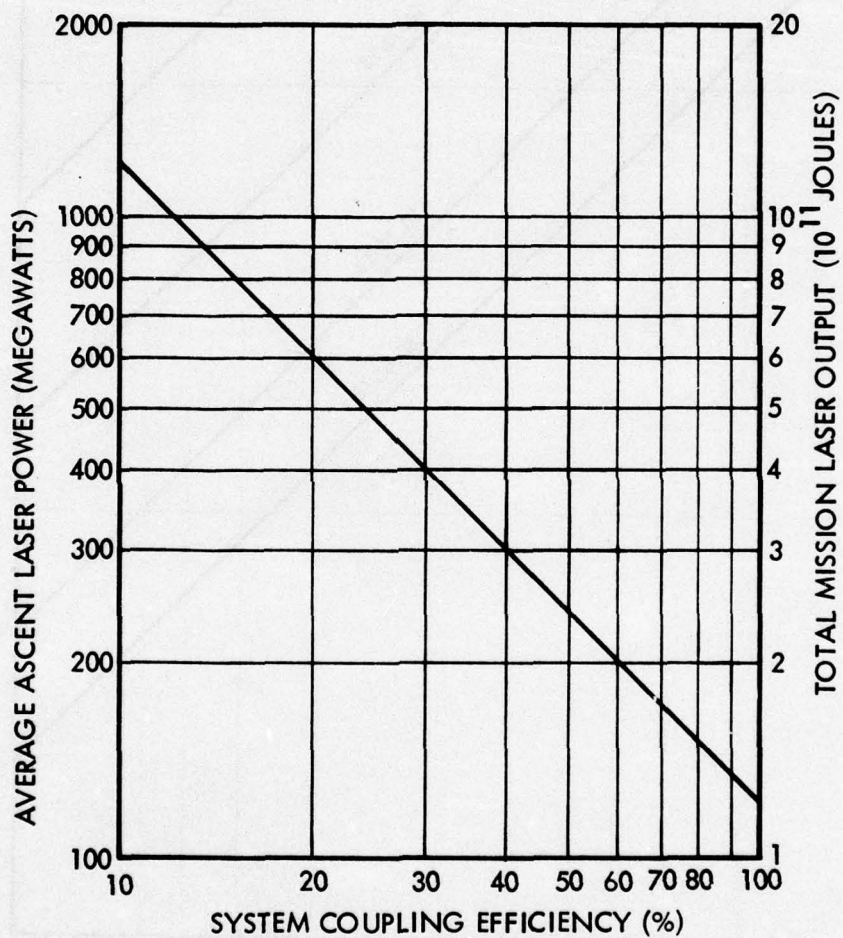


Figure 8. Laser Powered Tug: Total Laser Energy and Power Requirement as Functions of System Coupling Efficiency.

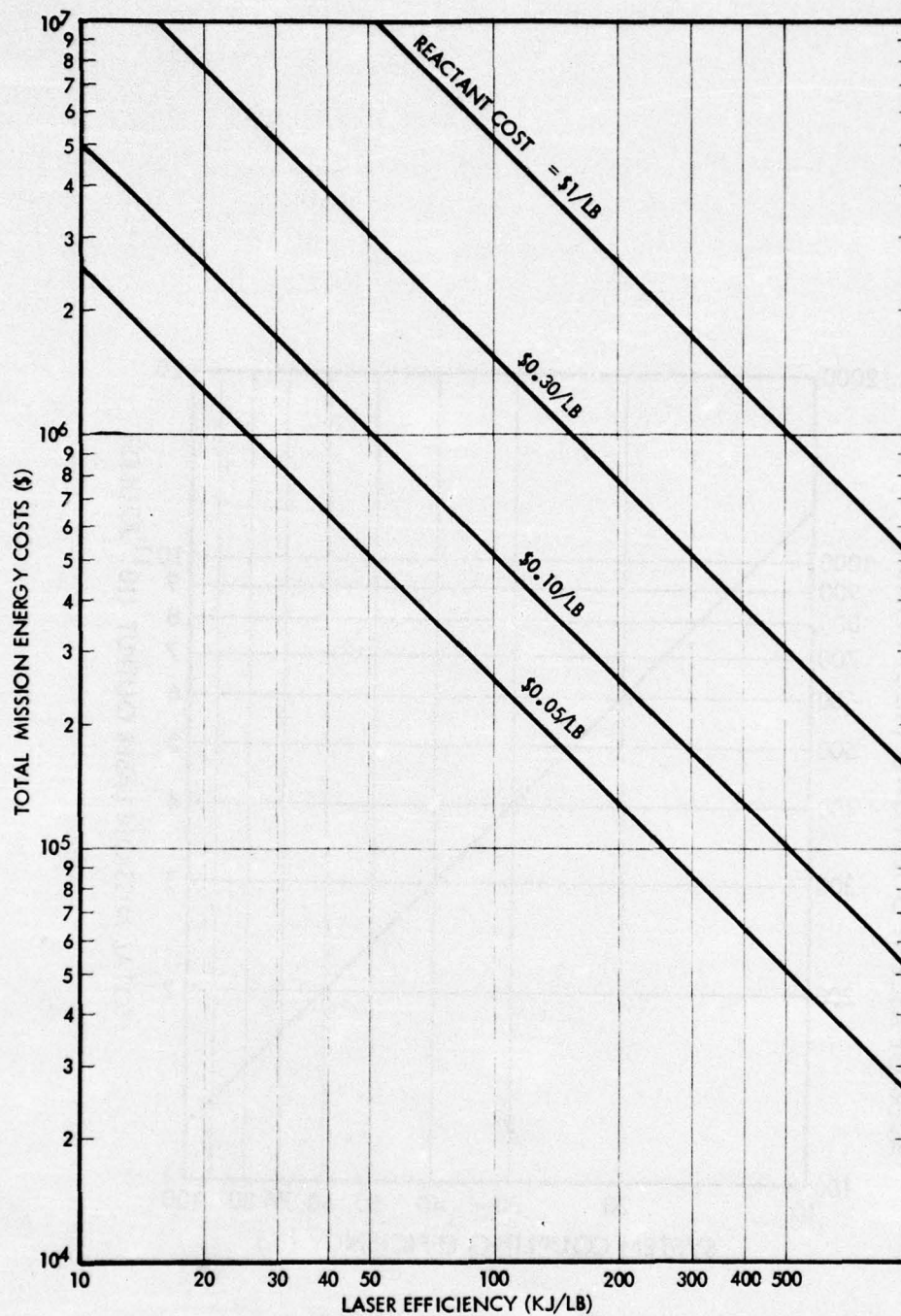


Figure 9. Total Mission Energy Cost as a Function of Reactant Cost and Efficiency for 24.5% Laser Propagation and Coupling Efficiency (5.06×10^{11} Joules Total Laser Output).

and a heat capacity of 0.2 cal/gm/°K (800 joules/Kg/OK) the temperature rise during a 50 second pulse would be 348°K. This may be tolerable. However, further specific design analysis will be required before the possible requirement for additional heat transfer hardware can be ruled out.

The smallest, and hence most critical, reflecting component to receive the full beam is the concentrator. Since the concentrator orientation is fixed relative to the spacecraft and propulsion unit, the most straightforward solution would be to route incoming propellant through a concentrator heat exchanger. The first mirror is greater than three times more massive than the concentrator, and hence will have a much lower average temperature rise even though receiving a greater portion of the incident beam.

The potential exists for huge heat fluxes throughout the thruster structure. Obviously, active cooling is required. The approach taken here is to assume that incoming propellant is the coolant (i.e., regenerative heat transfer) and that practically all the laser energy exits through the exhaust gas. To achieve this in practice may require highly complex intricate thermal designs. The thermal inertia of the thruster unit itself will considerably dampen thermal transients since the thruster weighs 200 pounds as compared with a propellant mass expulsion of 280 pounds for each 50 second thrusting period. However, careful thermal integration with the remainder of the spacecraft is still a major requirement.

2.4.4 Cost Comparisons

The three main cost elements for a reusable tug are (1) recurring mission costs, (2) tug manufacturing cost, and (3) research and development costs. This section discusses the major cost differentials between the LPT and ACT.

2.4.4.1 Recurring Costs Per Mission

The major recurring costs are (1) shuttle transport, (2) tug refurbishment and maintenance, and (3) reactant and energy costs. Amortized manufacturing and R&D costs will be treated separately.

The major transport cost is the shuttle launch to orbit. The cost to the Air Force for carrying 65,000 pounds to parking orbit has been quoted as being \$15.2 million⁽²⁾, which averages out to \$233/pound for ascent, resulting in a \$1,404,000 launch cost advantage for the LPT over the ACT.

A future shuttle launch cost escalation of \$10.8 million would result in an additional \$1 million dollar cost advantage for the LPT. This assumes that weight, not volume, is the limiting cost analysis factor. It should be noted, however, that the LPT will fill approximately 900 ft³ greater volume than the ACT as a result of its greater hydrogen tankage requirement. The laser collection and coupling will also take up additional volume within the cargo bay. Because of their sizes these elements will have to be stowed disassembled and then assembled in space. The 6.3 m diameter of the 31 m² circular concentrator exceeds the inner diameter of the shuttle bay. The first mirror length of approximately 19 meters exceeds the length of the shuttle bay.

The heavier burn out weight of the LPT (by 847 pounds) results in a corresponding weight disadvantage for the shuttle trip back to earth. No simple charge formulas for return trips have yet been developed. Current NASA thinking^(3,4) is to provide a free ride back if it can be scheduled into a normal return flight, i.e., no extra flight required. This however, neglects the cost impact of extra fuel that must be carried by the shuttle to handle the increased return mission weight. To the extent that the latter cost is ultimately passed on to the user it will decrease the round trip cost advantage to the heavier burn out weight of the LPT.

The longer mission duration for the LPT should not significantly affect retrieval costs. The 7-day round trip duration for the ACT would make it possible in principle to return on the same shuttle flight. However, since approximately 60 shuttle flights per year are anticipated, LPT return scheduling on succeeding flights should be no problem provided that the cargo bays are suitably standardized. If the return flight must carry additional interface hardware on the way up, there would be a cost impact.

2.4.4.2 Propellant and Energy Costs

Table 4 shows the propellant costs per mission figured on a basis of 3¢/pound for LO₂ and 40¢/pound for LH₂. APS propellant and fuel cell reactant cost differentials are negligible in comparison with propellant costs. As can be seen from Table 4 there is a \$1413 cost advantage for the ACT due to the lower cost of oxygen compared to hydrogen.

Table 4
Tug Propellant Costs per Mission

	LPT	ACT
LH ₂	\$2550	\$788
LO ₂	---	349
Total	\$2550	\$1137

The energy costs at 2-1/2¢/KWH and 30% conversion efficiency are \$11.7K per mission based on early 1976 industrial electric costs. This number is small enough so that a factor of 10 increase due to lower efficiency or higher energy costs will not seriously affect the major mission cost comparisons. For reactant powered lasers, a reactant cost of \$0.05/lb, would result in a mission reactant cost of from \$100K to \$1M depending on the laser efficiency (see Figure 9).

Ground station operation and maintenance will be of the order of \$1 million per year. This can either be amortized over perhaps 10 flights per year or completely charged to other functions that the station performs. The latter consideration follows from the fact that the primary impetus for developing high power laser systems will probably be for either weapons or other energy transmission applications, with the propulsion function serving as an add-on capability. The present study assumes that the ground station costs will be borne by non-propulsive commitments.

There is not sufficient information to assess tug refurbishment and maintenance costs between flights. For the purposes of this study refurbishment and maintenance costs per flight will be assumed to be 10% of the initial tug cost; \$4.04M and \$3.17M for the LPT and ACT respectively.

2.4.4.3 Fabrication Costs

At the present level of definition insufficient information is available to fully cost each competing tug concept to the accuracy required for meaningful R&D and fabrication cost differentials. However, weight cost comparisons have been derived from the use of the SAMSO Unmanned Spacecraft Cost model, adjusted for inflation, complexity and technology. The resultant numbers were then compared and averaged on an approximate dollar per pound

basis with two current spacecraft projects; the Defense Support Program spacecraft and the FLTSATCOM Space Vehicle. The resultant recurring production costs average out to \$9,500 per pound of dry weight, which translates to \$40.4 million for the LPT and 31.7M for the ACT. The cost differential is \$8.7M per tug, or \$174K/mission based on a 50 mission life.

Overall spacecraft R&D costs can run 2 or 3 times the recurring manufacturing cost. Assuming a total buy of the order of 4 to 6 tugs, DDT&E will add an additional 50% (\$87K) differential to the effective tug amortization cost per mission. These considerations would apply to typical spacecraft related development programs. In addition, the LPT requires development of a fundamentally new propulsion technology prior to initiation of a specific engine development. The overall complexity is roughly equivalent to that of ion propulsion, which has cost of the order of \$100M to develop to its present status. Assuming a similar cost amortized over 200 missions for the LPT would add an additional \$500K/mission. Adapting the technology to other applications would greatly decrease the per mission allocation. For the present exercise it is assumed that other applications effect a factor of 2 decrease to \$250K/mission in amortized DDT&E costs.

2.4.4.4 Cost Differential

The various cost elements are summarized in Table 5. It can be seen that the LPT has a potential cost advantage of \$800K/mission. Furthermore, future escalation of shuttle launch costs could add another \$1 million to the LPT cost advantage. Figure 10 shows the LPT cost advantage as a function of shuttle launch cost.

Table 5

Per Mission Cost Differential of LPT Compared to ACT (76 dollars)

	<u>Millions of Dollars</u>
Shuttle Transport to Orbit	- \$1.404 ^a
Reactants	+ 0.001
Energy	+ 0.012
Ground Station Maintenance	b
Tug Refurbishment and Maintenance	+ 0.870
Tug Production Costs	+ 0.174
Spacecraft R&D	+ 0.087
Laser Propulsion Technology R&D	+ 0.250 ^c
Total Cost Differential	- 0.010 ^a

a - Future escalation of shuttle costs could result in an additional \$1M/mission advantage for the LPT

b - \$1,000,000/year costs assumed to be amortized by non-propulsive commitments

c - \$100M R&D costs amortized over 400 missions (includes applications other than tug)

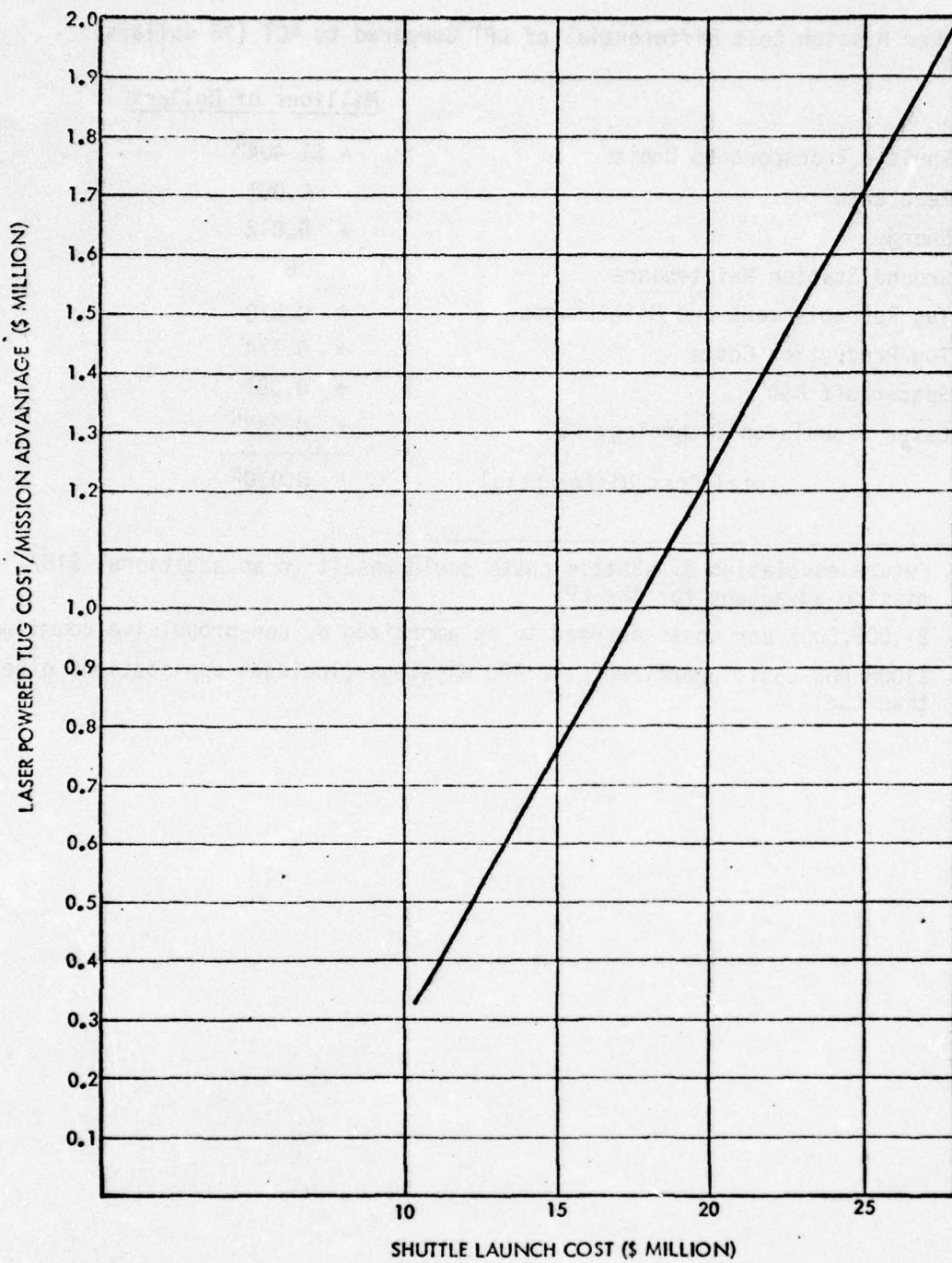


Figure 10. Cost Advantage Per Mission As a Function of Shuttle Launch Cost.

2.5 SUMMARY

Both space based and land based transmitters have been initially considered for beamed laser propulsion systems. For space based reactant powered lasers, the calculations showed that the required reactant weights will always exceed the propellant weight savings for the target vehicle. Consequently, to be cost effective, a space based laser would require either nuclear or solar space power sources in the megawatt range. Since no such sources are currently under development it has been concluded that the earliest opportunities for laser propulsion reside with ground based transmitters.

For ground based transmitters laser range considerations indicate that beam transmission periods should be limited to approximately $\pm 2^\circ$ of orbital arc centered around azimuth. For a 100 nautical mile altitude satellite this corresponds to a 50 second burn time.

Based upon the above considerations three missions were determined to be feasible for beamed laser propulsion applications. These were; 1) apsidal rotation and/or nodal regression correction; 2) drag make-up and 3) a reusable tug for orbit raising to synchronous altitude. The first two missions can be performed with a 10 megawatt laser while orbit raising will require of the order of 500 megawatts.

For apsidal rotation or nodal regression 8,000 pounds of laser powered space storable 800 second specific impulse propellant will perform a mission that would otherwise require 93,600 pounds of conventional 220 second hydrazine. For drag make-up, a 10 megawatt laser power system can produce a propellant weight saving of approximately 7,500 pounds per year.

Significant weight advantages exist for the laser powered tug as compared to an advanced cryogenic propellant powered tug. Thus a significant reduction in the cost of shuttle transport to orbit can be afforded. However these cost advantages tend to be cancelled out by other costs associated with the laser powered system.

For any of the mission concepts studied energy costs can be quite significant for reactant powered lasers. The energy costs will not be a significant factor for closed cycle lasers which employ available central station power.

3. MISSION REQUIREMENTS

The main motivation for beamed energy is to provide a means of providing higher than conventional specific impulses in order to achieve corresponding propellant weight savings. One of the first tasks required for the program was to identify mission requirements which would potentially offer the greatest propellant weight savings and hence the greatest opportunity for cost effective application of the beamed energy concept.

The initial mission requirements work emphasized space based transmitter concepts in order to maximize the available target view time, thus allowing longer energy transmission intervals and correspondingly lower average power levels for a given total energy requirement. This strategy could potentially avoid having to develop special ultra-high power laser systems solely for propulsion applications. Later on in the program it became apparent that reactant powered space based laser systems would require space transport of excessive quantities of reactants. Thus, to be effective, space based transmitters would require the development of megawatt nuclear or solar power sources. Since ground based transmitter concepts have no such requirement, they would be expected to be cost effective at an earlier implementation date.

The discussion that follows relates mainly to the space based transmitter concept. However, the results can be easily modified to apply to ground based transmitter concepts as required. The main correction required would be to recalculate the available thrusting periods for ground based transmitting geometries. The power requirements would then be scaled accordingly.

3.1 PROBABLE AIR FORCE MISSIONS

The probable Air Force missions fall into two categories; missions within the earth's dense atmosphere and geocentric space missions. The probable atmospheric missions consist of:

- Aircraft take off and landing
- Aircraft rapid climb to altitude
- Aircraft cruise

- Air to air missile
- Air to earth missile
- Earth to earth ballistic missile.

The probable space missions are:

- Earth launch to low parking orbit
- Communications, navigation, and reconnaissance, geocentric circular and eccentric orbits.
- Repositioning in synchronous orbit
- Maintaining orbit position

The geocentric circular orbits include synchronous altitude at 19,323 NM, medium altitude of 11,000 NM, and low altitudes of 600 and 450 NM. The eccentric geocentric orbits include those as high as 21,000 NM apogee with 100 to 300 NM perigees. Lower eccentric orbits at altitudes of 600 x 250 and 300 x 74 are also possible.

Synchronous orbit repositioning can be required with or without plane change. The repositioning requirement could be for survivability against attack, replacement of a malfunctioning satellite, or inspection of another vehicle.

Maintaining orbit position includes:

- Stationkeeping
- Drag make-up
- Nodal regression
- Apsidal rotation

Stationkeeping requires removing the perturbations that result in drift in East-West, North-South and Radial directions. These perturbing forces are secular, long term; and diurnal, daily.

3.2 VELOCITY INCREMENT DETERMINATION

The velocity increments were established by calculation, use of references, and previously prepared curves. For the geocentric orbits, equations were derived for changing altitude and circularization of the orbits. These derivations are shown in Appendix A.

3.2.1 Atmospheric Mission Velocity Increment Determination

Velocity increments for the atmospheric missions involving aircraft takeoff, landing or rapid climb to altitude, were calculated by assuming a representative final velocity and providing a velocity increment band that would encompass the generation of the needed velocity and overcome the associated drag.

A velocity of about 150 miles per hour is assumed as the final velocity needed to complete a take-off maneuver. A change in speed from about 150 to about 1000 miles per hour and the associated climb to altitude constitute the next maneuver. It follows that 200-400 ft/sec encompass a reasonable range for take off and 1000 to 2000 ft/sec for climb to altitude.

Air to air missiles accelerate to about 3000 miles per hour which requires a velocity increment of 4000 to 8000 ft/sec. The velocity increments for ballistic missiles are listed in the TRW Space Data Book, third edition, page 69. They are:

IRBM, 1000 NM range, 12,230 ft/sec

ICBM, 5000 NM range, 22,610

ICBM, 10,000 NM range, 25,350

For the earth launch to 100 NM parking orbit, NASA TMX2510 by Rom, Franke, and Putre, calculate the required velocity increment as 30,000 ft/sec including drag losses and an assumed average gravity constant of 0.8g.

3.2.2 Geocentric Circular Orbit Velocity Increment

The velocity increments for circular orbit raising from a shuttle parking orbit of 100 nautical miles are shown in Figure 11 which plots data given in the TRW space log, third edition, page 32. Use of the curve results in the following values:

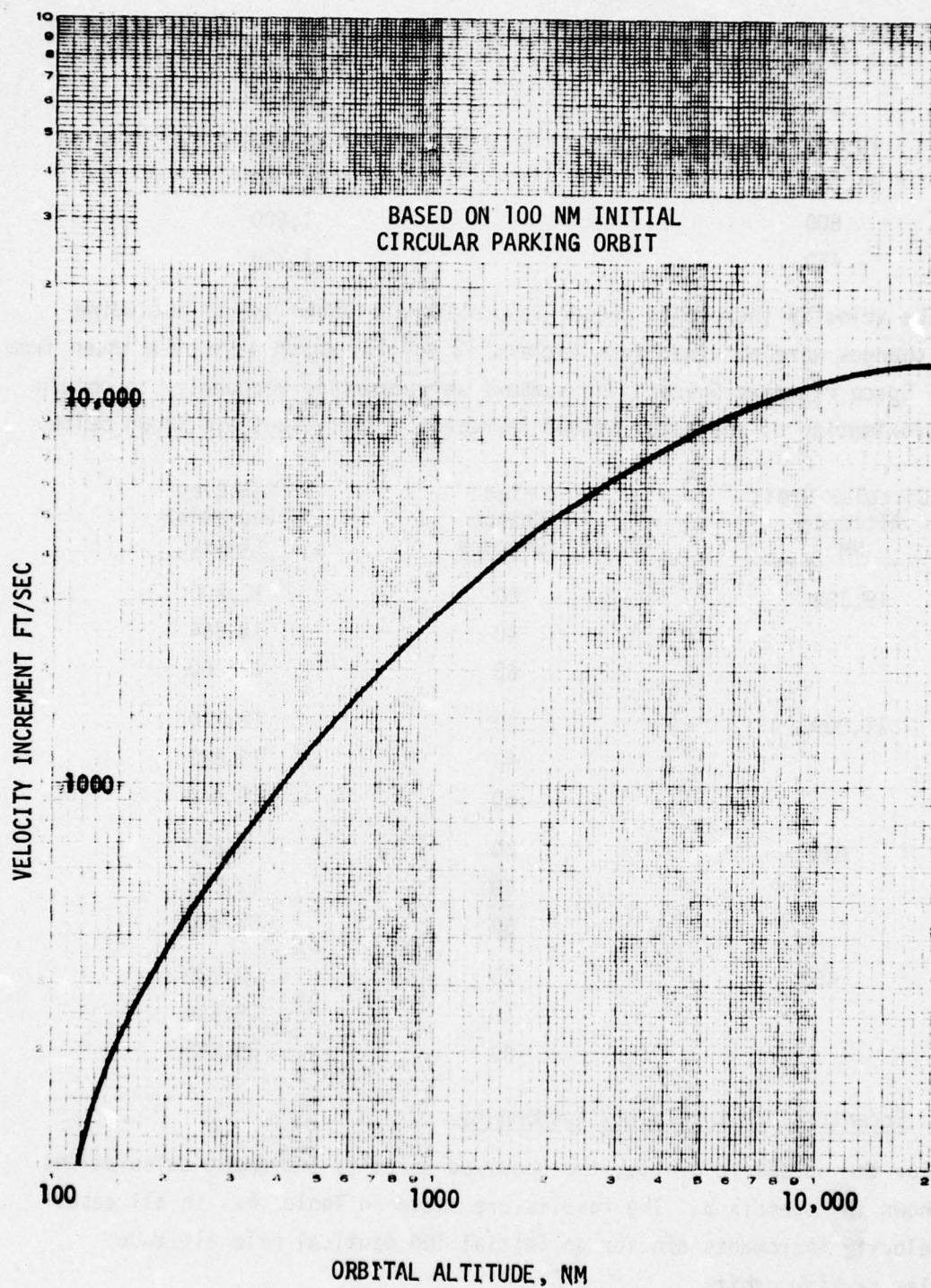


Figure 11. Velocity Increment to Achieve Circular Orbit

<u>Circular Orbit Altitude, NM</u>	<u>Velocity Increment ft/sec</u>
19,323 (synchronous)	13,000
11,000	12,000
600	1,600
450	1,200

The velocity increments needed to provide the above orbits including plane changes were obtained from Figures 12 and 13, which have been taken from the AF Space Planners Guide. The numbers were combined vectorally to obtain an approximation of the total needed increment. The values are shown below.

<u>Circular Orbit Altitude NM</u>	<u>Plane Change Degrees</u>	<u>Velocity Increment ft/sec</u>
19,323	20	13,600
	40	15,264
	60	17,060
11,000	20	12,170
	40	13,890
	60	18,440
600	20	8,650
	40	17,075
	60	25,550
450	20	8,830
	40	17,540
	60	26,280

3.2.3 Eccentric Orbit Velocity Increments

For the eccentric orbits, the required velocity increment calculations are shown in Appendix B. The results are shown in Table 6. In all cases the velocity increments are for an initial 100 nautical mile altitude circular parking orbit.

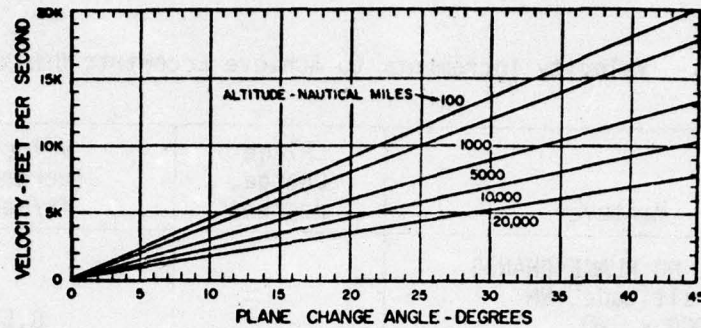


Figure 12. Plane Change Velocity
for Circular Orbits

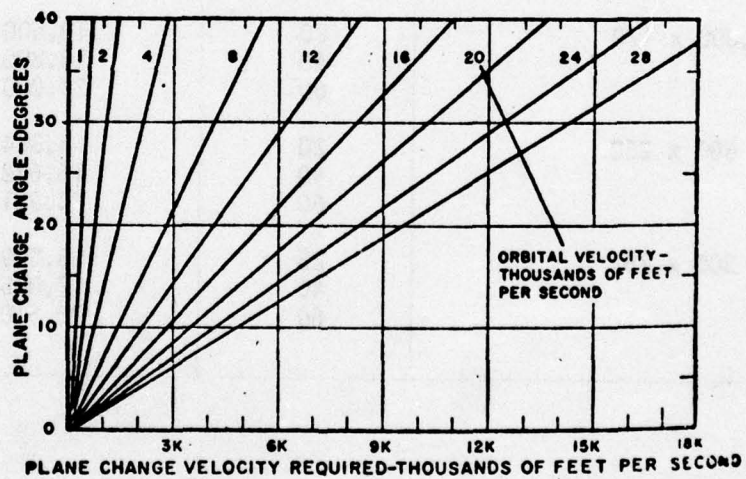


Figure 13. Performance for Any
Plane Change

Table 6. Velocity Increments to Achieve Eccentric Orbits

Maneuver	Plane Change, degrees	Velocity Increment, ft/sec
ECCENTRIC, NO PLANE CHANGE		
Orbital altitude, NM		
21,000 x 300		8,516
21,000 x 170		8,607
600 x 250		1,032
300 x 75		705
ECCENTRIC WITH PLANE CHANGE		
Orbital altitude, NM		
21,000 x 300	20	10,400
	40	14,700
	60	19,900
21,000 x 170	20	10,500
	40	14,800
	60	21,000
600 x 250	20	8,364
	40	16,632
	60	24,921
300 x 75	20	8,529
	40	17,005
	60	25,510

3.2.4 Repositioning in Synchronous Orbit Velocity Increment Determination

The repositioning velocity increment for a synchronous orbit is as follows:

$$\Delta V = 18.7 \frac{\theta}{t_{\theta}}$$

TRW I.O.C., G. S. Stern
to Meissinger 3431.5-240
dtd 2 Nov 1986

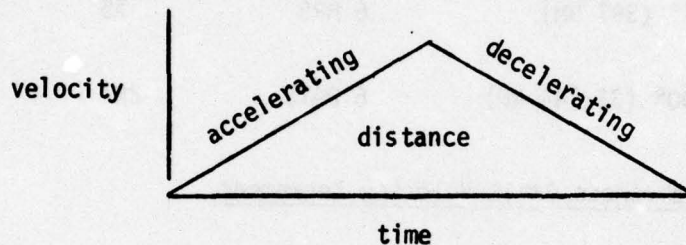
where

ΔV = velocity increment, ft/sec needed to reposition for impulsive maneuver

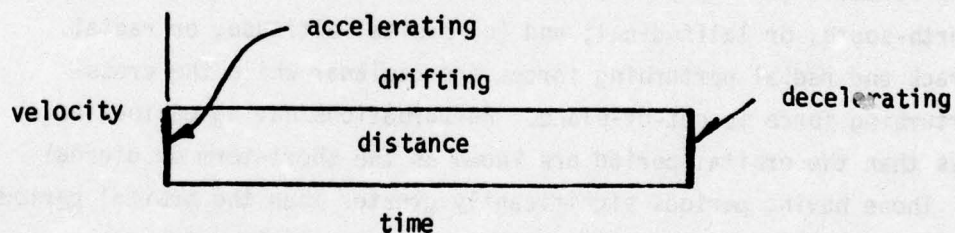
θ = repositioning angle, deg

t_{θ} = time for repositioning maneuver, days

For continuous maneuver or constant thrusting



For impulsive maneuver or instantaneous thrust



The areas under the curves, velocity x time = distance must be the same because the distance to be traveled, θ^0 is the same. If the areas are equal, then the height of the triangle must be twice the height of the rectangle. Therefore continuous thrusting requires twice the final velocity (or starting from rest, twice the ΔV) that is required for impulsive thrusting during a repositioning maneuver.

Figure 14 is a plot of the impulsive thrusting maneuver for repositioning. Since the ΔV for an impulsive maneuver is one-half that required for continuous, the figure can be utilized for continuous maneuvers as well.

For survival against satellite attack in synchronous orbit there will be about 6 hours warning time. The distance required to insure survival is about 450 miles or 1 degree. Maneuvering 1 degree requires about 75 ft/sec for an impulsive burn as shown in Figure 14.

Repositioning of a communication satellite by 90° to replace a degraded vehicle, might involve a 6 day maneuver which requires 281 ft/sec. To summarize, typical repositioning velocity increments are:

<u>Mission</u>	<u>Repositioning Angle, deg</u>	<u>Repositioning Time</u>	<u>ΔV ft/sec</u>
Satellite survival	1° (397 NM)	6 HRS	75
Degraded Satellite replacement	90° (35,744 NM)	6 DAYS	281

3.2.5 Stationkeeping in Synchronous Orbit Velocity Increment Determination

Stationkeeping in synchronous orbit involves corrections for three perturbing forces: (a) in-track, east-west, or longitudinal; (b) cross-track, north-south, or latitudinal; and (c) orbital altitude, or radial. The in-track and radial perturbing forces are coplanar while the cross-track perturbing force is out-of-plane. Perturbations having periods equal to or less than the orbital period are known as the short-term or diurnal effects. Those having periods significantly greater than the orbital period (in other words on the order of a month or more) are the long-term or secular effects. The short term effects, which cause diurnal variations in the satellite's unperturbed orbit, are on the average of 4 or more times greater than the long-term or secular effects. These effects result in in-lane position drifts and an out-of-plane widening inclination build-up which cause the satellite to inhabit an ever widening space relative to the earth. In most missions, correcting the secular perturbing forces will provide the needed satellite orbital position accuracy. However,

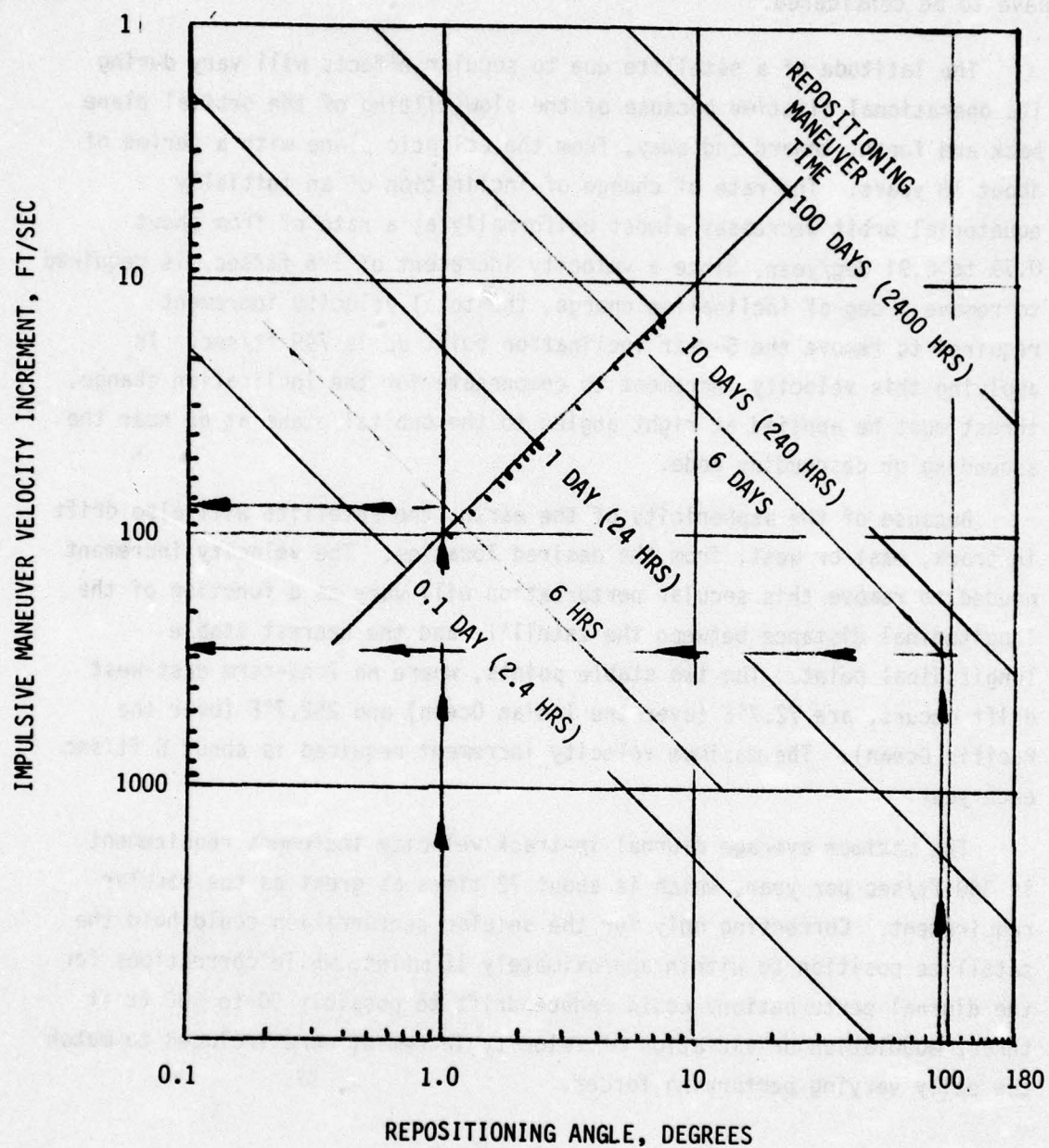


Figure 14. Synchronous Orbit Velocity Increments for Repositioning

for precise navigational satellites, particularly when attempts are made to reduce user equipment to a minimum, the diurnal perturbations may have to be considered.

The latitude of a satellite due to secular effects will vary during its operational lifetime because of the slow tilting of the orbital plane back and forth, toward and away, from the ecliptic plane with a period of about 18 years. The rate of change of inclination of an initially equatorial orbit decreases almost uniformly at a rate of from about 0.79 to 0.91 deg/year. Since a velocity increment of 176 ft/sec. is required to remove 1 deg of inclination change, the total velocity increment required to remove the 5-year inclination built up is 749 ft/sec. In applying this velocity increment to compensate for the inclination change, thrust must be applied at right angles to the orbital plane at or near the ascending or descending node.

Because of the asphericity of the earth, the satellite will also drift in track, east or west, from the desired location. The velocity increment needed to remove this secular perturbation will vary as a function of the longitudinal distance between the satellite and the nearest stable longitudinal point. The two stable points, where no long-term east-west drift occurs, are 72.7°E (over the Indian Ocean) and 252.7°E (over the Pacific Ocean). The maximum velocity increment required is about 5 ft/sec each year.

The maximum average diurnal in-track velocity increment requirement is 360 ft/sec per year, which is about 72 times as great as the secular requirement. Correcting only for the secular perturbation could hold the satellite position to within approximately 15 miles, while corrections for the diurnal perturbations could reduce drift to possibly 50 to 100 ft if thrust modulation or variation of velocity increment were included to match the daily varying perturbing forces.

The radial motion or drift in orbit is caused by the earth-moon effect exerting forces similar to those causing tidal motion on earth. The result of this perturbation is an oscillating in-plane drift about the orbital track. In general east-west drift implies first an inplane radial displacement which causes the satellite orbital period to be other than synchronous. Correcting this radial in plane displacement also eliminates the east-west perturbation. Therefore, in correcting the radial displacement perturbations, east-west drift is also corrected. In other words these two perturbations are always interrelated.

Table 7 summarizes the required velocity increments.

Table 7. Stationkeeping Velocity Increment Requirements

Perturbation	Velocity Increment			
	Diurnal		Secular	
	per/yr	per/day	per/yr	per/2 weeks
East-west	360	0.99	5	inconsequential
North-south	197	0.54	150	5.75
Radial	393	1.08	---	

The values are presented per two weeks for the secular forces because that is the usual period that drift is allowed to accumulate (about 15 miles) before a correction is made. The diurnal corrections require daily corrections.

3.2.6 Drag Make-Up Velocity Increment Determination

Low altitude missions have, in general, spanned a rather narrow band of altitudes. The orbital altitudes are constrained by drag limitations and their effect on orbital lifetime for the lower altitudes and by radiation hazards or the sensor resolution limitations for the higher ones. Once the orbit altitude and inclination have been selected, perturbing forces must be contended with in order to retain the selected flight path.

The major influence on the lower orbits is the density of the atmosphere and the resultant drag it imparts to the satellite. Figure 15

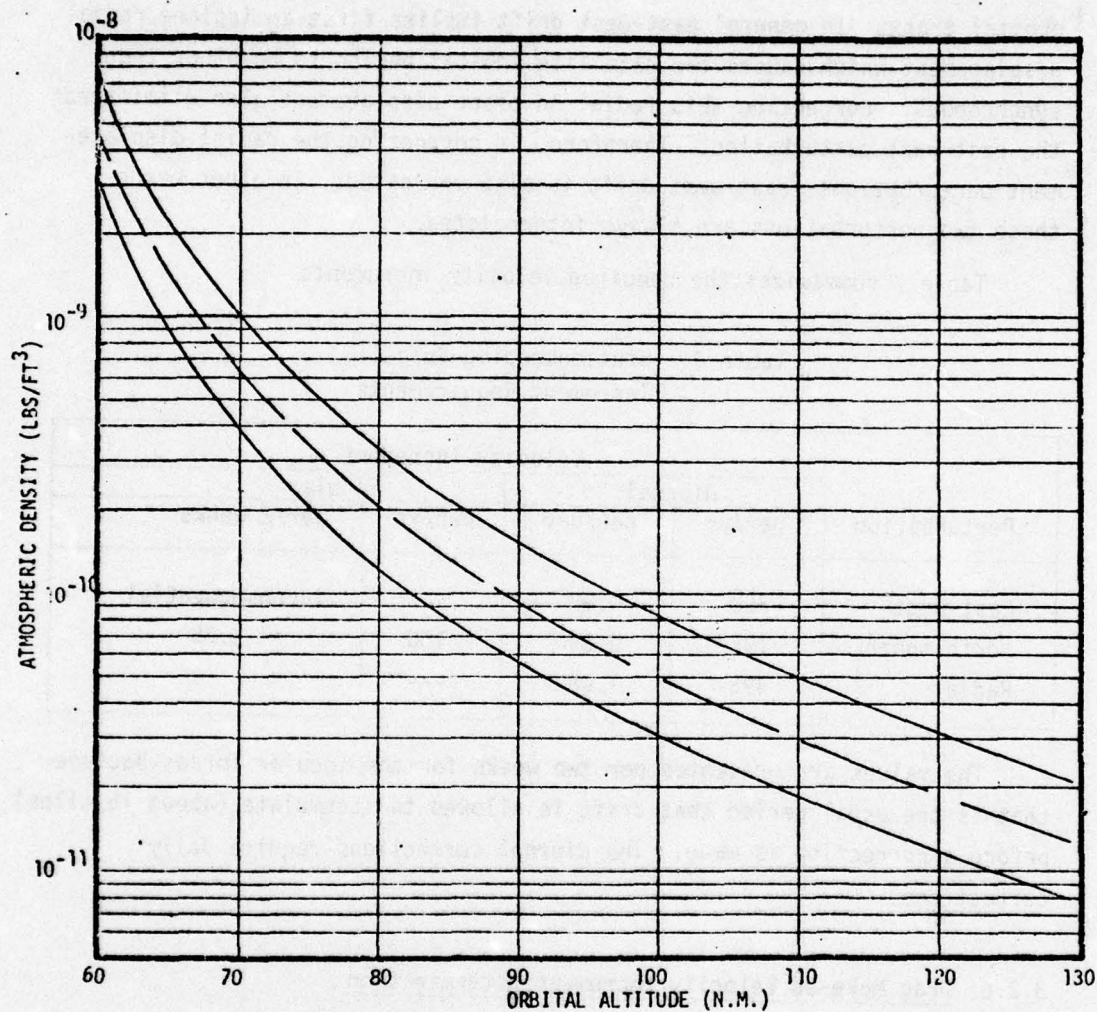


Figure 15. Atmospheric Density

illustrates the nominal atmospheric density band that encompasses four models. They are the ARDC 1959, COESA 1962 and COESA January and July 1966. The lower limit reflects the ARDC 1959 model while the upper limit reflects the COESA January 1966 values.

The drag (D) imparted to the satellite by the atmospheric density, is: $D = C_D A_p V^2/2$, where A is the projected frontal area and V is the spacecraft velocity. The $pV^2/2$ term is the dynamic pressure while C_D is the drag coefficient which is a function of the Reynolds number.

Figure 16 illustrates the nominal variation of C_D with altitude. As seen from the equation, the nominal drag on the spacecraft will vary depending on the orbital altitude. The satellite orbital velocity will vary with altitude as will the atmospheric density and drag coefficient. The only constant term will be the projected frontal area of the spacecraft.

Figure 17 illustrates the nominal drag resulting from using the mid-point atmospheric density values of Figure 15 and the C_D values from Figure 16. The values given are nominal values. There is a considerable variation of these values which include both secular (long term) and diurnal (short term) effects. These variations are caused by solar heating changes. The variation in solar energy causes changes in the atmospheric density. Increases in solar absorption cause atmospheric molecules at lower altitudes to move upward to higher altitudes. This increases the density at higher altitudes and can result in a net reduction of density at the lower levels.

The secular variations occur over about an 11 year cycle. They will be minimum in 1974-75 and peak in 1978-79. The density variations, and therefore the resultant drag forces, can increase as much as 10 to 20 percent at 70 NM, 200 to 300 percent at 200 NM and up to 1000 percent at 500 NM orbital altitude.

The diurnal variations, which involve the sunlight side versus the dark side of the earth, involve changes of about 10-20 percent at 70 NM, 60 to 70 percent at 200 NM and 300 percent at 500 NM. The change is so much greater at the very high altitudes because at very low densities the increased number of molecules have a very pronounced effect.

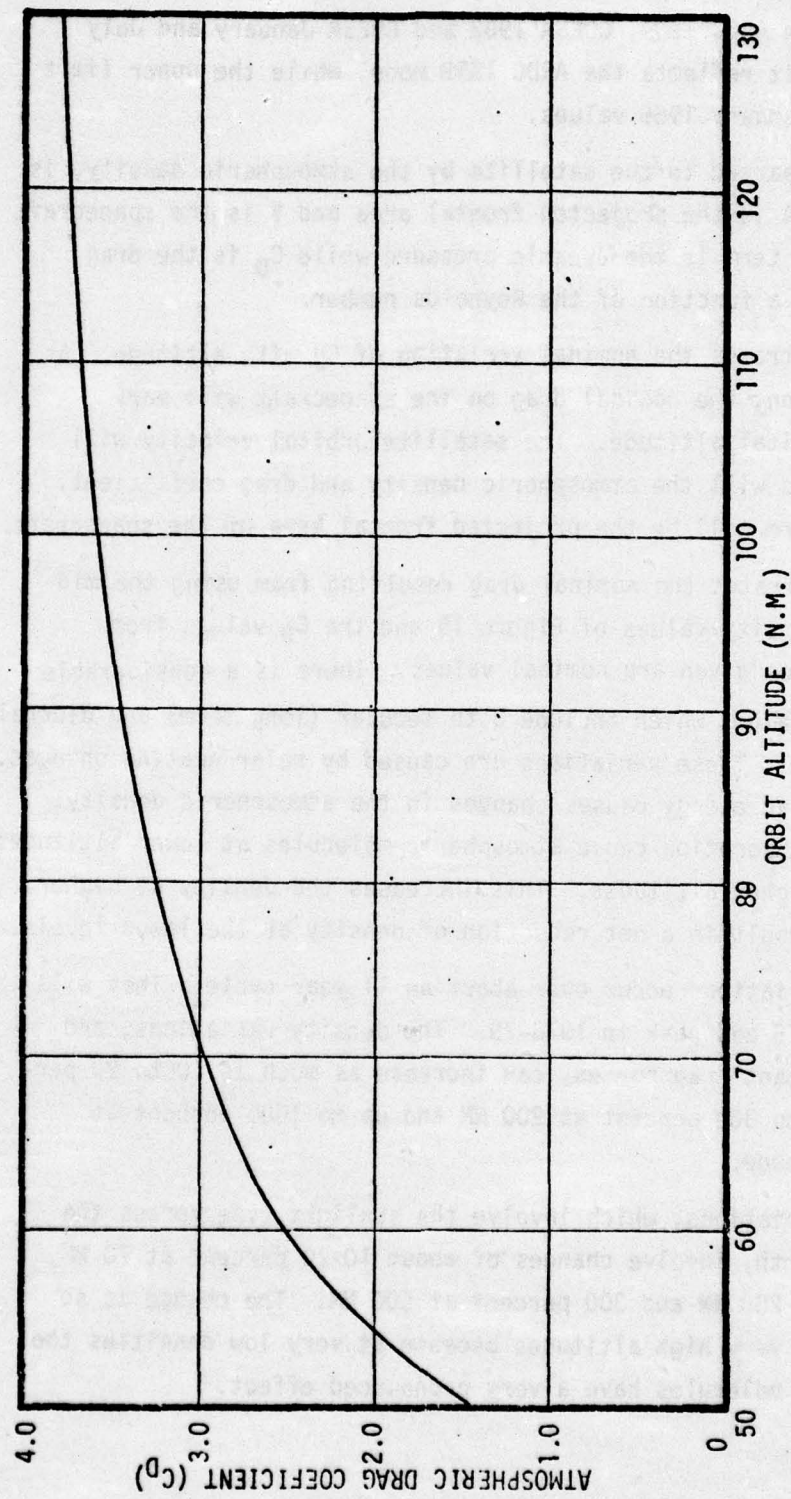


Figure 16. Drag Coefficient

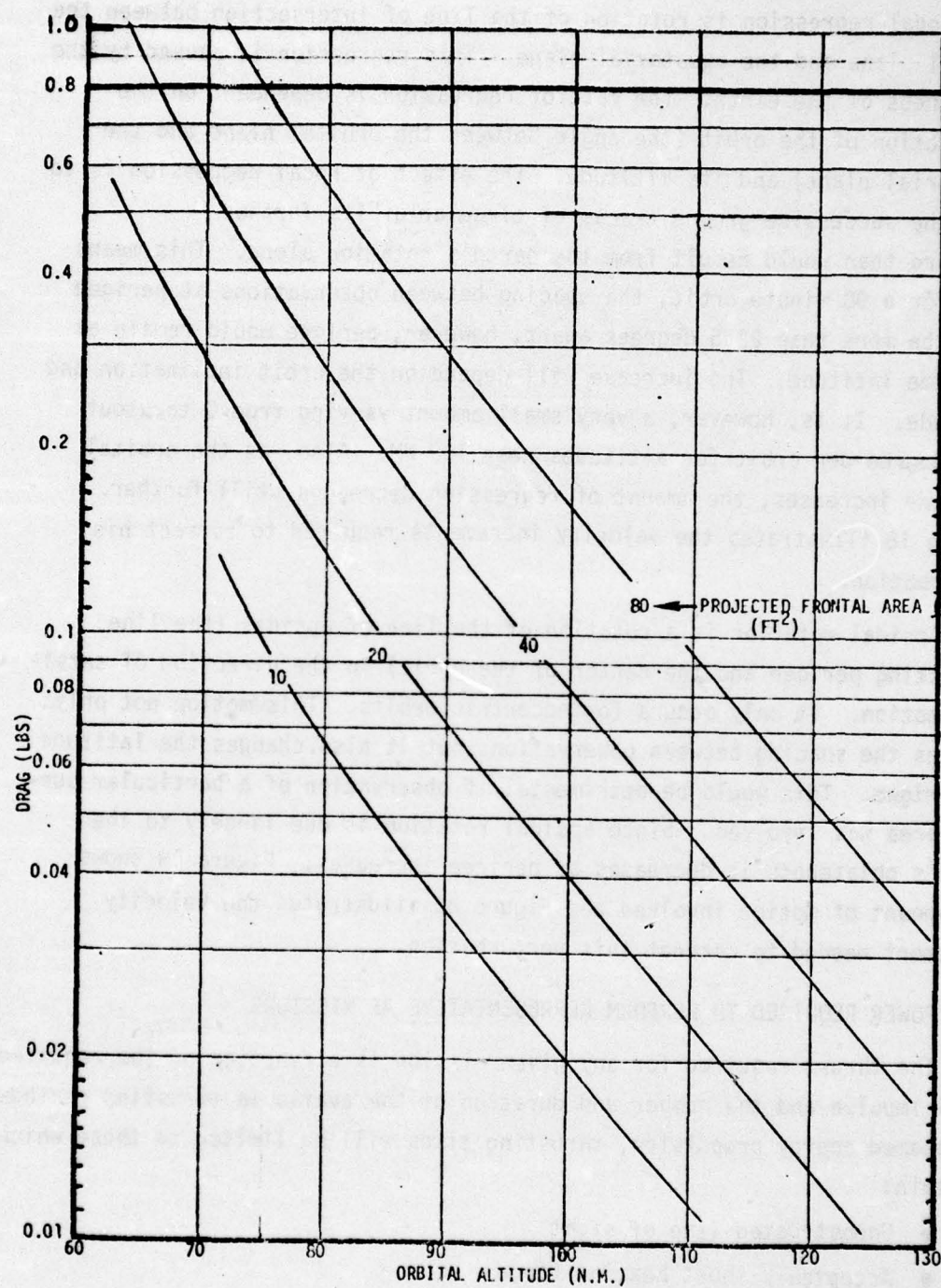


Figure 17. Drag

3.2.7 Nodal Regression and Apsidal Rotation Velocity Increment Determination

Nodal regression is rotation of the line of intersection between the orbital plane and the equatorial plane. This regression is caused by the oblateness of the earth. The rate of regression is dependent on the inclination of the orbit (the angle between the orbital plane and the equatorial plane) and its altitude. The effect of nodal regression is to make the successive ground tracks of circular orbits further westward than would result from the earth's rotation alone. This means that for a 90 minute orbit, the spacing between observations at perigee would be more than 22.5 degrees apart, however, perigee would remain at the same latitude. The increase will depend on the orbit inclination and altitude. It is, however, a very small amount varying from 0 to about 0.57 degree per orbit for altitudes near 100 NM. Also, as the orbital altitude increases, the amount of regression decreases still further. Figure 18 illustrates the velocity increments required to correct his perturbation.

Apsidal rotation is a rotation of the line of apsides (the line connecting perigee and the center of the orbit) in the direction of satellite motion. It only occurs for eccentric orbits. This motion not only changes the spacing between observations but it also changes the latitude of perigee. This would be detrimental if observation of a particular surface area was involved. Since apsidal rotation is due largely to the earth's oblateness it decreases as perigee increases. Figure 19 shows the amount of motion involved and Figure 20 illustrates the velocity increment needed to correct this perturbation.

3.3 POWER REQUIRED TO PERFORM REPRESENTATIVE AF MISSIONS

The thrust required for any given mission is a function of the required total impulse and the number and duration of the available thrusting periods. For beamed energy propulsion, thrusting times will be limited to those which maintain:

- Unobstructed line of sight
- Acceptably short beaming range
- Adequate orbital thrust efficiency
- Adequate view angle above horizon (for ground based transmitters)

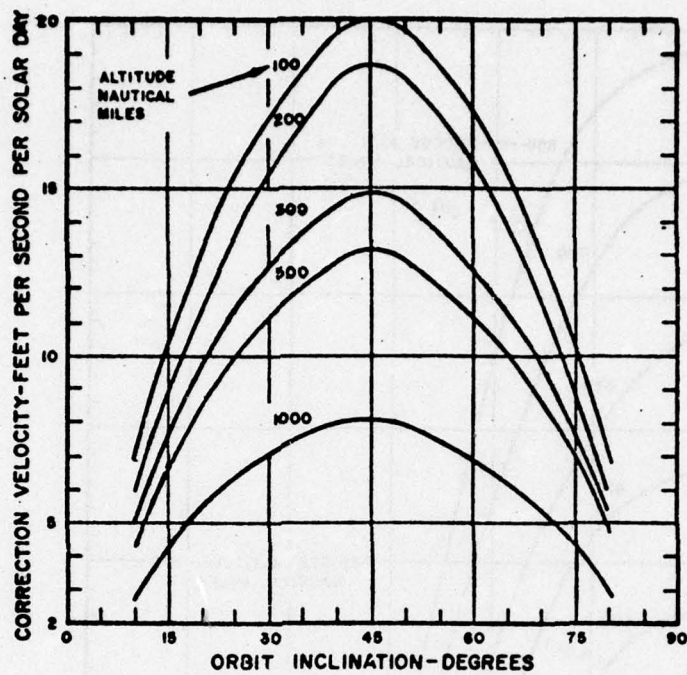


Figure 18. Nodal Regression ΔV

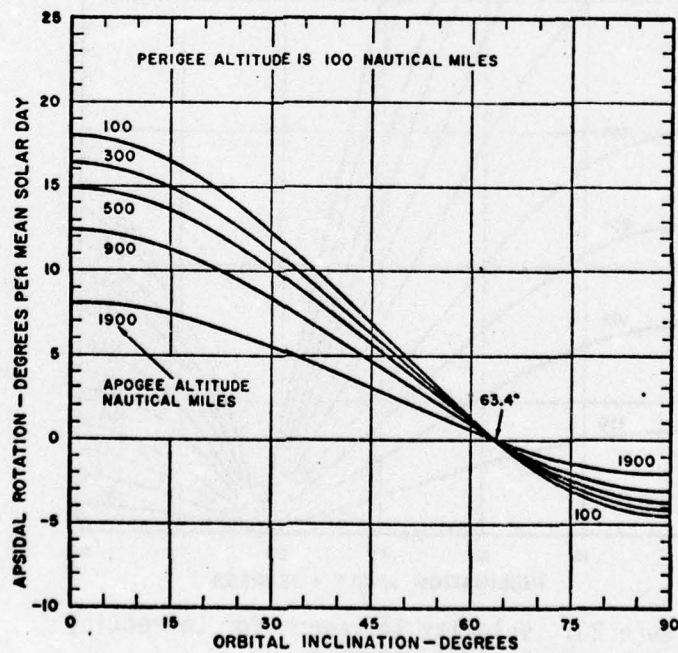


Figure 19. Apsidal Rotation Rate

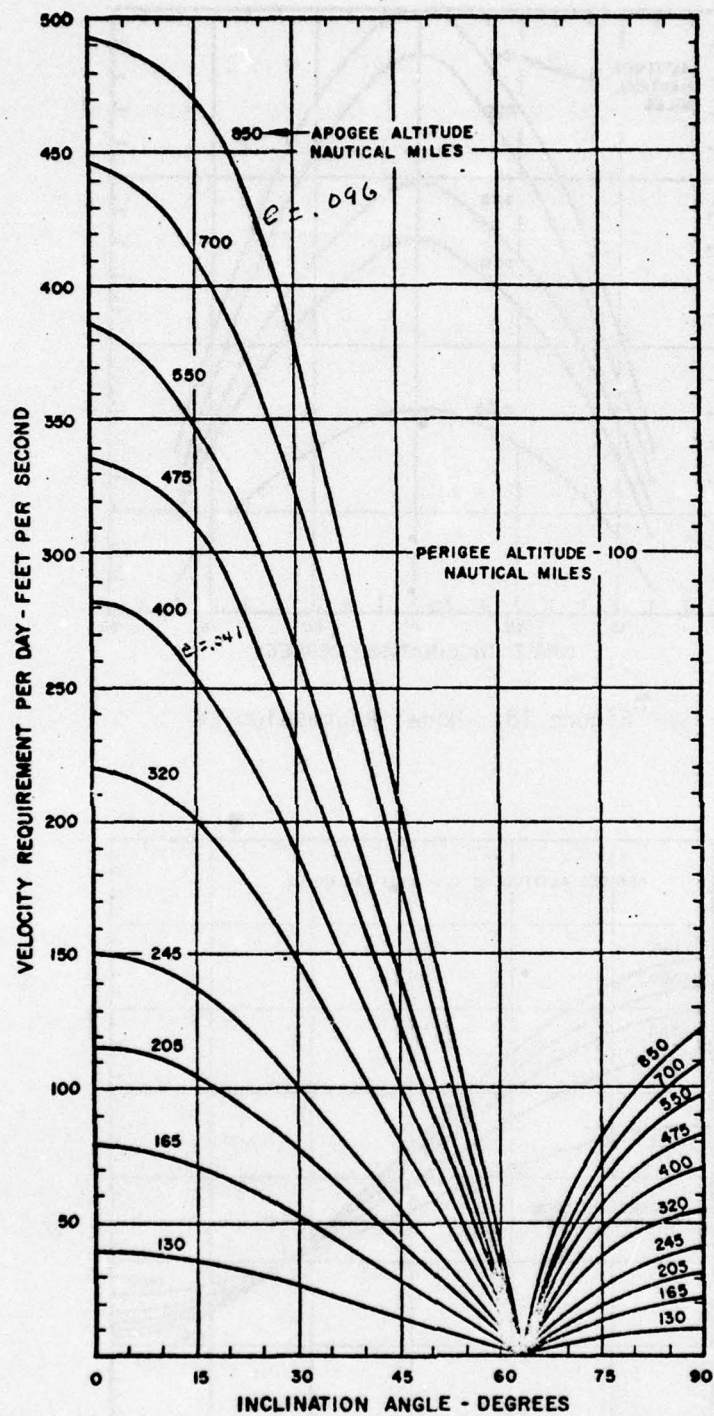


Figure 20. Velocity Increment for Correcting
Apsidal Rotation

Once the thrust level is known, the required power is easily calculated from:

$$P = F I_{sp} g / 2k\eta_R$$

where

P = power

$$g = 32.2 \text{ ft/sec}^2$$

F = Rocket thrust (lbs)

$$k = 737.6 \text{ ft lbs/sec/kw}$$

I_{sp} = specific impulse (seconds)

η_R = rocket efficiency* (ratio of ideal thruster power to collected laser power)

for power at the rocket, P_R , in kw while assuming η_R of 0.5 for rocket efficiency:

$$P_R = \frac{F I_{sp} g}{737.6} \text{ kw, or } 0.0437 F I_{sp}, \text{ kw}$$

In terms of S/C weight and needed velocity increment, assuming,
 $F = W\Delta V/gt$,

$$P_R = \frac{W\Delta V I_{sp}}{t \times 737.6}, \text{ kw for } \eta_R = 0.5$$

where

W = S/C weight, lbs

ΔV = velocity increment, ft/sec

t = firing time, sec

*The rocket efficiency factor includes all efficiency factors imposed by the spacecraft in converting incident power into propulsive power. This definition includes heat recovery due to the use of incoming propellant as a coolant.

If we assume 10% laser beam generating efficiency, 70% propagation efficiency and 80% optics train efficiency then the power required by the power generating plant, P_G , is:

$$P_G = P_R / 0.1 \times 0.8 \times 0.7 = P_R / 0.056$$

The beam output power, P_B , is then:

$$P_B = P_R / 0.08 \times 0.07 = P_R / 0.56$$

3.3.1 Power Required for Space Missions

This section applies the previous considerations to calculating the power requirements for various typical maneuvers for a 4,000 pound average weight satellite.

3.3.1.1 Power for Ground Launch to Orbit

A launch vehicle with a 200,000 lb thrust (Atlas Centaur class) with a beam powered propulsion system having a specific impulse of 1000 sec would require power of:

$$\begin{aligned} P_R &= 0.0437 \times 200,000 \times 1000 = 8.7 \text{ GW, } P_R \text{ (Power delivered to rocket)} \\ &= 155 \text{ GW, } P_G \text{ (Power supplied by generating plant)} \\ &= 15.5 \text{ GW, } P_B \text{ (Laser beam power)} \end{aligned}$$

3.3.1.2 Power for Circular Orbit Transfer

Included are circular orbit transfer with and without plane change.

Power for Circular Orbit Transfer without Plane Change. The power needed at the rocket, P_R , for a circular orbit transfer, assuming a spacecraft weight of 4000 lbs including payload, propulsion and inerts, a specific impulse of 1000 sec, and a 1000 second firing period is:

$$P_R = \frac{4000 \times \Delta V \times 1000}{1000 \times 737.6} = 5.42 \Delta V, \text{ KW}$$

$$P_G = P_R / 0.056, \text{ KW, } P_B = P_R / 0.56, \text{ KW}$$

The power for circular orbits with and without plane changes when transferring from a 100 NM parking orbit are shown in Tables 8 and 9.

Table 8. Power for Circular Orbit Without Plane Change

Final Orbit Altitude NM	ΔV ft/sec	Power, MW		
		P_R	P_B	P_G
19,323	13,000	70	126	1,258
11,000	12,000	65	116	1,161
600	1,600	8.7	15.5	155
450	1,200	6.5	11.6	116

Table 9. Power for Circular Orbits With Plane Change*

Final Orbit Altitude NM	Plane Change, (deg)	ΔV ft/sec	Power, MW		
			P_R	P_B	P_G
19,323	20	13,600	74	132	1316
	40	15,260	83	148	1477
	60	17,060	92	165	1651
11,000	20	12,170	66	118	1178
	40	13,890	75	134	1344
	60	18,400	100	179	1785
600	20	8,830	48	86	855
	40	17,540	95	170	1698
	60	26,280	142	254	2544

3.3.1.3 Power for Eccentric Orbits

Tables 10 and 11 show the power for eccentric orbits with and without plane change, assuming 4000 lb S/C, 1000 sec I_{sp} and firing time of 1000 sec and 100 NM initial parking orbit.

Table 10. Power for Eccentric Orbit Without Plane Change

Final Orbit NM	ΔV ft/sec	Power, MW		
		P_R	P_B	P_G
21,000 x 300	8516	46	82	824
21,000 x 170	8607	47	83	833
600 x 250	1032	5.6	10	99.9
300 x 75	705	3.8	6.8	68.2

*Based on 4000 lb S/C, 1000 sec I_{sp} and firing time of 1000 sec.

Table 11. Power for Eccentric Orbits With Plane Change

Final Orbital Altitude NM	Plane Change (deg)	ΔV ft/sec	Power, MW		
			P_R	P_B	P_G
21,000 x 300	20	10,400	56	101	1007
	40	14,700	80	142	1423
	60	19,900	108	193	1926
21,000 x 170	20	10,500	57	102	1016
	40	14,800	80	143	1432
	60	21,000	114	203	2033
600 x 250	20	8,364	45	81	810
	40	16,632	90	161	1610
	60	24,921	135	241	2412
300 x 75	20	8,529	46	83	825
	40	17,005	92	165	1646
	60	25,510	138	247	2469

3.3.1.4 Power for Repositioning in Synchronous Orbit

The power for the 2 nominal cases where ΔV was previously defined, i.e., for an assumed 1° movement in 6 hrs for satellite survival against attack, and a 90° satellite reposition in 6 days to repair a degenerating satellite; the power requirements are shown in Table 12.

Table 12. Power for Repositioning in Synchronous Orbit

Mission	Repositioning Angle, degrees	Repositioning Time	ΔV ft/sec	Power, MW		
				P_R	P_B	P_G
Satellite Survival	1° (400 NM)	6 Hrs	75	0.41	0.7	7.3
Degraded Satellite Replacement	90°	6 Days	281	1.5	0.3	27.2

3.3.1.5 Drag Make-Up Required Power

For a 75 mile orbit, the drag for an 80 ft^2 frontal area vehicle is about 1 lb. The power required at the rocket would be

$$P_R = 0.0437 F I_{sp} \text{ KW}$$

The resultant power requirements are shown in Table 13. It is assumed here that thrusting directly counteracts the drag on a one-to-one basis. The power requirements can scale dramatically if only a limited segment of orbital arc and not every orbital period is available for thrusting.

Table 13. 1 lb Drag Make-Up Power

Orbital Altitude NM	Frontal Area ft ²	Drag Force, lb	Power, MW		
			P _R	P _B	P _G
75	80	1	0.043	0.08	0.77

3.3.1.6 Power for Changing Altitude from a Parking Orbit

Changing altitude from a parking orbit normally involves applying a velocity increment at the perigee of the desired transfer ellipse. The allowable firing time will depend on the losses that can be tolerated during the maneuver. The losses include gravity, pointing and altitude. A conservative estimate of the allowable firing arc before thrust efficiency is excessively degraded is 40 degrees centered around perigee. On the other hand, the maximum arc before the range to a 100 nm altitude from a fixed ground station is doubled is approximately $\pm 2^\circ$ (4° total). Most of the following is calculated for a 40° arc. Thus the calculated power levels must then be multiplied by 10 for a ground based transmitter.

At 100 NM parking orbit, the vehicle velocity is 25,560 ft/sec (4.2 NM/sec). The arc distance per degree at 100 NM is 22,256.3 NM circumference/360° or 61.82 NM. Therefore the time to span that distance is 61.82/4.2 or 14.72 sec per degree. For 40° it would be 589 sec. Table 14 lists the available time for 100, 200 and 300 NM orbits.

Table 14. Firing Time Available for 40° Arc

Parking Orbit, NM	Circular Velocity		Circumference of Orbit, NM	NM per Degree	Available time for 40° arc, sec
	ft/sec	NM/sec			
100	25,560	4.20	22,256.3	61.82	589
200	25,213	4.15	22,859.2	63.50	612
300	24,874	4.09	23,487.2	65.24	638

To transfer to synchronous orbital altitude, requires 8128 ft/sec. The rocket power required to accomplish this maneuver, assuming a 50% rocket efficiency with a specific impulse of 1000 sec in 589 sec for a 4000 lb average weight vehicle is:

$$P_R = \frac{W \Delta V I_{sp}}{t \times 737600} = \frac{(4 \times 10^3) (8128) (1000)}{589 \times 737600} \text{ Megawatts}$$

$$P_R = 74.84 \text{ MW}$$

Required beam power would be $P_R / .56$ of 133.63 MW assuming 70% propagation efficiency, and 80% optics train efficiency. For a 10% laser generating efficiency it would require a power input of 1336.3 MW or 1.34 GW.

A means for reducing these required power levels would be to accomplish the transfer to altitude maneuver in smaller discrete steps. If the laser beam generating device were, for instance, in a 100 NM circular orbit, then it could provide an energy impulse to the vehicle each time the vehicle and the beam generating station were in close proximity.

For instance, if the first altitude raising transfer orbit had a period of exactly twice the 100 NM parking orbit, then the beam generating station after traversing two revolutions would again encounter the vehicle and another energy increment could be imparted to raise the transfer ellipse once more. Again if the new ellipse had a period of exactly 3 times the 100 NM orbital period, the vehicle would be available for still another energy input after 3 revolutions of the beam generating station. This

could be continued until the desired orbital altitude was reached where the circularization maneuver could be accomplished if desired. Figure 21 illustrates this concept.

The arrangement in Figure 21 allows a beamed energy transfer everytime the vehicle passes perigee. Transfer orbit harmonics of 1.5, 2, 2.5, 3, etc. would increase the number of available transfer orbits but would result in some passing of perigee without being in conjunction with the laser beam generating plant.

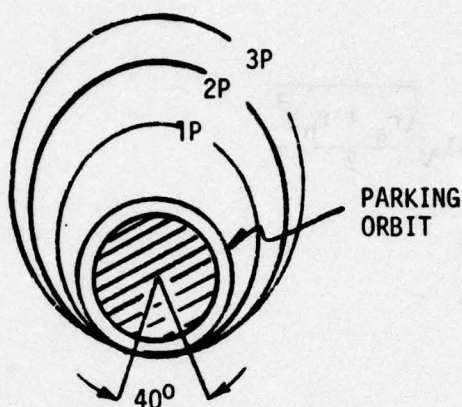


Figure 21. Orbit Transfer Concept

The transfer ellipse orbital altitude is a function of integer increments of the parking orbit period. Periods are shown for several parking orbital altitudes in Table 15.

Table 15. Orbital Periods

Parking Orbital Altitude, NM	Period			
	Days	Hrs	Min	Sec
100	0.06125	1.47	88.2	5292
200	0.06316	1.53	91.8	5508
300	0.06651	1.60	96.0	5760

Now the orbital period of a transfer ellipse, τ , is:

$$\tau = \sqrt{\frac{4\pi^2 a^3}{u}}$$

where

$$a = \frac{r_a + r_p}{2}$$

and $u = 62628 \text{ NM}^3/\text{sec}^2$

Then:

$$\tau_{\text{sec}} = .0251 \sqrt{\frac{(r_a + r_p)^3}{2}}$$

now $r_a = h_a + r$

and $r_p = h_p + r$

where:

h_a = altitude to apoapsis, NM

h_p = altitude to periapsis, NM

r = earth radius, NM

then

$$\tau_{\text{sec}} = .0251 \sqrt{\left(\frac{h_a + h_p + 2r}{2}\right)^3}$$

For a perigee of 100 NM altitude, the period, τ , for an eccentric orbit is:

$$\tau_{\text{sec}} = .0251 \sqrt{\left(\frac{h_a + 6988}{2}\right)^3}$$

$$\tau_{\text{sec}}^{2/3} = .0251^{2/3} \left(\frac{h_a + 6988}{2}\right)$$

$$\tau^{2/3} = .0857 \left(\frac{h_a + 6988}{2}\right) = .04286 (h_a + 6988)$$

$$\tau^{2/3} = .04286 h_a + 299.5$$

Then the altitude at apogee, h_a , for a 100 NM perigee is:

$$h_a = \frac{\tau^{2/3} - 299.5}{.04286} \text{ for 100 NM perigee}$$

where:

h_a = altitude at apogee in NM

τ = orbital period of eccentric orbit in sec

and

$h_a = (\tau^{2/3} - 303.8)/.04286$ for 200 NM perigee

$h_a = (\tau^{2/3} - 308.1)/.04286$ for 300 NM perigee

Table 16 lists the apogee altitudes for each transfer ellipse with a multiple of the parking orbit.

Table 16. Apogee Altitudes of Transfer Ellipses

Parking Orbital Altitude NM	Parking Orbital Period sec	Number of Parking Orbit Periods	Eccentric Orbit Period, τ , sec	$\tau^{2/3}$	$\tau^{2/3} - 299.5$	Altitude at Apogee, h_a NM	Orbit Identification Number
100	5292	2	10584	482	182.5	4258	1
		3	15876	632	332.5	7758	2
		4	21168	765	465.5	10861	3
		5	26460	888	588.5	13731	4
		6	31752	1003	703.5	16414	5
200	5508				$\tau^{2/3} - 303.8$		
		2	11016	495	191.2	4461	6
		3	16524	649	345.2	8054	7
		4	22032	786	482.2	11251	8
		5	27540	912	608.2	14190	9
300	5760	6	33048	1030	726.2	16943	10
					$\tau^{2/3} - 308.1$		
		2	11520	510	201.9	4711	11
		3	17280	668	359.9	8397	12
		4	23040	810	501.9	11710	13
		5	28800	940	631.9	14743	14
		6	34560	1061	752.9	17566	15

The velocity at perigee for each eccentric transfer ellipse will determine the time available for beam on-time when the laser and the vehicle are in conjunction. The velocity at perigee is:

$$V_p = V_{c_1} \sqrt{\frac{2n}{n+1}}$$

where:

V_{c_1} = velocity of parking orbit

$$n = R_a/R_p$$

and

R_a = radius from center of earth to altitude at apogee

R_p = same for perigee

also

$$R_a = h_a + r \text{ and}$$

$$R_p = h_p + r$$

where

h_a = altitude of apogee

h_p = altitude of perigee

r = earth radius

The velocities at perigee for the apogee altitudes determined in Table 16 are shown in Table 17.

Table 17. Velocity at Perigee

Orbit Identification Number	Altitude, NM		Radius, NM		R_a/R_p n	$\frac{\sqrt{2n}}{\sqrt{n+1}}$	Velocity at Perigee, V_p	
	Apogee, h_a	Perigee, h_p	Apogee, R_a	Perigee, R_p			ft/sec	NM/sec
For 100 NM Parking Orbit with circ. vel., $V_{ci} = 25,560$ ft/sec, 4.2040 NM/sec								
1	4258	100	7702	3544	2.1733	1.1703	29,914	4.9201
2	7758	100	11202	3544	3.1608	1.2326	31,506	5.1818
3	10861	100	14305	3544	4.0364	1.2661	32,369	5.3224
4	13731	100	17175	3544	4.8462	1.2876	32,911	5.4130
5	16414	100	19858	3544	5.6033	1.3027	33,298	5.4766
For 200 NM Parking Orbit with circ. vel., $V_{ci} = 25,213$ ft/sec, 4.1469 NM/sec								
6	4461	200	7905	3644	2.1693	1.1700	29,500	4.8520
7	8054	200	11498	3644	3.1553	1.2324	31,071	5.1104
8	11251	200	14695	3644	4.0327	1.2659	31,918	5.2497
9	14190	200	17634	3644	4.8392	1.2874	32,460	5.3388
10	16943	200	20387	3644	5.5947	1.3026	32,842	5.4016
For 300 NM Parking Orbit with circ. vel., $V_{ci} = 24,874$ ft/sec, 4.0911 NM/sec								
11	4711	300	8155	3744	2.1781	1.1708	29,122	4.7898
12	8397	300	11841	3744	3.1627	1.2327	30,662	5.0431
13	11710	300	15154	3744	4.0475	1.2664	31,501	5.1811
14	14743	300	18187	3744	4.8576	1.2879	32,034	5.2688
15	17566	300	21010	3744	5.6116	1.3029	32,408	5.3303

The time available for performing the perigee orbit raising maneuver will depend on the vehicle speed at perigee, the allowable firing arc in degrees, and the orbit altitude. Table 18 presents the allowable beam on-times for a 40° arc at perigee.

Table 18. Allowable Beam On-Times

Orbit Identification Number (See Table 17)	Altitude, NM		Velocity at Perigee, V_p , NM/sec	NM per Degree at Perigee	Available Beam On-Time at Perigee, sec	
	Apogee, h_a	Perigee, h_p			Per Degree	Per 40° arc
1	4258	100	4.9201	61.82	12.56	502.6
2	7758	100	5.1818	61.82	11.93	477.2
3	10861	100	5.3224	61.82	11.62	464.6
4	13731	100	5.4130	61.82	11.42	456.8
5	16414	100	5.4766	61.82	11.29	451.52
6	4461	200	4.8520	63.50	13.09	523.5
7	8054	200	5.1104	63.50	12.43	497.0
8	11251	200	5.2497	63.50	12.10	483.8
9	14190	200	5.3388	63.50	11.89	475.8
10	16943	200	5.4016	63.50	11.76	470.23
11	4711	300	4.7898	65.24	13.62	544.8
12	8397	300	5.0431	65.24	12.94	517.5
13	11710	300	5.1811	65.24	12.59	503.7
14	14743	300	5.2688	65.24	12.38	495.3
15	17566	300	5.3303	65.24	12.40	489.6

The velocity increments needed to achieve each incremental transfer orbit can be determined from Table 17 by subtracting each prior velocity at perigee from the subsequent one. For instance at 100 NM parking orbit, the velocity at the selected perigee point is the circular orbit velocity of 25,560 ft/sec. The velocity needed to achieve the first selected transfer orbit, no. 1, with a period of twice the initial circular orbit is 29,914 ft/sec. The difference is $29,914 - 25,560 = 4353$ ft/sec.

Table 19 lists the needed velocity increments for each transfer orbit.

Table 19. Velocity Increments for Transfer Orbits from Initial 100 NM Parking Orbit

Orbit Identification Number	Altitude at Apogee, NM		Perigee Velocity, ft/sec		Needed Velocity Increment ft/sec
	Initial	Desired	Initial	Desired	
1	100	4258	25560	29914	4354
2	4258	7758	29914	31506	1592
3	7758	10861	31506	32360	854
4	10861	13731	32360	32911	551
5	13731	16414	32911	33298	387

To achieve the 4354 ft/sec velocity increment from initial circular parking orbit in the allowable time of $61.82 \text{ NM/deg} \times 40 \text{ deg} = 4.204 \text{ NM/sec} = 588.2 \text{ sec}$ for a 40° arc at perigee would require a beam power in MW of the following, based on the previous assumptions:

$$P_B = \frac{W \Delta V I_{sp}}{t \times 737600 \times .56} = \frac{(4000) (4354) (1000)}{(588) (737600) (.56)}$$

$$P_B = 71.7 \text{ MW } (40^\circ \text{ Arc})$$

$$\text{or } P_B = 717 \text{ MW } (4^\circ \text{ Arc})$$

This can be reduced by employing additional orbits as mentioned initially in relation to the discussion of Figure 21. The result will be that the vehicle will not receive an energy boost each time it passes perigee. For instance with a transfer ellipse with a period of 1-1/2 instead of 2 as was the case for orbit no. 1 in Table 15, the vehicle will traverse two eccentric orbit revolutions while the laser generating station will traverse three revolutions in circular orbit before both meet again at perigee so that an energy transfer can again take place. For instance below are some additional candidate orbits in Table 20.

Table 20. Additional Candidate Transfer Orbits for Initial 100 NM Parking Orbit

Period in Multiples of Parking Orbit	Orbital Revolutions Before Encounter		Period sec	$\tau^{2/3}$	$\tau^{2/3} - 299.5$	Altitude at Apogee h_a , NM	Orbit Identification Letter
	Vehicle	Laser Stations					
1-1/2	2	3	7938	398	98.5	2298.18	A
1-1/3	3	4	7056	368	68.5	1598.23	B
1-1/4	4	5	6615	352	52.5	1224.92	C
1-1/5	5	6	6350	343	43.5	1014.93	D
1-1/6	6	7	6174	337	37.5	874.94	E
1-1/7	7	8	6048	332	32.5	758.28	F
1-1/8	8	9	5954	329	29.5	688.29	G
1-1/9	9	10	5880	326	26.5	618.29	H
1-1/10	10	11	5821	324	24.5	571.63	I

The velocities at perigee for these additional transfer orbits, V_p :

$$V_p = V_{ci} \sqrt{\frac{2n}{n+1}}$$

and for 100 NM circular parking orbit,

$$V_p = 25,560 \sqrt{\frac{2n}{n+1}}.$$

The perigee velocities are shown in Table 21.

Table 21. Additional Candidate Transfer Orbit Velocities at Perigee - For 100 NM Initial Parking Orbit

Orbit Identification Letter	Altitude, NM		Radius, NM		R_a/R_p	$\frac{\sqrt{2n}}{\sqrt{n+1}}$	Velocity at Perigee, V_p	
	Apogee, h_a	Perigee, h_p	Apogee, R_a	Perigee, R_p			ft/sec	NM/sec
					n			
A	2298.18	100	5742.18	3544	1.6203	1.11207	28424.4	4.6751
B	1598.23	100	5042.23	3544	1.4228	1.08373	27700.1	4.5559
C	1224.92	100	4668.92	3544	1.3174	1.06629	27254.4	4.4826
D	1014.93	100	4458.93	3544	1.2582	1.05561	26981.3	4.4377
E	874.94	100	4318.94	3544	1.2187	1.04811	26789.7	4.4062
F	758.28	100	4202.28	3544	1.1857	1.04163	26624.2	4.3790
G	688.29	100	4132.29	3544	1.1600	1.03905	26558.1	4.3681
H	618.29	100	4062.29	3544	1.1462	1.03352	26416.7	4.3449
I	571.63	100	4015.63	3544	1.1331	1.03072	26345.1	4.3331

The available firing times for each of the transfer orbits of Table 21 for a 40° arc at perigee are shown in Table 22.

Table 22. Available Beam On-Time at Perigee for Additional Candidate Transfer Orbits

Orbit Identification Letter	Velocity at Perigee, V_p , NM/sec	NM per Degree at Perigee	Available Beam On-Time at Perigee, sec	
			per Degree	per 40° arc
A	4.6751	61.82	13.22	528.93
B	4.5559	61.82	13.57	542.77
C	4.4826	61.82	13.79	551.64
D	4.4377	61.82	13.93	557.23
E	4.4062	61.82	14.03	561.21
F	4.3790	61.82	14.12	564.70
G	4.3681	61.82	14.15	566.10
H	4.3449	61.82	14.23	569.13
I	4.3331	61.82	14.27	570.68

The velocity increments needed to achieve each additional candidate incremental transfer orbit as a first step in the incremental transfer train can be determined from the data of Table 8. These results are shown in Table 23.

Table 23. Velocity Increments with Additional Candidates for 1st Transfer

Orbit Identification Letter (See Table 15)	Altitude at Apogee, NM		Perigee Velocity, ft/sec		Required Velocity Increments,	
	Initial	Final	Initial	Final	ft/sec	NM/sec
A	100	2298.18	25,560	28424.4	2864.4	0.4711
B	100	1598.23	25,560	27700.1	2556.0	0.4204
C	100	1224.92	25,560	27254.4	2140.1	0.3520
D	100	1014.93	25,560	26981.3	1421.3	0.2338
E	100	874.94	25,560	26789.7	1229.7	0.2023
F	100	758.28	25,560	26624.2	1064.2	0.1750
G	100	688.29	25,560	26558.1	998.1	0.1642
H	100	618.29	25,560	26416.7	856.7	0.1409
I	100	571.63	25,560	26345.1	785.1	0.1291

Using the I orbit as the initial transfer orbit in order to reduce maximum power levels results in a required beam power of:

$$P_B = \frac{4000 \times 785 \times 1000}{589 \times 737600 \times .56} = 12.9 \text{ MW}$$

This is close enough to the available state of the art to be a viable solution for the initial altitude transfer ellipse.

To remain near the 10 MW beam power level, assuming this power level is viable for our purposes, would allow as the second orbit around 700 ft/sec velocity increment since the times available for performing the higher orbit transfers decreases.

Orbit D (see Table 23) requires a velocity increment of 1421.3 - 785.1 = 636.2 ft/sec when applying beam power at the perigee velocity of

orbit I. The beam power required would be:

$$P_B = \frac{(4000)(636.2)(1000)}{(557.2)(7376.00)(.56)} = 11.06 \text{ MW}$$

Still close to 10 MW. Table 24 shows the sequence of transfer ellipse orbits that would keep the needed power level near 10 MW with $P_B = 9.6839 \times$ velocity increment \div by allowable beam on-time for a 4000 lb vehicle with a specific impulse of 1000 sec and transmission, collection and conversion efficiency of 0.56.

Table 24. Sequential Transfer Orbits That Have a Required Beam Power Level of About 10 MW For 100 NM Initial Parking Orbit

Orbit Identification	Altitude at Apogee, NM		Velocity at Perigee, ft/sec		Required Velocity Increment, ft/sec	Allowable Beam On-Time sec	Needed Beam Power, MW	Number of Revolutions Between Beams Turn-Ons	
	Initial	Final	Initial	Final				Vehicle	Laser Station
I	100	571.63	25560	26345.1	785.1	589	12.9	10	11
D	571.63	1014.93	26345.1	26981.3	636.2	557	11.06	5	6
B	1224.92	1598.23	26981.3	27700.1	718.8	542.77	12.8	3	4
A	1598.23	2298.18	27700.1	28424.4	723.9	528.93	13.25	2	3
requires additional intermediate orbits to keep power level around 10 MW									
1	2298.18	4258	28424.4	29714	1490	502.6	28.7	1	2
requires additional intermediate orbits to keep power level around 10 MW									
2	4258	7758	29914	31506	1592	477.2	32.3	1	3
requires additional intermediate orbits to keep power level around 10 MW									
3	7758	10861	31506	32360	854	464.6	17.8	1	4
4	10861	13731	32360	32911	551	456.8	11.7	1	5
5	13731	16414	32911	33298	387	451.5	8.3	1	6

As shown in Table 24, a series of sequential elliptical transfer orbits can be utilized to perform the orbital raising maneuver while keeping the required beam power level near 10 MW. The needed intermediate orbits as shown in Table 24 were not determined in order to save time. However, the previous orbits indicate the feasibility of doing so.

3.3.1.7 Circularization from a Raised Orbit Power

For circularization maneuver after orbit raising the vehicle would be in view of the laser generating station over almost an 180 degree arc. The time available would then be 180 degrees x 61.82 NM per degree + 4.204 NM/sec = 2646.9 sec. At synchronous altitude the circularization ΔV is about 4851 ft/sec which would require a one pass beam power level of:

$$P_B = 9.6839 \times 4851/2646.9 = 17.75 \text{ MW}$$

Two passes would reduce this to 8.87 MW.

In summary, employment of beamed propulsion for orbit raising missions, even out to synchronous altitude can be accomplished by employing incremental changes in altitude.

The number of orbits of the vehicle and the laser beam generating plant (if space based) between energy transmissions would vary per incremental elliptical altitude raising orbit. The transmission of energy between laser beam generating plant and the vehicle whose orbit altitude was being raised or lowered would only take place when both were in close proximity to the transfer orbit perigee.

3.3.1.8 Plane Change Power

Changing the plane of an orbit requires applying thrust near the ascending or descending nodal points. The thrust must be applied at right angles to the plane of the orbit in order to generate the needed momentum vector. The direction of the applied thrust and the particular nodal point at which it is utilized will determine which direction the orbital plane will move. Figure 22 illustrates the phenomena involved:

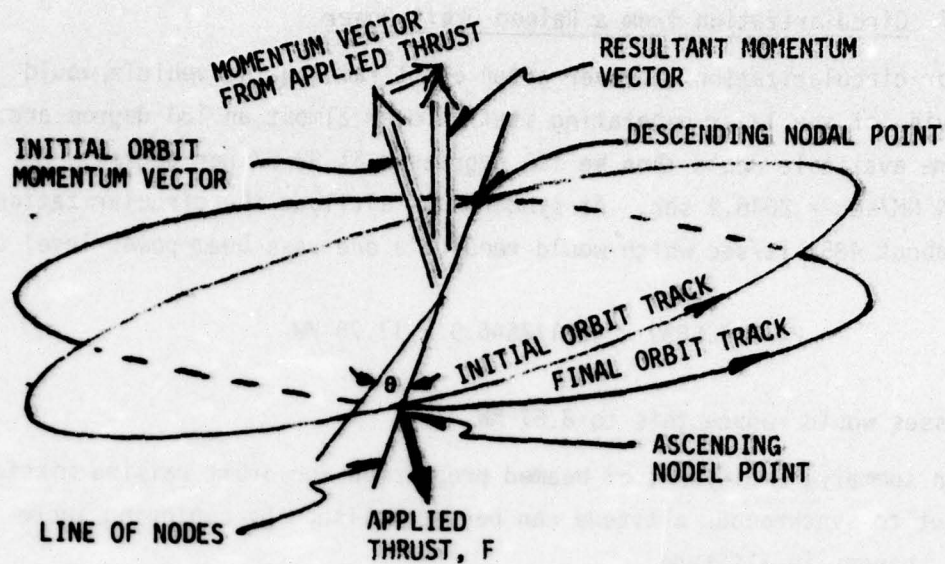


Figure 22. Plane Change Nomenclature

The greater the arc around the nodal point where thrust is applied to rotate the orbital plane, the less effective is the energy input for making the plane change. At 90 degrees from the nodal line, the application of thrust has no effect in rotating the plane about the line of nodes. The effectiveness varies with the cosine of the angular distance from the nodal point.

The average loss is $1 - \sin \theta / \theta$ and the efficiency of performing the maneuver is $\sin \theta / \theta$ where θ is the firing half arc angle at the nodal point.

Table 25 lists the efficiencies and losses as a function of nodal half angle.

Table 25. Plane Changing Thrust Application Efficiency

Nodal Point Half Angle, θ	$\sin \theta$	θ Radians	Average Efficiency, %	Average Loss %
			$\frac{\sin \theta}{\theta}$	$1 - \frac{\sin \theta}{\theta}$
10	.174	.175	99.4	0.6
20	.342	.349	98.0	2.0
30	.500	.524	95.4	4.6
40	.643	.698	92.1	7.9
50	.766	.873	87.7	12.3
60	.866	1.047	82.7	17.3
70	.940	1.222	76.9	23.1
80	.985	1.396	70.6	29.4
90	1.00	1.571	63.7	36.3

For a synchronous orbit it takes 176 ft/sec to move the orbit plane 1 degree. The time available per firing assuming an allowable average loss of about 5% could be a half angle of 30° of a 60° full arc. Transmission constraint, would of course greatly lower the permissible arc.

For a synchronous orbit it takes 176 ft/sec to move the orbit plane 1 degree. The time available per firing assuming an allowable average loss of about 5% could be a half angle of 30° or a 60° full arc.

At synchronous altitude the orbit period is 24 hrs. The time available for 60 degrees is 4 hrs, or 14,400 seconds. The beam power required for a 4000 lb S/C, with 1000 sec I_{sp} and system transmission, collection and conversion efficiency of 56% to effect a plane change of one degree is:

$$P_B = 9.6839 \times \Delta V / t_b \times \text{maneuver efficiency}$$

$$P_B = 9.6839 \times 176 / 14,400 \times .954 = .124 \text{ MW}; 124 \text{ KW}$$

Table 26 lists Beam Power for various synchronous orbit plane changes for the above conditions.

Table 26. Power for Synchronous Orbit Plane Change*

Plane Change Angle Degrees	Rocket Power MW	Beam Power MW	Laser Generating Plant Power, MW
1°	.069	.124	1.24
10°	0.69	1.24	12.4
20°	1.38	2.48	24.8
30°	2.07	3.72	37.2
40°	2.76	4.96	49.6
50°	3.45	6.20	62.0

*Based on 4000 lb vehicle with a specific impulse of 1000 sec. and 60° thrusting arc.

As can be seen from Table 26, large plane changes can be accommodated in synchronous orbit without exceeding about 10 MW of beam power.

The plane change might also be desired as the vehicle is being placed in orbit. This could be accomplished during the orbit raising firings required to attain the sequential elliptical orbit raising trajectories. The orbit plane changes can also be made incrementally at many of the nodal crossings whenever the vehicle and the laser beam generating station are in sight of each other. The required beam power levels can therefore be kept to low values, i.e., around the 10 MW level because of the great number of incremental plane change opportunities.

3.3.1.9 Nodal Regression Power Requirements

The power required to correct nodal regression, i.e., rotation of the line of intersection between the orbital plane and the equatorial plane, depends on the inclination of the orbit, its altitude, and the spacecraft weight specific impulse and firing time. The required velocity increments needed per day as a function of orbital inclination and altitude are shown in Figure 18.

In different orbital altitudes the time available to perform the maneuver would vary with altitude assuming a constant allowable 40 degree maneuver arc. Beyond 1000 NM, the correction velocity increment becomes relatively insignificant. The rocket power required for a 4000 lb vehicle with a 1000 sec specific impulse would then be:

$$P_R = \frac{4000 \times \Delta V \times 1000}{t_b \times 737600} = 5.4230 \frac{\Delta V}{t_b} \text{ MW}$$

Table 27 provides the power as a function of orbital altitude, and inclination.

Table 27. Power to Daily Correct Nodal Regression for Various Orbital Altitudes for a 4000 lb Vehicle with an $I_{sp} = 1000$ sec.

Orbital Altitude NM	Orbit Inclination degrees	Time (1) Available for Maneuver sec	Required Velocity Increment ft/sec		Power, MW		
			Per Day	Per Year	Rocket P _R	Beam(2) P _B	Generating Plant(3) P _G
100	10	589	7	2555	0.06	.11	1.1
	20	589	12	4380	0.11	.20	2.0
	30	589	17	6205	0.16	.28	2.8
	40	589	20	7300	0.18	.32	3.2
200	10	612	6	2190	0.05	0.10	1.0
	20	612	11	4015	0.10	0.17	1.7
	30	612	16	5840	0.14	0.25	2.5
	40	612	18	6570	0.16	0.28	2.8
300	10	638	5	1825	0.04	0.08	0.8
	20	638	10	3650	0.08	0.15	1.5
	30	638	13	4745	0.11	0.19	1.9
	40	638	15	5475	0.12	0.22	2.2

(1) Assumes a 40° arc

(2) Assumes propagation efficiency of 70%, optics train efficiency of 70%

(3) Assumes beam generation efficiency of 10%

3.3.1.10 Apsidal Rotation Power Requirements

The power required to combat apsidal rotation of elliptical orbits depends on the orbital altitudes, orbit inclination, spacecraft weight, specific impulse and available firing time. The required velocity increments needed per day is shown in Figure 20.

Table 28 presents the power as a function of orbital altitude and inclination, for a perigee of 100 NM.

Table 28. Power Per Day to Correct Apsidal Rotation for a 4000 lb Vehicle with a Specific Impulse of 1000 sec

Orbital Altitude NM	Orbital Inclination degrees	Time(1) Available for Maneuver sec	Required Velocity Increment ft/sec		Power Per Day, MW		
			Per Day	Per Year	Rocket P_R	Beam P_B ⁽²⁾	Generating Plant ⁽³⁾ P_G
110	10	589	10	3,650	0.09	0.16	1.6
	20	589	9	3,285	0.08	0.15	1.5
	30	589	7	8,555	0.06	0.12	1.2
	40	589	5	1,825	0.05	0.08	0.8
200	10	612	105	38,325	0.93	1.66	16.6
	20	612	90	32,850	0.80	1.42	14.2
	30	612	73	26,645	0.65	1.16	11.6
	40	612	52	18,980	0.46	0.82	8.2
300	10	638	196	71,540	1.67	3.0	30
	20	638	167	60,955	1.42	2.5	25
	30	638	134	48,910	1.14	2.0	20
	40	638	96	35,040	0.82	1.46	14.6

(1) Assumes a 40° arc

(2) Assumes propagation efficiency of 70% optics train efficiency of 70%

(3) Assumes beam generating efficiency of 10%

3.3.2 Atmospheric Missions

3.3.2.1 Power Required for Aircraft

From the American Airlines flight plan for a specific flight, the fuel consumption of a 747 is:

Climb 23,100 lbs/33 min = 42,000 lbs/hr

Cruise 65,200 lbs/3 hrs, 43 min = 17,543 lbs/hr

Takeoff estimated at 60,000 lbs/hr

Assuming the heat release on jet fuel is 19,000 BTU/lb, the thermal power or power used in the engine, P_u , required for each flight phase is given by:

$$P_u = \frac{\text{lbs/hr} \times 19,000 \text{ BTU/lb}}{3415 \text{ BTU/HR/KW}} = 5.564 \times \text{lbs/hr, KW}$$

Takeoff 333.82 MW

Climb 233.67 MW

Cruise 97.60 MW

Within the next 10 years, improved engine efficiency will reduce the fuel consumption by 1/2. The required power levels will therefore be as shown in Table 29.

Table 29. 747 Class Future Aircraft Power Requirements

Aircraft Maneuver	Power, MW		
	Used in Engine	Beam Power(2)	Input to Beam Powerplant(3)
Takeoff	167	299	2990
Climb	117	209	2090
Cruise	49	88	880

(1) Based on 70% transmission efficiency, 80% optics train efficiency

(2) Based on 10% Beam generation efficiency

AD-A034 995

TRW DEFENSE AND SPACE SYSTEMS GROUP REDONDO BEACH CALIF F/G 20/5
INVESTIGATION OF BEAMED ENERGY CONCEPTS FOR PROPULSION. SYSTEMS--ETC(U)
OCT 76 M HUBERMAN, J M SELLEN, R BENSON F04611-76-C-0003

UNCLASSIFIED

AFRPL-TR-76-66-VOL-1

NL

2 OF 3

AD
A034995



3.3.2.2 Ground Launched Vehicle Power

The power required for ground launched vehicles assuming an improvement from conventional propulsion to 1000 sec specific impulse propulsion are shown in Table 30.

Table 30. Power Required for Ground Launched Vehicles*

Vehicle Class	Thrust Level lbs	Power, Giga Watts		
		Rocket P_R	Beam P_B (1)	Beam Generation P_G (2)
Scout	100,950	4.4	7.9	79
Thor	170,000	7.4	13.2	132
Minuteman	180,000	7.9	14.1	141
Atlas	300,000	13.1	23.4	234
Titan I	400,000	17.5	31.3	313
Titan IIIC	2,400,000	105	187.5	1875
Saturn V	7,600,000	332	592.9	5929

*Based on specific impulse of 1000 sec and 50% rocket efficiency.

(1) Based on 70% propagation efficiency, 80% optics train efficiency

(2) Based on 10% beam generation efficiency.

3.3.2.3 Air to Air Missile Power

The air to air missiles encompass a wide range of thrust levels. The range of interest would be between 1000 to 10,000 lbs. Table 31 provides the power levels required for this range of thrust using the same assumptions that were used for the ground launched vehicles of Table 30.

Table 31. Power Required for Air to Air Missiles

Thrust Level, lbs	Power, MW		
	Rocket P_R	Beam P_B	Beam Generation P_G
1000	43.7	78.0	780
2000	87.4	156.1	1561
4000	174.8	312.1	3121
8000	349.6	624.3	6243
10000	437.0	780.4	7804

3.3.2.4 Power Required for Ballistic Missiles

The thrust level range for ballistic missiles are from 100,000 to 400,000. As shown in Table 30, Minuteman is 180,000 lbs thrust, Atlas, 300,000 and Titan 400,000. Table 32 indicates the power levels encompassed by this range of thrusts using the same assumptions as used in Section 3.3.2.2, Ground Launched Vehicles.

Table 32. Power Required for Ballistic Missiles

Thrust Level, lbs	Power, GW		
	Rocket P_R	Beam P_B	Beam Generation P_G
100,000	4.37	7.80	78
200,000	8.74	15.6	156
300,000	13.11	23.4	234
400,000	17.48	31.2	312

3.4 SUMMARY OF MISSION REQUIREMENTS

The beam power needed to perform the various missions depends on the thrust levels needed, and the propulsion system specific impulse. The power required is directly proportional to these parameters. For missions where thrust level is not specified, the power required will be a function of the vehicle weight velocity increment required and the time available for its application.

From a mission standpoint, the time available for applying the energy required, will depend on the mission characteristics and energy losses associated with the times involved. The power required will increase as beam on-time is decreased. The mission related energy losses however, will decrease as beam on-time is decreased. A tradeoff therefore exists between these two competing factors. For this study beam on-times were constrained to keep mission related losses compatible with past experience.

The mission characteristic that defined maximum beam on-time was, in general, the view angle between a space based laser beam generation station and the vehicle. It was assumed for instance in the orbit raising mission that the beam generation station was in low earth orbit to increase view angle, minimize transmission losses and the hazards of inadvertent interception of the high energy beam. Naturally, much shorter beam times will be available for ground based stations.

The power required for atmospheric missions considering available beam on times where applicable are shown in Table 33. Table 34 summarizes space mission requirements.

Table 33. Summary of Power for Atmospheric Missions

Atmospheric Missions	Power - Megawatts	
	Delivered To Vehicle P_R	Beam Output P_B
1. 747 Type Future Aircraft		
Take off	167	299
Climb	117	209
Cruise	49	88
2. Ground Launched Vehicles		
Scout 100,950 lb thrust	4,400	7,900
Thor 170,000 " "	7,400	13,600
Minuteman 180,000 " "	7,900	14,100
Atlas 300,000 " "	13,100	23,400
Titan I 400,000	17,500	31,300
Titan IIIC 2,400,000	105,000	187,500
Saturn V 7,600,000	332,000	592,900
3. Air to Air Missiles		
1,000 lb thrust	44	78
2,000 " "	88	156
4,000 " "	175	312
8,000 " "	350	624
10,000 " "	437	780
4. Ballistic Missiles		
100,000 lb thrust	4,370	7,800
200,000 " "	8,740	15,600
300,000	13,110	23,400
400,000	17,480	31,200

Table 34. Summary of Power for Space Missions*

Space Missions	Power - Megawatts	
	Delivered To Vehicle P_R	Beam Output P_B
1. Orbit raising (based on suitable increments)	8	13
2. Orbit circularization at synchronous (based on two increments)	5	9
3. Plane change in synchronous orbit		
10°	0.7	1.2
30°	2	3.7
50°	3.5	6.2
4. Nodal regressions (correction each ten days)		
Altitude Orbit Inclination		
NM deg.		
100 10	0.6	1.1
40	1.8	3.2
200 10	0.5	1.0
40	1.6	2.8
300 10	0.4	0.8
40	1.2	2.2
Power requirements keep decreasing with increased altitude.		

*Assumes 4,000 pound average weight vehicle, 1000 seconds specific impulse, space based transmitter and thrusting through 40° of orbital arc. For ground based transmitter multiply powers by ~ 10 .

Table 34. Summary of Power for Space Missions (Continued)

Space Missions		Power - Megawatts	
		Delivered To Vehicle P_R	Beam Output P_B
5. Apsidal rotation (correction each 10 days)			
Apogee Altitude NM (Perigee 100 NM)	Orbit Inclination deg.		
110	10	.9	1.6
	40	.5	.8
200	10	9.3	16.6
	40	4.6	8.2
300	10	16.7	30
	40	8.2	14.6
Power requirements keep increasing with increased apogee.			
6. Repositioning in synchronous orbit			
Satellite survival (1° in 6 hours)		.41	.7
Satellite replacement (90° in 6 days)		1.5	.3
7. Drag make-up			
Orbital Altitude NM	Frontal Area Ft ²		
75	80	.043	.08

*Assumes 4,000 pound average weight vehicle, 1,000 seconds specific impulse, space based transmitter and thrusting through 40° of orbital arc. For ground based transmitter multiply powers by ~10.

4. LASER GENERATING DEVICES

Beamed energy propulsion generates severe power, total energy and range requirements upon the laser system. Although significant advances in the state of the art are still needed, there are no known fundamental obstacles to the development of lasers for the required power. However, technical breakthroughs may be required to assure adequate efficiency of generation, propagation and delivery at extremely high power levels.

From a total systems viewpoint, the high power requirements would be easily met by combustion driven gas dynamic or chemical (HF or DF) lasers. From a cost effectiveness viewpoint, the high total mission energy requirements favor closed-cycle electrical energy such as would be available from central power stations. The long transmitting range required for propulsion would favor the shorter wavelength HF, DF and CO lasers in order to minimize diffraction spread. On the other hand, ground based laser transmitter concepts would benefit from the superior atmospheric propagation characteristics of the DF and CO₂ wavelengths.

In the following section the characteristics, operating efficiency limits, and state of the art of high powered laser concepts are discussed. The intent is to describe relevant characteristics rather than attempting a comprehensive beamed laser propulsion plant design study. It is too early to definitely predict which laser concept will win out. Independent of the relative benefits of the various laser types it is anticipated that the first laser powered propulsion systems will use those lasers which first become operationally available as the result of non-propulsion oriented development efforts. A significant proportion of the data relating to high power laser development is classified, and is included in the classified volume of this report.

4.1 LASER TYPES

4.1.1 Gas Dynamic Lasers

The earliest and most highly developed high energy laser type is the gas dynamic laser (GDL). This laser uses combustion heated gases that expand rapidly through supersonic flow nozzles to a low ambient temperature to create the population inversion in what was initially a thermally equilibrated gas. Specifically, a fuel and oxidizer are reacted in a combustor and are expanded with a diluent through supersonic nozzles into the optical cavity (Figure 23).

The metastable vibration states do not thermalize on the time scale of the nozzle flow and therefore remain as an energy source to supply the lasing energy.

An important example of this concept is the N_2 - CO_2 gas dynamic laser which operates at 10.6 microns in the usual CO_2 laser transition. The energy exchange process in the gas dynamic laser is the key to its ultimate capability and includes several energy transfers, the most significant of which is the relatively efficient transfer of energy from the single vibrational mode of the nitrogen diluent to the first asymmetric-stretch level of CO_2 from which the 10.6 micron transition can occur.

Candidate reactant combinations include air and an aircraft fuel such as JP-4, or air and natural gas for ground installations. Typical reactant combinations for experimental devices are $CO/O_2/N_2/CH_4$, $CO/Air/CH_4$, and $CO/N_2O/CH_4$. Highest performance has been obtained with the last combination. All these fuels and oxidizers can be stored as either gases or cryogenic liquids; but considerable effort is being spent in formulating more easily stored fuels for the GDL application. The pressures and temperatures in the combustor are typically 20 to 60 atmospheres and 1300 to 2000°K, respectively. In general, the higher the pressure and temperature, the more efficient the system is. Upon expansion through the nozzles, the pressure and temperature drop and the flow velocity increases. The flow consists of an $N_2/CO_2/H_2O$ mixture, the lower energy states of which are depopulated by the flow process faster than the upper states resulting in a population inversion and lasing. The laser beam (10.6 micron) typically leaves the cavity through an aerodynamic window, and the gases proceed through the diffuser to the exhaust.

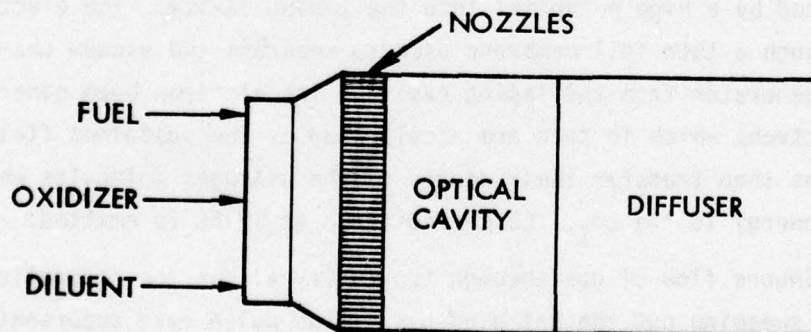


Figure 23. Gas Dynamic Laser Schematic

For high power applications, the CO_2 GDL is an attractive candidate. Although it is presently the least efficient of the high energy lasers, it has high theoretical efficiency and it can operate on virtually any energy source. For example, even a gas turbine engine could conceivably supply the heated plenum gases for such a laser. In addition, the CO_2 wavelength has an acceptable low altitude, atmospheric window.

A variation of the gas dynamic laser is the Mixing Nozzle Gas Dynamic Laser, MNGDL. This device mixes CO_2 with other gases in the supersonic nozzle to produce higher lasing efficiency than a conventional GDL.

Another variation of the gas dynamic laser is the DF- CO_2 transfer laser. In this laser the chemical reaction of D_2 and F_2 is used to vibrationally pump the CO_2 to an excited (population inverted) state. Mixing of the resultant DF and CO_2 makes this an open cycle device.

4.1.2 Electric Discharge Laser

In electric discharge lasers, an electric discharge is used to create a population inversion in the flowing gas. For the CO_2 lasers, the gas mixture typically consists of helium, nitrogen, and carbon dioxide. The nitrogen is easily excited by the electric discharge and transfers its energy to the CO_2 upper levels. For the CO lasers, the gas mixture consists of carbon monoxide, nitrogen, or helium. Filling the entire cavity with the electric discharge allows high power generation from small volumes.

A typical EDL configuration is shown in Figure 24. A high energy electron gun is used to generate the electrons and deliver them to the lasing cavity. Alternately, a thermionic emitter can be used to generate electrons which are then accelerated by a high potential into the lasing cavity. The electrons penetrate through a thin foil membrane used to separate the vacuum chamber of the electron generator from the lasing cavity. The electron beam generates secondary electrons which in turn are accelerated by the sustainer field. These electrons then transfer their energy to the nitrogen molecules which transfer the energy to the CO_2 . Laser radiation at 10.6μ is emitted.

The continuous flow of gas through the cavity allows the generation of high power by sweeping out the hot used gas. High pulse rate supersonic CO_2 devices are also being investigated. These devices eliminate acoustic disturbances and reduce the weight of the system.

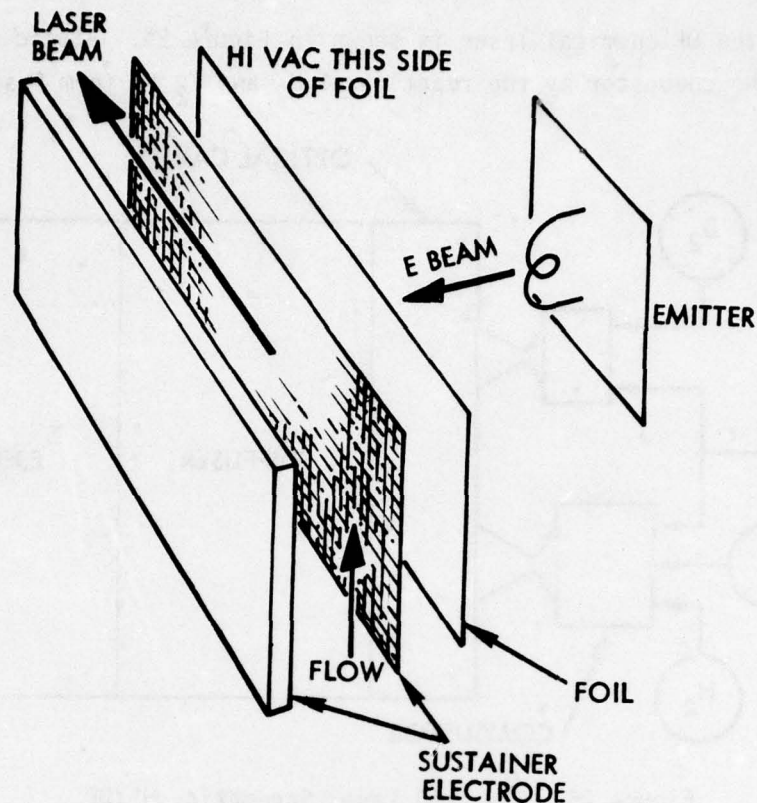


Figure 24. Electric Discharge Laser Schematic

The primary advantage of the EDL over the other high power lasers is that it can operate in a closed as well as open cycle. The cavity mass flow efficiency of the EDL is also considerably higher than the efficiency of the GDL. Furthermore, the EDL can be operated using CO as the lasing medium. The CO electric lasers tend to be more efficient than the CO₂ electric lasers in converting electrical energy delivered to the optical cavity to laser light energy. However, the CO laser does not propagate as well through the atmosphere, but could be well suited for high power transmission either in space (from a space station source to a satellite) or at high altitude (for example, from a large aircraft). Another systems advantage of CO lasers for either airborne or spacecraft installations is that they are more compact and lighter weight than other lasers.

4.1.3 Chemical Lasers

In the chemical laser, deuterium (or hydrogen) and fluorine are used in a chemical reaction to create the DF (or HF) inversion and lasing. A schematic

diagram of the DF chemical laser is shown in Figure 25. Atomic fluorine is formed in the combustor by the reaction of H_2 and F_2 to form F and HF. In

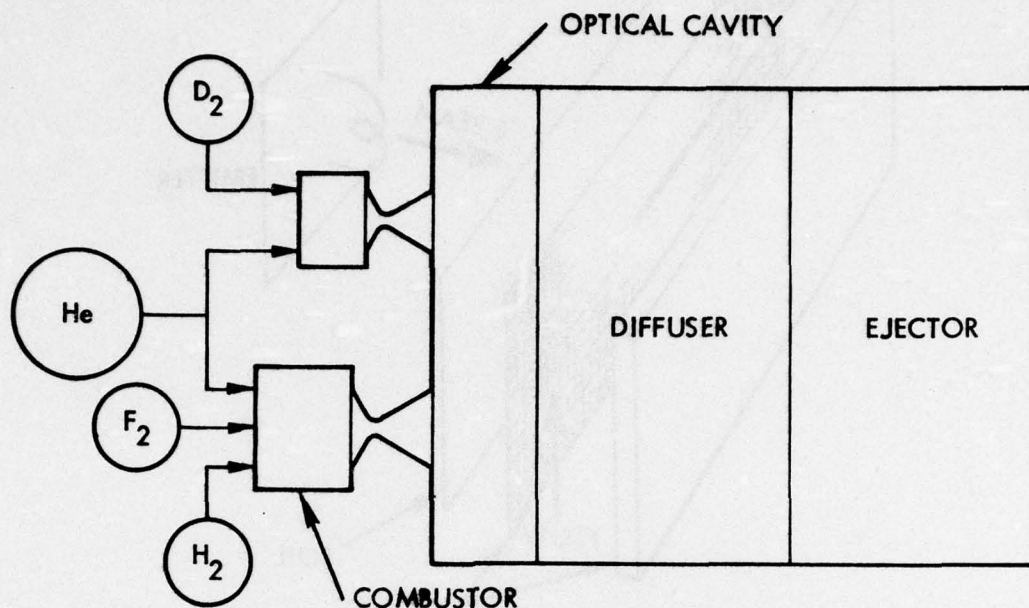


Figure 25. Chemical Laser Schematic, HF/DF

some lasers, F_2 is replaced by a fluorine compound. Helium is used as a diluent and the mixture undergoes supersonic expansion. Deuterium is introduced into the combustor flow stream through separate nozzles. The reaction between the deuterium and fluorine atoms creates the DF inversion, in metastable vibration states, and the lasing.

To minimize deactivation, the pressure in the cavity must be very low, on the order of 5 to 10 torr. A critical problem in the design of the chemical laser is the design of the ejector to allow pressure recovery for in-atmosphere operation. For a space-based laser this problem is, of course, of no concern. For a land based laser the problem is simplified since weight is not critical and an adequate ejector can be designed. Alternately, a chemical pump may be used.

Since the laser exhaust contains hydrofluoric acid and other toxic materials, containment of the exhaust or scrubbing to remove toxic components may be required when operating in the earth's atmosphere. Conventional water scrubber and steam ejector technologies are adequate to handle the toxic

products and maintain the low optical cavity pressure needed for efficient lasing. The fuel is more expensive for the DF laser than for the GDL and this would have to be traded against its advantages of substantially better atmospheric propagation (a better atmospheric window and a shorter wavelength) and more compact collection optics. Since there is no pressure recovery problem in space, higher efficiencies than those obtained on the ground can be achieved by operating at lower laser cavity pressures. Furthermore, beam quality is improved.

The HF laser has a 2.7 micron wavelength, which is the shortest wavelength available for the present generation of high power lasers and thus would have the least diffraction spreading for space applications. The 3.8 micron DF chemical laser wavelength is more favorable for atmospheric propagation.

4.2 OPERATING EFFICIENCY AND REACTANT UTILIZATION

Total energy expenditures can significantly affect the cost effectiveness of the beamed laser propulsion concept. This section discusses some of the basic operating efficiency limitations for various candidate laser/reactant combinations. State-of-the-art performance figures are discussed in Volume 4.

Theoretical quantum efficiency* limitations of laser devices are shown in Table 35. Practical limitations are much lower and the best results to date are summarized in the classified annex. Table 36 lists the heat of reaction of selected candidate chemical energy sources. All of these are space storable and could be used in liquid form in space, airborne or in a fixed ground based beam generation plant. Operational systems would almost assuredly use the liquid form to minimize system inert weights and transportation costs. The reactions in Table 36 include those for combustion driven GDL's and chemical energy to drive turbo-alternators for EDL's.

For CO_2 GDL's, present experience indicates a 14/85/1 molar mixture ratio of $\text{N}_2/\text{CO}/\text{H}_2\text{O}$ is the optimum reactant mixture. The water acts to depopulate the laser excitation levels and gives best performance. There are efficiency limitations imposed by the physics of the energy transfer to the

*Based on the available chemical or electrical energy.

Table 35. Theoretical Efficiency Limits

TYPE	TYPICAL SPECIES	WAVELENGTH MICROMETERS	THEORETICAL EFFICIENCY, %		
			QUANTUM	CHEMICAL	NET
<u>LOW OR HIGH ALTITUDE</u>					
1. Gas Dynamic	$N_2-CO_2-H_2O$	10.6	40.6*	28.5	11.6
Transfer	DF- CO_2		35.8**	62.8	22.5 ⁽⁵⁾
2. Electric Discharge	$CO_2/He/N_2$	10.6	45 ⁽⁶⁾ (41) ⁽⁷⁾	NA	43
3. Chemical	DF	3.8(3.6-3.9)	NA	20 ⁽⁸⁾	20
<u>HIGH ALTITUDE TYPES</u>					
4. Gas Dynamic	$N_2-CO_2-H_2O$	10.6	40.6*	28.5	11.6
5. Electric Discharge	$CO/N_2, CO/N_2/Ar$	4.9-5.7	>65 ⁽⁹⁾	NA	>65
6. Chemical	HF	2.7(2.6-2.9)	NA	20 ⁽⁴⁾	20

* $N_2^* + CO_2 \rightarrow CO_2^* + N_2$; $4.3 \mu m / 10.6 \mu m = .405$ ** $DF^* + CO_2 \rightarrow CO_2^* + DF$; $3.8 \mu m / 10.6 \mu m = .358$

Table 36. Selected Candidate Energy Sources

<u>No.</u>	<u>Location</u>	<u>Fluid</u>	<u>Type</u>	<u>Power Source</u>	<u>Undiluted Heat of Reaction</u>	<u>Remarks</u>
1A	SPACE BASED	CO	EDL	LOX/RP-1	4,330 KJ/lb _R	500-600 KJ/LB BY TURBO-GENERATOR* 1000 BY MHD 2500 BY TURBOGENERATOR
B	SPACE BASED	CO	EDL	LOX/LH ₂ NUCLEAR	5,753 KJ/lb _R HIGH	
2	SPACE BASED	HF	CL	F/H ₂	2,900 KJ/lb _R	6,150 BY CHAIN REACTION
3	AIRBORNE	CO ₂	GDL	CO/N ₂ O AIR/JP-4	2,300 KJ/lb _R 19,200 KJ/lb _R	AIR/CARBON 14,900 KJ/lb
4A	AIRBORNE	HF	CL	F/H ₂	2,900 KJ/lb _R	
B		DF	CL	F/D ₂	2,600 KJ/lb _R	
5	GROUND BASED	DF	CL	F/D ₂	2,600 KJ/lb _R	
6A	GROUND BASED	CO ₂	GDL	CO/N ₂ O	2,300 KJ/LB _R	
B		CO ₂	GDL	AIR/HYDROCARBON	19,200 KJ/LB _R	
7A	GROUND BASED	CO ₂	EDL	AIR/HYDROCARBON	19,200 KJ/LB _R	
B		CO ₂	EDL	COMMERCIAL ELECTRIC		

CO_2 and the transition. In addition, the N_2 molecule begins significant dissociation above 2400°K . This in turn imposes a severe specific energy penalty at higher temperatures, except for air breathing systems where the nitrogen is obtained essentially at no cost to system performance.

Air/hydrocarbon mixtures are attractive from the operational standpoint, although efficiency may be low due to heavy deactivation by the considerable water products (1:1 with CO_2). The following reactant combinations are presently of greatest interest for producing the desired molar mixture ratio:

1. CO , gaseous/ O_2 , gaseous/ N_2 , CH_4 , gaseous
2. CO , gaseous/Air/ CH_4 , gaseous
3. CO , gaseous/ N_2O , liquid/ N_2 , gaseous/ CH_4 gaseous

For an air breathing airborne or ground based laser, the weight of the air used in the reaction and as the diluent would not be chargeable to the reactant consumption thus increasing the theoretical power per unit reactant by a factor of three to four. The following candidates for intermediate and far term reactants may also be considered.

	<u>Intermediate</u>	<u>Far Term</u>
Space	$\text{LCO}/\text{LO}_2/\text{LN}_2/\text{C}_3\text{H}_8$	$\text{C}/\text{LO}_2/\text{LN}_2/\text{Hydrocarbon}$
Airborne	$\text{Air}/\text{C}_6\text{H}_6$	$\text{Air}/\text{C}/\text{Hydrocarbon}$

C refers to carbon in some form such as fine powder, perhaps in a jelled hydrocarbon base. This would allow direct reaction with air without excess deactivating water.

The reactant weights and overall system efficiency of electric discharge lasers are determined in great part by the properties of the particular chemical reactions which power the generator system. In some cases the chemical reactions are similar to those which supply the CO_2 gas dynamic laser, i.e., oxygen reacting with carbon and hydrogen to form CO_2 and water.

Candidate turbo-alternator fuels include:

	<u>Specific Fuel Consumption</u>	<u>Specific Power</u>
N_2H_4	1.2×10^{-3} lb/kw-sec; ⁽¹⁾	833 kj/lb
LOX/JP-4	2.2×10^{-3} lb/kw-sec; ⁽¹⁾	454 kj/lb
LOX/LH ₂	$.37 \times 10^{-3}$ lb/kw-sec; ⁽¹⁾	2,702 kj/lb
LOX/NH ₃	1.4×10^{-3} lb/kw-sec; ⁽¹⁾	714 kj/lb

Liquid hydrogen is potentially a very high specific power fuel for a turbine driven system. However, it has limited space storability. Furthermore turbine temperature limitations reduce the specific power obtainable by not allowing a stoichiometric LO₂/LH₂ mixture ratio.

Similarly, although the stoichiometric O₂/JP-4 reaction is capable of producing 4.3 MJ/lb, much lower yields are achieved in practice as a result of lowering the mixture ratio in order to keep the turbine temperature in the 1600 to 1800°F range. Reference 1 quotes the resultant LOX/JP-4 yield as 2.2×10^{-3} lb/kw-sec or 454 kj/lb. This is further reduced by turbine and laser inefficiencies.

Obviously, a key technology item would be development of a higher temperature turbine. This would allow use of less reactants by burning closer to the stoichiometric mixture ratio, producing more energy per weight of reactants.

Another alternative would be to develop another type of electric generator to convert fuel and oxidizer with high efficiency and reasonable weight to electricity. One candidate might be the magnetohydrodynamic (MHD) generator. This device is in a state of early development for ground applications. It offers the potential of high efficiency with high temperature gas, but there are significant unknowns as to practicality since large magnetic fields are required. Matching of the electric output of the MHD generator to the laser may also involve some losses.

Non-chemical electric power sources are also possible. These include nuclear and solar sources. The specific power of nuclear fuel is very high but must be realized over a considerable time. Solar energy could be collected and used to generate electricity either by photovoltaic, thermoelectric or

turbine systems. Spaceborne nuclear or solar power capabilities would obviously favor electric discharge lasers in order to avoid excessive reactant weight penalties.

Chemical lasers achieve efficient conversion of the chemical reaction energy of atomic fluorine with molecular hydrogen into excited HF and H in the so-called cold reaction. Under some conditions, some power may also result from the succeeding chain reaction. However, it is much less efficient at producing the proper excited levels.

The specific energy is degraded further by the addition of fuel to dissociate the fluorine; diluents; and, for ground based systems, ejector flow. Space versions of the laser device would be operated at low pressures to achieve high specific power, while ground based versions are operated at higher pressure to be able to recover more pressure from the flow to minimize the required ejector flow.

The optimum space laser may operate at such low pressures that heat losses become significant and partial recombination of the fluorine is permitted. This involves a trade-off between system size and weight and specific power efficiency.

Airborne lasers would have intermediate characteristics. Water deactivates the chemical laser so oxygen as a heat source oxidizer is not permitted in the laser gas flow. It might be used indirectly in some forms of chemical laser. This might allow a more economical ground or airborne chemical laser by using air for the heat source oxidizer to dissociate the fluorine.

4.3 SUMMARY

Various high powered laser concepts are in a rapid state of competitive development. At this time it is difficult to predict which concept will ultimately be developed to the capability required for the beamed laser propulsion concept. Therefore the main emphasis in this section has been to provide a brief summary of the general characteristics of the various devices currently being developed. Specific operating capabilities, which are classified, are discussed in classified Volume 3 of this report (AFRPL-TR-76-67).

5. MICROWAVE BEAMED ENERGY

This section will consider both the conceptual functions necessary for conversion of DC electrical energy to Spacecraft microwave or DC energy using a microwave transmission link, and the present and near future technological capabilities to implement these components. The system necessary for conversion of the spacecraft energy, microwave or DC, to propulsion will not be considered.

The functions of a microwave beam propulsion system, shown in Figure 26, are:

- DC to microwave conversion
- Microwave beaming (antenna)
- Microwave collection
(microwave focusing antenna)
(microwave to DC converter)
- Power conversion to propulsion

The important conclusions of this study are summarized as follows. The second and third functions are not feasible at microwave frequencies for most spacecraft mission parameters. Further, for many mission parameters the direct conversion of solar energy is to be preferred. And finally, for appropriate mission parameters, efficiencies involved in the first three functions of the microwave system are very high and may be compared favorably to laser system efficiencies.

The reasons for these conclusions are summarized. Microwave antennas cannot be fabricated with sufficient precision for the required beam collimation for the transmission distances involved. With a transmitting antenna, power can only be beamed to a microwave to DC converter whose size is prohibitive for many orbit distances. Solar energy is a preferred source of power for many missions where the power density of the microwave beam is far less than the power incident from the sun.

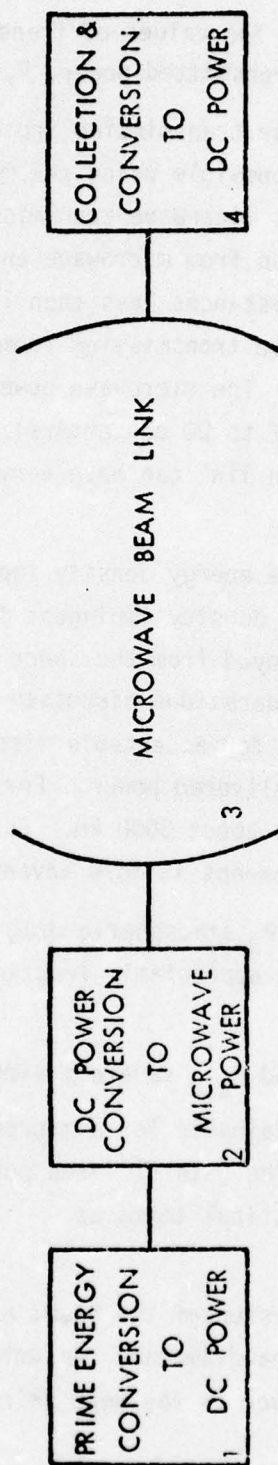


Figure 26. Components of a Beamed Power System.

5.1 MICROWAVE CONCEPTS AND LIMITATIONS

This section will show that for values of transmission distance, d , microwave wave lengths, λ , and transmitted power, P , such that:

- $d > d_1$ and $\lambda < \lambda_1$, then power transmission from microwave antenna to microwave antenna is impossible using the most precisely made antennas. For efficient microwave transmission and for microwave wavelengths, transmission from microwave antenna to microwave antenna is limited to distances less than 100 nautical miles. For this reason microwave transmission from antenna to antenna will not be considered. The microwave power receiver must be a rectenna (an array of RF to DC converters). The microwave antenna to rectenna transmission link can have very high efficiency but for:
 - $d > d_2$, $\lambda > \lambda_2$ and $P < P_2$ the energy density impinging on the rectenna is less than the energy density impinging from the sun and the use of solar cells deployed from the space vehicle is more appropriate. The considerations discussed here show a maximum distance of propagation for acceptable missions of 100 NM for 10 cm waves and a 10 meg W delivered power. For .1 cm waves and 1000 Meg W the maximum distance is about 3000 km. For missions demanding less power the solar cell concept is more advantageous.
 - for $d < d_3$, $\lambda > \lambda_3$, and $P < P_3$ atmospheric drag associated with the rectenna will absorb an appreciable fraction of the transmitted power.
 - The values of $d_{1,2,3}$ and $P_{2,3}$ severely limit the available missions.
1. The highest directivity obtainable for a microwave beam is generated by a large parabolic antenna. The gain of large parabolic antennas may be approximately expressed in optical terms as

$$\theta = 1.22 \lambda / d \quad (1)$$

where θ is the half angle dispersion of the beam, λ is the wavelength of propagation, and d is the antenna diameter. Assuming a uniform intensity over the beam and negligible power in the beam skirts, θ may be related to the gain by

$$G = 4/\theta^2 \quad (2)$$

which is valid for small θ .

This equation assumes a perfect focusing antenna which has zero phase error across the aperture. This assumption is valid for low gain antennas, but phase errors, caused by construction tolerances, limit the gain of larger antennas. This loss in gain due to phase errors may be expressed by:

$$\frac{G}{G_0} = 1 - \delta^2 \quad (3)$$

where

G = Antenna gain accounting for phase errors

G_0 = Antenna gain with zero phase error

δ^2 = Mean phase plane deviation

Equation (3) indicates that for a one dB loss in gain, the RMS phase variation about the mean phase plane must be less than $(.4/2\pi)\lambda$ or $\lambda/14$. For shallow reflectors Equation (3) is no longer valid and the surface error must be less than $\lambda/28$.

For a given antenna, Equations (2) and (3) indicate that gain increases as the square of the frequency until, at a sufficiently high frequency, tolerance effects predominate and a rapid gain deterioration occurs. It may also be concluded that for a given frequency, as the antenna size is increased, the tolerance effect must be minimized to provide increased gain.

Figure 27 shows the wavelength versus gain characteristics of a selection of the world's largest parabolic microwave antennas. Each of the antenna shows an increase in gain with decrease in wavelength to a characteristic wavelength below which tolerance effects predominate and their gain falls. The antennas have been built over a period of 20 years, using different techniques, for various purposes. The most remarkable feature of Figure 27 is the gain and wavelength at which each of the antennas is limited by tolerance effects. For instance, the maximum gain obtainable for 10 cm waves is 65 dB (or $\theta = 1.15$ m rad). A 6 dB improvement can be expected for an antenna designed for 1 cm waves and a 12 dB improvement for .1 cm waves.

Assuming that the technology of parabolic antenna fabrication cannot be significantly improved, the transmission efficiency, η , from microwave

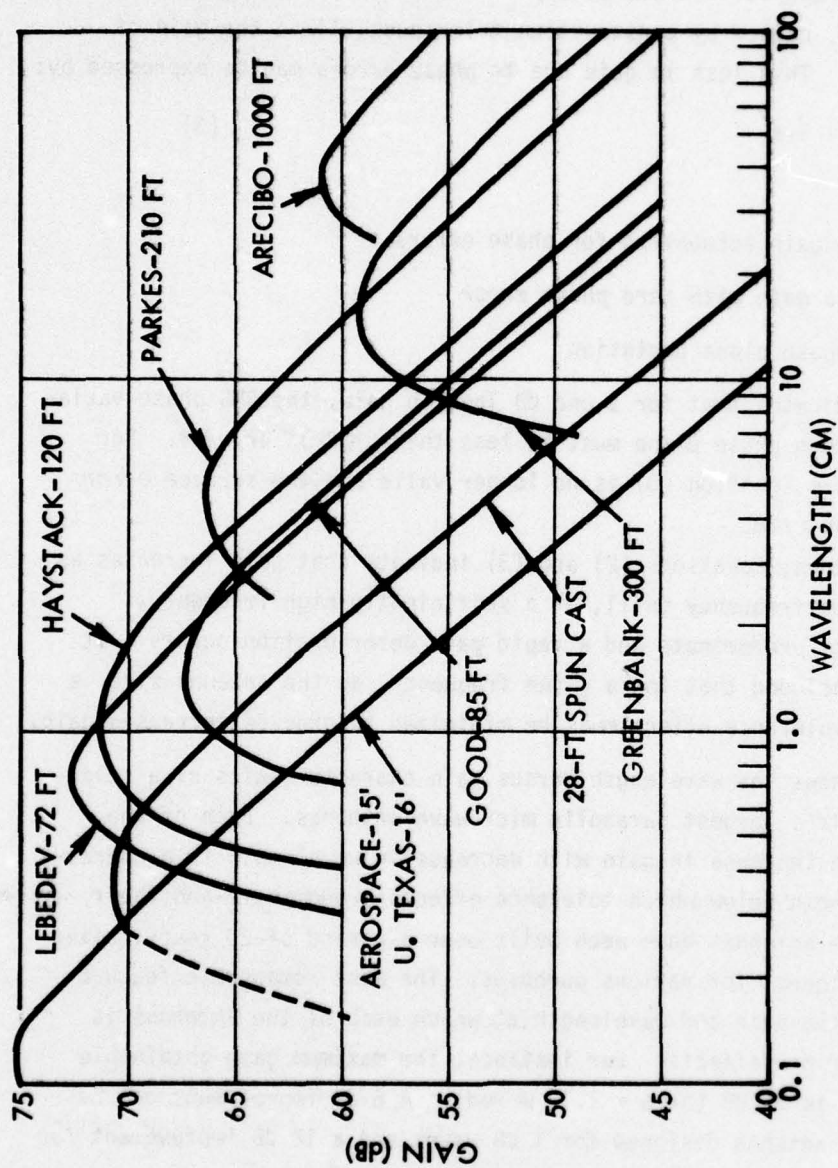


Figure 27. Gain of Large Antennas

antenna to microwave antenna as a function of wavelength and transmission distance may be summarized by Figure 28. For maximum transmission efficiency two antennas of equal diameter have been chosen. For example, using a transmission wavelength of 1.0 cm, two 72 ft. antennas are used and Figure 28 shows a transmission efficiency of 1% at an antenna distance of 100 NM.

The Lebedev 72 ft. (22 meter) parabolic antenna at $\lambda = 1.0$ cm has a gain of 72 dB. Assuming a uniform intensity over the beam spread and negligible power in the beam skirts, this gain corresponds to an angular beam dispersion of .505 milliradians. For the large gains involved, the half angle dispersion may be expressed as:

$$\theta = \sqrt{4/G}$$

where G is the antenna gain.

Note that .505 m rad is close to the calculated angular dispersion, .57 m rad, derived from the usual optical formula, equation 1. At 70 km the beamwidth for a .5 m rad beam is $70 \text{ Km} \times 2 \times .5 \times 10^{-3} = 70$ meters. Thus for total beam collection at 70 km, a 70 meter antenna with theoretical gain at 1.0 cm is necessary. Such an antenna is well beyond the fabrication capabilities available today. For instance the Parkes 70 meter (210 ft.) antenna has a gain of 20 dB below theoretical (1% efficiency) due to fabrication tolerances.

Based on the precision of fabrication evidenced in Figure 28, the maximum diameter of matched antennas is:

$$d = 92 \log \lambda$$

where λ is transmitted wavelength in centimeters and d is in meters. For transmission of 525 cm waves, the minimum wavelength for 30% reception at 100 NM, the diameter of the receiving and transmitting antennas is 250 meters.

2. To obtain transmission efficiency for parameters in the shaded regions of Figure 28, a different concept for energy reception must be developed. If the receiving "antenna" is designed to convert microwave power to dc or low frequency power at several localities within the "antenna", then phasing problems incurred in power combining at a central location are avoided. An "antenna" which rectifies microwave fields and produces dc power at several localities is called a rectenna. With the relaxation of

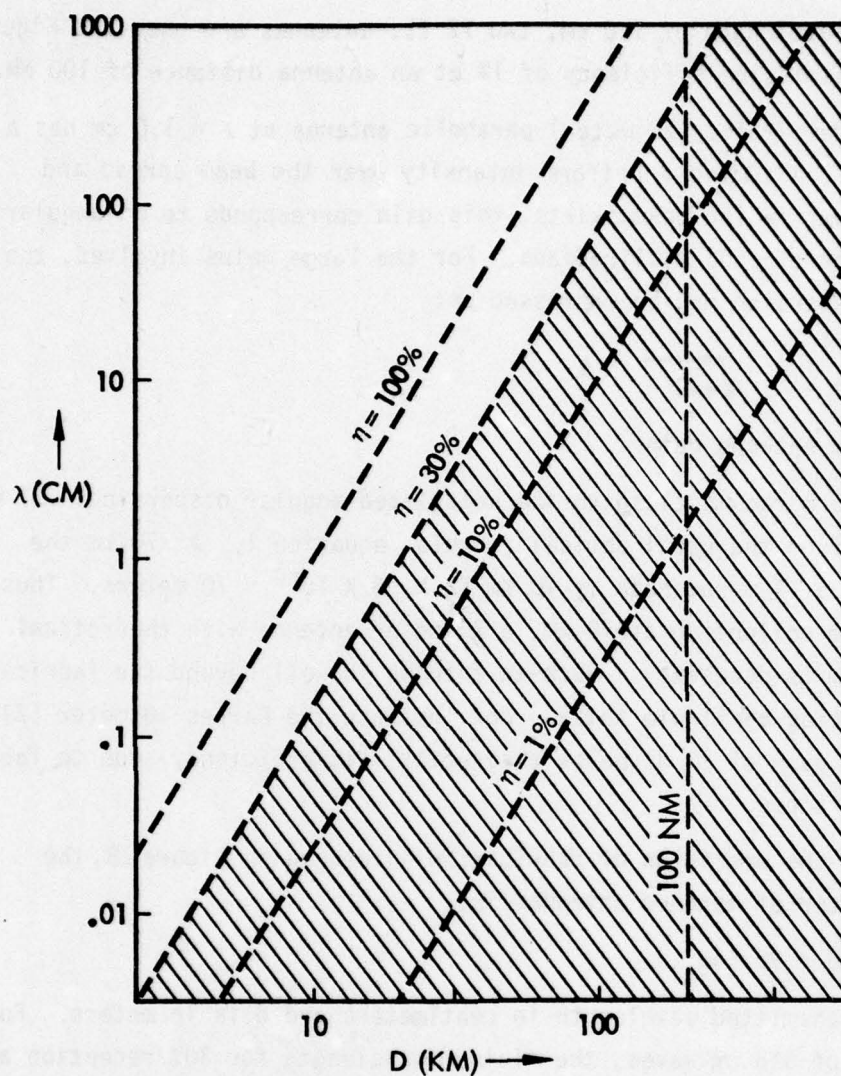


Figure 28. Theoretical Microwave Antenna-to-Antenna Transmission Efficiency as a Function of Wavelength and Transmission Distance. (The figure assumes present state-of-the-art capabilities for a parabolic antenna.)

dimensional tolerances extremely large rectennas can be constructed. As well, the directivity of the large array becomes that of the small aperture, and pointing difficulties are largely avoided. The rectenna concept also makes possible the convenient use of the only efficient rectifying device that exists at the present time. This rectifying device is the Schottky-barrier semiconductor diode. Diodes have exhibited efficiencies of over 75% and it would appear that further improvement in its efficiency can be made. When improved diodes are properly incorporated into the rectenna, an overall collection and rectification efficiency approaching 85% should result. Gallium arsenide diodes have an 80% rectification efficiency and a single diode can handle 6 watts.

The use of a rectenna allows construction of a very large receiver of microwave power of theoretical efficiency. Using the beam spread data derived above, the radius of a microwave beam is plotted versus the distance of propagation for several microwave frequencies. See Figure 29. The beam diameter monotonically increases with increasing wavelength. Each decade of wavelength increases the diameter by a factor of two. The minimum size of a rectenna which receives the entire beam is thus found.

The concept of rectenna reception of a microwave beam must be compared to a similar beamed power receiving system: a solar cell array aimed at the sun. The size of the rectenna is fixed by the transmitting antenna and the rectenna's distance from the antenna, and is independent of the power beamed in the microwave link. The size of a solar cell array is, of course, proportional to the energy received. By dividing the total power converted by the rectenna for a particular mission application, taken as 1, 10, and 1000 meg W, with the necessary rectenna area as determined by Figure 29, the DC power available per square meter is determined in Figure 30. The power density, of course, is a function of wavelength, transmission distance and mission power requirements. The power converted from a solar cell array is greater for transmission distances greater than 350 km and total powers less than 10 meg W. Solar insolation is 1400 W/M^2 and conversion efficiency is assumed to be 20%.

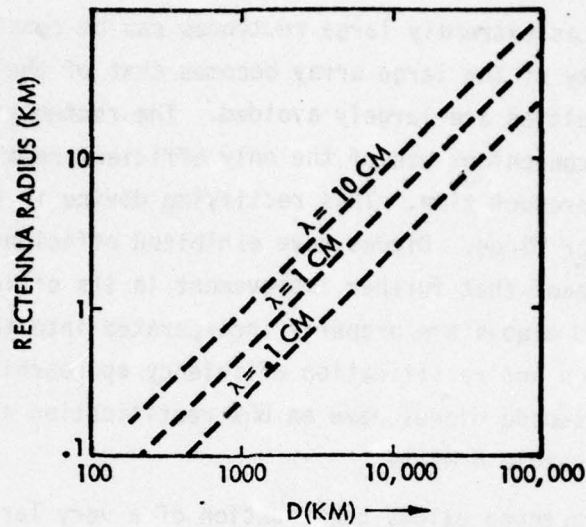


Figure 29. Necessary Rectenna Diameter for Total Beam Collection as a Function of Orbit Altitude and Transmission Wavelength. (The graph assumes the gain limitations incurred by present large parabolic antennas.)

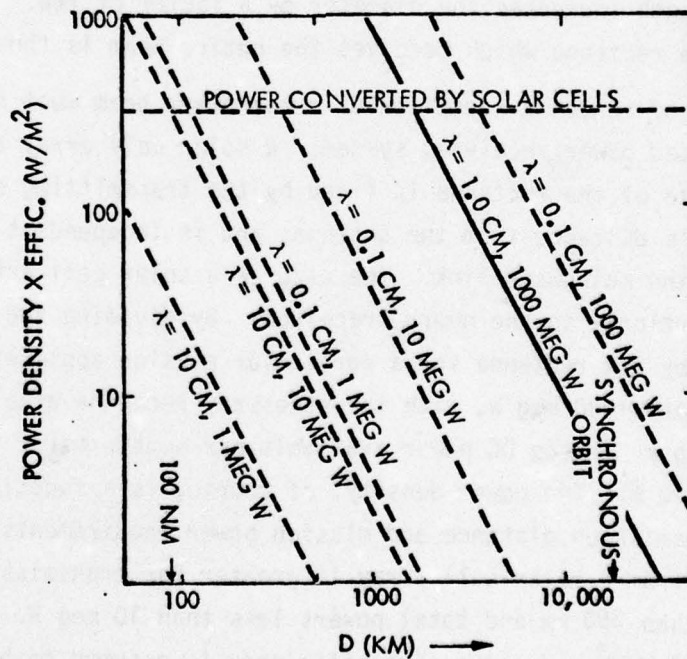


Figure 30. DC Power Density Converted by a Rectenna as a Function of Transmission Distance, Propagated Wavelength, and Total Power Transmitted. (DC power available per square meter of solar cell array is shown for comparison.)

3. Finally, an additional problem of a large power receptor in low orbit is the energy lost to molecular drag. The drag incurred by an orbiting vehicle may be expressed as:

$$D = 1/2 \rho v^2 C_D S$$

where ρ is the molecular density in kg/m^3 , v is the orbiting velocity, C_D is a constant which may be approximated by 2.2 for a wide region of altitude and vehicle cross section, and where S is the effective vehicular cross section in the velocity direction.* The molecular density surrounding the earth at altitudes greater than 160 km may be expressed as

$$\rho = 3.3 \times 10^{-8} e^{-.023h} \text{ kg/m}^3$$

where h is in kilometers. This expression for ρ has been derived from molecular mean free path vs altitude data published by G. E. Cook and a well established relationship between mean free path and vapor pressure.

The resulting power lost, $D \cdot v$, is plotted in Figure 31 as a function of altitude and transmission frequency. A minimum rectenna size is assumed. S is assumed to be the entire rectenna size, which is a worst case.

For a low orbit mission, propulsion from a ground based antenna has a duty cycle of approximately 1%. Therefore, power levels for drag makeup alone would be approximately 100 times the plotted quantities.

From this figure, a minimally sized rectenna for 10 cm waves, 100 NM above the earth's surface, losses energy to the atmosphere at the rate of 5 meg W. Unless the rectenna's cross section in the direction of flight can be minimized, i.e., by turning the rectenna, this drag power is lost during the entire 360° of the orbit. Since a single earth based microwave source can supply energy over less than 3% of the orbit, power supplied to the spacecraft for drag make up alone must be greater than 500 meg W.

*G. E. Cook, "Satellite Drag Coefficients", Planetary & Space Science, Vol. 13, pp. 929 - 946 (1965).

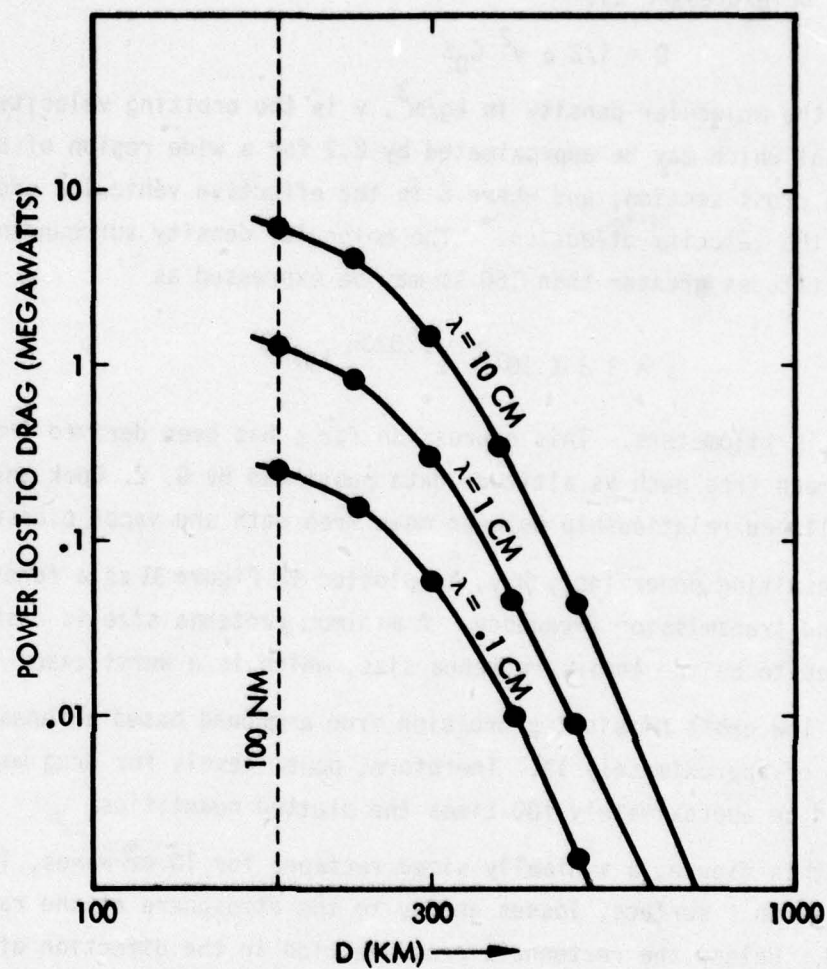


Figure 31. Power Lost to Drag for a Minimally Sized Rectenna vs Altitude of Rectenna. (The power may be reduced by rotation of the rectenna during orbit. Note that the energy lost must be replaced during a small fraction of orbit.)

An expression which relates the orbital angle, θ , to the angle, α , seen by an earth bound observer, is

$$\cos \alpha = \left[\cos \theta - \frac{R}{R+h} \right] \left\{ \left(\frac{h}{R+h} \right)^2 + \frac{2R}{r+h} (1 - \cos \theta) \right\}^{-1/2}$$

where R is the earth's radius and h is the altitude of the orbiting vehicle. Note that for most microwave frequencies the atmospheric attenuation incurred by the beam is not substantial even for non vertical beaming. Thus, the beaming angle is not limited by the atmospheric path traveled, as in a laser system, but by the beam spreading incurred for the excess path length involved.

Using the above expression, using Figure 30, which compares the energy density delivered by a microwave beam to the energy density delivered by a solar cell array as a function of altitude, and using Figure 31 which relates rectenna energy lost to drag versus rectenna altitude and wavelength of propagation, we can define a range of possible missions in altitude and power levels used by the satellite. Figure 30 defines a maximum acceptable altitude and Figure 31 defines a minimum acceptable altitude. The additional consideration of generation capabilities must be met. If a lower limit of a 4 - 5 cm wave is demanded by generation considerations then the following missions may be characterized as follows:

A 400 km (220 NM) altitude and a 4 - 5 cm wave operation requires a 60 meter diameter antenna and a 600 meter diameter rectenna as calculated from Figure 27 and Figure 29. The 600 meter rectenna, whose cross section in the direction of flight is not controlled, will lose power to drag at the rate of 0.2 megW as calculated from Figure 31. Since power can be delivered to the satellite during approximately 8% of its orbit (a duty cycle), as calculated by the equation above, the power delivered during this period to counteract drag alone is 2.5 meg W. This lost power must be subtracted from the efficiency of the overall system. The power density incident on the rectenna is 40 W/M^2 .

A system at an altitude of 600 km and using wavelength of less than 10 cm suffers no appreciable drag. Rectenna array diameter for 5 cm waves is 900 meters and incident power density is 20 watts/meter^2 .

5.2 TECHNOLOGY OF BEAMED MICROWAVE ENERGY

The technological parameters of beaming microwave energy are very favorable.

- Projected conversion efficiencies, from ground based 60 Hz power to DC power on the space vehicle, is 70%.
- A suitable RF generator for the project (the amplitron) is a simple, long lived (>20 - 30 yrs.) and efficient device.
- Suitable antennas for the project exist.
- A power receiver, the rectenna, is relatively non-directional, non-phase dependent, mechanically easy to build (large but relatively crude), and has a highly efficient DC output.

Table 37 delineates the efficiencies of a microwave beamed transmission system. The table shows present efficiencies, expected efficiencies, and probably future efficiencies as described by W. C. Brown, inventor of the Amplitron and principal proponent of the satellite solar power station concept. Similar values may be found in "Status of the Technology and Applications of Free-Space Microwave Power Transmission", by W. C. Brown, 1971 IEEE Microwave Symposium. It should be noted that the efficiency of the transmitting antenna has not been included in Table 37.

The state-of-the-art in microwave power obtainable from a single tube has been greatly advanced as a result of the development of the super power CW Amplitron. Continuous 400 kilowatt operation has been achieved with 70% efficiency. This represents an average power level significantly greater than that obtainable at this frequency from a single tube of any other type.

As shown in Figure 32, the Amplitron consists of a cathode surrounded by a slow wave structure and a magnetic field whose direction is normal to the plane of the illustration. The slow wave structure serves both as a means for carrying the RF wave and a collection surface for the electrons which are emitted from the cathode and subsequently impinge upon the anode. Operation is achieved by placing a DC potential between the cathode and the anode. As the potential is raised, electrons emitted from the cathode rotate in concentric orbits, ultimately reaching the anode.

Table 37. Microwave Power Transmission Efficiencies

	Efficiency Presently Demonstrated*	Efficiency Expected with Present Technology*	Efficiency Expected with Additional Development*
Microwave Power Generation Efficiency (η_g)	76.7**	85.0	90.0
Transmission Efficiency from Output of Generator to Collector Aperture (η_t)	94.0	94.0	95.0
Collection and Rectification Efficiency (Rectenna) (η_r)	64.0	75.0	90.0
Transmission, Collection, and Rectification Efficiency ($\eta_g \eta_t \eta_r$)	60.2	70.5	85.0
Overall Efficiency ($\eta_g \eta_t \eta_r$)	26.5***	60.0	77.0

* Frequency of 2450 MHz (12.2 cm wavelength)

** This efficiency was demonstrated at 3000 MHz and a power level at 300 kW cw.

*** This value could be immediately increased to 45% if an efficient generator were available at the same power level at which the $\eta_t \eta_r$ efficiency of 60.2% was obtained.

Microwave Power Transmission Efficiencies
as published by W. C. Brown.

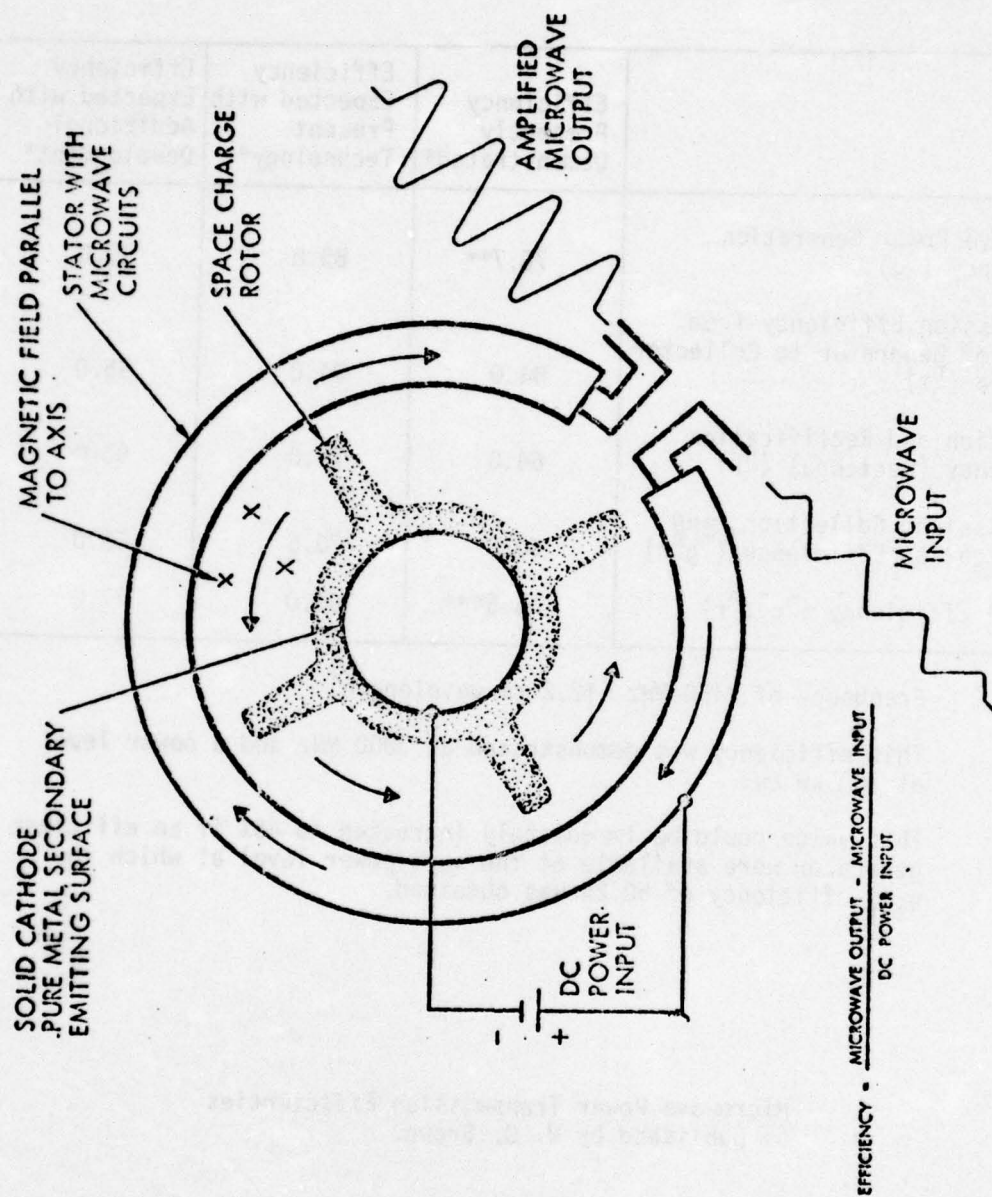


Figure 32. Conceptual View of Amplitron Device.

During the transit, the electrons become synchronous with the phase velocity of the RF wave on the network. Interaction occurs causing the electrons to coalesce into spokes of space charge which then induce RF currents into the slow wave structure. The several RF currents so induced caused energy to travel along the RF structure.

In terms of energy conversion, the electron has maximum potential energy at the cathode surface. As it moved toward the anode, it loses its potential energy. About 80 to 90% of this loss is converted directly into useful RF energy. The remaining 10 to 20% is converted into kinetic energy of motion which in turn appears as heat as the electrons strike the anode.

It is evident that an increase in efficiency will decrease the amount of dissipation at the anode and therefore permit more DC power input with correspondingly more RF power output. It is further evident that if the heat dissipation capabilities of the anode surface could be improved, greater power handling capability would result. Finally, by making the RF circuit larger, more anode dissipation is permitted, and therefore, more power output.

A simple expression which relates the RF power output to efficiency and anode dissipation is

$$\begin{aligned}
 \text{RF power generated} &= (\text{anode dissipation}) (\text{efficiency factor}) \\
 &= (\text{anode area}) (\text{dissipation density}) (\text{efficiency factor}) \\
 &= \left(\frac{K}{f^2} \right) (\rho) \left(\frac{\eta_e}{1-\eta_e} \right) \quad (4)
 \end{aligned}$$

where ρ = dissipation density Kw/cm²

η_e = conversion efficiency of DC to RF power

f = frequency of operation

K = a constant function of the number of vanes, operating potential level, etc.

It can be seen from equation (4) that the RF power generated is highly dependent both upon efficiency and dissipation density. It will be noted that a rapid increase in the power output is possible with moderate increase in efficiency. For example, an efficiency of 75% will produce twice the power output that would be obtained at 60%.

On the assumption that a dissipation density of 10 kw/cm^2 and an electronic efficiency of 80% can be realistically achieved, it should be possible to generate about 40 kilowatts for each square centimeter of anode area. Anode area determined from wavelength and other considerations typically amounts to about 30 cm^2 . A total power capability of about 1200 kilowatts of RF power is thus indicated. With allowances made for non-uniformity of dissipation along the vanes, a power output of about 600 kilowatts could be reasonably expected.

Published results have shown power generation of 400 kw. Table 38 summarizes the power generation and dissipation for a demonstrated amplatron.

Table 38. Distribution of Power in the CW Amplatron

RF Power Generated	71.7%	350 Kw
Anode Dissipation	21.4%	104.5 Kw
Cathode Dissipation	5.0%	24.6 Kw
Transmission Line	1.9%	9.3 Kw
	<hr/>	<hr/>
TOTAL	100.0%	488.4 Kw
RF Drive Power		55 Kw
RF Power Generated		350 Kw
		<hr/>
Total RF Output Power		405 Kw

Developmental programs for high power continuous wave amplitrons are presently in progress and are sponsored by NASA. The primary frequency is 2450 MHz. Parameters of amplitrons which will soon be available include 5-10 kW continuous output, 85 - 90% efficiency, and greater than 20 years lifetime. Similar development at 6000 MHz (5 cm) is expected to yield tubes of similar output power and lifetime and 75% efficiencies.

A planned usage of the 2450 MHz tubes is for RF generation on the solar cell power station. Arrays of solar cells deployed in synchronous orbit will be used to generate 10,000 Meg W of DC power which will be converted to RF power by an array of one million 10 kW amplitrons. By proper phasing of the amplitrons outputs energy will be beamed to earth to be received by a 7 by 7 kilometer rectenna receiver. Proponents of the program admit to difficulties in the output phasing concept. Difficulties include construction and thermal contraction problems in the waveguide feeds. The use of fewer, but higher power amplatron tubes cannot be made since the high power tubes require water cooling.

High power klystrons are being developed in competitive programs. Varian Associates is presently developing windowless klystrons for ERDA for use on the solar cell power station.

There exists frequency limitations to both the efficiency and maximum power output of the amplatron. The maximum power output of the device is limited by the maximum power dissipation density allowed on the anode. The anode area is proportional to $1/f^2$; hence the maximum power wasted due to inefficiencies is proportional to $1/f^2$. In addition the amplatron device is limited by the maximum magnetic fields which are presently obtainable. The theoretical efficiency of an amplatron device, as a function of the parameter B/B_0 , is shown below. The parameter B_0 , which is the value of magnetic flux for the grazing of the anode by electrons at synchronous velocity, may be expressed as:

$$B_0 = \frac{21,200}{N \left(\frac{\pi - \theta}{2\pi} \right) \lambda \left[1 - \left(\frac{r_c}{r_a} \right)^2 \right]} \quad \text{gauss}$$

B = value of magnetic flux produced by the magnet in Gauss

r_a = radius of anode in centimeters

r_c = radius of cathode in centimeters

λ = operating wavelength of tube in centimeters

N = number of vanes (assumed equally spaced)

N typically is as high as 15. See Figure 33.

Since the number of vanes cannot be arbitrarily increased, the value of B/B_0 decreases as λ decreases. While amplatron efficiencies for 10 cm waves are about 85%, efficiencies for 5 cm waves are about 75%. Not only does the inefficiency waste power, but it reduces the maximum obtainable output power below the $1/f^2$ limitation.

Size of the 10 cm 400 kW generator is less than one cubic foot. Thus 10 meg W generator would occupy a three foot cube, and proper phasing of each output, necessary for the power combining, should not be difficult. A 10 meg W generator for 5 or 1 cm waves would be slightly larger and phasing problems would be more difficult as the wavelength decreases.

Klystrons capable of 500 kW with 40% efficiency and 40 dB gain are catalog items and have existed for 10 years. Frequencies are presently limited to 10 GHz, but present ERDA contracts propose building 100 kW tubes for 1 cm waves. 40% efficiency is proposed. Sizes of the 10 cm devices are large, approximately 5 ft by 1 ft by 1 ft. Gains are high, 40 dB, which implies a common drive may be used; an array of amplatron devices, which has a gain of 10 dB, needs a more complicated drive. Maximum power output of the klystron is limited by a $1/f^2$ dependence. As well, tube life of the klystron may be limited to approximately 1000 hours. The tube life of the amplatron is approximately 20 years.

Figure 34 and Tables 39 - 42 show the physical outline and specifications of the commercially available Varian VKS-7773.

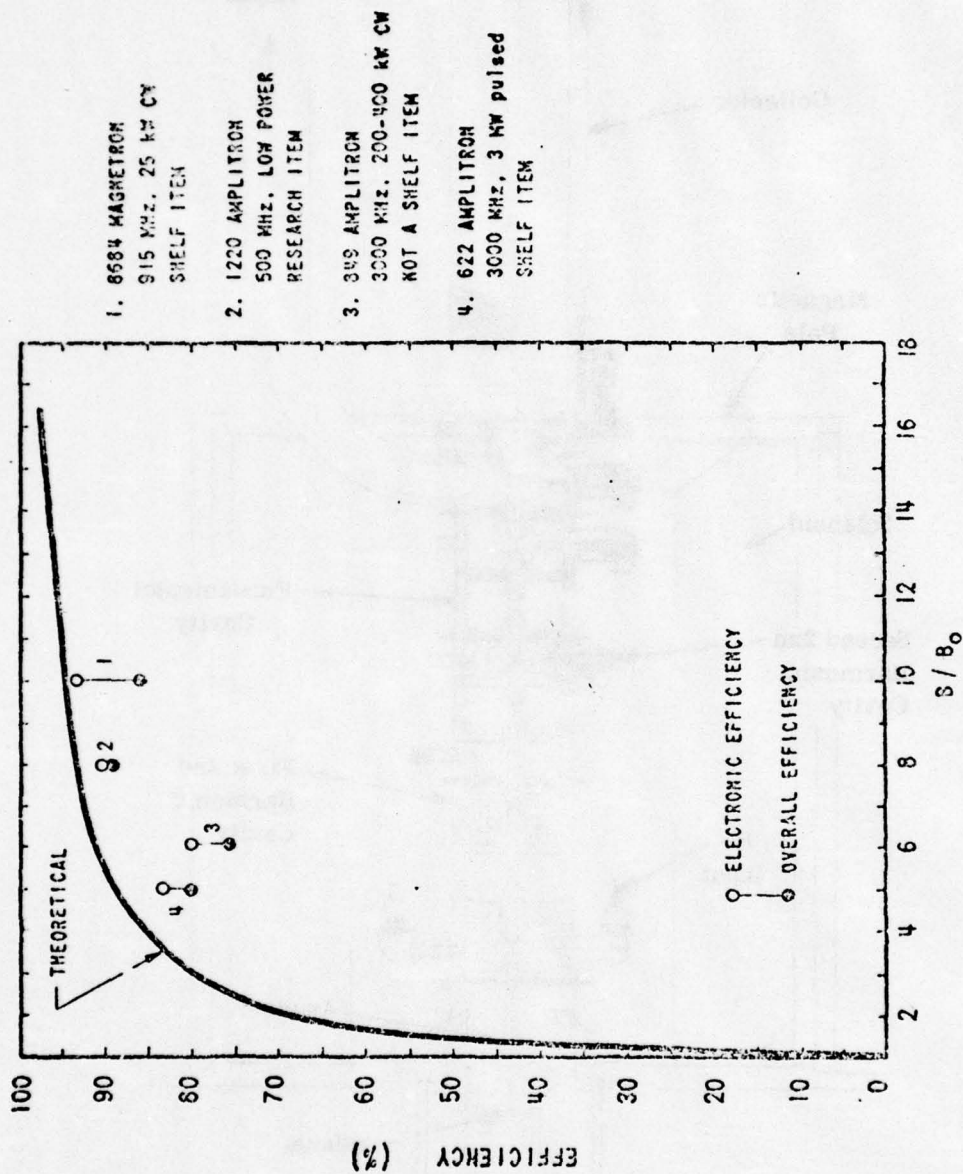


Figure 33. Efficiency of Microwave Generation vs the Normalized Magnetic Field, B/B_0 .

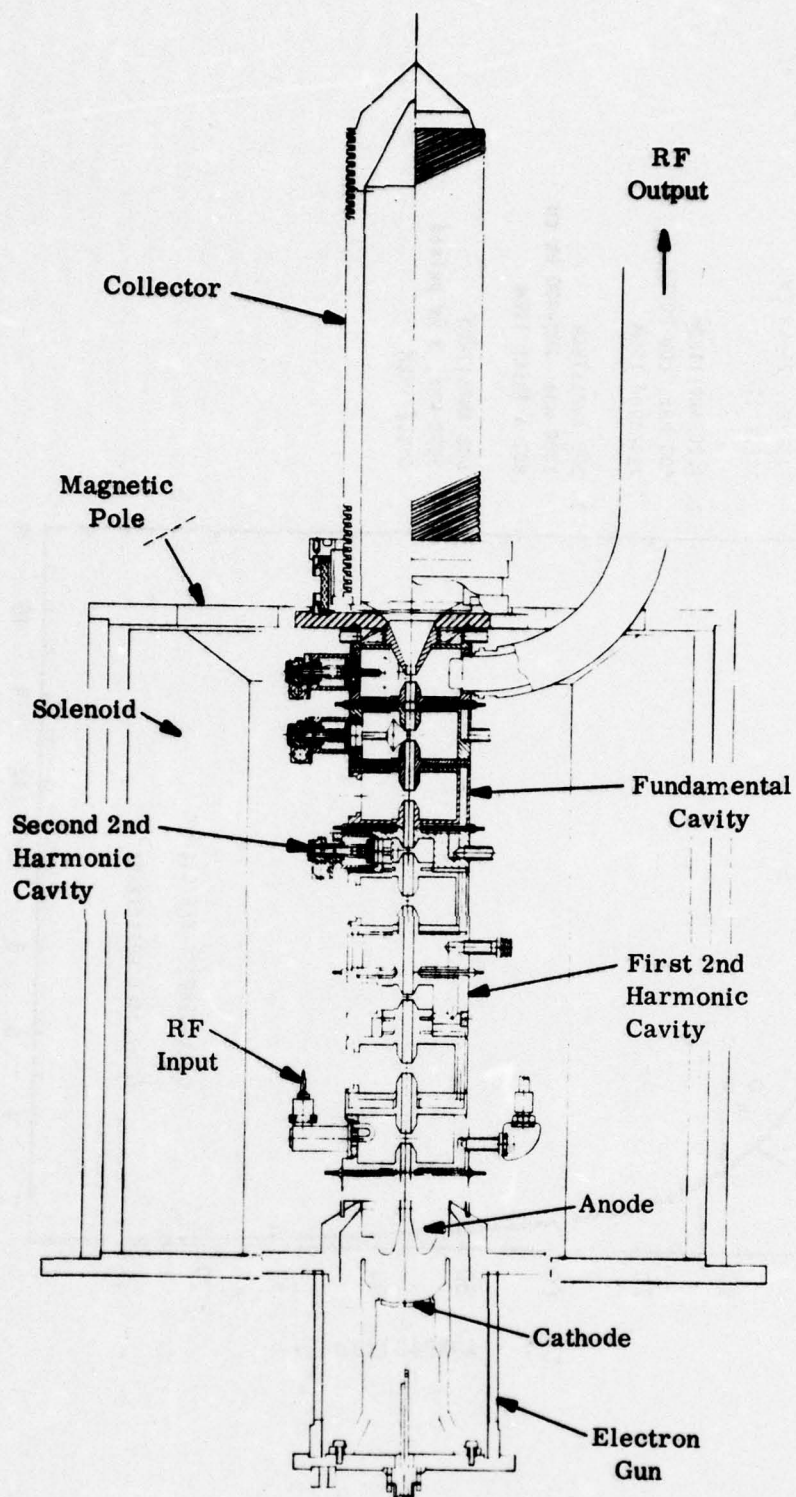


Figure 34. VKS-7773

Table 39
VKS-7773 Klystron CW Amplifier Operating Characteristics

Frequency	2450 MHz
Tuning Range	± 25 MHz
Bandwidth (3 dB)	3 MHz
Beam Voltage	28 kV
Beam Current	2.4 Amperes
Power Output	50 kW
Efficiency	74%
Saturated Gain	50 dB
Heater Power	95 Watts
Electromagnet Power	1.9 kW
Cooling	Liquid

Table 40
High Efficiency Klystron CW Amplifier
for Space Applications

Summary of steps for increasing Klystron efficiency:

- Improve Electronic Conversion Efficiency
 - Optimize output cavity γ_a (output drift tube)
 - Reduce electron beam perveance (0.5 to $\sim 0.3 \mu P$)
 - Optimize electronic bunching
- Improve Output Cavity Circuit Efficiency
 - Use toroidal-shaped cavity for higher Q_0
 - Optimize output coupling
 - Simplify tuner structure
- Employ Depressed Collector to Improve Collector Efficiency
- Reduce Solenoid Power with Smaller Size Unit

Table 41. Proposed High Efficiency Klystron CW
Amplifier Operating Characteristics

Frequency	2450 MHz
Bandwidth (3 dB)	3 MHz
Beam Voltage	34-40 kV
Beam Current	1.8-2.4 Amperes
Beam Perveance	0.3 μ P
Power Output	48-77 kW
Beam Efficiency	75-80%
Overall Efficiency*	84-86%
Saturated Gain	40-50 dB
AM Noise**	-130 dB
PM Noise**	-115 dB
Heater Power	40 Watts
Electromagnet Power	\sim 1 kW

*Includes heater and electromagnet power and requires depressed collector.

** Measured in 1 kHz bandwidth 50 kHz from carrier.

Table 42. High-Efficiency Klystron CW Amplifier
For Space Applications

ADVANTAGES

- High Gain Amplifier
 - Low RF drive
 - Phase control at low RF level
- High Power Output
- High Efficiency (optimum in narrow bandwidth Klystron)
- Low Noise Output (amplified shot noise)
- Harmonics Over 30 dB Down
- Long Life
- Bakeable Solenoid (tube bakeout with solenoid power)
- Small Efficiency Change with Temperature
- Control and Protective Electrodes

DISADVANTAGES

- Requires Solenoid and Heater Power
- Requires Phase Control (multiple tube use)
- May Require Tuner Trimming Control
- High Beam Voltage
- Requires Depressed Collector for Highest Efficiency
- Efficiency Somewhat Lower than Crossed-Field Devices

5.3 SUMMARY

Microwave beaming to space and subsequent collection by a spacecraft is not feasible for the beamed energy propulsion concept. Microwave antennas cannot be fabricated with sufficient precision to provide the degree of beam collimation required for the distances involved. With a transmitting antenna based on current technology, the required collector diameter exceeds the limits achievable for a reflecting type antenna. Thus the power will have to be collected by a rectenna microwave to a DC converter whose size is prohibitive for many orbit distances. Furthermore, the power conditioning required to handle the converted DC would greatly increase the system weight and heat rejection.

6. LASER BEAM PROPAGATION

6.1 GENERAL CONSIDERATIONS

Section 4 has discussed the generation of the laser beam and Sections 7 and 8 will discuss the ultimate collection of the laser energy at the spacecraft and the concentration of that radiation for injection into the thruster. The discussion in this section will consider the propagation of that radiation from the beam source to the beam collector.

Two principal features in the laser beam propagation will be emphasized in this section. The first of these is the cross sectional area of the propagating beam as a function of distance from the source. This beam area specifically determines the required collector area at the spacecraft. Also of interest in the collector design (but not to be treated in depth in this present section) is the shape of the beam as it reaches the collector (since propagation effects will cause the beam to assume, on occasion, non-circular cross sections). The second principal feature of the laser beam propagation is the total transmitted energy for a given initial beam energy, as a function of distance along the beam path for the various laser wavelengths of interest and for various beam launching properties (optical aperture and focal length). This total energy content determines the possible thrust level in the laser aided thruster, following beam injection into the thruster and the coupling with the propellant.

It is acknowledged here that many of the parameters of the laser beam propagation will involve specific features of the device utilized. In addition to the laser source itself, these features include the required mirrors and mirror pointing and pointing control systems. The pointing control system for the laser mirror will require a variety of signal inputs including those which allow initial acquisition of the spacecraft and, following acquisition, those which center the laser beam on the collecting surface. The discussion here will not examine these pointing and pointing control systems in detail. The discussion will, however, examine the effects of various levels of angular jitter as that motion acts to require additional collection area for the laser beam.

6.2 OPTICAL DIFFRACTION AND BEAM QUALITY EFFECTS

The spacecraft systems requirements on allowable laser beam collector weight argue for laser beams which possess the minimum possible cross sectional area. That minimum cross section will be derived, for actual beams, from a series of beam quality factors, from the jitter in the mirror pointing system and from broadening effects of laser beam propagation through the atmosphere (considering here that propagation will, more likely than not, involve passage through the atmosphere). The combination of the factors above, with appropriate convolution of the various effects, may be difficult to estimate. It is comparatively straightforward, however, to obtain a lower bound estimate on beam cross sectional area.

The minimum possible beam cross sectional area is that obtained as a result of optical diffraction. For an ideal wavefront of light at wavelength, λ , emerging from an ideal source of diameter, d , an angular divergence in the propagating beam is obtained with a half angle, ψ , of

$$\psi = \frac{1.22\lambda}{d} \quad (5)$$

This half-angle defines that cone which contains .84 of the beam energy and encloses the circular area which extends to the first dark ring of the diffraction pattern.

The diameter of the laser beam from this ideal source of aperture width d and wavelength λ is given by

$$D = 2\psi R = \frac{2(1.22)\lambda R}{d} \quad (6)$$

where R is the distance (range) from the laser to the point of beam diameter D . This equation neglects the finite size of the light source. This finite source size neglect is a valid approximation if $D \gg d$ (i.e. if $2(1.22)\lambda R \gg d^2$).

In order to diminish the beam diameter at distance R , aperture size, d , may be increased and ψ will diminish according to Eq. 5. This direction of system development is clearly indicated as worthwhile

and later sections will utilize values of aperture size which are as that sufficient increases in d may ultimately invalidate the approximation of $2(1.22)\lambda R \gg d^2$, and finite source size must then be taken into account in calculations of the diameter of this ideal (diffraction limited only) beam.

For actual beams a series of beam quality factors, including phase coherence and frequency purity, will create additional beam spreading. A convenient descriptive term for such additional spreading is the beam n value. The n value of the beam is determined by that area required to encompass 0.84 of the beam energy compared to that area required to encompass this same energy fraction for an ideal (diffraction limited) beam. For $n = 2$ this area is doubled, (relative to an ideal beam), and beam diameter, D , has increased by $\sqrt{2}$ from its value for an ideal beam. For this practical beam

$$\begin{aligned}\psi &= \frac{1.22\sqrt{n} \lambda}{d} \\ &= \frac{1.22\sqrt{2} \lambda}{d}\end{aligned}\tag{7}$$

is the appropriate half-angle expression.

Figure 35 illustrates values of the far-field half angle of the beam as a function of wavelength, λ , aperture size, d , and beam quality, n . The value of n has been allowed to range from unity to 2.7, this latter figure being a considered state of laser optical development.

The significant feature in Figure 35 is that for systems utilizing current laser wavelengths (of the order of several microns) and for present possible aperture sizes (several meters), characteristic far-field half-angle values will be approximately 5 microradians and that total beam angles will be, characteristically, 10 microradians, considering here only the limitations of diffraction and beam quality. This 10 μ radian total beam divergence angle has significant implications in terms of required collector size and allowable range which will be discussed in the following section.

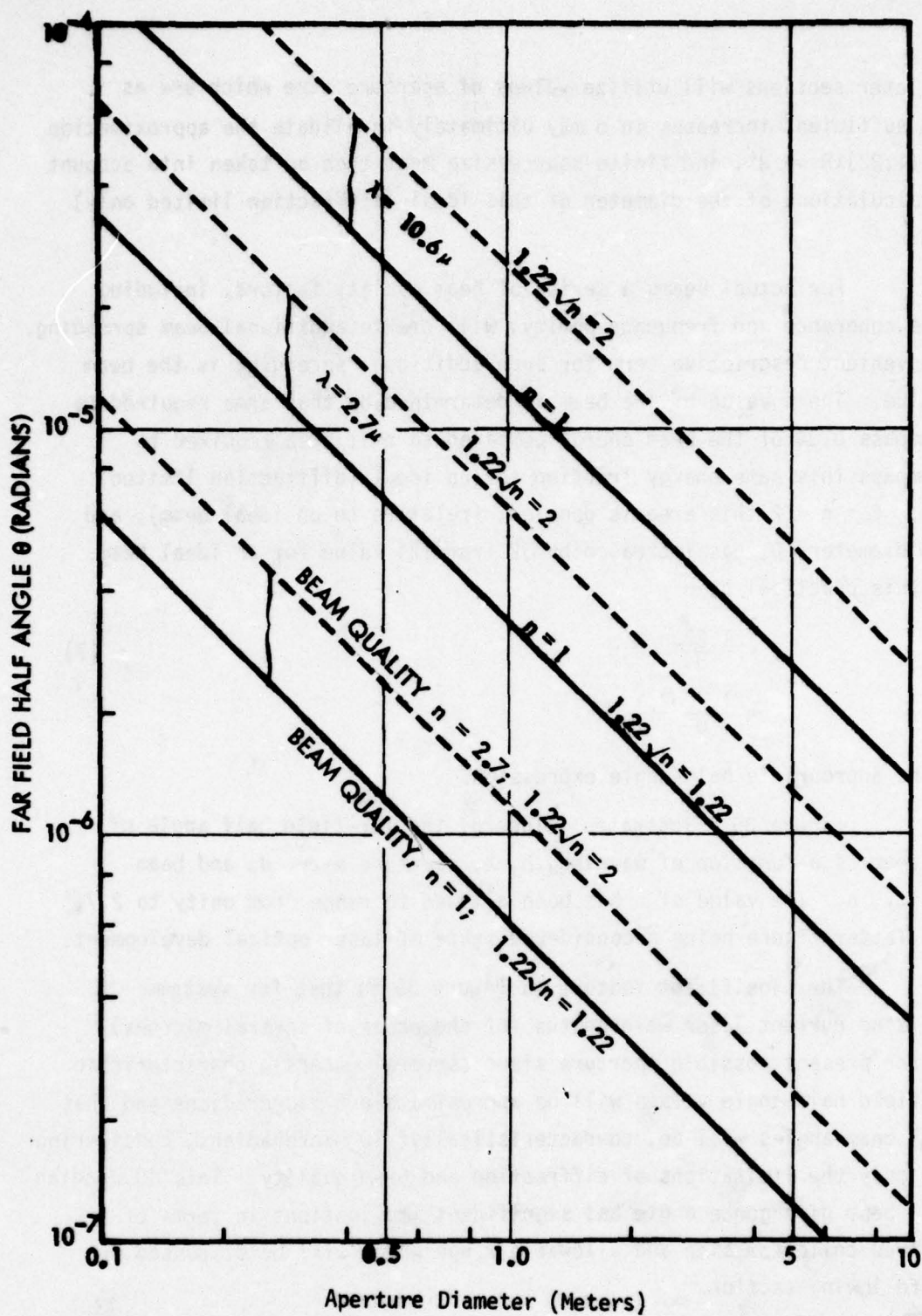


Figure 35. Far field half angle versus aperture size for various wavelengths (corresponding to the wavelengths produced by various common lasers) and for two levels of beam quality. Far field half angle calculated for a circular aperture on the source.

6.3 LASER-TO-TARGET RANGE EFFECTS AND REQUIRED COLLECTOR SIZE

The laser beam collector must possess a target half-angle which, at the very least, exceeds ψ . Figure 36 illustrates the target half-angle of a series of targets of various diameters for ranges of from 10^3 kilometers to 10^5 kilometers. Also indicated on Figure 36 are the ranges encountered in six reference missions of this study.

Examining Figure 36 and utilizing the results of the previous section of minimum practicable beam half angles of approximately 5 μ radians leads immediately to a conclusion that location of the target at geosynchronous altitudes (Missions 2, 3, and 4) will require beam collectors of several hundred meters in diameter. These collector sizes have been considered impractically large, and emphasis in the discussion to follow will be directed increasingly toward those missions involving smaller maximum ranges. From Figure 36, it would appear that practically sized collectors (of the order of 10 meters in diameter) can be employed to ranges of approximately 1000 kilometers. It should be emphasized, however, that the calculations of Figure 36, and the results of Figure 35 have been for diffraction limited beams, propagating in the absence of both an atmosphere and perturbation jitter in the transmitter. The inclusion of these factors in the sections to follow will result in increased beam spreading and increased requirements on laser beam collection area.

6.4 TRANSMITTER JITTER BEAM BROADENING

Transmitter jitter for currently operating systems includes a specification for both low frequency and high frequency movement. In this section, and for the qualitative discussion to be given here, a separation of specifications will not be made. This discussion will consider various levels of " 2σ " jitter where the 2σ notation indicates that the center axis of the laser beam will remain (for 95% of the time) within a cone whose half angle is $\theta_{2\sigma}$. Figure 37 illustrates the increase which this jitter imposes on required diameter of the laser beam collector as a function of range, from 10^3 to 10^5 kilometers, and for $\theta_{2\sigma}$ from 10^{-5} to 10^{-8} radians. From previous considerations of beam diffraction, operation at geosynchronous altitudes had been considered to require impractically large collectors. These considerations remain

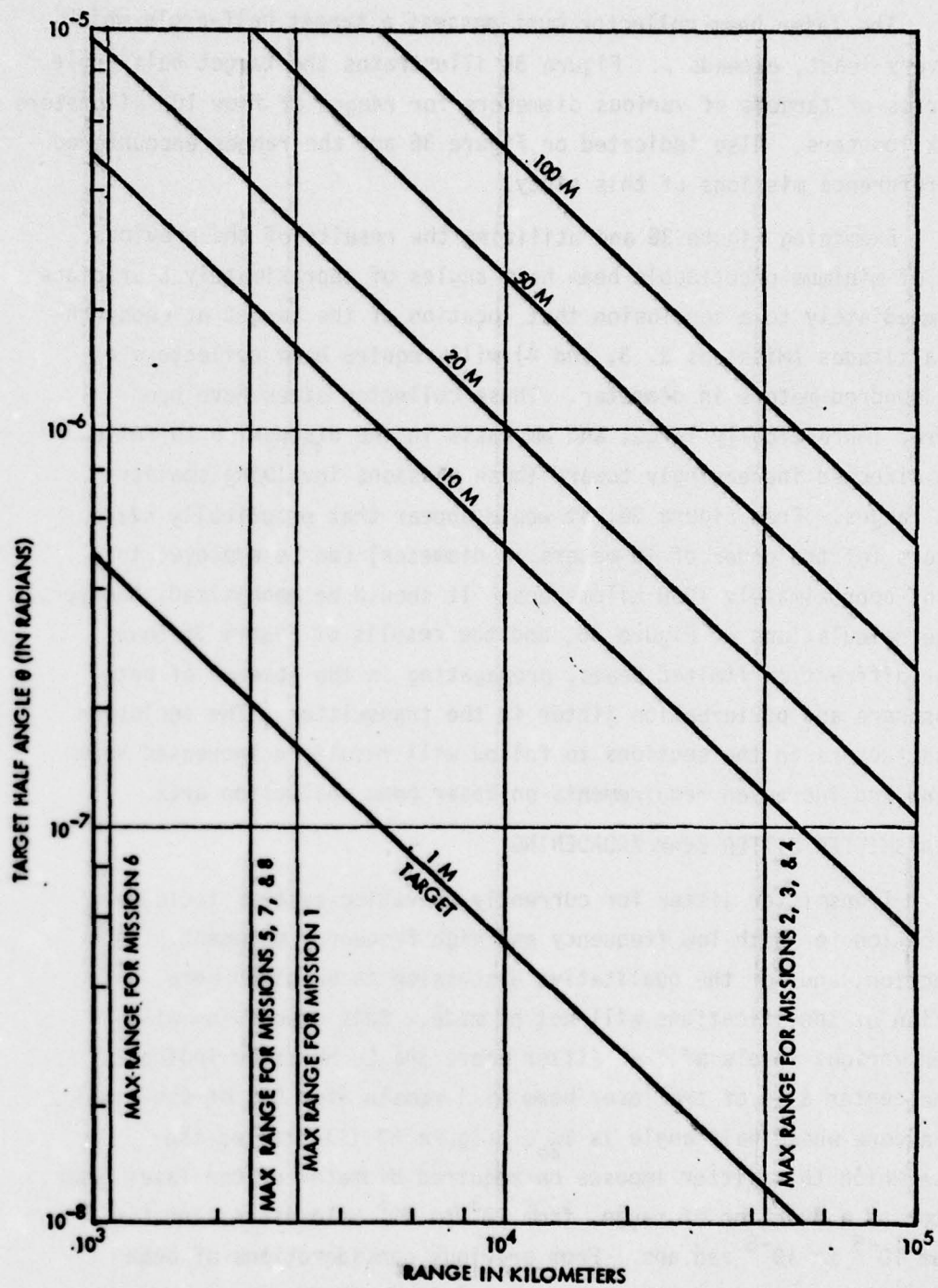


Figure 36. Target Half Angle versus Range for Various Sized Target Diameters

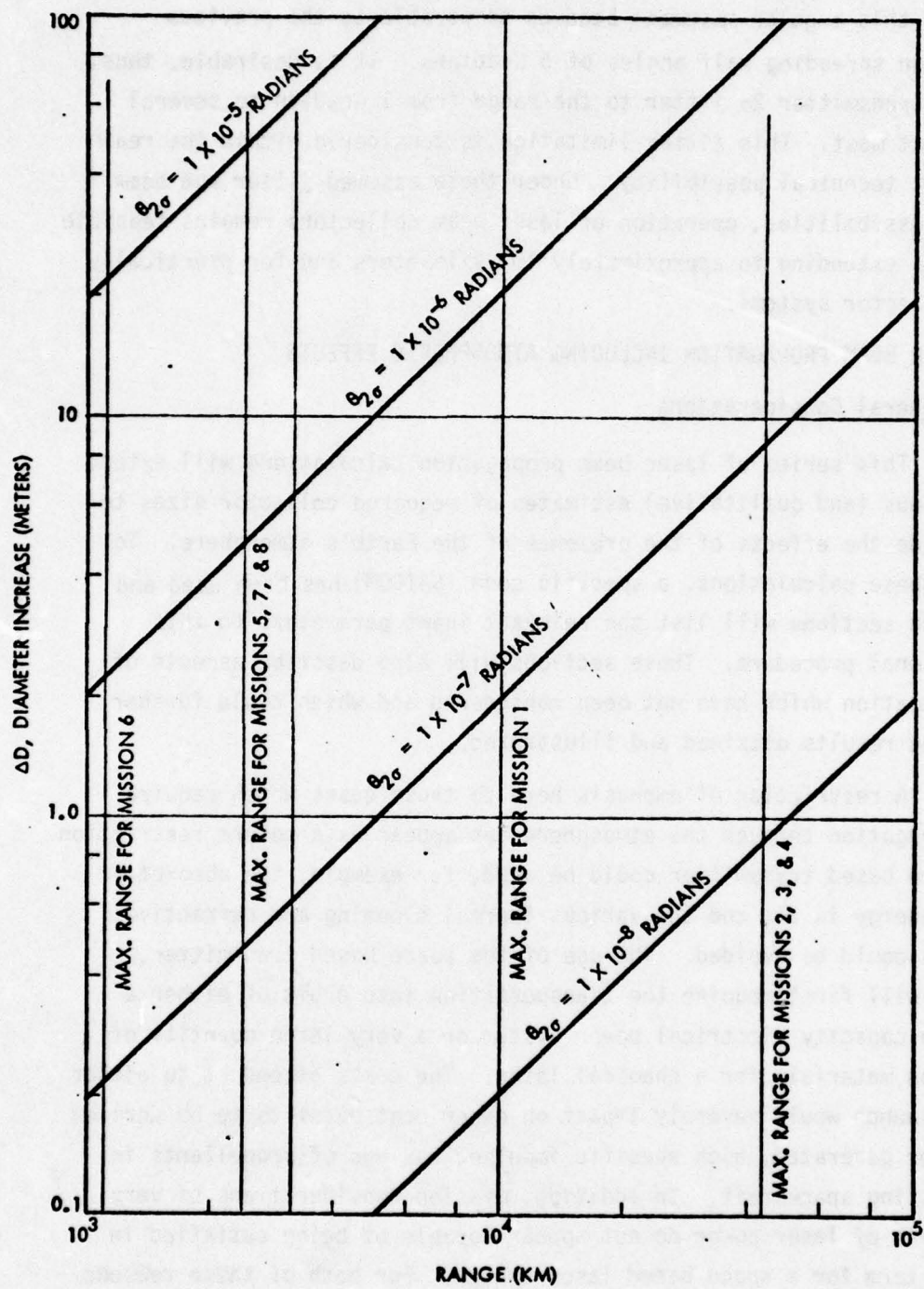


Figure 37. Diameter Increase Due to Jitter versus Range for Various Levels of 2σ Jitter

valid, since jitter cannot alleviate these previous beam broadening problems. System jitter can however, impact on the spacecraft collector system if this angular movement becomes comparable to the previous diffraction spreading half angles of 5 μ radians. It is desirable, thus, to limit transmitter 2σ jitter to the range from 1 μ radian to several μ radians at most. This jitter limitation is considered within the realm of current technical possibility. Under these assumed jitter and beam quality possibilities, operation of laser beam collectors remains feasible for ranges extending to approximately 10^3 kilometers and for practically sized collector systems.

6.5 LASER BEAM PROPAGATION INCLUDING ATMOSPHERIC EFFECTS

6.5.1 General Considerations

This series of laser beam propagation calculations will extend the previous (and qualitative) estimates of required collector sizes to now include the effects of the presence of the Earth's atmosphere. To perform these calculations, a specific code (SAICOM) has been used and subsequent sections will list the relevant input parameters to this calculational procedure. Those sections will also describe aspects of the propagation which have not been considered and which could further modify the results obtained and illustrated.

A restriction of emphasis here to those cases which require beam propagation through the atmosphere can appear as a severe restriction. If a space based transmitter could be used, for example, the absorption of beam energy in air and the various thermal blooming and refractive processes could be avoided. The use of the space based transmitter, however, will first require the transportation into orbit of either a very high capacity electrical power system or a very large quantity of combustion materials for a chemical laser. The costs attendant to either form of launch would severely impact on other cost benefits to be derived from laser generated, high specific impulse, savings of propellants in the thrusting spacecraft. In addition, mission considerations of very high levels of laser power do not appear capable of being satisfied in the near term for a space based laser system. For both of these reasons

further discussion of this transmitter location restriction are given in other portions of this report, emphasis will be restricted in this section to transmitters at or near sea level.

A second general restriction in emphasis will be made upon the altitude of the receiver spacecraft orbit at the time of radiation reception. Although some of the calculated values will extend to collectors at geosynchronous altitudes, the major emphasis of this section will be given to collectors at altitudes of 75 nautical miles and 100 nautical miles (190 kilometers). This emphasis in receiver altitude follows from the findings earlier in this section of impractically large required receiver areas for range values in excess of 1000 kilometers.

6.5.2 Range and Slue Rate Calculations

Required inputs for the SAICOM propagation code calculations are the range from the transmitter to the receiver and the slue rate of the path joining these two points. These quantities are illustrated in Figures 38, 39, 40, and 41 for collector altitudes of 75 and 100 NM and transmitter altitudes of 0, 12 kilofeet, and 40 kilofeet. These calculations have assumed a coplanar laser and receiver. Figures 38 and 39 illustrate these ranges, in meters, as a function of orbital arc separation in degrees. From the curves illustrated there it may be seen that ranges in excess of 10^6 meters (10^3 kilometers) occur for orbital arc separations in excess of approximately 8° . Since 10^3 kilometers appeared earlier as a range limitation for practically sized collectors, it would appear that transmission of laser radiation to the spacecraft would be limited from practical considerations to total orbital arcs of approximately 16° . In subsequent calculations in this section additional limitations on total orbital arc will be encountered.

Figures 40 and 41 illustrate the slue rates, in radians per second, of the lines joining the laser to the laser collector. Motion of the source is not present for the 0 and 12 kilofeet level. Source motion for the 40 kilofeet level (aircraft based) is present but is not significant. The principal area of significance in the illustrated slue rate calculations is the low levels of rate (of the order of 10^{-3} radians/second) for orbital arc separations of approximately 8° . These

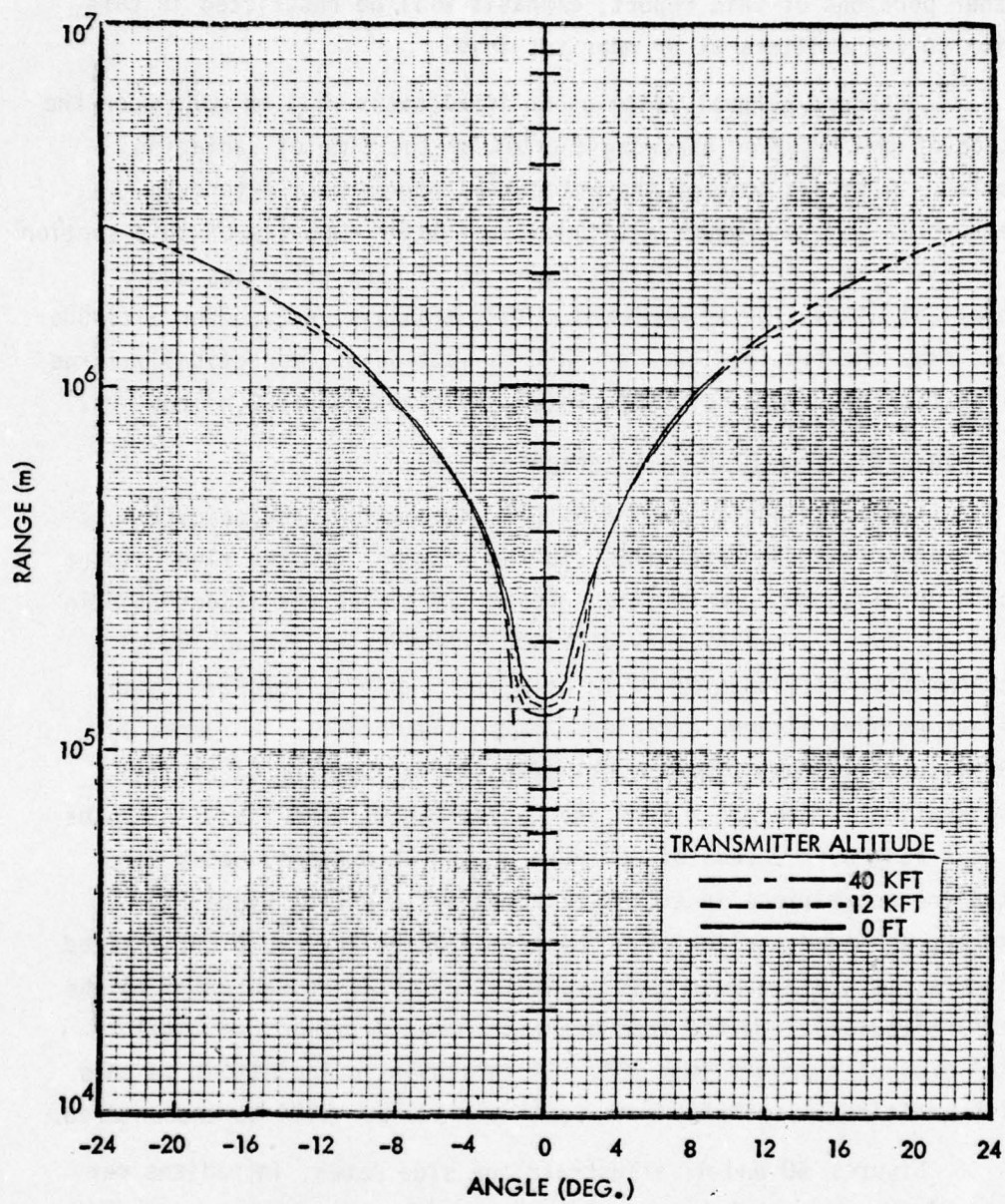


Figure 38. Instantaneous Range for Collector Altitude of 75 nm

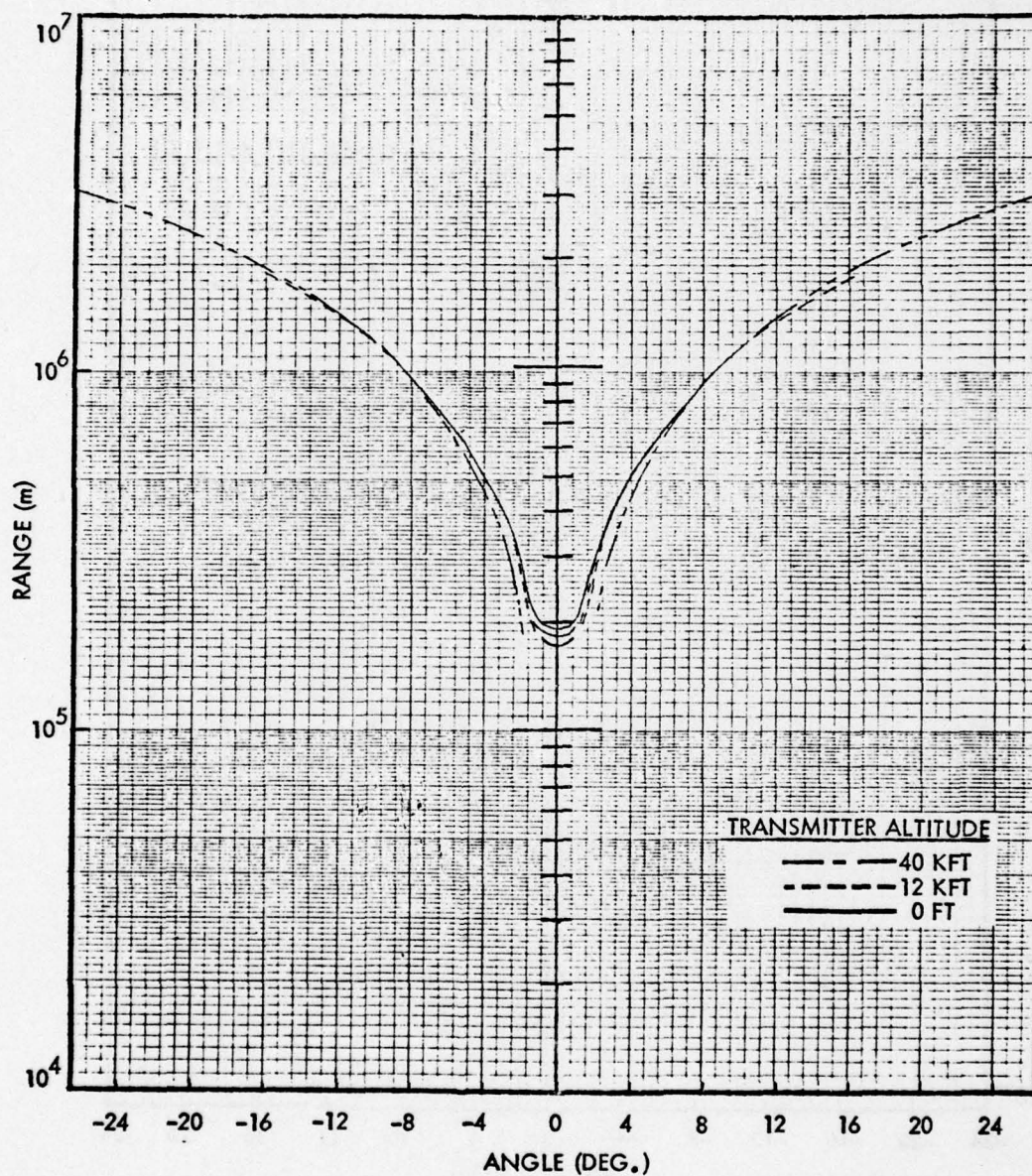


Figure 39. Instantaneous Range for Collector Altitude of 100 nm

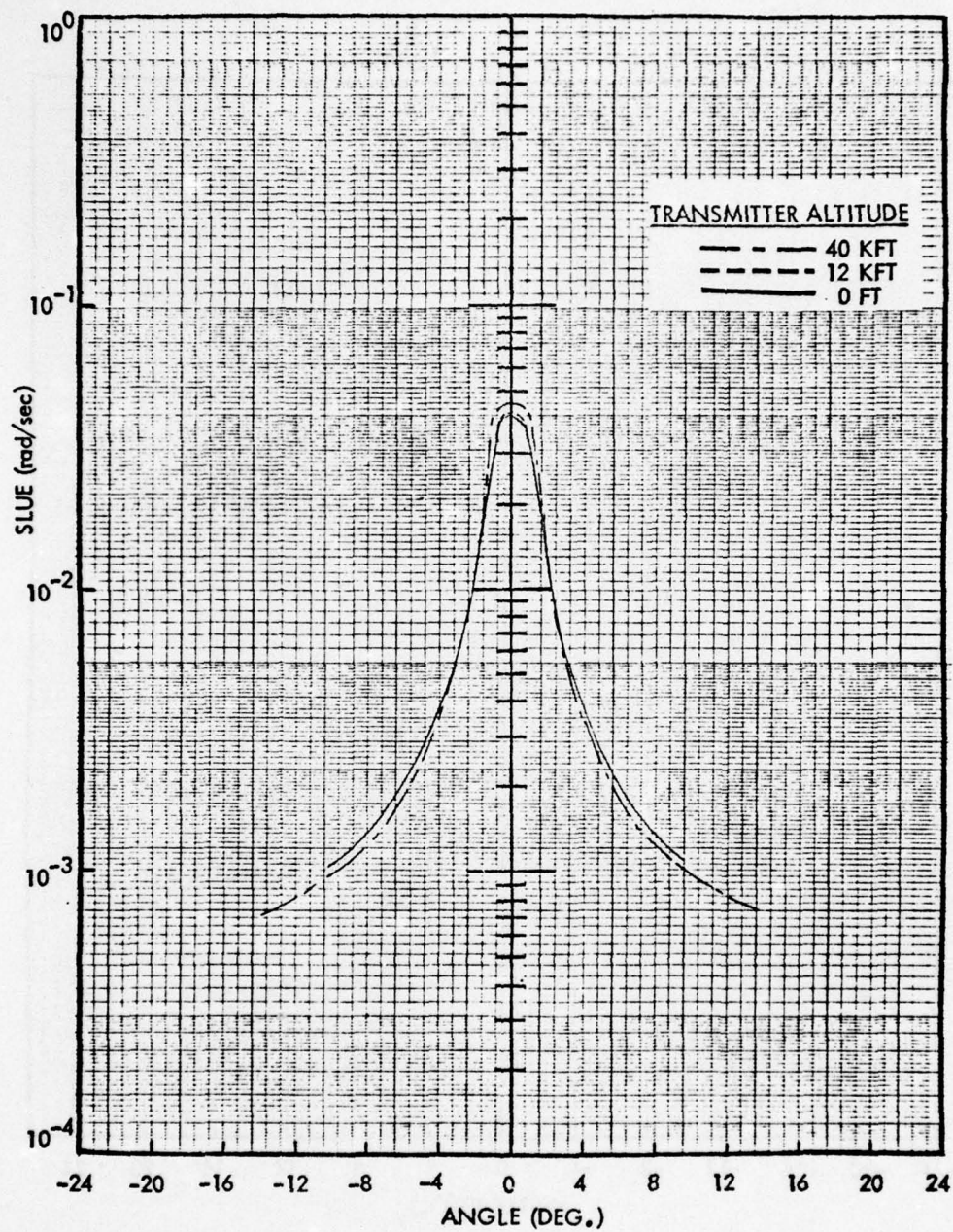


Figure 40. Slue Rates for 75 nm Collector Altitude

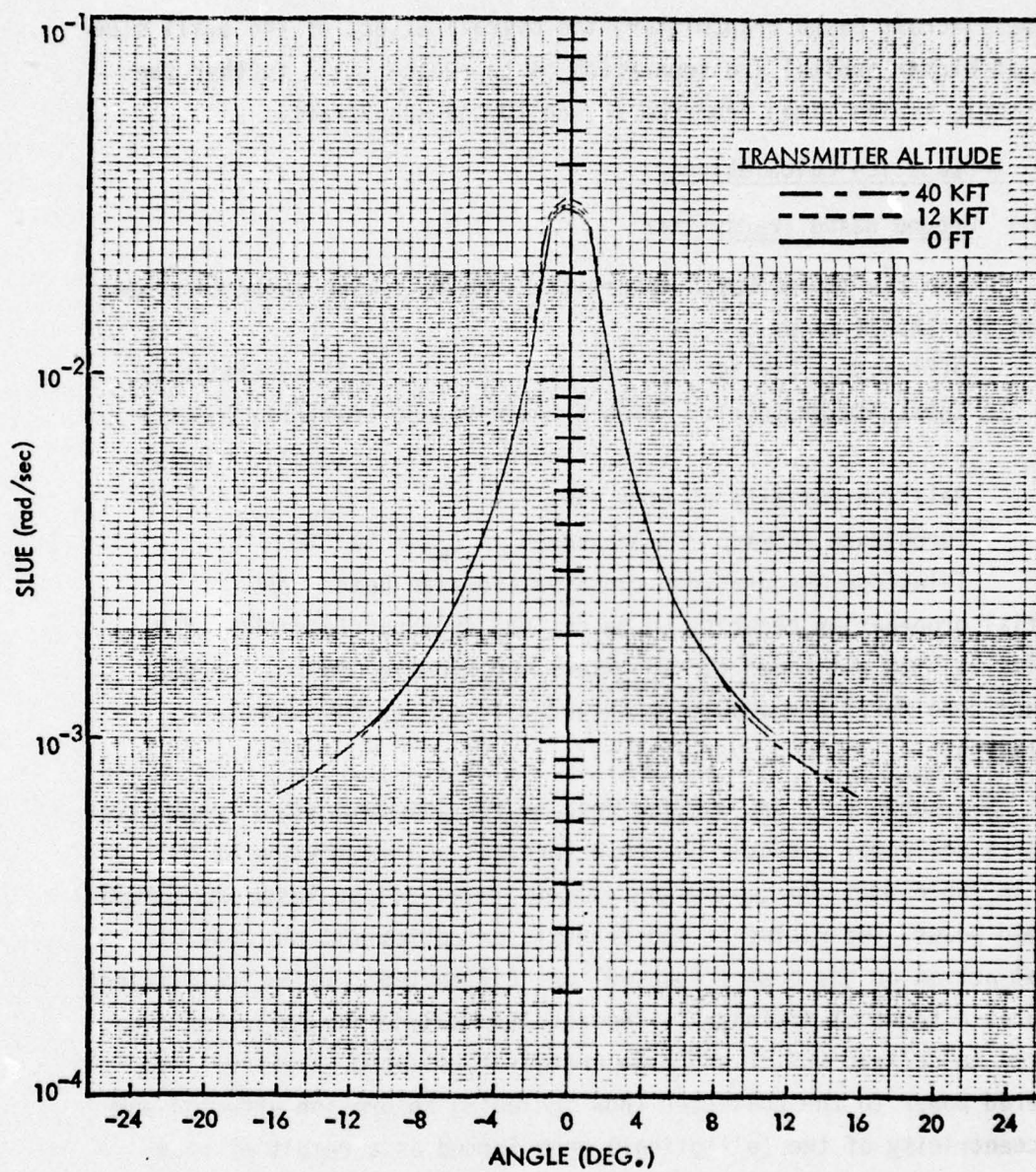


Figure 41. Slue Rates for 100 nm Collector Altitude

low slue rates lead to prolonged irradiation of the ambient air and enhanced thermal blooming beam broadening, and, although some alleviation of these thermal blooming effects is provided by source motion for the aircraft based transmitter, the overall effect of the small slue rates at higher orbital arc separation is to reduce still further the permissible firing times from the source to the spacecraft.

6.5.3 Propagation Calculations

6.5.3.1 Ground Based Transmitter

For the ground based transmitter the following parameters were used in the SAICOM code:

Diffraction Limited Performance: $n = 1.3$ (all wavelengths)

Total Jitter Level: (High Frequency) $0.5 \mu\text{rad}$ (1σ , 1 axis)
(Low Frequency) $0.5 \mu\text{rad}$ (1σ , 1 axis)

Relative Humidity of Air: 50%

Turbulence (Nominal at Sea Level): $C_N^2 = 10^{-13} M^{-2/3}$

Telescope Obscuration Truncated Gaussian Beam: 23%.

Potential propagation benefits to be derived from consideration of N_2 kinetics at high altitudes for DF lasers and kinetic cooling for CO_2 were not considered and should be included in other, more complete, calculations.

A summary of propagation results for a ground based transmitter and for a collector directly overhead (orbital arc separation of 0°) is given in Table 43. The parameters varied there include laser wavelength, launched power, the radius of the transmitter optics and the mode of optical action on the beam ("focused" or "collimated", where "collimated" indicates a focus at infinity). The results include the collector area required to collect 80% of the beam energy at collector altitude, the delivered power to the collector (now including absorption effects) and the eccentricity of the (elliptical) beam formed as a result of beam passage through the atmosphere (NOTE: orientation of the beam ellipse is with the ellipse major axis perpendicular to the direction of motion of the beam as it follows the laser collector. This orientation will be of interest in the ultimate design and fabrication of the laser beam collector).

Table 43. Parametric Results for Ground Base (Sea Level)
Transmitter Directed at Overhead Collector

TRANSMITTER							
COLLECTOR ALTITUDE (NM)	LASER TYPE	BEAM TYPE	OPTICS RADIUS (m)	COLLECTOR AREA (m ²)	ECCENTRICITY OF SPOT	DELIVERED POWER (MW)	LAUNCHED POWER (MW)
75	DF	FOCUSED	5.0	10.159	1.0	5.87	10.0
100	DF	FOCUSED	5.0	18.061	1.0	5.87	10.0
1.932E4	DF	FOCUSED	5.0	67.4E4	1.0	5.87	10.0
75	DF	FOCUSED	5.0	10.159	1.0	7.04	12.0
100	DF	FOCUSED	5.0	18.061	1.0	7.04	12.0
1.932E4	DF	FOCUSED	5.0	67.4E4	1.0	7.04	12.0
75	DF	FOCUSED	2.5	12.63	.865	7.04	12.0
100	DF	FOCUSED	2.5	21.59	.887	7.04	12.0
1.932E4	DF	FOCUSED	2.5	75.6E4	.927	7.04	12.0
75	HF	FOCUSED	5.0	16.934	.722	2.34	10.0
100	HF	FOCUSED	5.0	28.060	.753	2.34	10.0
1.932E4	HF	FOCUSED	5.0	89.0E4	.833	2.34	10.0
75	DF	COLLIM	5.0	10.159	1.0	11.73	20.0
100	DF	COLLIM	5.0	18.061	1.0	11.73	20.0
1.932E4	DF	COLLIM	5.0	67.4E4	1.0	11.73	20.0
75	DF	COLLIM	5.0	10.159	1.0	5.87	10.0
100	DF	COLLIM	5.0	18.062	1.0	5.87	10.0
1.932E4	DF	COLLIM	5.0	67.4E4	1.0	5.87	10.0
75	DF	COLLIM	2.5	14.89	.779	5.87	10.0
100	DF	COLLIM	2.5	26.47	.779	5.87	10.0
1.932E4	DF	COLLIM	2.5	98.84E	.779	5.87	10.0
75	CO	FOCUSED	2.5	18.159	.592	6.46	12.0
100	CO	FOCUSED	2.5	30.667	.713	6.46	12.0
1.932E4	CO	FOCUSED	2.5	10.1E5	.770	6.46	12.0
75	CO ₂	FOCUSED	2.5	21.432	.637	3.64	12.0
100	CO ₂	FOCUSED	2.5	35.137	.665	3.64	12.0
1.932E4	CO ₂	FOCUSED	2.5	11.48E5	.717	3.64	12.0

Several conclusions may be drawn from the calculations. The first of these is that collector size is well within the limits of practicality for collectors at 75 and 100 NM. For collectors at geosynchronous altitude the resultant collector sizes are, as previously concluded, well beyond present practical limits.

A second conclusion is that the benefits of the use of a focused beam, in preference to a collimated beam, are small for those systems using the 2.5 meter radius optics and have been eliminated at the larger, 5.0 meter radius, aperture size.

The transmission of HF laser radiation is not effective (2.34 megawatts incident on 16.9 square meters of collector at 75 NM altitude for 10.0 megawatts of launched power). DF laser radiation, on the other hand is transmitted effectively (5.87 MW incident on 10.1 m^2 for 75 NM collection and 10.0 MW launched). The CO laser radiation is approximately at the same fractional power transfer as DF but has required an increase in collector size (for the 75 NM case) to 18.1 m^2 . The CO₂ laser radiation transmitted to 21.4 m^2 is 3.64 MW for 12.0 MW launched and 75 NM collection.

These results were obtained with the SAICOM code as described in Peckham, L.N. et al, "Propagation Modeling and Analysis for High Energy Lasers," SAI-74-629-WA; and Simas, R., "Report on Modification to SAICOM," SAI-76-514-WA, 1976. These publications also discuss the absorption data on which these calculations are based. The 2.7 micron HF absorption coefficients are based on a five line approximation, the 3.8 micron DF is calculated for a three line approximation, the 10.6 micron CO₂ is calculated for a one line approximation. The CO₂ calculations did not take into account kinetic cooling which if included would have resulted in decreased CO₂ blooming.

The CO absorption was based on McClatchey's data (AFCRL-71-0279, "Optical Properties of the Atmosphere," 10 May 1971 and AFCRL-71-0370, "Atmospheric Attenuation of CO Laser Radiation," 1 July 1971) for a single CO "typical" line. The chosen line is the P15 transition in the 5 → 4 band; this corresponds to a wavelength of 5.05 microns. The calculation assumes there has been some line selection to reduce the effects of highly

absorbing CO laser lines. This has not yet been achieved in practice and therefore the true atmospheric absorption for future CO lasers may be significantly higher. For the SAICOM code McClatchey's absorption coefficients are converted to the following empirical function of water vapor partial pressure (P_W):

$$\alpha_A = 1.5 \times 10^{-3} (P_W)^a e^b \quad m^{-1}$$

where:

$$a = 1.9222$$

$$b = 1.4032$$

$$\text{for } P_W \leq 4.5 \times 10^{-4} \text{ torr}$$

$$\text{and } a = 1.14256$$

$$b = -4.605$$

$$\text{for } P_W > 4.5 \times 10^{-4} \text{ torr}$$

Of the several laser wavelengths considered, the best performance has been obtained with DF. As noted earlier, consideration of N_2 kinetics at high altitude will provide additional propagation benefits for the DF laser. Additional propagation benefits are also anticipated for the CO_2 laser when kinetic cooling effects are included in the propagation calculations.

Figures 42 and 43 illustrate the results of more general propagation calculations. In Figure 42, a DF laser at sea level and with 2.5 meter diameter optics is directed against a collector at 75 NM altitude. Given there is the required collector area (in meter²) to collect 80% of the power at altitude, the delivered power and launched power and the laser beam eccentricity at the collector. These values are given as a function of orbital arc separation. Figure 43 repeats these calculations with the laser unchanged and the collector orbital altitude increased to 100 NM.

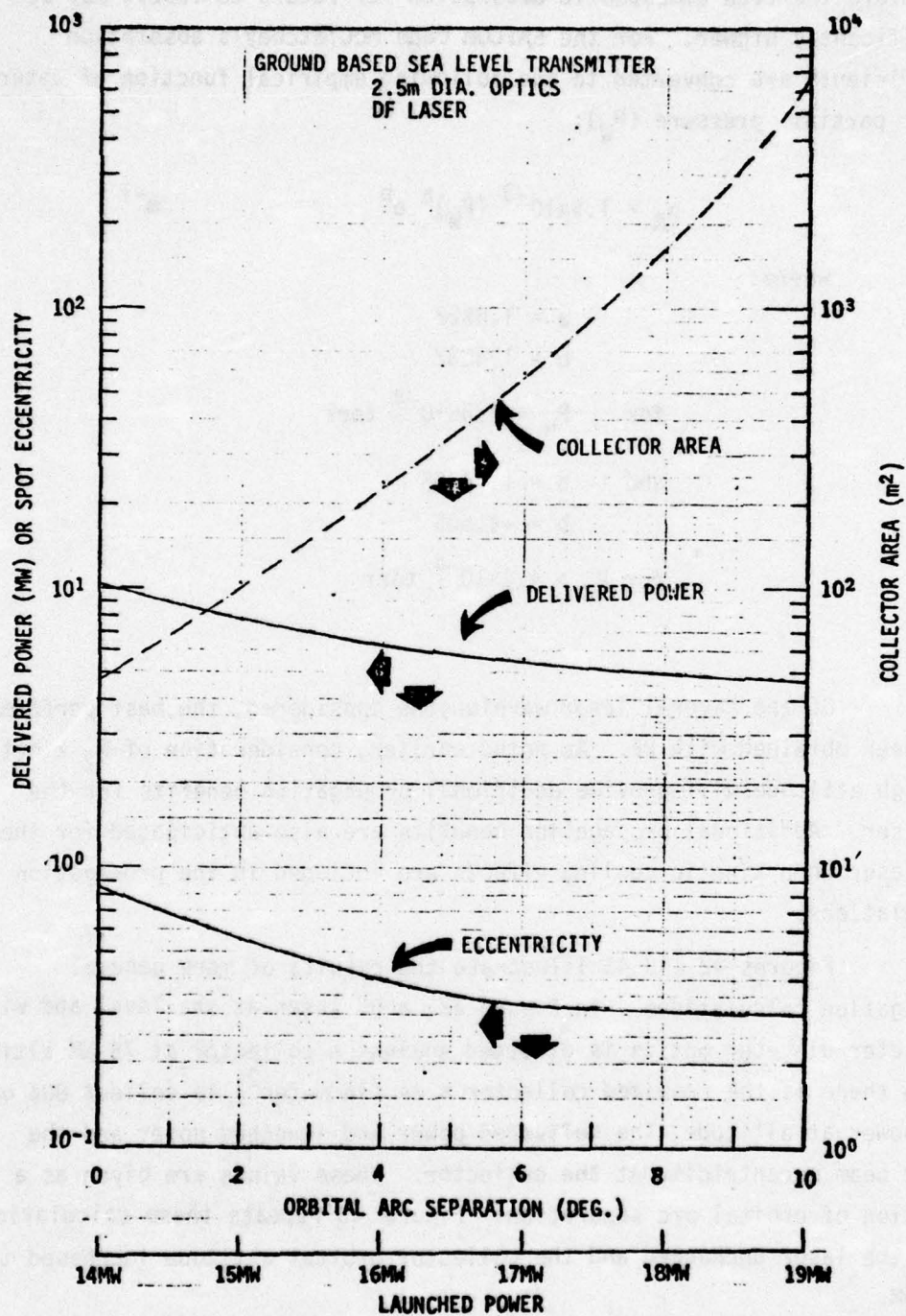


Figure 42. Power Variation for 75 nm Collector Altitude

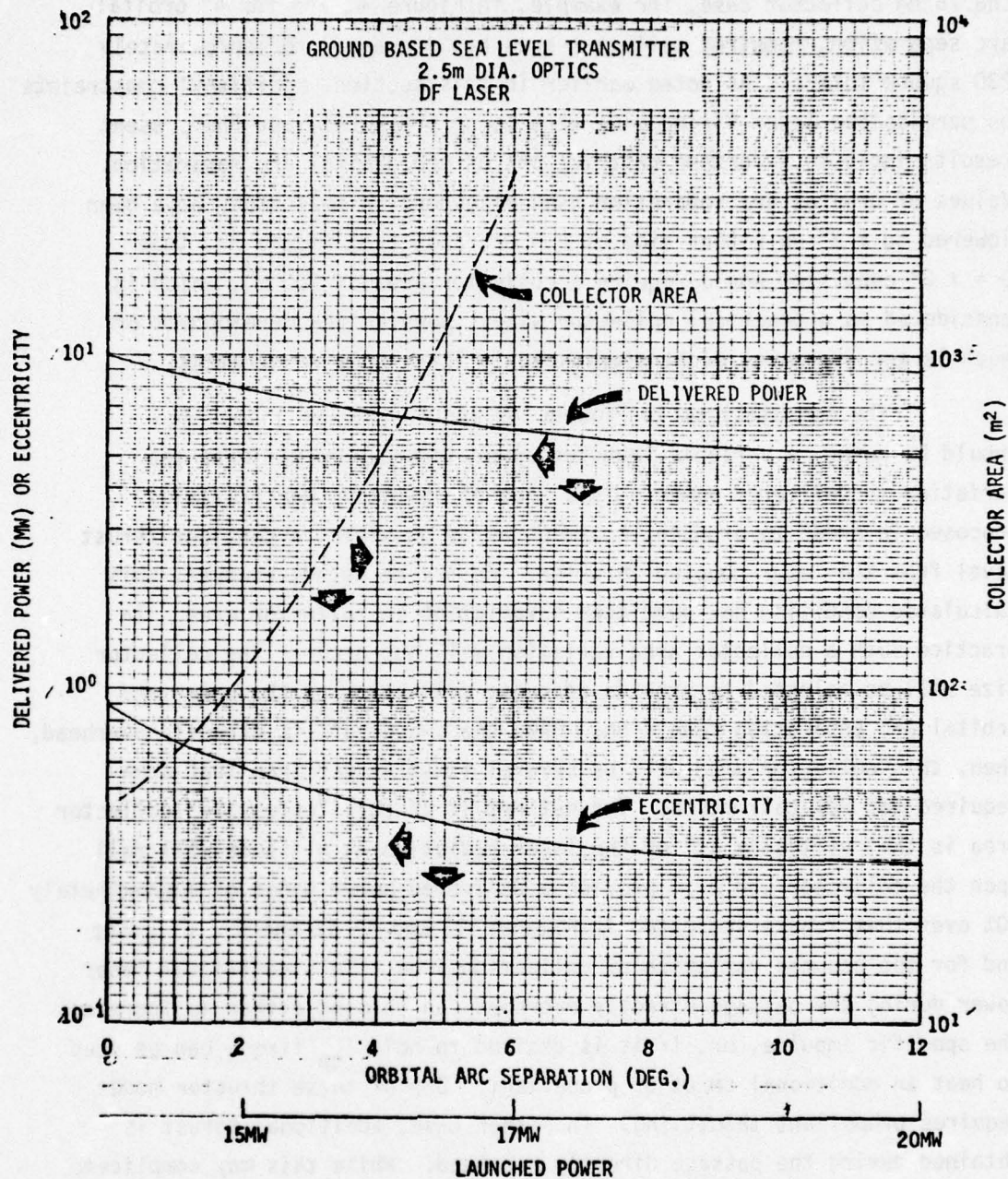


Figure 43. Power Variation for 100 nm Collector Altitude

The principal feature of the calculations given in Figures 42 and 43 is the rapid increase in the required area of the collector. For the 75 NM collector case, for example, in Figure 42 and for 4° orbital arc separation, required collector area has increased to approximately 230 square meters. As noted earlier in this section, additional constraints on permissible laser firing time were to be presented, and the present results imply such further restrictions on the orbital arc separation. Values of orbital arc separation used elsewhere in this study have been lowered to $\pm 2^\circ$ on either side of $\theta = 0^\circ$, and, from Figure 42, this $\theta = \pm 2^\circ$ condition would require a collector area of 100 m^2 , which is considered as a practical collector size. However the development of much larger apertures might significantly lower this requirement.

The computations in Figures 42 and 43 have utilized, it should be noted, a variable launched power in order to minimize the variation in delivered power. This mode of operation was initially proposed in order to produce, inasmuch as is possible, a constant thrust level from the laser coupled thruster. As may be noted, however, this calculated condition has permitted a variation in collector area. In practice such a collector area variation will not occur. The collector size will be selected to provide adequate collection at the upper end orbital arc separation condition. When the spacecraft is directly overhead, then, this collector area will be several times larger than that area required for 80% collection. The net result of this "excessive" collector area is that virtually all of the laser radiation at altitude will fall upon the collector and will provide a delivered power boost of approximately 20% over that figure indicated in Figures 42 and 43 at the $\theta = 0^\circ$ point and for the assumed variation of collection area. This additional laser power during the passage directly overhead can be used either to increase the specific impulse, or, if it is desired to hold I_{sp} fixed, can be used to heat an additional dM/dt of propellant. One of these thruster modes requires propellant throttling. In either case, additional thrust is obtained during the passage directly overhead. While this may complicate the orbital calculations somewhat, it is not considered as a significant

problem, and, if experience should indicate a more serious orbital software problem than considered here, then the laser launched power should be diminished further during passage directly overhead.

One final consideration as a result of beam size changes during flyover is that the laser beam power density on the collector will change significantly and the collector design should be examined to insure against an excessive heat input into specific regions of the collector at the periods of smallest beam size. This problem can be alleviated, if necessary, by a pullback of laser launched power during direct overhead passage.

6.5.3.2 Aircraft Based Transmitter

The SAICOM code inputs for the case of the aircraft based transmitter are the same as given at the beginning of Section 6.5.3.1. In addition, an aircraft ground speed of 220 meters/second has been utilized in the code.

Table 44 provides a series of calculated results for a focused DF laser utilizing transmitter optics of .5 m and 1.0 m radius, and for collectors at a position directly overhead and at 75 NM, 100 NM, and geosynchronous altitudes.

Table 44. Parametric Results for Aircraft Based Transmitter Directed at Overhead Collector

TRANSMITTER							
COLLECTOR ALTITUDE (NM)	LASER TYPE	BEAM TYPE	OPTICS RADIUS (m)	COLLECTOR AREA (m ²)	ECCENTRICITY OF SPOT	DELIVERED POWER (MW)	LAUNCHED POWER (MW)
75	DF	FOCUSED	0.5	8.96	1.0	6.2	9.0
100	DF	FOCUSED	0.5	16.71	1.0	6.2	9.0
1.932E4	DF	FOCUSED	0.5	30.61E5	.679	5.16	9.0
75	DF	FOCUSED	1.0	8.36	1.0	3.45	5.0
100	DF	FOCUSED	1.0	15.59	1.0	3.45	5.0
1.932E4	DF	FOCUSED	1.0	17.62E5	.939	2.87	5.0

The results of the DF laser calculations in Table 44 are of particular interest in that the motion of the source has produced a substantial lessening of thermal blooming effects. As a result, only 8.96 m^2 of collector area is required to collect 6.2 MW of the 9.0 MW launched power for the 0.5 meter radius optics. The increase in optics radius to 1.0 meter causes a minor reduction in required collection area to 8.36 m^2 .

Figures 44 and 45 illustrate the results of the more generalized propagation calculations. The quantities shown there are those described earlier for Figures 42 and 43 for the sea-level transmitter except that in the present case the (DF) laser is airborne and possesses a 1.0 meter diameter optics. If the orbital arc separation is not permitted above 2° , then required collector area remains below 40 m^2 . The selection of the collector size will result in an "appropriate" collector at the orbital arc separation end points and an "excessive" area collector at $\theta = 0^\circ$. The considerations here on thruster throttling and resultant thrust variability during the passage are the same as discussed earlier in Section 6.5.3.1, and reference is made to that discussion.

6.6 SUMMARY

This section will not attempt to present, in re-summary, all of the propagation calculation results discussed and summarized in earlier sections. Reference is made to those sections. The principal point in summary here is that a variety of beam broadening factors generally eliminate from consideration the location of the laser collector at very high altitudes, such as geosynchronous. The study has found, however, that spacecraft passage at lower altitudes (examples considered: 75 NM and 100 NM) do not require inordinately sized collectors and do provide a reasonable period of laser transmission. The most promising results have been obtained with a DF laser, with additional propagation benefits having been produced for an airborne transmitter system as compared to the ground based transmitter system. It is acknowledged that many other cost considerations will be present in a laser base condition selection in addition to these propagation benefits.

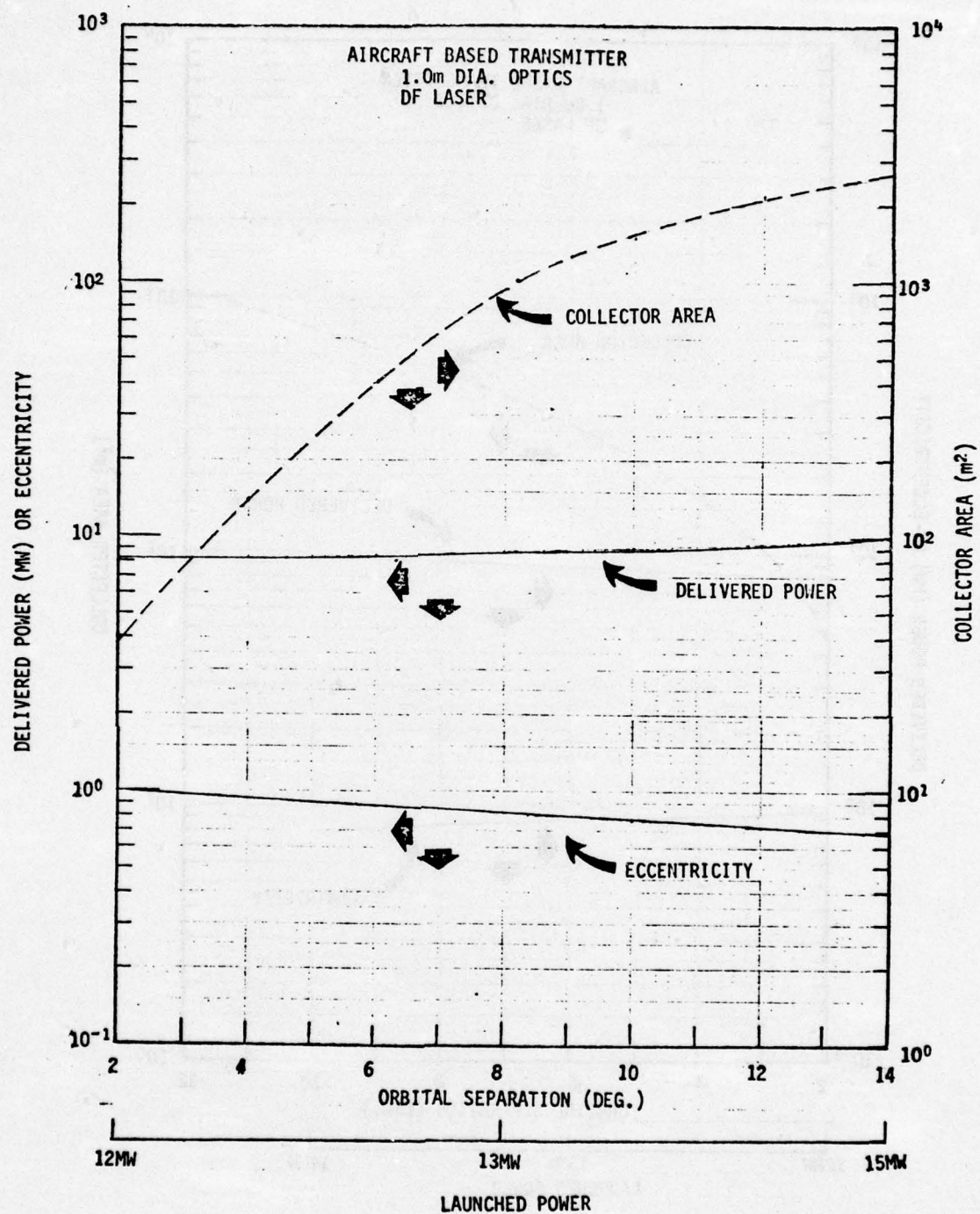


Figure 44. Power Variation for 75 nm Collector Altitude

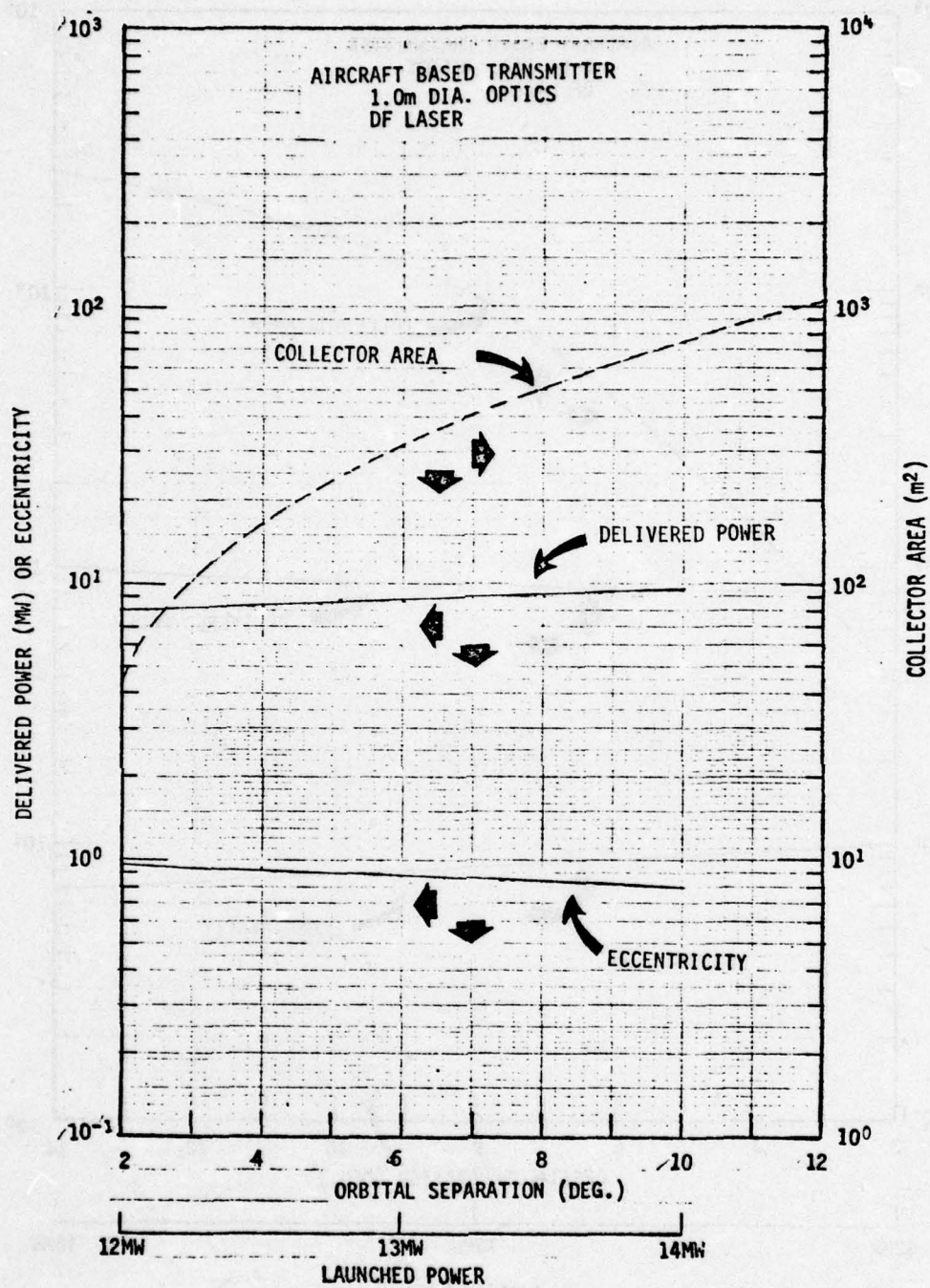


Figure 45. Power Variation for 100 nm Collector Altitude

7. LASER RECEIVER SYSTEM

7.1 SYSTEM COMPONENTS

The laser receiver system causes incoming laser energy to be directed into the thrust chamber, where absorption of laser energy in the propellant material causes increases in propellant temperature and (following release) in specific impulse. Since the scale size of the thruster will be small, in general, compared to the width of the laser beam at representative spacecraft altitudes, a concentrator will be required. A second requirement will be for a window through which laser radiation passes on its way into the thruster and which prevents the propellant gas from escaping in the non-thrust direction. This second requirement assumes that laser energy will not be coupled into the propellant by entry through the thruster exhaust.

The simplest form of a laser receiver would consist, in principle, of a concentrator, a window, a thruster, and alignment and attitude control sensors and devices in order to keep the concentrated laser beam directed through the window. In some portions of the discussion in this section, such simplified systems will be utilized in order to estimate certain aspects of system performance. In practice, however, a more complicated system may be required because of generally varying orientations between the incoming laser beam direction and the direction of propellant release by the thruster. These more complicated and more realistic systems will employ a mirror, a concentrator, and a thruster, along with appropriate attitude control and sensing devices.

Figures 46 and 47 illustrate two versions of this mirror/concentrator/thruster system, entitled an f_1 and an f_2 system because of the ratio of concentrator focal length to concentrator diameter. The inclusion of the figures in this introductory section is for convenience. Other and later sections will describe elements of this total system in further detail.

7.2 GENERAL SCALE SIZE

The scale size in the laser receiver system will be determined primarily by the width of the laser beam (including pointing and tracking

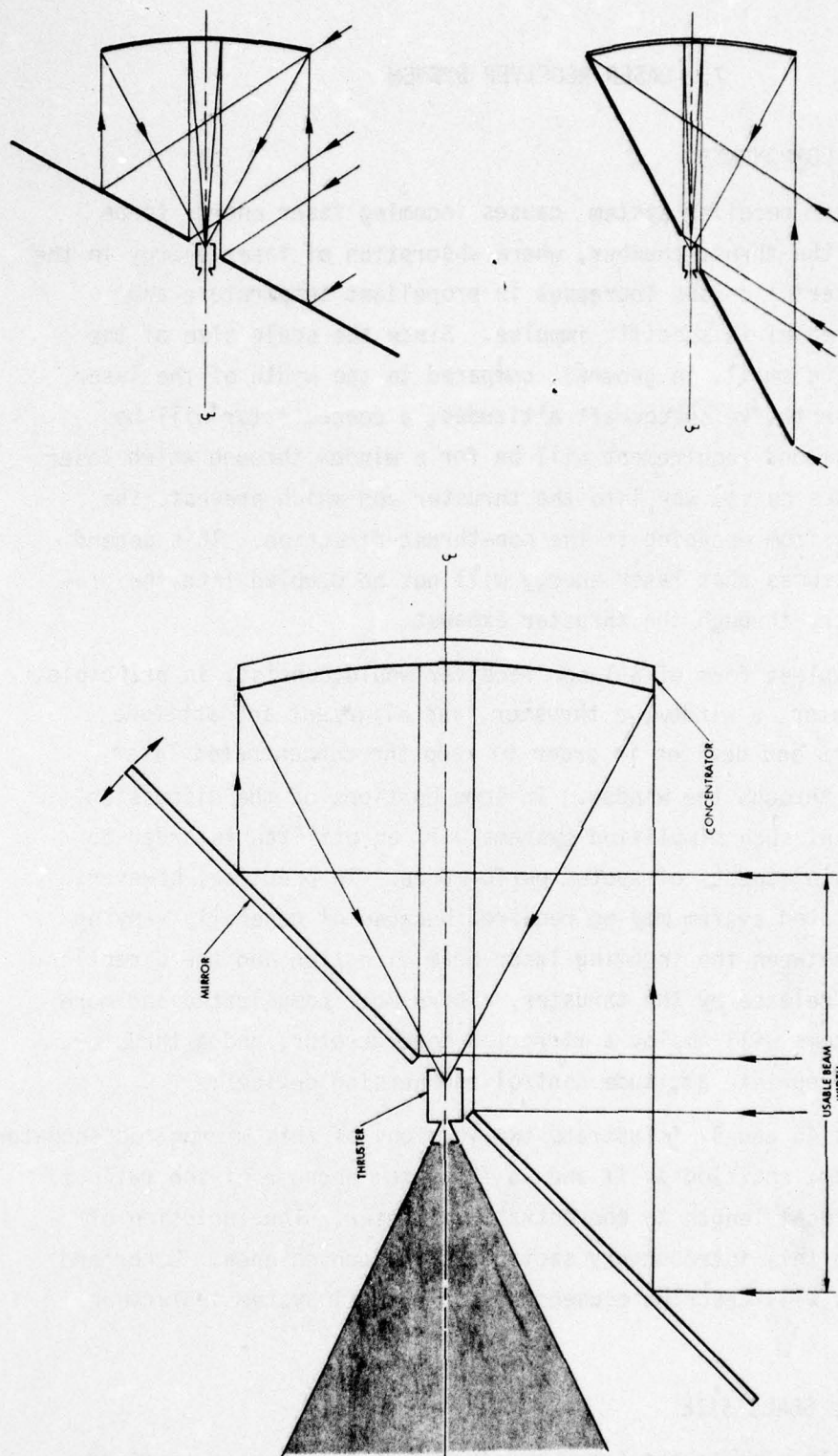


Figure 46. Laser Receiver System With Mirror, Concentrator, and Thruster for f_1 System

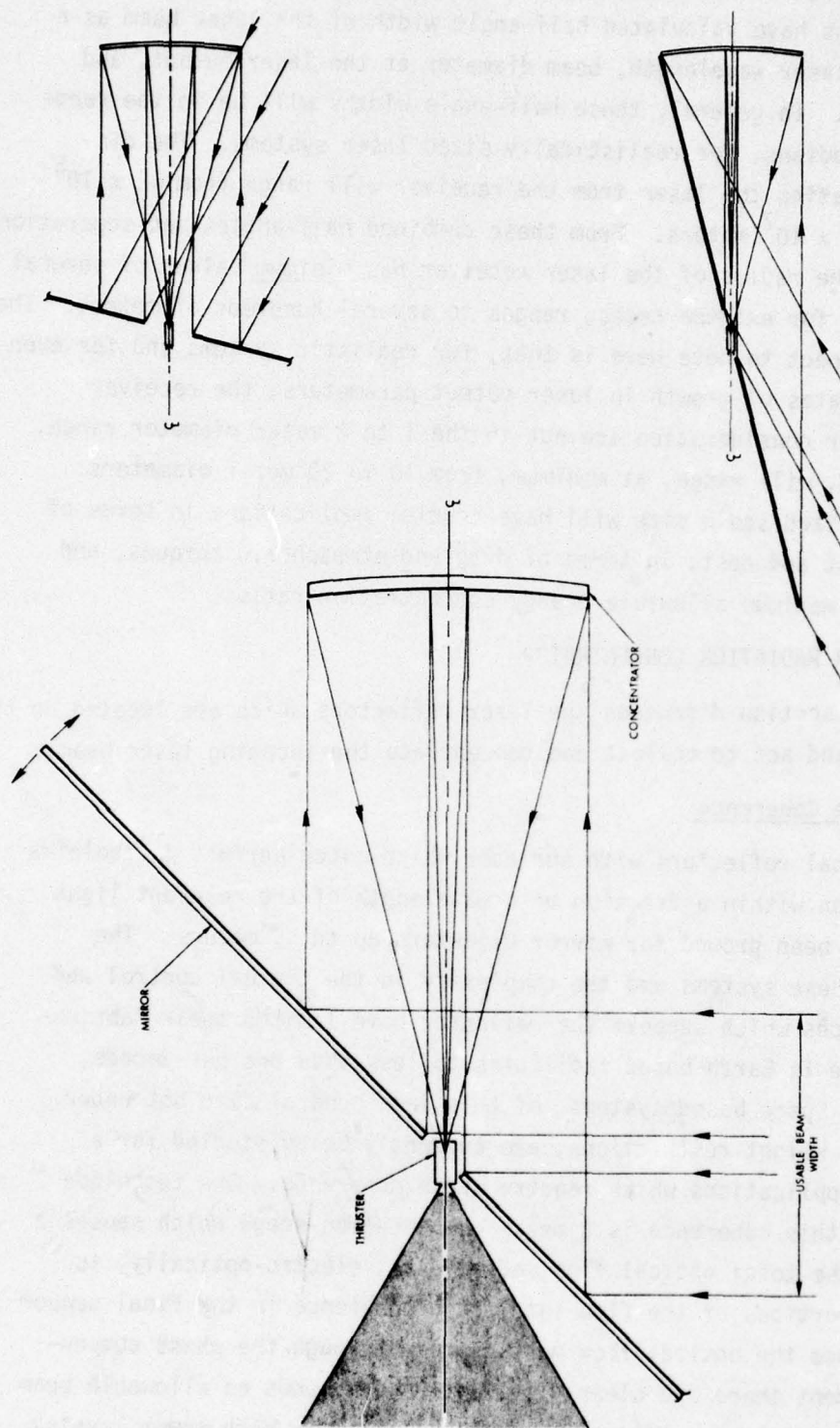


Figure 47. Laser Receiver System With Mirror, Concentrator, and Thruster for f_2 System

jitter) at spacecraft altitudes and for ground based laser systems. Previous sections have calculated half-angle width of the laser beam as a function of laser wavelength, beam diameter at the laser output, and beam quality. In general, these half-angle widths will be in the range above 10^{-5} radians, for realistically sized laser systems. The distances separating the laser from the receiver will range from $\sim 2 \times 10^5$ meters to $\sim 4 \times 10^7$ meters. From these combined half-angles and separation distances, the radius of the laser receiver has minimum values of several meters, and, for extreme cases, ranges to several hundreds of meters. The important aspect to note here is that, for realistic systems and for even optimistic rates of growth in laser output parameters, the receiver systems under consideration are not in the 1 to 2 meter diameter range, but, instead, will range, at minimum, from 10 to 20 meter diameters. This generalized scale size will have crucial implications in terms of system weight and cost, in terms of drag and atmospheric torques, and in terms of maximum allowable energy concentration ratios.

7.3 LASER RADIATION CONCENTRATOR

This section discusses the laser reflectors which are located on the spacecraft and act to collect and concentrate the incoming laser beam.

7.3.1 Phase Coherence

Optical reflectors with surfaces which match perfect paraboloids of revolution within a fraction of a wavelength of the relevant light quanta have been ground for mirror diameters up to ~ 5 meters. The weight of these systems and the complexity in the thermal control and in the devices which support the reflector have limited their fabrication and use in Earth based facilities to less than one per decade, worldwide. Space based systems, of this same general size but under more severe weight restrictions, are currently being studied for a series of applications which require phase coherence. One technique to produce this coherence is a phase compensation stage which senses a sector of the total optical flow and adjusts, electro-optically, to bring all portions of the flow into phase coherence in the final sensor plane. Since the optical flow must proceed through the phase compensation element there are clearly evident upper bounds on allowable beam power, and, for laser aided propulsion and the very high power levels in the photon beam, the use of phase compensation does not appear

practical. A second technique under examination for large space based reflector systems (which also require phase coherence) is "adaptive" optics. Under the adaptive optic approach sections of the reflector are individually sensed and positioned. While this adaptive optic, flexible mirror, approach does not have the apparent power restrictions of the phase compensation technique, it is, nevertheless, a highly complex system and is considered only because phase coherence is a mission critical item for the applications under study.

This system study will assume that the laser reflector surfaces possess uncorrected root mean square deviations from perfect paraboloidal shape by values of $\sim 10^2 \lambda$. Phase coherence, thus, will not be present in approaching the focal point of the reflector. This will prevent the laser coupling to the propellant from utilizing the intense electric fields associated with laser breakdown of gases for optically perfect, highly focused, systems. An absence of phase coherence, however, is not considered crucial here. The absorption process is, after all carried out on a volume basis rather than a point basis. The major concern of the study will be that the laser radiation be gathered within as small a circle as is conveniently possible. Since the weight of the reflector is of major concern for total system feasibility, the strategy in this study will be to remove, inasmuch as is possible, extraordinary requirements in magnification and in phase coherence in order to provide reduced reflector weight.

7.3.2 Circle of Confusion

A circle of confusion may be defined as that area illuminated in the focal plane of a reflector by a point source of light infinitely distant from the reflector. This circle of confusion can be determined in principle by ray tracing over the surface of the reflector. If the normal to a reflector surface element dA at point (x,y) deviates by an angle $\delta\theta$ from the surface normal direction of an ideal paraboloid at the point (x,y) , then the ray from this element will be approximately $2f\delta\theta$ away from the optical axis of the system in the focal plane and where f is the reflector focal length. An estimate of the size of the circle of confusion, then, is $\sim 2f(\langle \delta\theta^2 \rangle)^{1/2}$ where the indicated average is taken over the surface of the reflector.

The value of $\delta\theta$ at a given surface element can be expected to depend on many factors. Among these factors are: (1), original fabrication accuracy, (2), thermal distortion of the reflector system from both absorbed and emitted radiation (where absorption must consider both solar radiation and laser radiation, and must consider optical processes on both the front and back surfaces of the reflector, and, (3), dynamically induced reflector shape changes, including here the forces derived from thruster operation, attitude control system operation (for both the reflector and the spacecraft) and atmospheric drag effects. An accurate treatment of expected $\delta\theta$'s for the various distortion factors above proceeds considerably beyond the limits of the present systems study. The discussion here will attempt to quantify expected performance to only that degree required to sense the general scale size of the focused radiation.

The bulk of present day technology is not concerned with optical radiation, but, rather, with microwave radiation. Adequate performance (good antenna gain for received signals, or appropriately narrow beams for radiated signals) is obtained for antenna diameters \sim two orders of magnitude in excess of the wavelength. For optical reflectors, and assuming that the principal source of technology development will be from microwave antennas, this suggests circles of confusion whose diameters are $\sim .01$ of the reflector diameter. A 10 meter diameter reflector, thus, would contain the focused laser radiation within a diameter of ~ 10 centimeters.

The acceptance of the comparatively small concentration ratios described above ($\sim 10^2$ in beam diameter, $\sim 10^4$ in beam intensity) eliminates consideration of very small scale thrust chambers. The use of a larger size thruster does not appear, however, as a sacrifice to the system since there is no major benefit to be derived from making the thruster absorption chamber diameter small compared to the absorption length. Since absorption lengths in the thruster diameter will be of the order of tens of centimeters, an appropriate scale size for the thruster chamber diameter is, again, of the order of tens of centimeters.

A system strategy, then, may be to accept this comparatively low magnification, utilize larger thruster chambers, and (since windows

connecting to the thrust chamber are now larger), move thruster chamber pressure to lower values. If a successful solution can be obtained with the larger thruster scale size and somewhat less than perfect optics, the direction of system evolution could be to continue to reduce reflector weight until the focus is barely adequate to bring the laser radiation into the thrust chamber. In short, there appears to be no major system benefit in reducing thruster size and demanding more perfect optics, while reducing reflector weight is of principal concern.

While the discussion here has not derived expected $\delta\theta$'s of the reflector under various loading conditions, it should be noted that computer programs presently exist for determining beam properties in and near the focal plane for an arbitrary perturbation function to the reflector surface and can be utilized as an element in future systems studies.

7.3.3 Concentrator Weight

The systems illustrated in Figures 46 and 47 have employed both a mirror (in the illustrated cases a planar mirror) and a concentrator (a paraboloid of revolution). While the discussion in this section will treat the weight of the concentrator, the analysis will also apply to a planar mirror on a per area basis. It should be noted that for the configurations illustrated in Figures 1 and 2, mirror area exceeds concentrator area by a factor of $(\cos \alpha)^{-1}$ where α is the maximum angle between the normal to the mirror and the concentrator axis. Total system mass of a mirror and a concentrator will be $\approx M_c (1 + (\cos \alpha)^{-1})$ where M_c is concentrator mass.

The concentrator total mass will be composed of three elements. These are the infrared reflecting film and the reflecting film substrate, a supporting plane of material (most likely a honeycomb core between two bonded planes of material), and a more coarse grain supporting adjustment structure for the reflector and its underlying plane. Figure 48 illustrates these elements.

The IR reflecting film has been bonded to a 12.5×10^{-3} cm thick glass substrate with metallized backing plus a thin bonding layer of epoxy. The weight assigned to this reflecting layer is .030 grams per

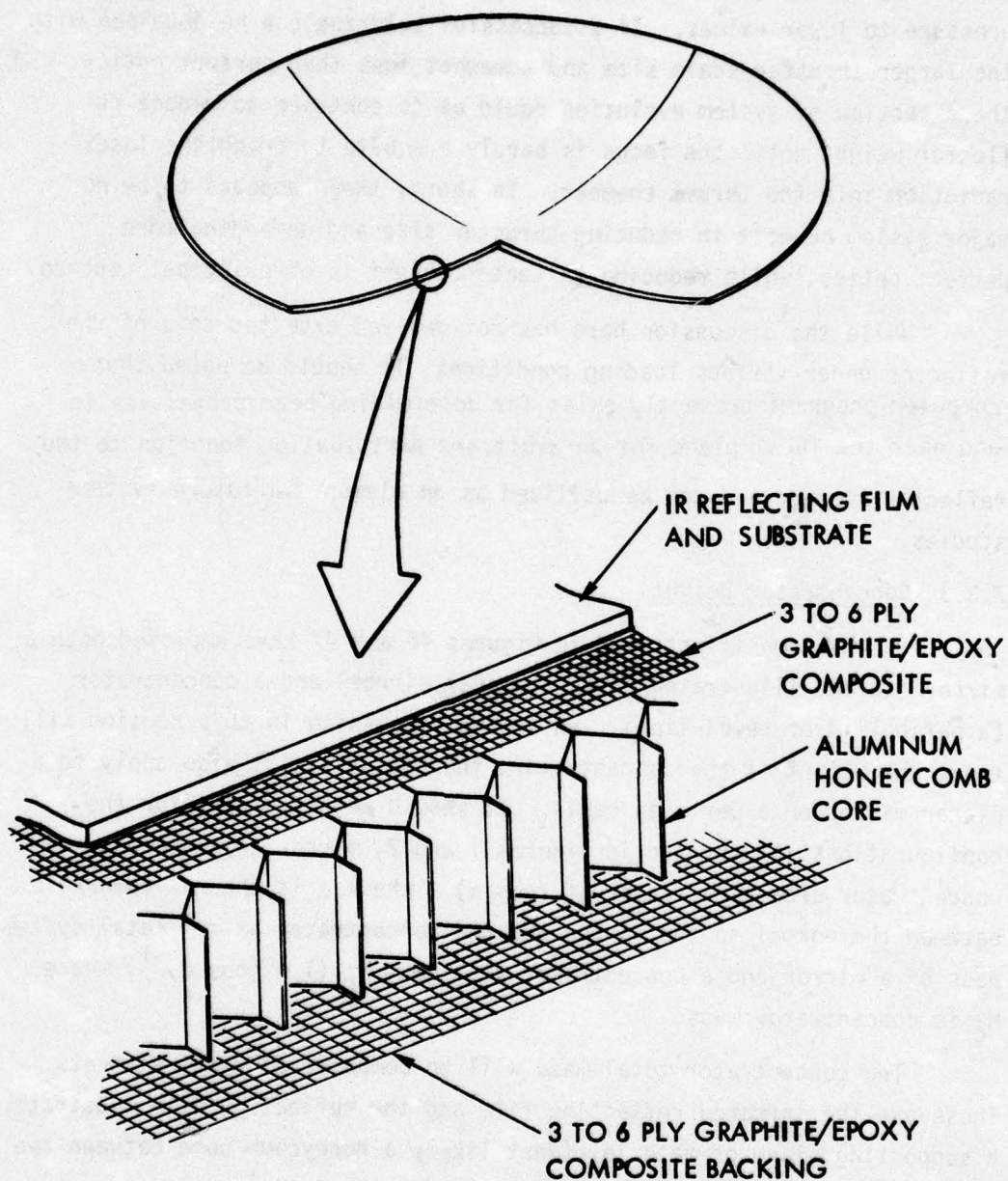


Figure 48. Lightweight Concentrator Construction Detail

square centimeter. This assumption of a glass substrate is not completely firm. In present practice, these IR reflecting materials (ZnS, ZnSe, ThF_4) are deposited at $\sim 150^\circ\text{C}$ upon a variety of glass surfaces. Other surface materials, however, including polymer films and graphite epoxy composites are also capable of stable properties at these temperatures. If the IR reflector can be deposited on these films and on the composites, important savings in both costs and weight can be realized. The underlying support plane has been assigned .095 grams per square centimeter (which is obtained in presently available Kevlar honeycomb board). This combined weight of 0.125 grams per square centimeter is assumed to be matched by another, averaged, 0.125 grams/cm^2 major support structure for a total concentrator weight per area of 0.250 grams/cm^2 . These weights are comparatively firm, since microwave antennas of graphite epoxy composites and in the range of 2 meters in diameter possess such mass per unit area figures ($\sim .5$ pounds per square foot).

If we assume that increases in concentrator size to the 10 meter diameter range can maintain this $.25 \text{ grams/cm}^2$ density figure (which assumes that all advances in the technology are being re-invested to maintain constant σ in the face of increasing system diameter, and, hence, increasing mass in the major supporting structure weight) then a 10 meter diameter concentrator would weigh 200 kilograms and a combined mirror and concentrator system would be ~ 600 kilograms for the fl system (Figure 46). This mass figure does not include the weight of attitude control systems for either the mirror or the collector.

The collector mass estimate given above may be optimistic by a factor of ~ 2 . Whether increased reflector weight will be required will depend upon rigidity during collector movement and thermal loading from solar and laser radiation. It is important to note that microwave systems generally retain good antenna characteristics for reflectors in the $.5 \text{ lb./ft.}^2$ to 1 lb./ft.^2 range and for diameters of the order of 100λ . This system study has concentrated its attention on systems built, essentially, to microwave antenna accuracy. If requirements are introduced for a focus into diameters of 10^{-3} of the concentrator diameter, then significant increases in the supporting mass to the

reflecting surface will be required. Since increases in concentrator mass, impact, in turn, on attitude control system mass and on dynamic stability problems of the total spacecraft, there are very cogent reasons for an attempted system solution using a comparatively "loose" focus. Separate systems studies for space borne, optically accurate, reflectors in the range from 5 to 15 meters in diameter have evolved mass estimates from 4000 pounds to 32,000 pounds, well beyond the point of attractiveness in terms of laser aided propulsive systems.

7.3.4 Required Window Diameter

7.3.4.1 Ideal (No-load) Conditions

Ideal conditions will be described here as a stationary reflector (no angular acceleration, no linear acceleration, no aerodynamic loading) with weakly incident laser light from infinity, and, if sunlight is present, with a uniform deposition of solar radiation over the reflector front or rear surface. Under these conditions the laser light will focus into a minimum area with diameter $\sim 2f(\langle \delta\theta^2 \rangle)^{1/2}$ where $\delta\theta$ is the angular deviation of the reflector surface normal from the surface normal for a true paraboloid of revolution. This RMS ($\delta\theta$) is specifiable and for present manufacturing techniques can be held less than 10^{-2} radians for light weight graphite epoxy reflectors in the range of several meters in diameter. Clearly the window at the input end to the thrust chamber must have a radius larger than $f\delta\theta_{\text{rms}}$.

A reflector fabricated as a single rigid piece and subsequently launched can be expected to possess significantly lower values of $\delta\theta_{\text{rms}}$ than a folded structure which deploys following launch. For conventionally sized reflectors (1 to 2 meters diameter, for example) the size of the reflector does not prohibit fabrication as a single rigid unit with subsequent launch. At some point, however, reflector size can exceed even the largest shrouds for boost vehicles and one or another of two alternatives must be considered. The first alternative is to utilize folded structures during launch with subsequent deployment and erection, accepting whatever penalties in increased $\delta\theta_{\text{rms}}$ may occur. A second alternative is launch of the reflector in the Space Shuttle bay with separate sectors intact and an assembly in space of a rigid structure

from these sectors. The limitations here are the length and breadth of the Shuttle cargo bay (~ 60 feet in length and 15 feet in width) and the ability of the Shuttle crew to assemble the reflector section and subsequently attach the reflector to the spacecraft. (A third alternative, not considered above because of weight and complexity is the launch of a folded, deployable structure with adaptive optics, both sensors and drivers, to align the reflector portions more accurately after deployment). Cost/value tradeoffs for the several possibilities outlined above clearly exceed the scope of the present systems study and will not be pursued further. It may be noted, however, that the Shuttle transportation system may be expected to be in service sufficiently early to allow that system to transport a total spacecraft, including a partially disassembled reflector, into orbit. For this approach, the Shuttle crew would complete the erection of the reflector before release of the total spacecraft.

The systems strategy of using only a moderately strong focus in the reflector, will also have the reflector accuracy as a stipulated quantity. A suggested $\delta\theta_{\text{rms}}$ range is $.01 > \delta\theta_{\text{rms}} > .003$ radians. For $\delta\theta_{\text{rms}} > .01$ radians excessive window diameters are obtained, and for $\delta\theta_{\text{rms}} < .003$, the laser focus is sufficiently tight to permit a tradeoff in this area to less accurate, less costly and perhaps less massive reflectors.

7.3.4.2 Angular Acceleration Loading

Some of the AF missions utilizing a laser aided propulsion system will require a reorientation of the mirror in the mirror/concentrator/thruster system illustrated in Figures 46 and 47 so that a ground based laser signal may be continuously received and concentrated by the moving spacecraft. The reorientation of the mirror necessarily involves angular acceleration of this structure, and, while this is not of concern for a totally rigid structure, a light weight reflector can be expected to deform and to cause a defocussing action in the concentrated laser rays.

At least two widely differing regimes of operation can be identified. In the first, the structure is sufficiently rigid under all possible

loading forces that the attitude control system may be programmed in advance of any required reorientation maneuver. This regime will be termed an "active" operational condition, in contrast to a "reactive" operational condition. In a reactive condition, deformation of mirrors and concentrators becomes an accepted possibility and the attitude control system, in conjunction with associated radiation sensors attempts to correct the mirror orientation or the concentrator orientation to keep the laser radiation directed through the central portion of the window on the thruster chamber. A principal distinction between active and reactive control conditions is that substantially higher angular accelerations may be expected to be present in the latter case, causing, in turn, still greater deformation in these large bodies. The discussion here will consider possible window diameter requirements as this control condition moves from the active to the reactive mode.

As an illustration of angular reorientation requirements, the discussion here will consider the boost of orbit apogee by thrust periods at orbit perigee for an initial circular orbit at 200 kilometers altitude. Figures 49, 50, and 51 illustrate the zenith angle during space-craft fly over for the initial (non-boosted) perigee velocity of 7.7 kilometers per second, and for a final (boosted) perigee velocity of 11 kilometers per second. Also shown there are $d\theta_z/dt$ and $d^2\theta_z/dt^2$ for these orbital end point conditions.

From an examination of Figure 51, the maximum angular acceleration of a mirror or a concentrator would be $\sim 10^{-3}$ radians/sec², which translates into spatial accelerations of $\sim 10^{-3}r$ cm/sec² where r is radial distance of a point on the mirror from the axis of rotation. Even for the outboard portions of comparatively large structures ($r \sim 10^3$ cm) these accelerations would only be in the range of centimeters per second square (~ 1 milli-g). Such small accelerations are unlikely to cause significant deformation of either mirrors or concentrators.

From the discussion above it would appear that, in principle, a structure designed with sufficient rigidity could be adequately pre-programmed in the attitude control system, and that this attitude control system, acting perfectly and under representative orbital

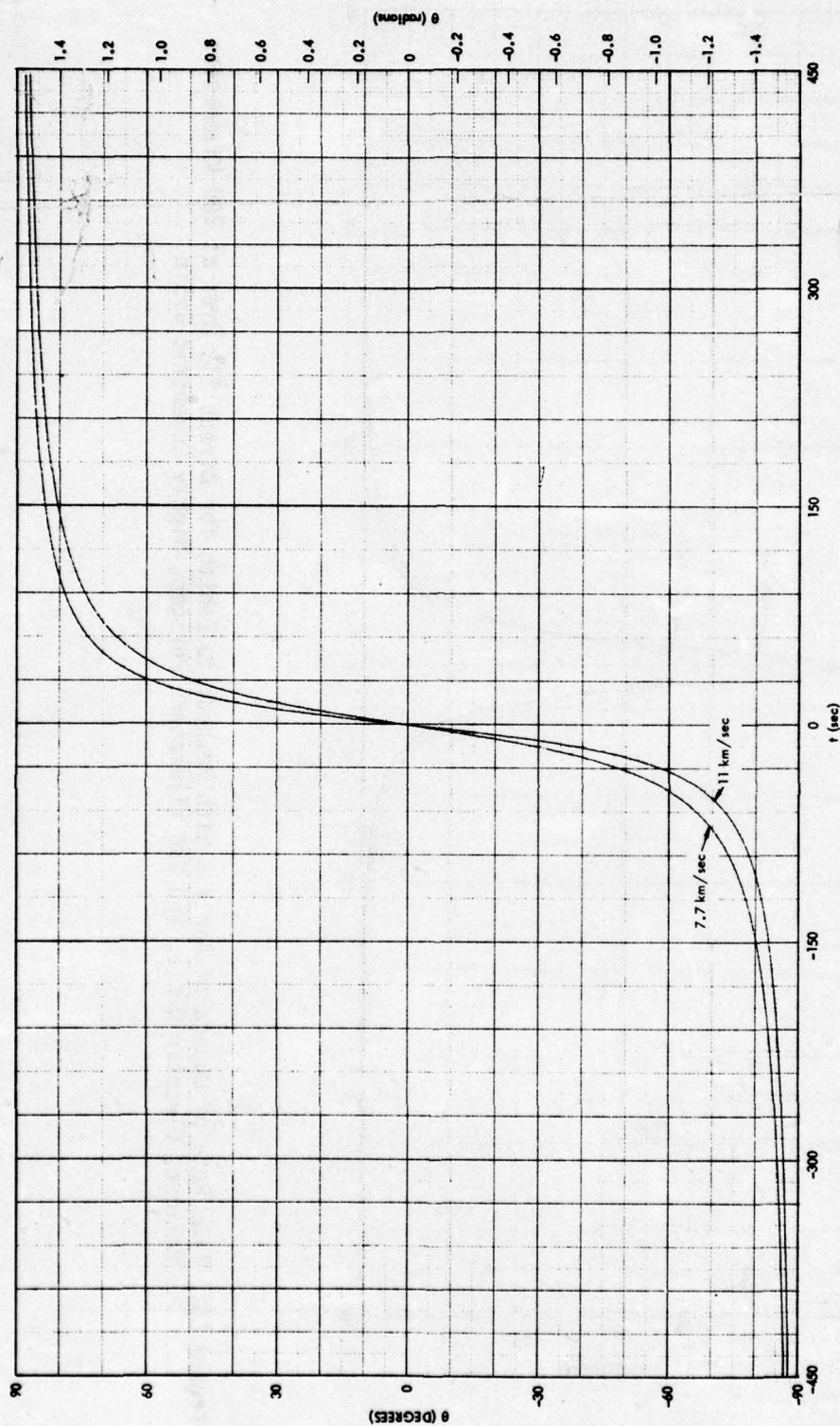


Figure 49. Angle θ Relative to the Zenith for Direct Fly Over at 200 Kilometers Perigee, Circular Orbit, and 200 Kilometers Perigee, Highly Eccentric Orbit

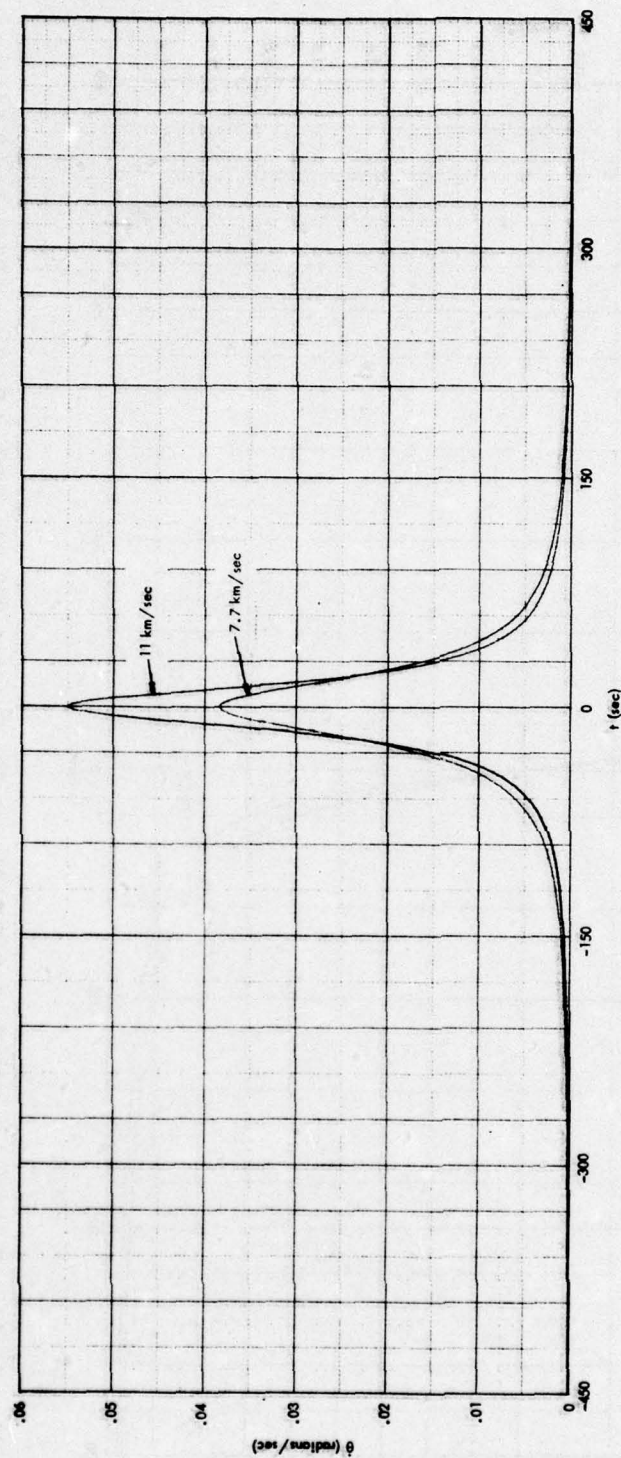


Figure 50. Time Rate of Change of Angle θ With Respect to Zenith for Direct Fly Over at 200 Kilometers Perigee, Circular Orbit, and 200 Kilometers Perigee, Highly Eccentric Orbit

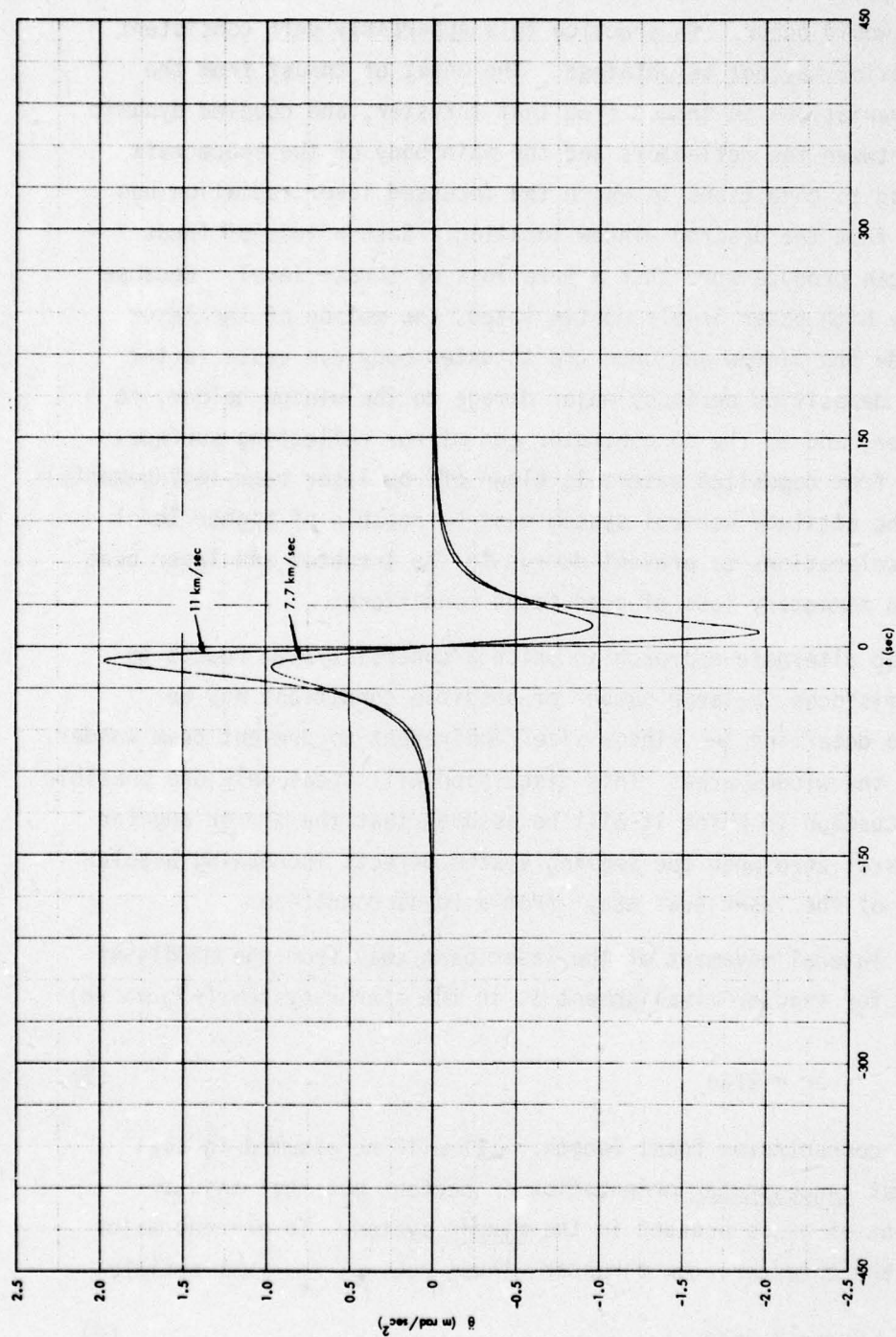


Figure 51. Angular Acceleration, $\ddot{\theta}$, for Direct Fly Over at 200 Kilometers, Perigee, Circular Orbit, and 200 Kilometers, Perigee, Highly Eccentric Orbit

conditions, would continue to maintain proper focus conditions and for sufficiently small accelerations that no deformation of the reflecting structures would occur. In practice this apparently self consistent system behavior may not be obtained. The onset of thrust from the thruster, variations in thrust from that thruster, and coupled dynamic behavior between the reflectors and the main body of the spacecraft can all lead to conditions in which the focussed laser radiation has moved away from the desired window location. Such a loss of focus condition can produce more than a mere loss of thrust level. Because of the very high power levels contemplated, the motion of the laser beam outside the window and onto the thruster body can cause (after only brief deposition periods) major damage to the window holder, to the thruster, and to the concentrator and mirror reflecting surfaces (this last from deposited materials blown off by laser beam impingement.) Clearly, the attitude control system must be capable of higher level angular accelerations to prevent damage to the thruster and laser beam system by a momentary loss of good focus conditions.

In an alternate approach in which a control system reacts to temporary misfocus, a large number of possible conditions may be examined to determine the window size requirement to prevent beam wander outside of the window area. This discussion will treat only one possible control situation in which it will be assumed that the mirror angular velocity is at zero when the sensing system detects increasing angular divergence of the laser beam away from a focus condition.

The lateral movement of the laser beam away from the middle of the window for angular misalignment $\delta\theta$ in the mirror system (Figure 46) will be

$$\Delta r = 2f\delta\theta \quad (8)$$

where f is concentrator focal length. (It will be assumed in this example that concentrator orientation is perfect but that angular misalignment of $\delta\theta$ is present in the mirror system. To prevent major damage to the thruster, the thruster window radius, r_w , must satisfy

$$r_w > 2f\delta\theta \quad (9)$$

Following the earlier choice of control situation it is assumed that at $t = 0$ the mirror rotation rate is zero. It will also be assumed that the sensitivity of the sensing system has a dead-band such that signals to refocus are not generated unless the laser beam has wandered to $\frac{1}{2}r_w$. The calculation assumes thus that an angular misalignment in the mirror of $r_w/4f$ is present at $t = 0$, and also that $\dot{\theta} = 0$ at this time.

The sensing of the beam wander at $r_w/2$ at $t = 0$ sets off angular acceleration $\ddot{\theta}$ in the control system. It should be noted, however, that spacecraft motion relative to the ground laser causes a growth in $\delta\theta$ at $t = 0$, determined by spacecraft position and orbit condition. From Figure 50 it will be assumed that a $\dot{\delta\theta}$ of 40 milliradians per second is occurring because of source motion relative to the spacecraft. Thus the beam wander at $t = 0$ is increasing by

$$\dot{r} = 2f\delta\dot{\theta} \quad (10)$$

and to prevent damage to the thruster

$$r_w > r(t)$$

where

$$r(t) = \frac{r_w}{2} + 2ft\delta\dot{\theta} \Big|_{t=0} + 2f \int_0^t dt \int_0^t dt \ddot{\theta} \quad (11)$$

and $\ddot{\theta}$ is the applied correction signal. Assuming $\ddot{\theta}$ at some maximum allowable angular acceleration leads to

$$r(t) = \frac{r_w}{2} + 2f(.040)t - f\ddot{\theta}_{\max}t^2 \quad (12)$$

and the control situation requires

$$\frac{r_w}{2} > 2f(.040)t - f\ddot{\theta}_{\max}t^2 \quad (13)$$

The maximum value of the RMS in Eq. (6) is at

$$t_m = \frac{0.040}{\ddot{\theta}_{\max}} \quad (14)$$

From Eq. (6) and (7) it follows that

$$r_w > \frac{f(0.040)^2}{\ddot{\theta}_{\max}} \quad (15)$$

The major question then becomes the maximum allowable mirror angular acceleration without mirror deformation. If the mirror total width is $2D$ and if the maximum loading at the edge of the mirror (without loss of mirror planarity) is βg , then

$$\ddot{\theta}_{\max} \sim \frac{\beta g}{D} \quad (16)$$

so that

$$r_w > \frac{fD}{\beta g} (0.040)^2 \quad (17)$$

is the final condition on minimum allowable window radius. As an example, consider $f = D = 10^3$ cm and $\beta g = 10^2$ cm/sec² so that $r_w > 16$ centimeters would obtain. The crucial question, of course, remains as the allowable βg on the mirror before this (light-weight) structure deforms and causes defocussing of the laser beam at the thruster window. For sufficiently complicated deformation of the mirror, the error signal which senses angular misalignment can be completely masked by these effects, thus disabling the control system. As noted throughout this discussion, strengthening of the mirror and concentrator can be achieved, but with costs in increased mass and increased attitude control torques to achieve angular correction.

An important factor to note is that small size windows (~ 1 cm) are not only denied by limits on allowable magnification but are also not indicated as feasible from attitude control considerations.

7.3.4.3 Thruster Firing Loading

The coupling of the laser radiation into the propellant in the thruster and the generation of thrust will impose a loading on the

large area structures of the mirror and the concentrator. Considering a mission to boost orbit apogee by thrusting during fly over and at perigee distance, P, estimates of the required acceleration may be made. If laser beam transmission to the spacecraft occurs during the period when the spacecraft is within $\pm \epsilon$ from the zenith, the thrusting period will be

$$\Delta t_{th} = \frac{2P \tan \epsilon}{v_s} \quad (18)$$

and the Δv_s per thrust period will be

$$\Delta v_s \sim \frac{2TP}{M_s v_s} \tan \epsilon \quad (19)$$

where T is generated thrust and M_s is spacecraft mass (including propellant) and, for a total of N "passes", a total velocity increment

$$\Delta v_{st} \sim \frac{2NTP}{M_s v_s} \tan \epsilon \quad (20)$$

results. For a major change in orbit apogee, $\Delta v_{st} \sim 3 \times 10^3$ meters per second is required. Using $\epsilon \sim 30^\circ$ and $P = 2 \times 10^5$ meters leads to values of

$$\frac{NT}{M_s} \sim 150 \quad (21)$$

The mission plan will assign a required value of N from which a required value of T/M_s is derived. Inserting reasonable values of N leads to values of T/M_s at the 1 g level. There is, thus, a basis for assuming significant acceleration loading on the mirror and concentrator structures.

The effect of thruster firing on the mirror and concentrator structures will be to cause a "bowing" of the mirror and a "closure" of the outer portions of the concentrator. It is of interest to note that these deformations differ significantly in shape from those occasioned by angular rotation of either the mirror and/or the concentrator. This raises questions, in turn, on the ability of sensing devices to

detect the appropriate angular acceleration if portions of the laser beam are being directed outside the thruster chamber window. Reducing these uncertainties by a total reduction in deformation through stiffer mirrors and concentrators leads to the previously noted problems of additional structure mass and additional attitude control torques to achieve a given angular acceleration level.

7.3.4.4 Aerodynamic Loading

Missions such as thruster firing at perigee to create an apogee boost will operate more effectively at lower perigee values where laser transmission distances are reduced. These lower perigee values, however, result in non-trivial aerodynamic loading on the large structures of the mirror and the concentrator. Using a formula for drag of

$$D_r = \frac{1}{2} \rho v^2 C_D S \quad (22)$$

and

$$\rho = 33 \times 10^{-9} \exp(-.023h) \quad (23)$$

where ρ is in kilograms per cubic meter and h is altitude in kilometers leads to the calculated values of drag/area in Figure 52. The calculations there have assumed $C_D = 2.2$.

From Figure 52 and for frontal areas in the mirror and concentrator of the order of 10^2 m^2 , the total drag at 200 kilometers would be of the order of a few newtons. An examination of Eq. (21) for required thrust levels to perform an orbit apogee boost clearly indicates much larger values of T in order to perform the mission in reasonable periods of time. The aerodynamic loading, thus, will not be as significant as the thruster firing in terms of mirror and concentrator deformation.

While aerodynamic drag may not be a significant contributor to deformation, the continuous presence of these forces can cause significant torques on the spacecraft and, in addition, result in a substantial expenditure of energy per orbit for each area of surface creating the drag. Figure 53 illustrates the energy loss per orbit per square meter of surface area as a function of altitude. At 200 kilometers, this

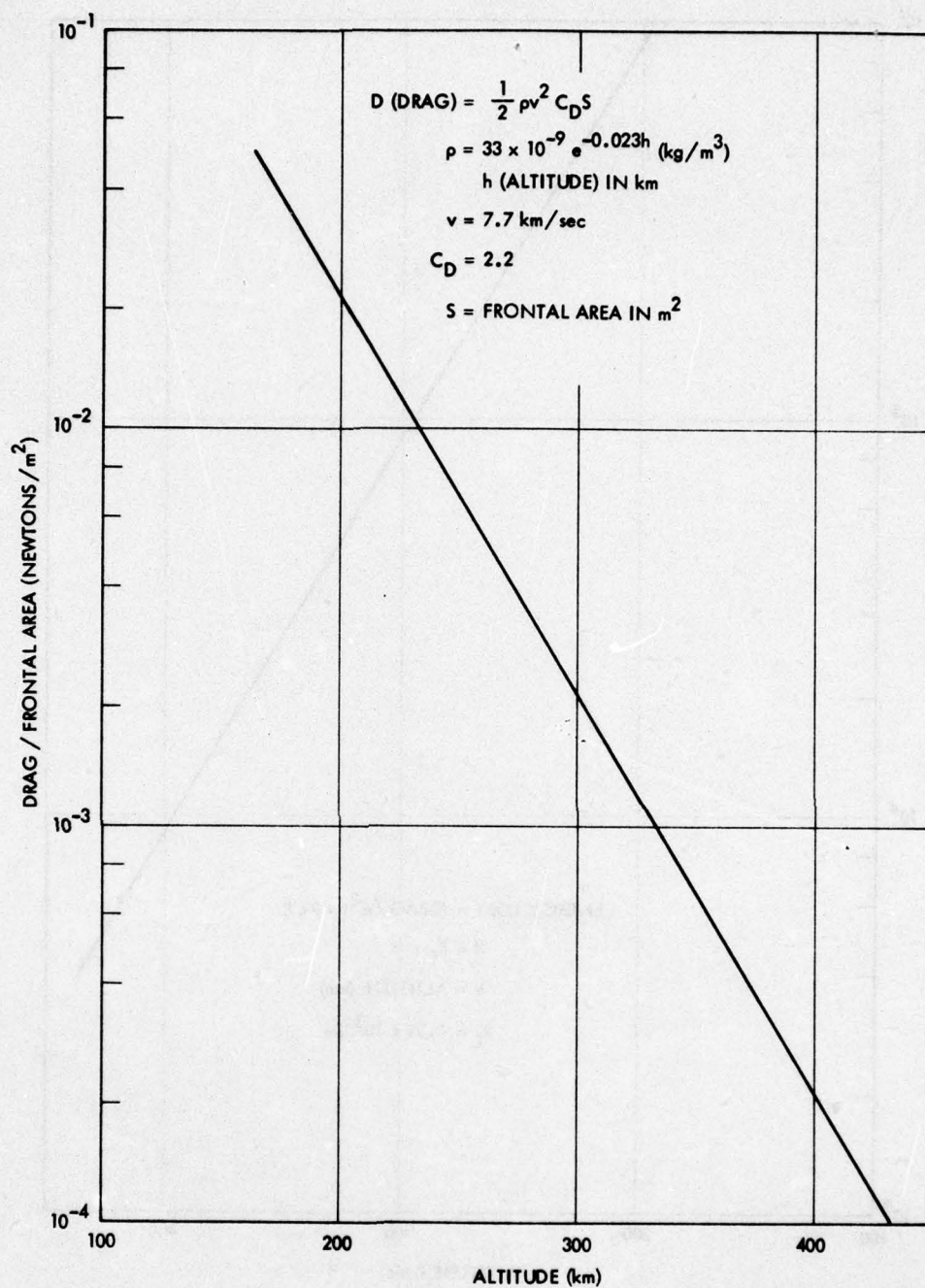


Figure 52. Aerodynamic Drag per Frontal Area as a Function of Altitude (Mean CIRA Atmosphere), (Spacecraft Orbit Velocity of 7.7 Kilometers per Second).

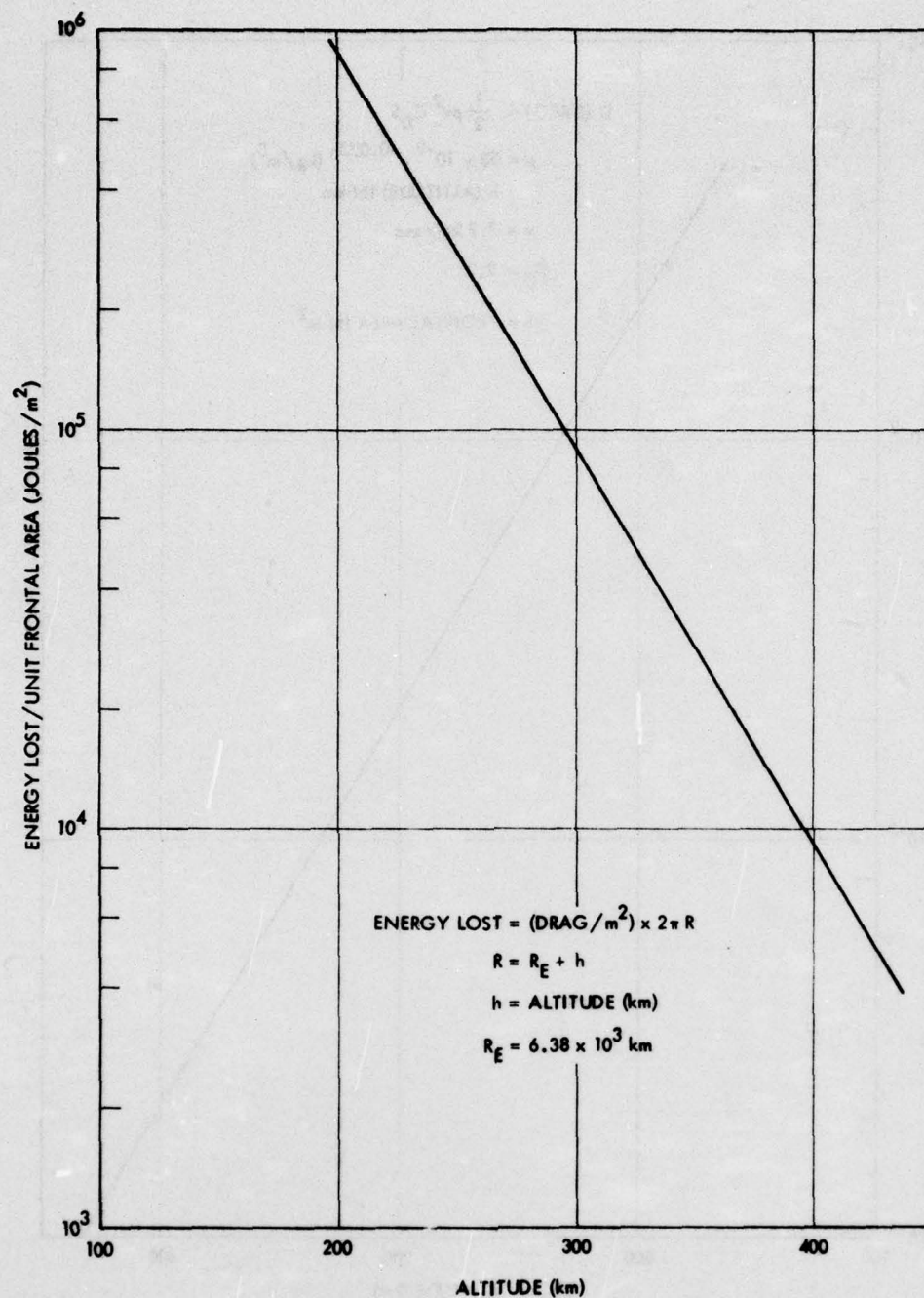


Figure 53. Energy Loss Per Unit Frontal Area to Aerodynamic Drag as a Function of Altitude (Mean CIRA Atmosphere) for Circular Orbit (Spacecraft Velocity of 7.7 Kilometers per Second)

loss is almost 1 megajoule per square meter per orbit.

In order to prevent decay of the orbit, the thruster firing during spacecraft flyover must have certain minimum values. Figure 54 assumes thruster firing for a variation of the spacecraft angle of $\pm 30^\circ$ with respect to the zenith. At 200 kilometers, and during this limited thruster burn, a thrusting force of ~ 4 newtons per square meter must be present merely to compensate aerodynamic drag. This thrust level, in turn, requires calculable power levels in the laser beam. Figure 55 illustrates the required laser beam power which must be converted to thrust during the -30° to $+30^\circ$ flyover period merely to compensate for aerodynamic drag. Figure 55 illustrates this "sustaining power" for various assumed values of beam half-angle width (increasing beam width requires increasing areas of mirror and concentrator) and as a function of altitude, assuming that the thruster operates at 770 seconds of specific impulse. Figure 56 repeats these calculations but with an assumed value of 1000 seconds specific impulse in the thruster. The clearly evident conclusion of these calculations is that laser beam half angle widths of 10^{-5} radians lead to significant aerodynamic drag problems and that still further increases in this width carry the mission totally away from feasibility.

7.3.4.5 Thermal Loading

Thermal loading can occur from absorption of either solar or laser radiation. It is interesting to compare the magnitudes of the radiant energy of these two sources. For laser beam half-angles of $\sim 10^{-5}$ radians, the beam area at an altitude of several hundred kilometers is $\sim 100 \text{ m}^2$. A 100 kw laser beam would have a radiant energy of $\sim 1 \text{ kw}$ per square meter, which is approximately the energy flux rate of solar radiation. The 100 kw, 1 mw and 10 mw laser beam energy missions, thus, will have energy fluxes of ~ 1 , 10, and 100 Suns.

While laser beam energy flux may range to many times that of solar radiation, it does not follow necessarily that laser light will thermally load the mirror and concentrator to the same level as sunlight. Section 3.3, in treating concentrator weight, has noted the IR reflective

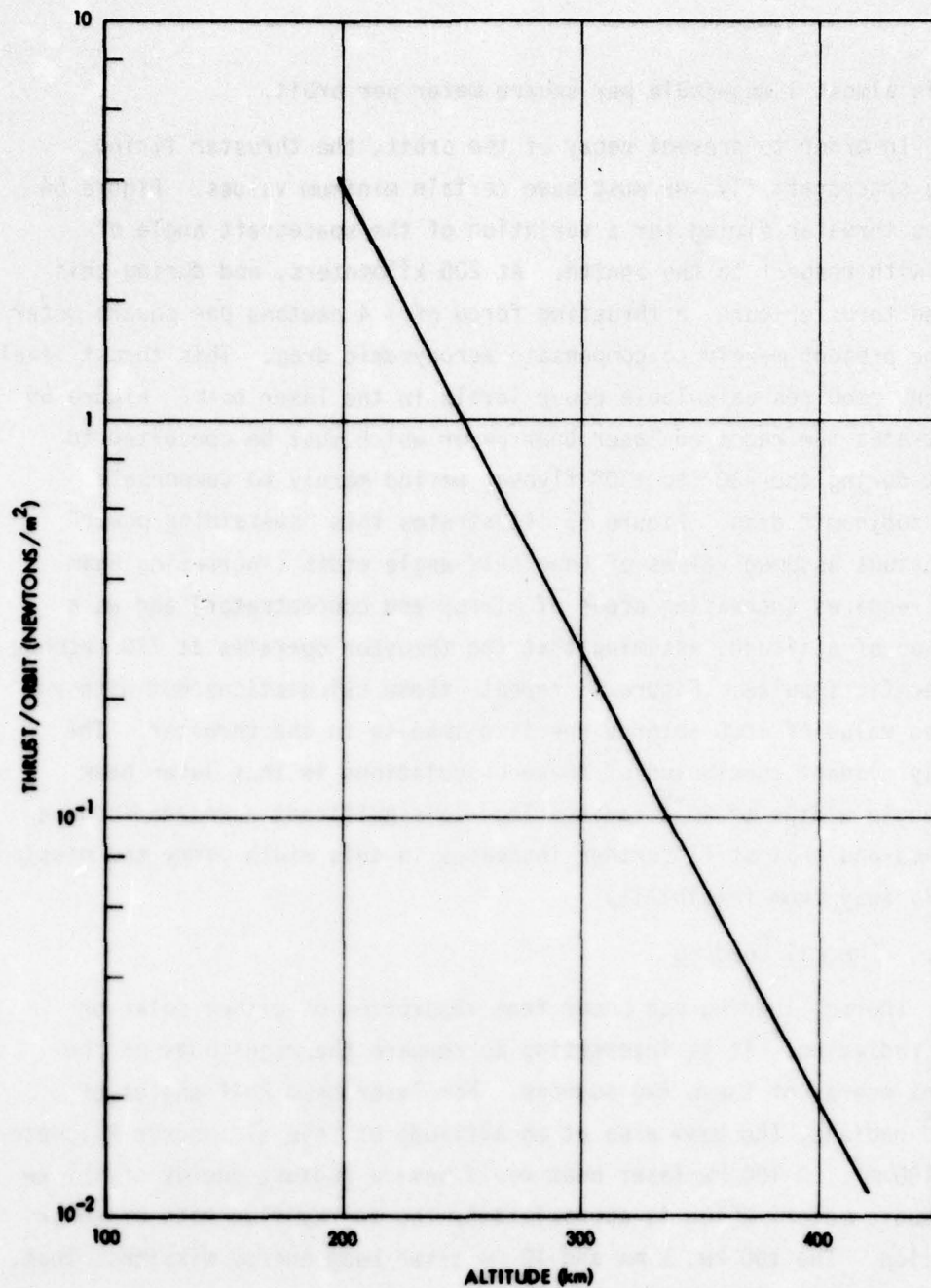


Figure 54. Required Thrust for Thrust Period During $\pm 30^\circ$ Angular Motion With Respect to Zenith, per Unit Frontal Area, as a Function of Altitude for a Circular Orbit

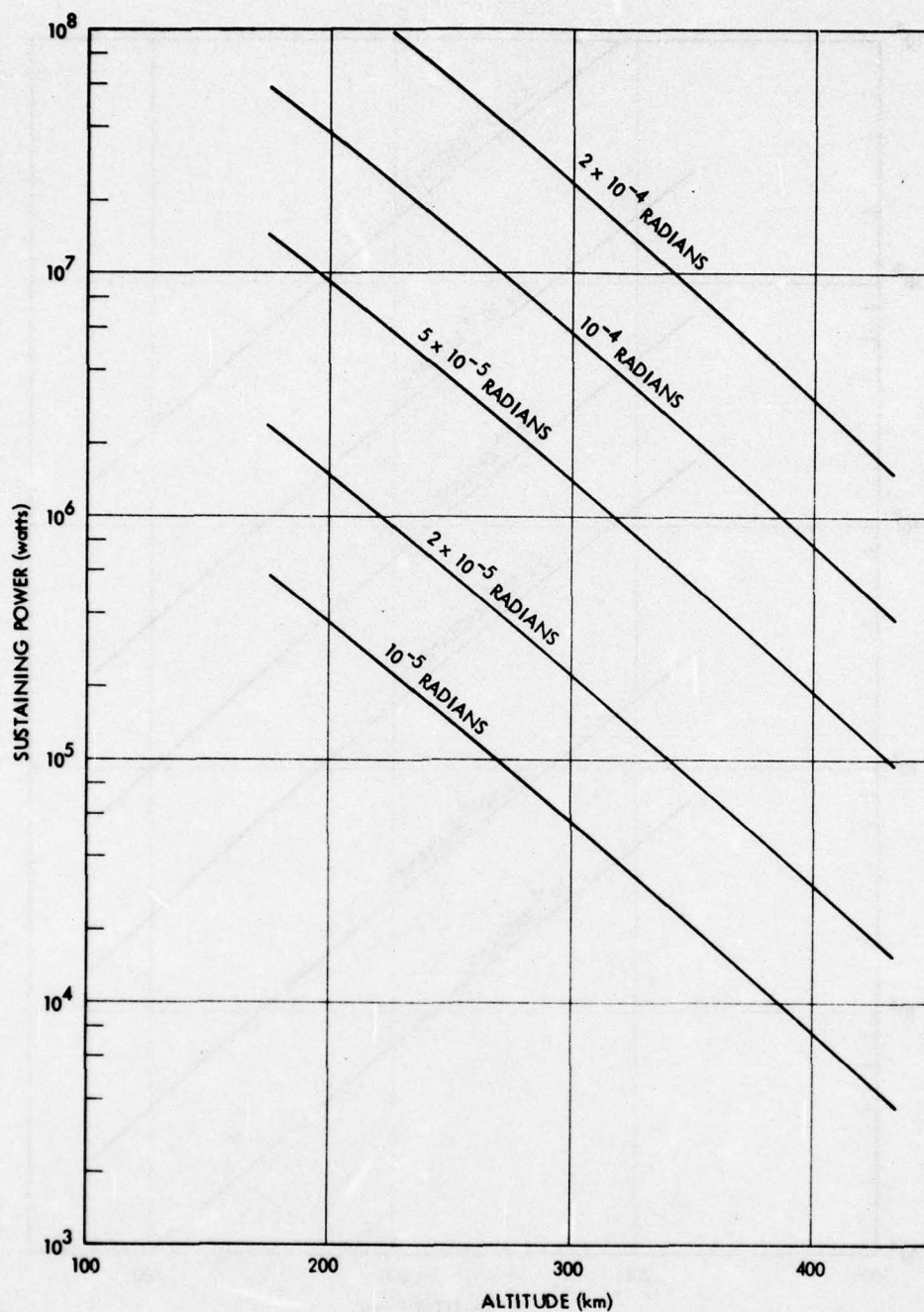


Figure 55. Required Laser Beam Power Conversion to Thrust (at $I_{sp} = 770$ seconds) to Sustain Orbital Altitude from Aerodynamic Drag for Thrust Period $\pm 30^\circ$ With Respect to Zenith, as a Function of Altitude, for Frontal Area Sufficient to Intercept Laser Beam at Indicated Half Angles

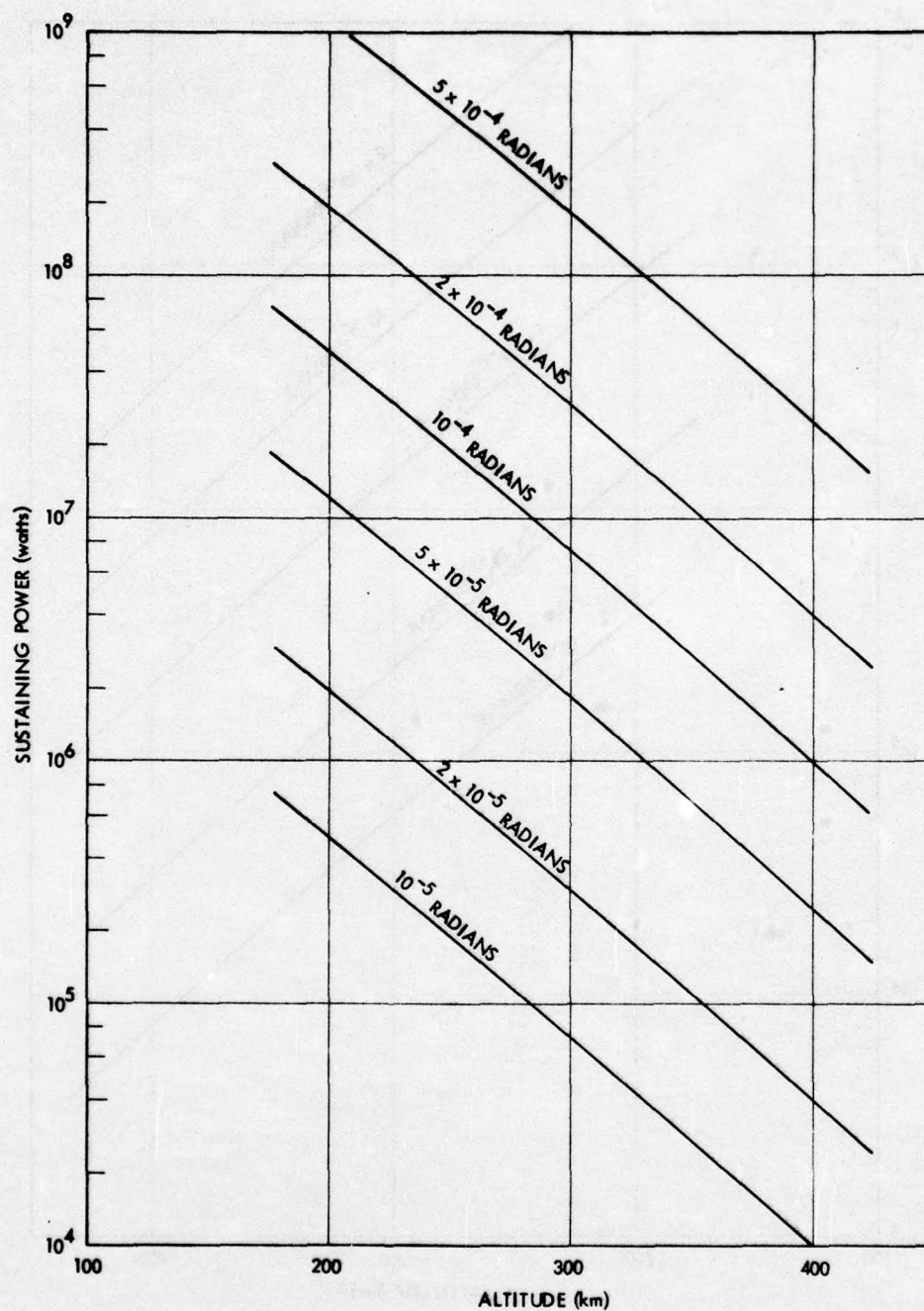


Figure 56. Required Laser Beam Power Conversion to Thrust (at $I = 1000$ seconds) to Sustain Orbital Altitude from Aero-sp^{dynamic} Drag for Thrust Period $\pm 30^\circ$ With Respect to Zenith, as a Function of Altitude, for Frontal Area Sufficient to Intercept Laser Beam at Indicated Half Angles

coating on the mirror and concentrator. These coatings, specifically cut for the relevant IR wavelength, have demonstrated reflectance of 0.998, over a comparatively broad range of arrival angle, away from normal incidence. If this indicated absorptivity of .002 is used, the absorptance per area reaches maximum values of only 200 watts per square meter (for 10 mw incident over 10^2 meters) or $\sim .2$ Suns. This is not considered as a significant perturbation.

The major area of concern for thermal loading is not the forward (reflecting) surfaces of either of these structures, but, rather the "rear" facing surfaces. Examining Figures 46 and 47, it may be seen that the incoming laser beam may be in close proximity to the rear surface of the concentrator and to other (assumed) portions of the spacecraft. In the design of Figures 46 and 47 the thruster is exposed to incoming laser radiation (although this may be corrected by minor relocations of the thruster). For these spacecraft surfaces, thruster surfaces, and rear concentrator surfaces, only brief periods of an inadvertent deposition of laser radiation can cause major damage (particularly for the 10 mw laser beam condition). In principle this damage can be averted by suitable sensing circuits which detect incoming laser radiation and command shutdown of the laser until it is repointed onto the mirror.

Two questions remain to be answered. The first of these questions is the rate of falloff in beam intensity for increasing lateral separation from the beam axis. If this fall-off is not sufficiently steep, then even a laser beam perfectly centered on the mirror will deposit excessive radiation on spacecraft surfaces. (A possible solution to this problem is configuration of the spacecraft so that most of the portions not associated with the beam are in the "shadow" of the mirror. A major problem with this design is the inability of a craft in this configuration to view the regions of the Earth immediately below it). A second remaining question is the extent of contaminant layers on the mirror and concentrator. The discussion here has assumed 99.8% reflectance, which is obtainable for non-contaminated reflectors. Only minor levels of material deposition,

however, are required to change these reflectances dramatically. Material blow-off from spacecraft surfaces under inadvertent laser irradiation (or even small levels of thruster plume contaminants) could alter the mirror surface at which point thermal loading of this element could become severe.

7.4 LASER RECEIVER ATTITUDE CONTROL SYSTEMS

7.4.1 Mirror Attitude Control System

7.4.1.1 Required Pointing Accuracy

Section 7.3.4.2 considered window diameter requirements imposed by angular acceleration loading and determined that

$$r_w > \frac{fD}{8g}(\dot{\epsilon})^2 \quad (24)$$

where f is concentrator focal length, D is the half width of the mirror, $8g$ is maximum allowable loading on the mirror without excessive deformation, and $\dot{\epsilon}$ is the rate of change of the angle of the laser beam-to-spacecraft direction relative to the zenith. In that derivation it was assumed that a dead-band for mirror reorientation is present so that if the beam remains within $0.5 r_w$ of the center of the window, angular correction is not applied. Clearly the pointing accuracy of the beam must be small compared to this selected dead-band, inasmuch as other source of beam wander (minimum circle of confusion, beam broadening from mirror deformation) are present. This discussion will consider that pointing accuracy of the mirror is satisfactory if an ideal (pencil) beam is positioned within $0.2 r_w$.

In 7.3.4.2 and Eq. (24), the use of $\dot{\epsilon} = 80$ milliradians per second, $\beta = .1$, and $f = D = 10^3$ cm led to $r_w > 16$ cm. Requiring pointing accuracy of the beam within $.2 r_w$ leads to a positioning within 3 cm. Since the angular displacement of the mirror by $\delta\theta$ causes positional offset of the beam at the thruster window location of $2f\delta\theta$ the required pointing accuracy is

$$\delta\theta < \frac{.2r_w}{2f} \quad (25)$$

Using $.2r_w = 3.2$ cm and $f = 10^3$ cm yields a required pointing accuracy of 1.6 milliradians for the mirror.

7.4.1.2 Required Torque

The required torque for the attitude control system is obtained from the moment of inertia of the mirror and the maximum allowable angular acceleration of this structure without unacceptable deformation.

Moments of inertia of the mirror are

$$I = \frac{2}{3} M_m D^2 \quad (26)$$

where M_m is mirror mass and D is the half length of the mirror. D is taken as $2.1 r_c$ for the f1 system and $4.1 r_c$ for the f2 system, where r_c is the concentrator radius. These moments of inertia are illustrated in Figure 57 as a function of r_c and for assumed levels of mass density, σ , consistent with earlier discussions of mirror construction. For the f1 system and a 10 meter diameter concentrator the moment of inertia for a mirror with surface density of 2 kilograms per square meters is $\sim 16,000$ kilogram meters².

The torque to drive a mirror of the indicated moments of inertia will depend on allowed $\ddot{\theta}$. If the mirror merely follows the $\ddot{\theta}$ required in a perfect active system, then from Figure 51, values of $\ddot{\theta}$ are $\sim 10^{-3}$ radians/second². In the discussion of 7.3.4.2, values of $\ddot{\theta} \sim .1$ radian per second² emerged for a "reactive" control situation. Figure 58 illustrates required torque for $.001 < \ddot{\theta} < .1$ radians/second² as a function of concentrator radius for a representative light weight structure. Maximum torques required for the mirror of the f1, 10 meter diameter, system are $L \sim 1,600$ kilogram meters² per second².

The comparatively large values of torque required to drive the mirror in a reactive system will clearly cause coupled dynamical problems to the remainder of the spacecraft unless it is quite massive and extended. Estimates of the disturbance on the spacecraft of the mirror reorientation torques will not be carried out here, but should be investigated further when the remainder of the spacecraft is more thoroughly defined. At that time the angular disturbance on the total spacecraft from the mirror

AD-A034 995

TRW DEFENSE AND SPACE SYSTEMS GROUP REDONDO BEACH CALIF F/G 20/5
INVESTIGATION OF BEAMED ENERGY CONCEPTS FOR PROPULSION. SYSTEMS--ETC(U)
OCT 76 M HUBERMAN, J M SELLEN, R BENSON F04611-76-C-0003
AFRPL-TR-76-66-VOL-1 NL

UNCLASSIFIED

3 OF 3

AD
A034995



END

DATE
FILMED

3-77

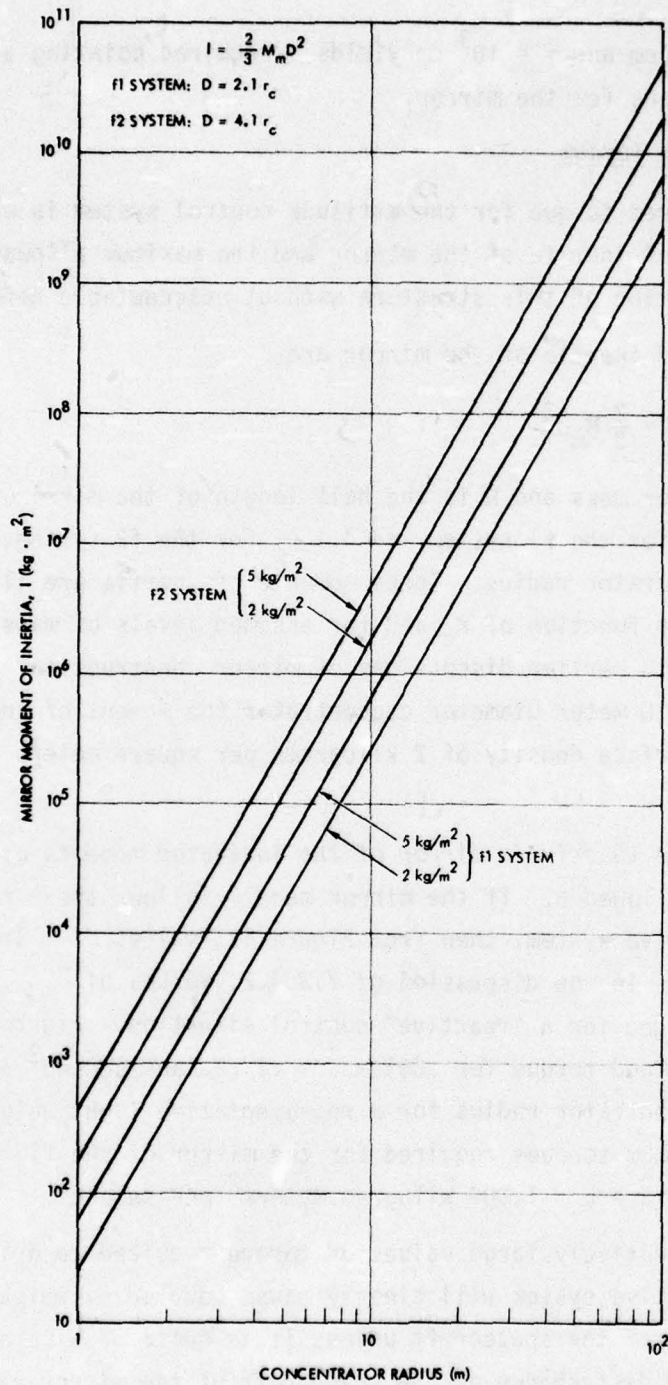


Figure 57. Moments of Inertia of Mirror as a Function of Concentrator Radius, and Assumed Levels of Surface Mass Density, σ

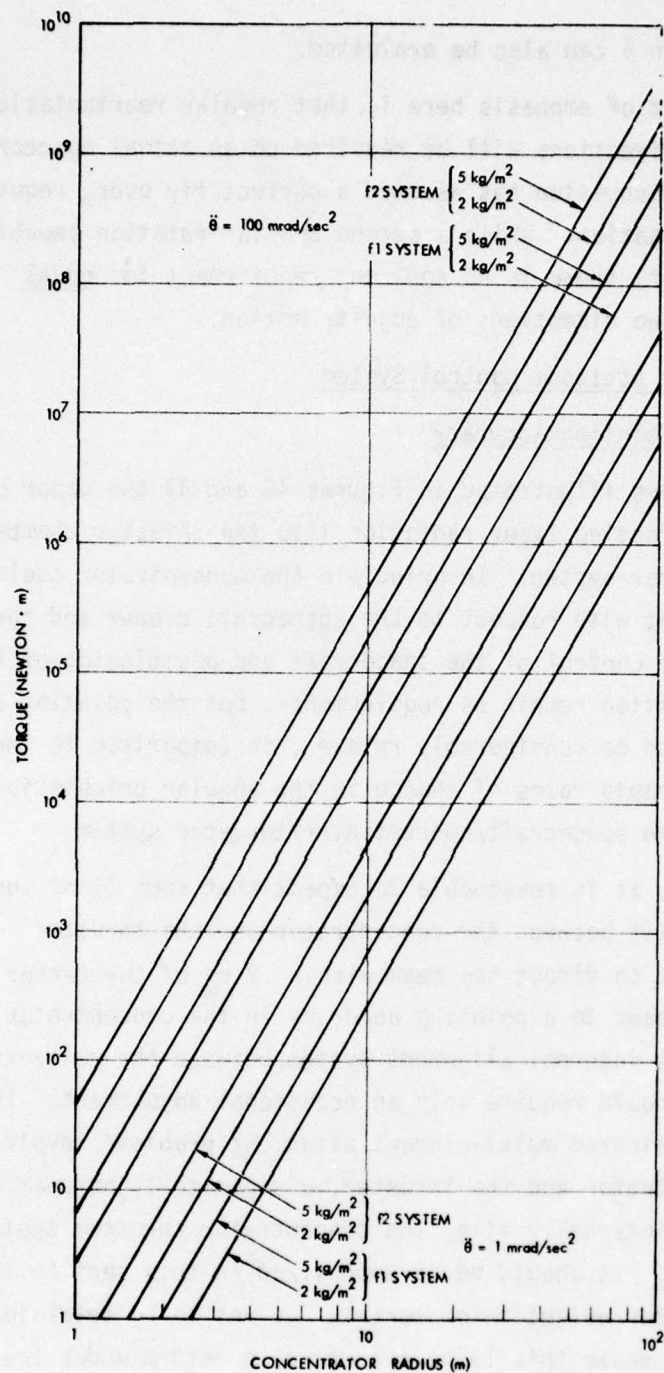


Figure 58. Required Torque to Move Mirror at Indicated Angular Acceleration Levels as a Function of Concentrator Radius

positional change in θ can also be evaluated.

A final point of emphasis here is that angular reorientation of the mirror in two directions will be required on an actual spacecraft, while the present discussion has assumed a perfect fly over, requiring only one angular rotation. While a second angular rotation capability must also be present, there is no apparent requirement for equal capability in the two directions of angular motion.

7.4.2 Concentrator Attitude Control System

7.4.2.1 Required Pointing Accuracy

In the systems illustrated in Figures 46 and 47 the major orientation requirement for directing laser radiation into the thruster chamber is imposed on the mirror system. In principle the concentrator could be in a fixed alignment with respect to the spacecraft proper and the thruster. Attitude control of the spacecraft and positioning of the thrust vector direction remain as requirements, but the pointing accuracies here are expected to be considerably relaxed, in comparison to the mirror and, in addition, rapid rates of change in the angular orientation are not expected for the spacecraft/concentrator/thruster system.

In practice, it is reasonable to expect that some "fine tuning" capability must exist between the concentrator and the thruster. Following Section 7.4.1.1 and to direct the beam within $.2 r_w$ of the center of the thruster chamber leads to a pointing accuracy in the concentrator of 10^{-3} radians. This internal alignment system between the concentrator and the thruster should require only an occasional adjustment. In order to avoid very complicated multi-element alignment problems involving the mirror, the concentrator and the thruster, a separate light beam and sensing system to internally align the concentrator/thruster system should be utilized. It should be re-emphasized in this section that reducing concentrator weight below certain (as yet to be determined) minimum levels may cause this large structure to deform under the various loading factors and that the various possible deformations can produce confusing (and non-specific) error signals to alignment sensing devices. What is required, in effect, for useful concentrator response is that the circle of confusion of the concentrator remain at the level

of $\sim .2 r_w$ under all loading conditions.

7.4.2.2 Required Torque

Since the concentrator is not required to track the angular motion of the laser source during a fly over (the beam steering mirror provides this action), torque requirements on the concentrator attitude control system are significantly reduced compared to those of the mirror control system. Moments of inertia of the concentrator and mirror are expected to be similar. If it is assumed that maximum angular acceleration of 10^{-3} radians per second squared are adequate, then torque requirements follow the minimum illustrated case ($\ddot{\theta} = 10^{-3}$) in Figure 58.

7.5 THRUSTER CHAMBER WINDOWS

7.5.1 General Considerations

This system study has relied on two general concepts in scaling the size of the thruster chamber window. The first of these is that the general scale size (both diameter and length) of the thruster chamber is determined by the absorption length. Absorption of radiation over a 10 centimeter distance, for example, will not be achieved efficiently in a thruster chamber in the ~ 1 centimeter diameter range. This necessarily points toward windows considerably in excess of centimeter diameter, effectively eliminating diamond as a possible thrust chamber window. The second general concept has been that mirror and concentrator diameters are, for realistic laser beam angular width and spacecraft altitude, of the order of 10 meters, and that magnification in excess of 100 will be difficult to maintain with light weight systems. These concepts, and the discussion in Section 7.3.4 have led to generalized notions of thruster chamber window diameters in the range of tens of centimeters. For these window sizes, use of the alkaline earth fluorides is indicated. Sections 7.5.2 through 7.5.4 will treat BaF_2 , CaF_2 and SrF_2 windows in terms of required window thickness, power transmission capability, and allowable surface and bulk absorptivity.

7.5.2 Required Window Thickness

For laser transmitters, two considerations enter into the required

window thickness. The first of these is the thickness required to prevent a fracture of the window because of applied pressure. Following Sparks and Chow (JAP 45, 1510-1517) the required window thickness, ℓ_f , to avoid fracture for a window of diameter D and strength σ is

$$\ell_f/D = 0.433 \left(\frac{PSF}{\sigma} \right)^{1/2} \quad (27)$$

where P is pressure applied to the window and SF is the safety factor against window fracture.

A second consideration in window thickness for laser transmitters is optical distortion, a particularly crucial item in view of the desired range of focal lengths. Sparks and Chow list this thickness as ℓ_o , where

$$\ell_o/D = 0.842[(n-1)(P/E)^2(D/\lambda)]^{1/2} \quad (28)$$

where n is index of refraction, E is Young's modulus, and P and D have been defined above.

For a thruster chamber window, only the first of the thickness requirements above is important, since transmission of the laser beam into the thruster chamber is over very short distances (of the order of tens of centimeters), and focal length considerations are not in effect. Figure 59 illustrates the value of ℓ_f/D in the range of (PSF) from 30 to 1200 pounds per square inch for BaF_2 , CaF_2 and SrF_2 windows. For a thruster chamber pressure of 125 psi and a safety factor, SF, of 2, $\ell_f \sim .1 D$ for these window materials. A 30 centimeter diameter window, thus, would be ~ 3 centimeters in thickness. Both the diameter and thickness figures stated here are within the capabilities of present day window technology.

7.5.3 Power Transmission Capability

7.5.3.1 Window Face Cooling

Energy deposited in the bulk of the window material by laser beam absorption there may be removed by either face cooling or edge cooling. The time constant for face cooling, using Sparks and Chow is

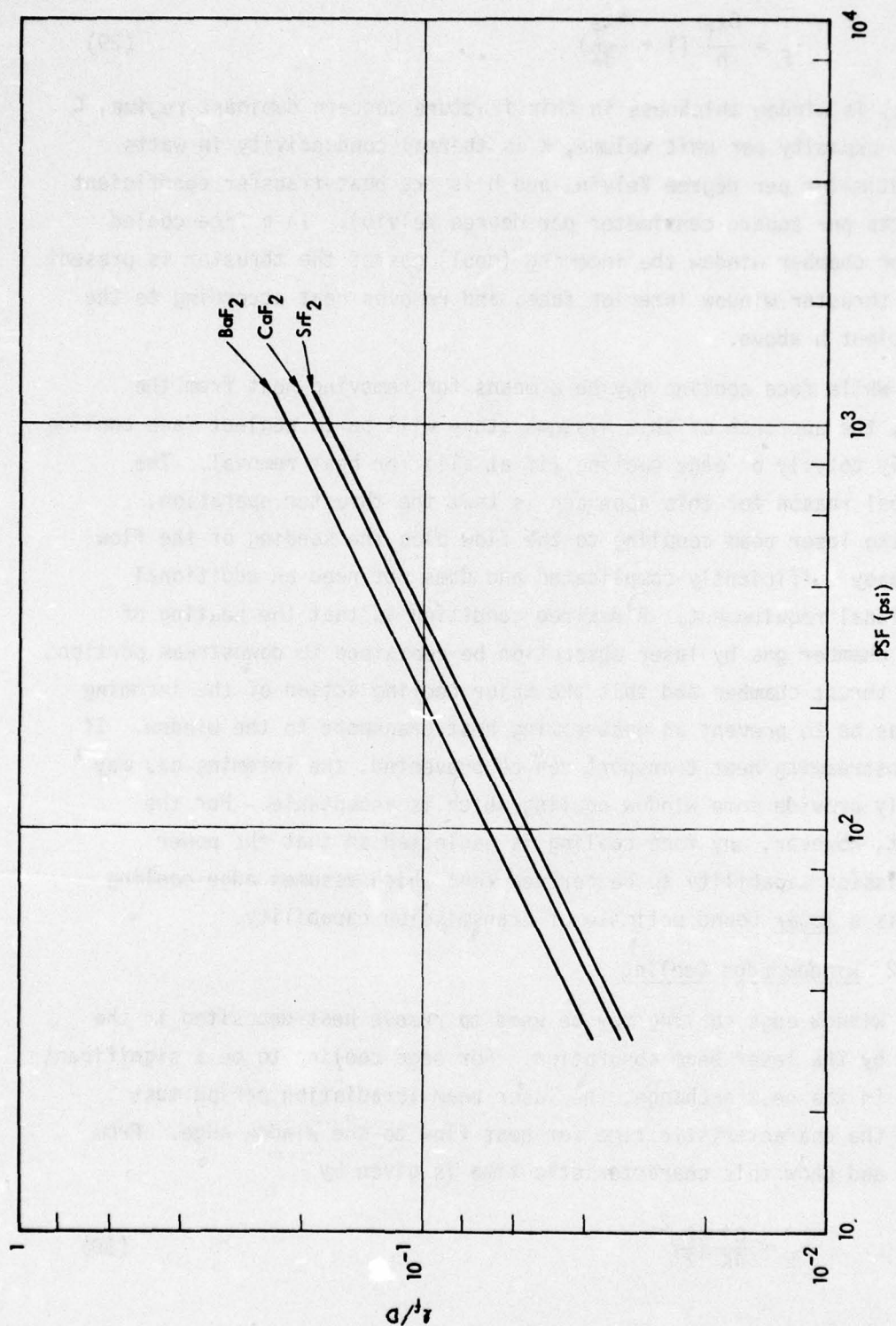


Figure 59. Required Window Thickness (Relative to Window Diameter) to Prevent Fracture as a Function of Pressure and Safety Factor for BaF_2 , CaF_2 , and SrF_2

$$\tau_F = \frac{C\ell_f}{h} \left(1 + \frac{h\ell_f}{3K}\right) \quad (29)$$

where ℓ_f is window thickness in this fracture concern dominant regime, C is heat capacity per unit volume, K is thermal conductivity in watts per centimeter per degree Kelvin, and h is the heat-transfer coefficient (in watts per square centimeter per degree Kelvin). In a face cooled thruster chamber window the incoming (cool) gas of the thruster is present on the thruster window interior face, and removes heat according to the coefficient h above.

While face cooling may be a means for removing heat from the window, the approach of this systems study will be to neglect face cooling and rely totally on edge cooling (if at all) for heat removal. The principal reason for this approach is that the thruster operation, including laser beam coupling to the flow plus the seeding of the flow is already sufficiently complicated and does not need an additional operational requirement. A desired condition is that the heating of thrust chamber gas by laser absorption be contained to downstream portions of the thrust chamber and that the major cooling action of the incoming cold gas be to prevent an upstreaming heat transport to the window. If this upstreaming heat transport can be prevented, the incoming gas may actually provide some window cooling which is acceptable. For the present, however, any face cooling is neglected so that the power transmission capability to be derived (and which assumes edge cooling only) is a lower bound estimate of transmission capability.

7.5.3.2 Window Edge Cooling

Window edge cooling may be used to remove heat deposited in the window by the laser beam absorption. For edge cooling to be a significant factor in the heat exchange, the laser beam irradiation period must exceed the characteristic time for heat flow to the window edge. From Sparks and Chow this characteristic time is given by

$$\tau_E = \frac{C}{4K} \left(\frac{D}{2}\right)^2 \quad (30)$$

where τ_E is in seconds for the terms and units previously described. Values of τ_E as a function of window diameter have been calculated for CaF_2 , BaF_2 , and SrF_2 windows and are given in Figure 60.

An important aspect of the data given in Figure 60 is that, for $D \sim 10$ centimeters, the characteristic time for edge cooling is of the order of 10^2 seconds. On a fly over mission, the period of laser beam irradiation will be of the order of 30 seconds (for 200 kilometers altitude) so that, for this mission at least, the energy transmission capability of the window will be determined by heat capacity of the window and by allowable temperature buildup in the window, rather than by any edge cooling. (Previous considerations of face cooling effects should be borne in mind for this laser burst period for $t < \tau_E$).

In order to calculate the power transmission capability (or the energy transmission capability for $t < \tau_E$), it is necessary to calculate allowable temperature buildup from the center to the edge of the window without fracture. From Sparks and Chow, this is given by

$$\Delta T_f = \frac{2\sigma}{\alpha E S F} \quad (31)$$

where σ is strength (in psi), E is Young's modulus (in psi), α is the linear thermal expansion, and SF is the desired safety factor. Table 45 provides calculated values of ΔT_f for CaF_2 , SrF_2 , and BaF_2 for safety factors of 2 and 4.

Table 45. Allowable Temperature Rise, ΔT_f , in Degrees Kelvin, without Window Fracture for Safety Factors of 2 and 4.

SF	Window Material		
	CaF_2	SrF_2	BaF_2
2	24.5	26.3	25.0
4	12.2	13.1	12.4

These allowable temperature elevations may then be used to calculate allowable energy transmission through the window. From Sparks and Chow:

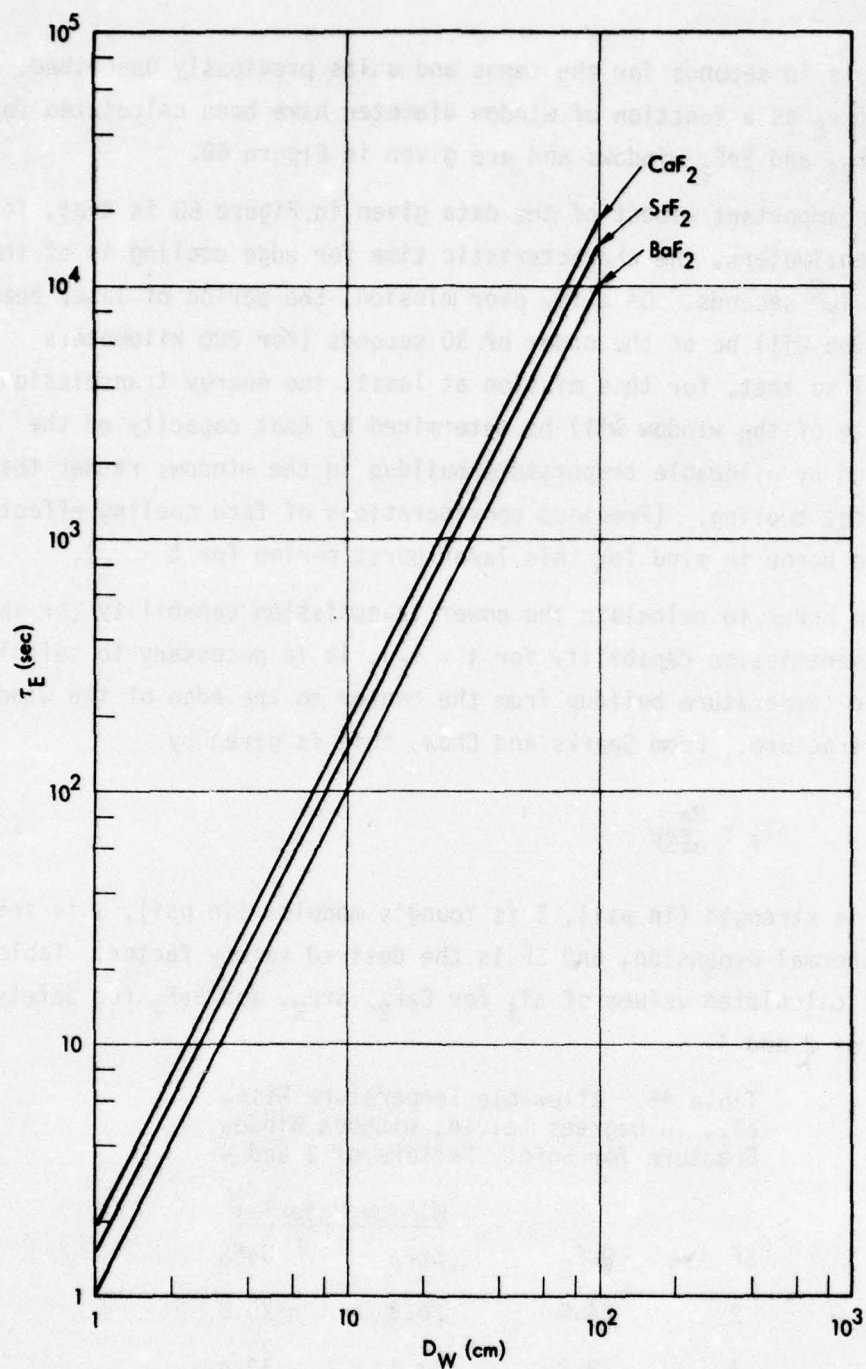


Figure 60. Characteristic Time, τ_E , for Edge Cooling of CaF_2 , SrF_2 , and BaF_2 Windows as a Function of Window Diameter

$$P_{\text{pulse}} = \frac{\pi D^2 C \Delta T}{4 \beta t_{\text{pulse}}} \quad (32)$$

where β is the absorption coefficient (per centimeter, and Eq. (32) is acknowledged to hold for $t_{\text{pulse}} < \tau_E$. For laser beam pulse durations greater than τ_E , τ_E is substituted in Eq. (32).

Figures 61, 62, and 63 illustrate the allowable laser beam power as a function of burst length for CaF_2 , BaF_2 , and SrF_2 as a function of window diameter and for a safety factor of 2 and for an assumed value of $\beta = 10^{-4}$ (see section 7.5.4 for further discussion of possible values of the bulk absorption coefficient).

As an example of the use of the data in Figures 60, 61, 62, and 63, consider a SrF_2 window 20 centimeters in diameter. For this window the characteristic time τ_E is 600 seconds and, for $t_{\text{burst}} > 600$ seconds, the power which may be safely transmitted through the window (at $\text{SF} = 2$, and assuming $\beta = 10^{-4} \text{ cm}^{-1}$) is ~ 330 kilowatts. For a fly over, however, lasting only 30 seconds, the safe power transmission capability of this window would be approximately 6 megawatts. For a 30 second fly over period, with 10 megawatts of laser power through the window, the minimum window diameter for SrF_2 would be ~ 30 centimeters, which is also approximately the size determined from mirror and concentrator diameter, and allowable magnifications. There appears to be, thus, a solution to the required window properties, based on present day window technology.

7.5.4 Surface and Bulk Absorption

Section 7.5.3 has used assumed values of β of 10^{-4} per centimeter for bulk absorption and has neglected surface absorption. This section will examine these assumptions.

A recent survey of optical transmission characteristics by Miles ("Ultimates, Pragmatism, and New Materials") has noted that only three materials (single crystal KCl at $10.6 \mu\text{m}$ incident, single crystal BaF_2 at $5.3 \mu\text{m}$, and fusion cast SrF_2 at $5.3 \mu\text{m}$) have achieved bulk absorptions of less than 10^{-4} cm^{-1} . Figure 64 (which is drawn from Figure 1 of Miles brief review) illustrates the state-of-the-art bulk absorption

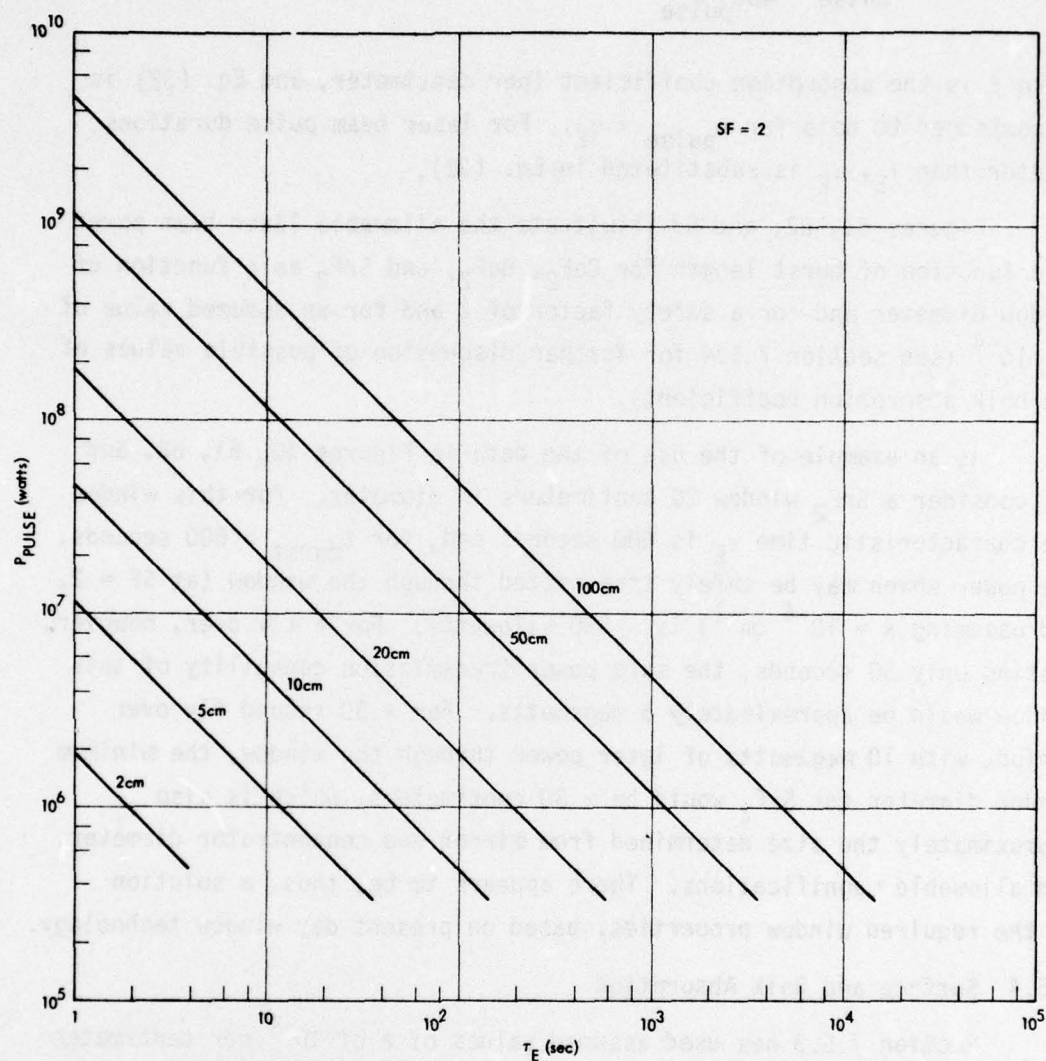


Figure 61. Allowable Power Transmission as a Function of Burst Length for Various Window Diameters for SrF_2 for $t < \tau_E$

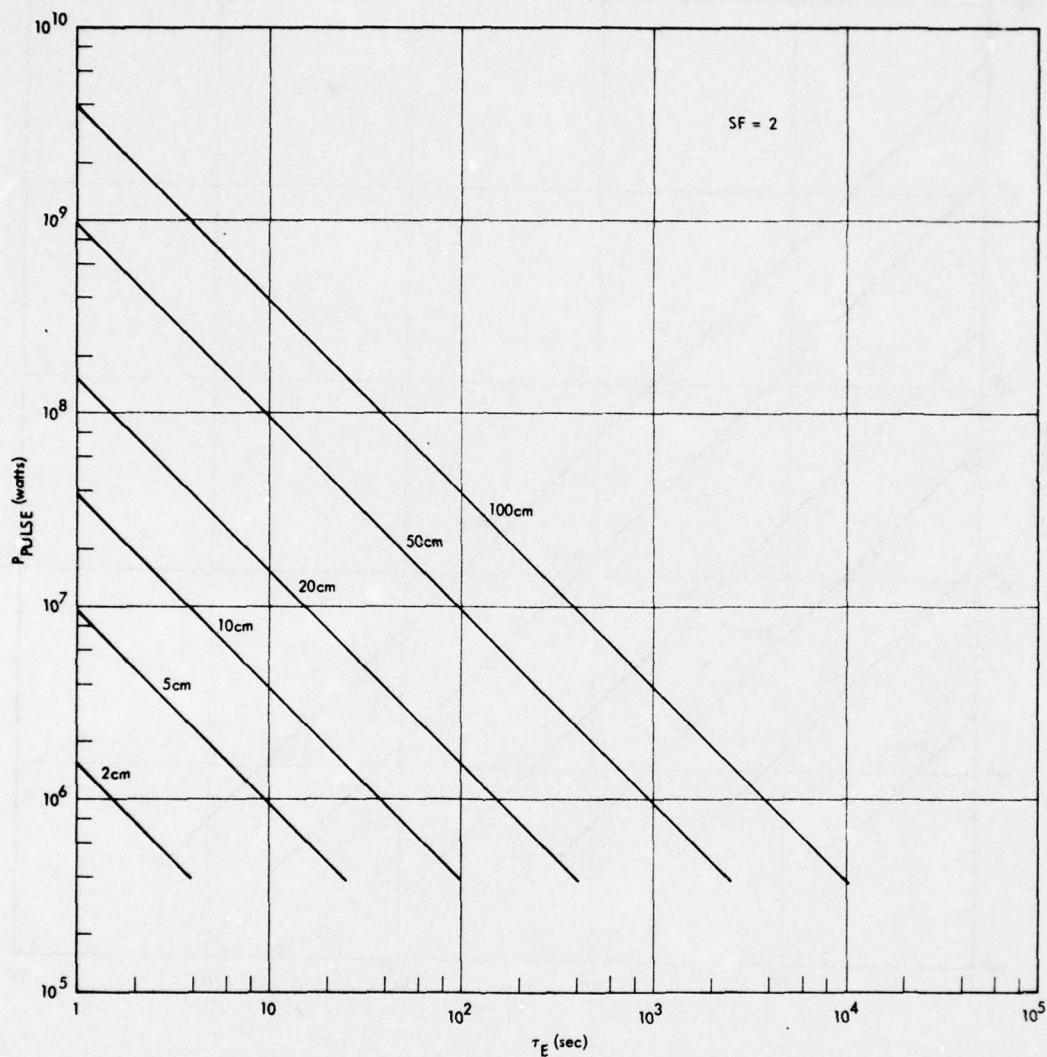


Figure 62. Allowable Power Transmission as a Function of Burst Length for Various Window Diameters for BaF₂ for $t < \tau_E$

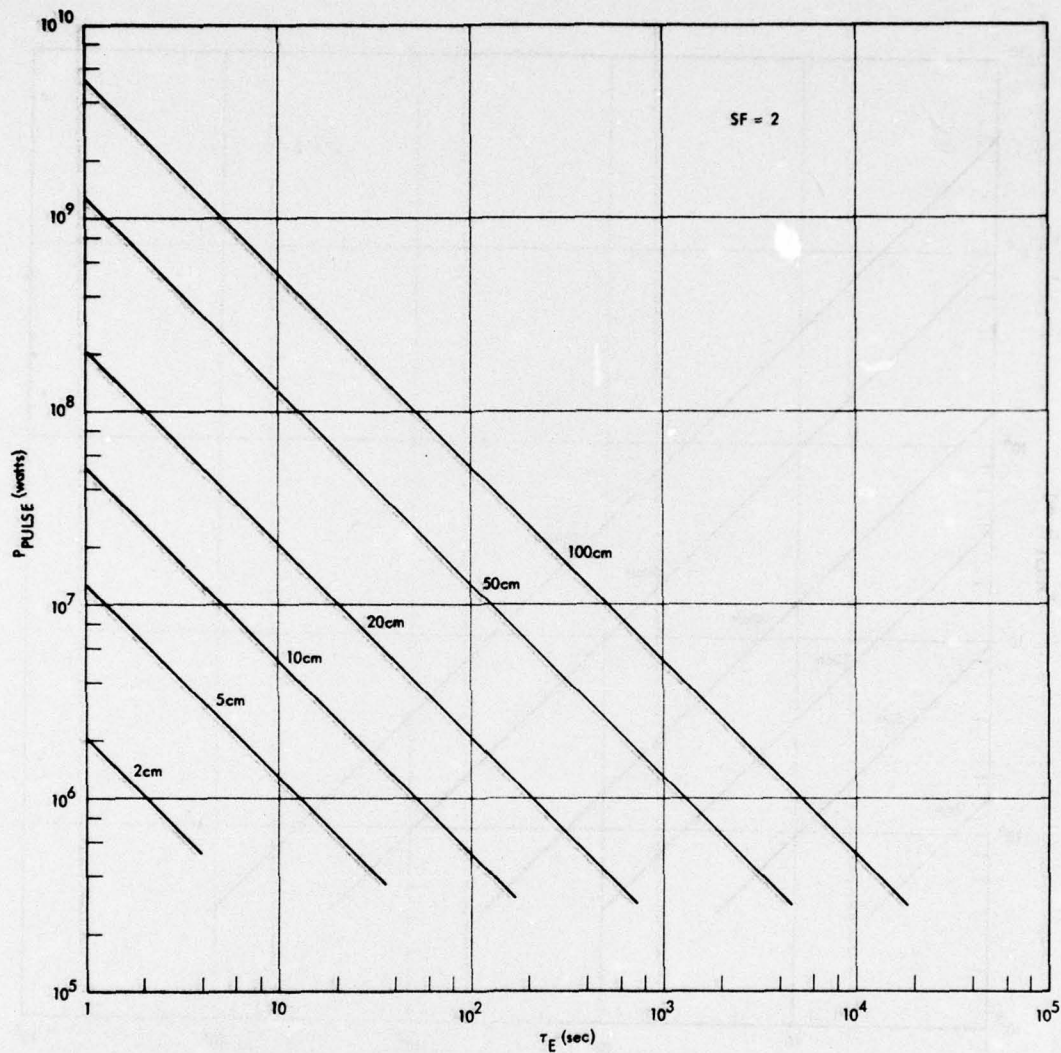


Figure 63. Allowable Power Transmission as a Function of Burst Length for Various Window Diameters for CaF₂ for $t < \tau_E$

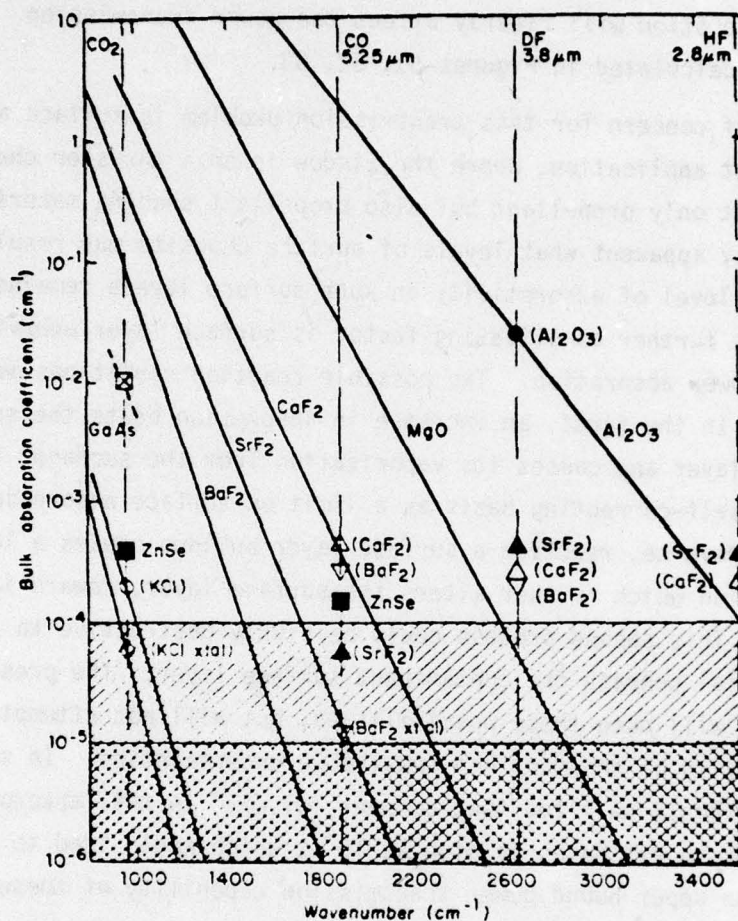


Figure 64. State-of-the-Art Bulk Absorption Coefficients for Laser Window Materials (from Miles)

coefficients for laser window materials as functions of the wavelength of incident light. From this data, it may be seen that values as low as 10^{-5} cm^{-1} are obtained, but that it is more likely that $10^{-4} < \beta < 10^{-3} \text{ cm}^{-1}$ will obtain, at least for present day materials. These higher values of absorption will clearly affect the power transmission capabilities calculated in Figures 61, 62, 63.

Also of concern for this transmission problem is surface absorption. In the present application, where the window is on a thruster chamber containing not only propellant but also propellant seeding material, it is not readily apparent what levels of surface deposits may result and, in turn, the level of absorptivity in such surface layers remains unknown. One further complicating factor is surface layer behavior under sufficient power absorption. Two possible reaction conditions may be considered. In the first, an increase in absorption heats the surface contaminant layer and causes its vaporization from the surface, thus acting on a self-correcting basis as a limit on surface absorption. In the second, reverse, reaction a surface layer buildup causes a local heat deposition which further alters the surface layer, toward increased absorption. This second process could be highly destructive to the window material beneath the contaminant surface layer. The present system study will note these possibilities, but will not attempt further solution in view of the many non-resolvable uncertainties. In summary, however, it should be noted that current "wisdom" in this absorption process leads to estimates as high as 10^{-3} , which would lead to significant influences on upper bound power transmission capability of these windows if such absorptions are, indeed, obtained.

7.5.5 Window Defocus of Transmitted Light

The discussion throughout this systems study has assumed that the thruster chamber windows are planar. It should be noted, however, that the laser absorption calculations have been performed for a laser beam of uniform cross section along the thruster axis. Figure 65 illustrates this assumed parallel flow light beam and also illustrates the converging light beam which would be obtained if a planar window is used. Figure 65 also illustrates the necessary lens action in the window in order to

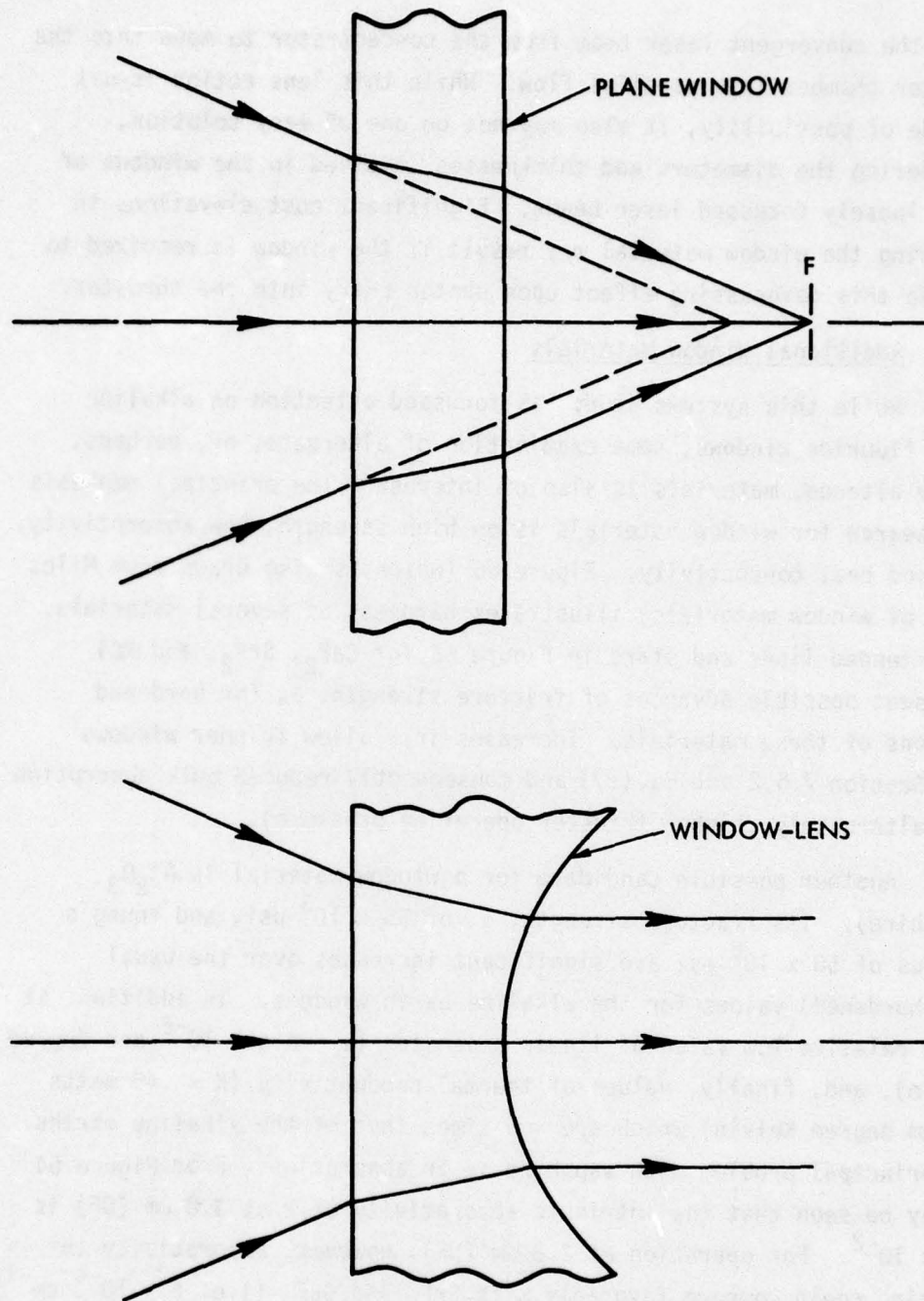


Figure 65. Laser Beam Shape for Planar Thruster Chamber Windows and Shaped Thruster Chamber Windows

cause the convergent laser beam from the concentrator to move into the thruster chamber in a parallel flow. While this lens action is not outside of possibility, it also may not be one of easy solution, considering the diameters and thicknesses involved in the windows of these loosely focussed laser beams. Significant cost elevations in providing the window material may result if the window is required to provide this defocussing effect upon photon entry into the thruster.

7.5.6 Additional Window Materials

While this systems study has focussed attention on alkaline earth fluoride windows, some examination of alternate, or, perhaps, merely altered, materials is also of interest. The principal emphasis in a search for window materials is on high strength, low absorptivity, and good heat conductivity. Figure 66 (which is also drawn from Miles study of window materials) illustrates hardness of several materials. The extended lines and stars in Figure 66 for CaF_2 , SrF_2 , and KCl represent possible advances of fracture strength, σ , for hardened versions of these materials. Increases in σ allow thinner windows (see Section 7.5.2 and Eq. (27) and consequently reduced bulk absorption (or, alternately, higher thruster operating pressure).

Another possible candidate for a window material is Al_2O_3 (sapphire). Its fracture strength, σ , of 65×10^3 psi, and Young's modulus of 50×10^6 psi are significant increases over the usual (non-hardened) values for the alkaline earth windows. In addition, it has a relative low value of linear expansion ($\alpha = 5.5 \times 10^{-6}$ per degree Kelvin), and, finally, values of thermal conductivity ($K \sim .45$ watts per cm degree Kelvin) which are ~ 5 times that of the alkaline earths. The principal problem with sapphire is in absorption. From Figure 64 it may be seen that the intrinsic absorptivity of β at $3.8 \mu\text{m}$ (DF) is $\sim 2 \times 10^{-2}$. For operation at $2.8 \mu\text{m}$ (HF), however, absorptivity in sapphire could compare favorably with SrF_2 and CaF_2 (i.e. $\beta \sim 10^{-4} \text{ cm}^{-1}$). Table 46 provides performance values of a sapphire window under HF ($2.8 \mu\text{m}$) laser radiation.

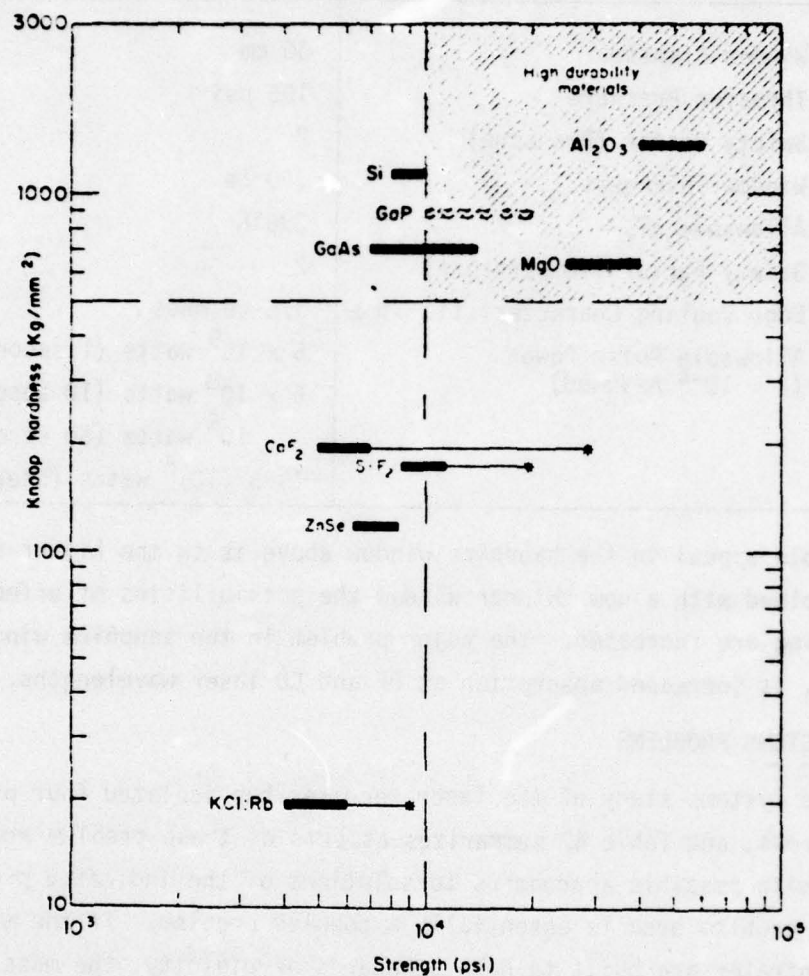


Figure 66. Strength and Hardness Characteristics of Potential Laser Window Materials (from Miles)

Table 46. Performance Parameters of a
30 cm Diameter Sapphire Thruster Window
(HF, 2.8 μm Incident).

Window Diameter	30 cm
Thruster Pressure	125 psi
Safety Factor (Pressure)	2
Window Thickness	.80 cm
Allowable ΔT_f	236°K
Safety Factor (Temperature)	2
Edge Cooling Characteristic Time	375 seconds
Allowable Pulse Power ($B \sim 10^{-4}$ Assumed)	5×10^9 watts (1 second) 5×10^8 watts (10 seconds) 10^8 watts (50 seconds) $13.3 (10)^6$ watts (Steady State)

One possible appeal in the sapphire window above is in the higher allowable ΔT_f . Combined with a now thinner window the possibilities of effective face cooling are increased. The major problem in the sapphire window, of course, is increased absorption at DF and CO laser wavelengths.

7.6 SYSTEMS PROBLEMS

The systems study of the laser receiver has isolated four principal problem areas, and Table 47 summarizes aspects of these problem areas together with possible approaches to solutions of the indicated problems. The first problem area is essentially a coupled problem. If the mirror and concentrator are built to high standards of rigidity, the mass of these elements becomes excessive, while, if the structures are built at low surface mass density, deformations of the structures may occur under the various loading factors which have been identified. The approach in this study has been to emphasize a mirror and concentrator system of only moderate (~ 100) magnification. This necessarily leads to larger thruster chamber windows and, in turn, to reduced allowable thruster chamber pressure.

A second problem area is in the mirror angular momentum and angular acceleration requirements. The angular momentum aspect of this

Table 47. Problem Areas in the Laser Receiver System and Possible Approaches to Solution

PROBLEM AREA	APPROACHES TO SOLUTION OF PROBLEM
<ul style="list-style-type: none"> • Excessive mirror and concentrator mass • Deformation of mirror and concentrator under various loading factors • Mirror angular momentum requirements • Mirror torque requirements 	<ul style="list-style-type: none"> • Acceptance of reduced rigidity in return for reduced mass, and system design using comparatively low magnification (~ 100) • Counter-rotation of other spacecraft mass • Design of loosely focused system to permit principal "active" control mode with limited or no reliance on "reactive" control measures
<ul style="list-style-type: none"> • Window fracture from thruster pressure • Window fracture from bulk absorption • Window fracture from surface absorption 	<ul style="list-style-type: none"> • Increased window thickness and selection of lower pressure range for thruster operation • Principal appeal to edge cooling with limited appeal to face cooling • Spatial separation of propellant seed injection from window with input gas flow cleaning
<ul style="list-style-type: none"> • Contamination of IR reflector surfaces by material transport and deposition 	<ul style="list-style-type: none"> • Thruster and other efflux source placement to reduce contaminant plume density

dynamics problem clearly will require available mass for counter-rotation. As for angular acceleration, the principal hope here is the loosely focussed system will not require the rather high levels of torque which may result in a purely "reactive" control situation.

Several aspects of window design present problems. To avoid fracture from thruster chamber pressure, the window must be thickened and, chamber pressure must be reduced. Satisfactory system design can be achieved for chamber pressures in the range of 10 atmospheres. Window fracture from bulk absorption can be avoided by the larger size windows (greater heat capacity), and by both edge and face cooling. As noted, the major appeal has been made to edge cooling. Window problems due to possible surface absorption (from accretion and alteration of surface contaminants) remain as largely undefined areas. Possible approaches to solution of contaminant problems are given in Table 47, but are basically speculative. The Baseline Test System (Section 7.7) could provide answers to some of these unknown performance areas.

A final problem area is in contaminant layer build-up on IR reflecting surfaces. As noted, these problems may be reduced by proper placement of the thruster and other efflux sources. It should be emphasized, however, that only very thin layers of contaminant can cause severe alteration of reflecting surface properties, so that a satisfactory solution of this problem may require considerable effort in shielding of efflux sources from the mirror and the concentrator.

7.7 BASELINE TEST SYSTEM

This systems study has based the design of the mirror/concentrator/window/thruster system on currently available technology. This permits a Baseline Test System to be proposed for an examination of performance parameters of eventual flight systems. Table 48 lists elements of the Baseline Test System. Also presented there are proposed initial tests for this system. Tests of the optical quality of the concentrated beam, using presently available microwave antennas (paraboloids) with appropriate reflecting coatings, can be conducted in the visible, with IR beams introduced in later tests, after appropriate IR reflecting coatings have been applied. This permits an increased development time

Table 48. Baseline Test System With Initial Systems Tests

<ul style="list-style-type: none"> ● Mirror 	<ul style="list-style-type: none"> ● 2 to 3 meters diameter ● Graphite/epoxy composite ● IR reflecting surface cut for incidence $\sim 45^\circ$ from normal
<ul style="list-style-type: none"> ● Concentrator 	<ul style="list-style-type: none"> ● f 1, 2 to 3 meters diameter ● Graphite/epoxy composite ● IR reflecting surface cut for normal incidence to $\sim 45^\circ$ from normal
<ul style="list-style-type: none"> ● Window 	<ul style="list-style-type: none"> ● Fusion cast SrF_2 ● 15-30 cm diameter
<ul style="list-style-type: none"> ● Thruster 	<ul style="list-style-type: none"> ● 125 psi chamber pressure
<ul style="list-style-type: none"> ● Initial tests 	<ul style="list-style-type: none"> ● Circle of confusion of mirror/concentrator system for distant point source under simulated loading conditions (these tests could be conducted using visible rather than IR) ● IR laser beam (100 kW) onto baseline test system with examination of laser beam quality after concentration and passage through window ● Propellant introduction into thruster chamber for 100 kW coupling experiments

for lost cost IR reflecting materials bonding to the graphite epoxy substrate material.

7.8 MIRROR-CONCENTRATOR CONFIGURATIONS FOR A LASER AIDED THRUSTER

Figures 46 and 47 of this laser receiver system have illustrated an f_1 and an f_2 mirror-concentrator system. It is of interest to consider a total system configuration of the spacecraft utilizing the laser aided thruster, and Figure 67 illustrates such a system.

While the spacecraft in Figure 67 represents one embodiment of the laser aided thruster system, it should be emphasized that system design in this area has not been exhaustive and that a variety of mirror-concentrator-thruster configurations may be considered. This section will review some of the design considerations which led to the configuration illustrated in Figures 46, 47, and 67, and will discuss possible advantages and disadvantages of an alternate mirror-concentrator arrangement.

A fundamental design factor is that the direction of laser beam propagation (from the ground station) will not, in general, coincide with the required direction of thrust. Because of the large angular separation of these two directions (consider, for example, direct flyover with thrusting along the spacecraft velocity direction), it follows that at least two optical elements must be used in the required redirection and concentration of the laser beam. Because of the motion of the laser beam source relative to the spacecraft, it also follows that the optical system must be capable of realignment as a function of spacecraft position along the flight path.

The simplest possible two element system to produce beam redirection and concentration will utilize a mirror and a concentrator. The remaining question then becomes the order in which the laser beam encounters these elements. In the method chosen in Figure 46 the first encounter is with the mirror, followed by the concentrator, and then having injection into the thruster. This will be denoted as an MCT configuration. The alternative to be discussed later (in which the first encounter is with the concentrator) will be denoted as CMT.

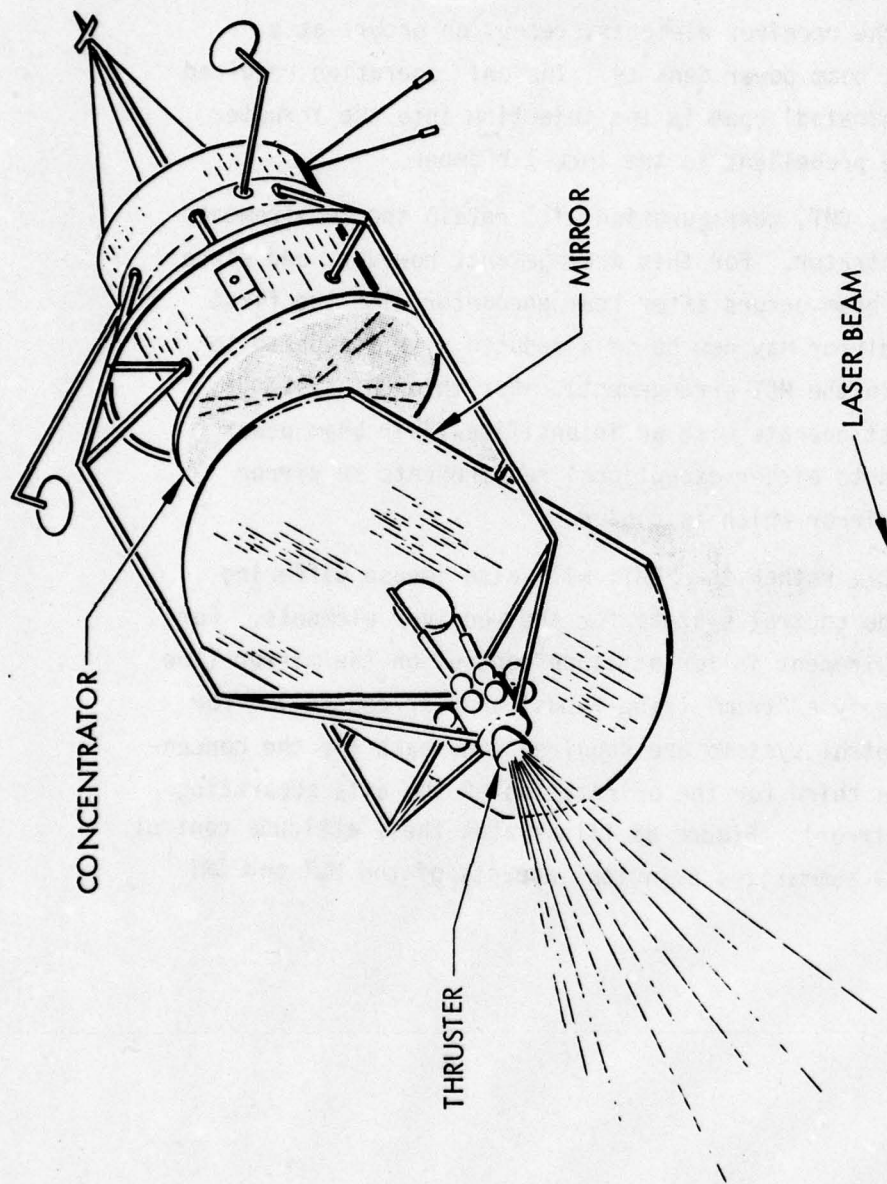


Figure 67. Beamed Laser Propulsion Spacecraft.

For the MCT configuration, a natural requirement will be that the mirror must have a large area (in order to efficiently collect the laser energy). Since the mirror merely reflects the laser beam, the concentrator in the MCT configuration must also be a large area element. This results in a useful practical situation that in both encounters of the laser energy with the receiver elements, reception occurs at a comparatively low level beam power density. The only operation required for the intense (concentrated) beam is the injection into the thruster and its coupling to the propellant in the thrust chamber.

The alternate, CMT, configuration will retain the requirement for a large area concentrator. For this arrangement, however, and since a concentration of the beam occurs after beam encounter with the first receiver element, the mirror may now be of a reduced size (compared to the size used earlier in the MCT arrangement). For this CMT system, however, the mirror must operate with an intensified laser beam power density. This may lead to either exceptional requirements in mirror reflectivity, or to a mirror which is cooled.

The use of MCT, rather than CMT, will also impose differing requirements in attitude control systems for the receiver elements. For MCT, the principal requirement is for attitude control on the mirror (the concentrator utilized only a "trim" (fine-focus) angular control). For CMT, three attitude control systems are required (one each for the concentrator and mirror and a third for the orientation of the axis separating the concentrator and mirror). Figure 68 illustrates these attitude control requirements. Table 49 summarizes principal aspects of the MCT and CMT configurations.

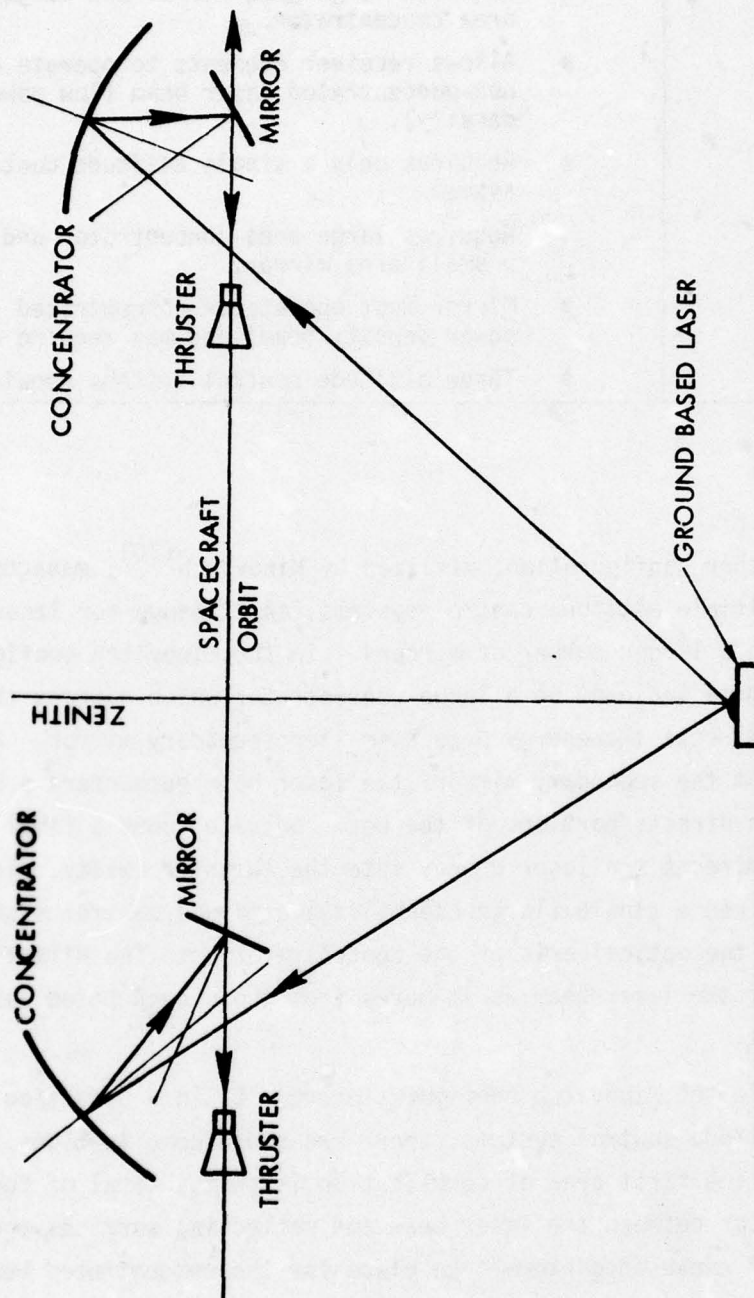


Figure 68. Reorientation of Concentrator, Mirror, and Concentrator-Mirror Axis During Direct Flyover of Laser Aided Thruster System.

Table 49. Principal Design Factors in Mirror/Concentrator/Thruster and Concentrator/Mirror/Thruster Configurations.

Configuration	Design Factors
<ul style="list-style-type: none"> • MCT 	<ul style="list-style-type: none"> • Requires large area mirror and large area concentrator. • Allows receiver elements to operate on non-concentrated laser beam (low power density). • Requires only a single attitude control system.
<ul style="list-style-type: none"> • CMT 	<ul style="list-style-type: none"> • Requires large area concentrator and only a small area mirror. • Mirror must operate on concentrated (high power density beam) and may require cooling. • Three attitude control systems required.

Another configuration, utilized by Minovitch⁽¹⁰⁾, manages to avoid the use of multiple attitude control systems, in exchange for laser beam encounter with a larger number of mirrors. In the Minovitch configuration, the laser beam is incident on a large concentrator which narrows the beam diameter and directs the energy onto a smaller secondary mirror. After reflection from the secondary mirror, the laser beam encounters a beam splitter which directs portions of the beam "outward" onto a final stage mirror which directs the laser energy into the thruster cavity. The laser receiver requires a single (large capability) attitude control system which directs the optical axis of the concentrator onto the direction of propagation of the laser beam as it moves from the ground based laser to the spacecraft.

While the Minovitch configuration results in a reduction in the number of attitude control systems, there are added complications in three areas. The first area of complication is that a total of four encounters occur between the laser beam and reflecting surfaces and the final three of these encounters take place for the concentrated beam. It is likely that cooling would be required on the secondary mirror, the

beam splitter, and the final stage (pre thruster cavity entry) mirror. The addition of required cooling is a major systems complication in view of the power levels in the beam and the required quantities of heat flow. A second complication in the 4 stage system (Concentrator, Secondary Mirror, Beam Splitter, Final Stage Mirror: C, SM, BS, FSM) is a requirement for the Secondary Mirror to be placed in the incoming laser beam, resulting in another heat input into this system element. A third complication in the configuration is the comparatively narrow separation angle between the thruster axis (and the thrust plumes) and the secondary mirror. Only very small quantities of material deposition (from the thrust beams to the mirror surface) can result in significant increases in absorptivity of the secondary mirror surface to laser beam radiation, and, in view of the power level in the concentrated laser beam at the secondary mirror position, the destruction of this mirror (in spite of a mirror cooling system) would be a likely result. Thus, although the Minovitch configuration simplifies the total system in terms of attitude control requirements, there are significant problems in the heat losses to the mirrors.

7.9 SUMMARY

A systems study has been carried out for a laser receiver consisting of a planar mirror, a concentrator, and a thruster together with appropriate attitude control and sensing devices. The general scale size in this system is determined by the angular width of the transmitted laser beam. For representative laser beams and for representative transmission distances, the required concentrator diameters are in the range of tens of meters. This generalized scale size has crucial implications in terms of system weight and costs, in terms of drag and atmospheric torques, and in terms of maximum allowable energy concentration ratios.

The study has not employed phase coherence for the concentrated laser beam. Instead the system development strategy has been to produce a non-phase coherent laser beam at comparatively modest magnification ratios ($M \sim 100$). This approach reduces the magnification and phase coherence requirements, thus reducing the weight of the laser beam reflector and

concentrator elements. The acceptance of comparatively modest concentration ratios leads, in turn, to an elimination of consideration of very small scale size thrusters. For representative systems, the thrust chamber diameters will be in the range of tens of centimeters. Because absorption lengths of the radiation in the propellant gas material are also of the order of tens of centimeters, the system design strategy above will yield concentrated laser beam diameters comparable in scale to the absorption length which is a desirable condition for a volume absorption process.

The concentrator and mirror (reflector) weight have been examined for the described system design criteria. It appears feasible to provide magnification ratios in the range $M = 100$ with optical elements in the specific weight range of 2.5 kilograms per square meter. A crucial factor in the ultimate design and fabrication of this system will be loss of optical quality as the mirror and concentrator are moved to provide continued interception of the beam and its direction into the thrust chamber. The "dynamic" qualities of the optical elements under attitude control system reorientation, thruster firing acceleration loading, radiation energy absorption, and atmospheric loading will determine the required diameter to the thruster inlet window. Two conditions have been examined for the actions of the attitude control system. These conditions span the range of possibilities and lead to major variations in attitude control system requirements. It is not possible at present to conclude the degree to which either the "active" attitude control situation or the "reactive" attitude control situation will exist for a flight system. A series of ground tests of the optical qualities of the reflector and concentrator under various vibration and acceleration loadings have been recommended.

In addition to a primary attitude control system which will align the mirror, a second attitude control system for the alignment of the concentrator is required. This second, or "trimmer," attitude control system has greatly reduced requirements in torque and angular range, compared to the primary attitude control systems for the mirror. The pointing accuracies of both attitude control systems are comparable, however.

The thruster chamber windows have been studied for window diameters in the range of a few tens of centimeters and for thruster chamber pressures

in the range of 8 atmospheres. Principal emphasis has been given to BaF_2 , CaF_2 , and SrF . The required window thickness for the window diameter and thrust chamber pressure ranges examined are ~ 3 centimeters in thickness. Both the diameter and thickness requirements derived from the study are within the capabilities of present day alkaline earth window technology.

The cooling of the thruster windows has been examined for both face and edge cooling approaches. Face cooling has not been appealed to in view of other possible requirements on the thrust chamber input gas flow to achieve optimum coupling with the laser radiation. The neglect of the face cooling heat withdrawal approaches produces a lower bound estimate on allowable laser power transmission through the windows. For edge cooling, the appropriate thermal delay times have been examined. It has been determined that many of the laser power absorption periods are less than the thermal transport time to the window edge and that the power transmission capability is limited by the allowable heat input into the windows, neglecting either of the two heat withdrawal paths. Even under these circumstances, however, it has been shown that multi-megawatt level laser beam power transmission through the windows is possible for the desired thruster burn times without window damage. These conclusions on allowable power transmission capability have not included surface absorption effects from (possible) contaminant films, and further study of surface absorption effects is recommended.

A final area of study for the thruster window has been alternative window materials. If the laser operation can be carried out at $2.8 \mu\text{m}$ (HF), then sapphire (Al_2O_3) can provide an attractive alternate window material.

A variety of possible systems problems have been identified and approaches to the solution of these problems have been proposed. These system problem areas are summarized in Table 47, and, for brevity, will not be repeated in this present summary section. In addition, a baseline test system has been proposed (Table 48), together with a series of proposed systems tests. A final area of study has been other possible mirror concentrator systems for a laser aided thruster. Specific problems with

a concentrator/mirror/thruster system (CMT), as compared to the earlier mirror/concentrator/thruster system have been identified. Those principal design factors have been summarized in a preceding table (Table 49). The study has also examined the system configuration utilized in earlier studies by Minovitch and has identified specific problem areas which are considered to be present in that configuration.

8. LASER POWERED THRUSTER

8.1 INTRODUCTION

This section will examine possible operational problems in the performance of a laser aided thruster. The thruster system will be consistent with the earlier laser receiver system discussed by Sellen⁽¹²⁾ and with the laser/propellant coupling calculations of Molmud⁽¹³⁾.

In this section it will be shown that the operation of a laser aided thruster will entail, in many areas, new technology. In specific areas, where the data base is inadequate, experiments will be required before a detailed design of the thruster can be carried out. These experiments can be conducted using currently available laser beams.

The Test Plan (Ref 14) describes these experiments and the eventual laser aided thruster in operation in the complete coupling/thrusting portion of the program.

The examination of thruster operational problems will be divided into three time periods: start-up, steady state, and close down operation. It will be assumed that multiple burns will be required by the thruster to satisfy the mission so that specific attention must be given to thruster close down conditions which will permit later, successful, restarts.

This study has used a methanol/H₂ propellant mixture as an example of a laser aided thruster. This is not meant to imply that only CH₃OH/H₂ is an acceptable propellant. It is however, a very promising propellant mixture. Hopefully, other promising propellant candidates will emerge during the laser/propellant coupling tests. An advantage favoring the use of methanol is its capability for prolonged storage in space, thus making possible the application of the laser aided thruster to long term propulsion missions such as apsidal rotation correction and drag make-up. The indicated H₂ component could be either a specific storage in LH₂ (which would lead to problems in long term storability) or as a released product from another, as yet unspecified, hydrogen bearing substance which does possess storability (e.g. CH₄, NH₃).

8.2 THRUSTER START-UP PROBLEMS

8.2.1 Inadvertent Laser Beam Deposition on Thruster End Walls

The treatment of the laser beam/thruster interaction will use the generalized thruster model illustrated in Figure 69. Three features illustrated there are of particular importance. These are: 1) the laser beam diameter, D_b , as it enters the thrust chamber, 2) the absorption path length, L , for laser radiation in the propellant, and 3) the throat diameter, D_t , of the thrust chamber, leading to the nozzle. From Reference 1, an emphasis has been placed upon a loosely focused laser beam in order to reduce requirements on the mirror and concentrator and on the rear end thruster window. For a 10 meter diameter concentrator and a 100:1 reduction in laser beam diameter, D_b will be of the order of 10 centimeters as the radiation enters the thrust chamber. From Reference 13, and for the 125 psi methanol injection condition discussed there, $L \approx 8$ cm.

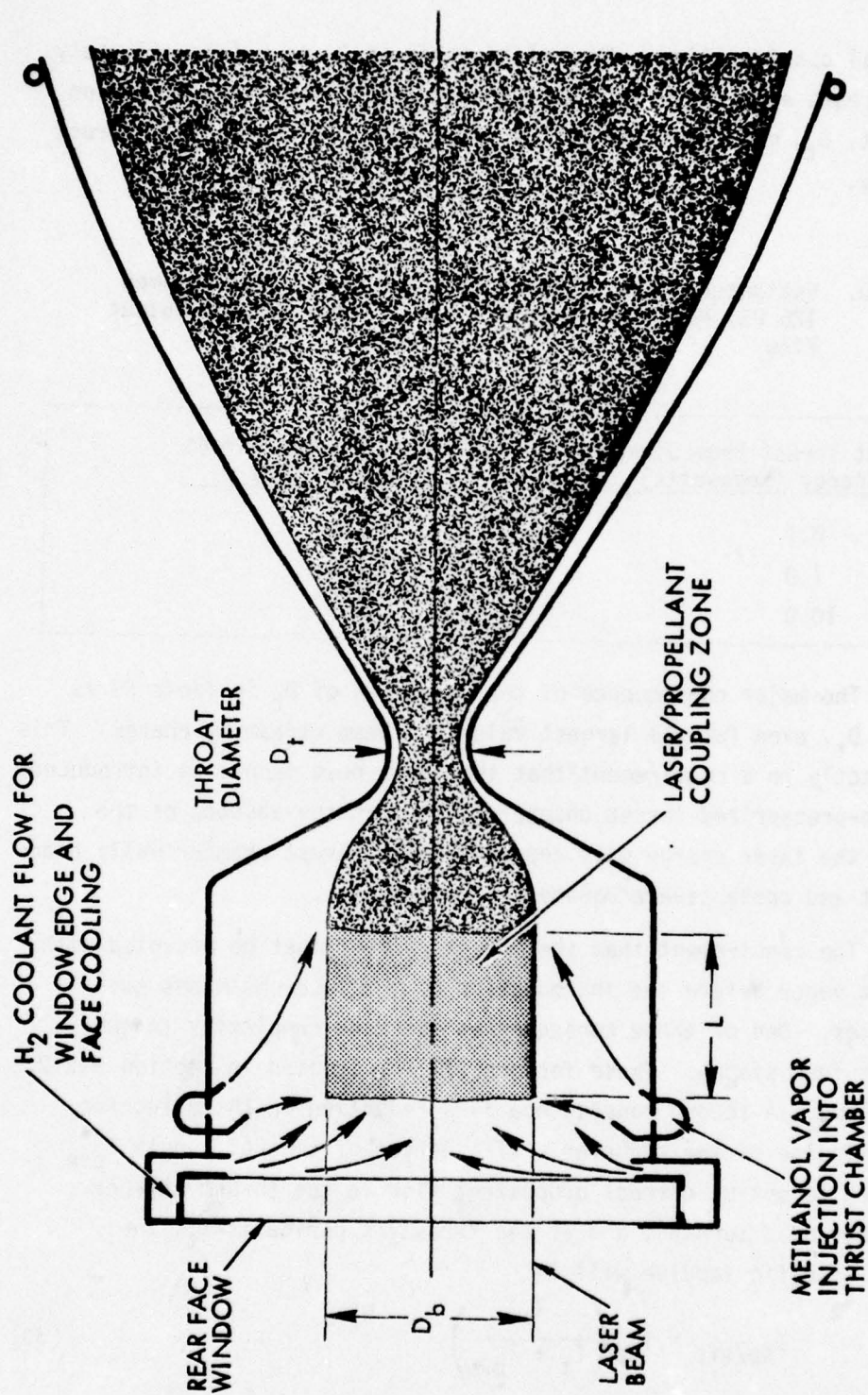


Figure 69. Laser Aided Thruster with H₂ Gas Cooling of Rear Face Window Face and Edges, and Methanol Vapor Propellant Injection.

From general considerations, the relationship of D_b to L (approximately 1 to 1) appears as a reasonable design condition. The final dimension of interest, D_t , may be estimated for three conditions of output thrust beam energy.

Table 50. Estimated Thrust Chamber Throat Diameter for Assumed 125 PSI Methanol Injection and $I_{sp} = 800$ Seconds Output Flow

Output Thrust Beam Streaming Energy (Megawatts)	Thrust Chamber Throat Diameter (cm)
0.1	.5
1.0	1.6
10.0	5.0

The major consequence of the estimates of D_t in Table 50 is that $D_b > D_t$, even for the largest values of beam streaming energy. This leads directly to a requirement that the laser beam cannot be introduced into a non-pressurized thrust chamber, since, in the absence of the methanol, the laser energy will deposit on the thrust chamber walls near the throat and cause severe damage to the thruster.

The requirement that the thrust chamber must be occupied with propellant vapor before the introduction of the laser beam has two consequences. One of these consequences is added complexity in the propellant feed system. These factors will be treated in Section 8.2.2, which follows. A second consequence is a reduction in the effective specific impulse of the thruster. If a period of time of length T_{pre} is required to set up correct propellant flow in the thrust chamber before laser beam turn-on, and if the thrusting period is T_t , the effective specific impulse will be

$$I_{sp/eff} \approx I_{sp} \left(\frac{T_t}{T_t + T_{pre}} \right) \quad (33)$$

where I_{sp} is the specific impulse achieved during laser coupled thrusting.

For a fly-over where the thrusting period is only of the order of 50 seconds, a preparatory period of several seconds can impose significant penalties in effective specific impulse. Section 8.4 will discuss thruster close-down problems and will show that, in addition to T_{pre} , a second period of propellant flow, T_{post} , will be required after laser beam turn-off, to prevent deposition of absorbing particulates on the thruster rear window which would interfere with thruster re-start. The generalized form of effective specific impulse then becomes

$$I_{sp/eff} = I_{sp} \left(\frac{T_t}{T_t + T_{pre} + T_{post}} \right) \quad (34)$$

8.2.2 Required Start-Up Flow Condition

Molmud⁽¹³⁾ has determined the decomposition products of methanol subject to laser beam heating. For heating to 750°K two features are of interest. The first of these is that, above some activation point, the decomposition leads to elevated product temperature without further heat input. All told, zero net heat input is required to elevate the material to ~ 750°K. A second feature of interest is that a significant amount of solid carbon is present at 750°K. In the presence of the laser beam, this solid carbon acts as the principal coupling mechanism. As the products heat to higher temperatures, the solid carbon diminishes, and CO forms which couples, in turn, to the incident laser light.

A major concern in the laser coupling is that the solid carbon act to absorb energy but not act as a reflector of incident light, since this reflection not only prevents entry of the light into the propellant regions, but also results in a significant radiative heat input to the thruster walls. If the solid carbon particles have sizes comparable to the laser light wavelength, significant reflection occurs. A requirement, then, is that particulate matter in the thrust chamber must have values of $(\frac{2\pi r}{\lambda}) \ll 1$. It follows that the presence of liquid methanol droplets is not allowable, since these large size particulates will certainly act to reflect the incident light, cause a heat input to the walls, and prevent the laser beam entry into the principal laser/propellant coupling regions.

From these several required features in the laser interaction with the methanol, it follows that the chamber must be occupied with methanol vapor prior to laser beam entry. It also appears as a reasonable requirement that the methanol be at temperatures below activation (prior to laser beam onset) so that solid carbon will not be present (deposition of carbon particles on the windows can lead to severe absorption and reflection problems there). These requirements are, then, that the methanol vapor be at sufficient temperature to remain in the gas phase for 125 psi. The chamber walls should also be at sufficient temperature to allow the methanol to remain in the vapor phase. Since it is not desired to have warm methanol in contact with the thruster windows during this time, the H_2 gas cooling of the windows must be in operation. Table 51 summarizes requirements for the chamber and propellant prior to laser beam entry.

Table 51. Propellant and Thruster Wall Conditions Required Prior to Laser Beam Entry

<u>Quantity</u>	<u>Condition</u>
H_2 Gas Flow	Present at edges and face of window to prevent methanol deposition and/or heating.
Methanol	Present in vapor phase at 125 psi with required pre-heating to sufficient temperatures for gas phase retention without condensation, but not at such temperatures as to cause decomposition, further heating, and carbon formation.
Chamber Walls	Pre-heat to sufficient temperature to prevent methanol condensation at 125 psi.

As may be noted in Table 51, pre-heating is required for both the methanol vapor and the chamber walls prior to laser beam entry, and appropriate heat sources must be found for these actions. It should also be noted that the required wall temperatures for this action are not, in general, consistent with the use of regenerative cooling of the walls by incoming

(liquid) methanol. The magnitude of the heat transport to the walls (to be discussed in Section 8.3.1) also tends to weigh against a regenerative cooling using the liquid propellant, although in this second instance, the principal problem will be a mismatch between heat input to the walls and heat capacity in the incoming fluid.

8.3 THRUSTER STEADY STATE OPERATION PROBLEMS

8.3.1 Heat Input to Thruster Chamber Walls and Rear Face Window

8.3.1.1 General Considerations

Two aspects of the laser aided thruster will act to create heat transport problems that are not generally encountered in thruster operation. The first aspect is a small value of throat area compared to wall area. In principle, this area ratio can be reduced by more tightly focusing the laser beam with subsequent diminutions in thrust chamber diameter. This leads, however, to excessive requirements in the concentrator magnification and in the pointing accuracy of the attitude control system. For the present system, then, there will be a large amount of wall area exposed to the heated propellant decomposition products.

The second aspect of the laser aided thruster which creates heat transport problems is, perhaps, more generic than the first and is the "unusual" relationship between the mass flow and the heat input to that flow. The central feature of the laser aided thruster is the reduction in required propellant mass by large increases in specific impulse. This leads to a condition of extremely high gas temperatures in the thruster chamber with only modest quantities of input material to act as a wall coolant (if regenerative cooling should be attempted), and, to repeat the argument of the previous paragraph, this process takes place in a chamber whose exposed wall area considerably exceeds the throat area. These two aspects combine to present the laser aided thruster with severe heat loading problems. As a final note, here, it should also be emphasized that portions of this total thruster (the window) must be maintained within a narrow temperature range to avoid damage.

8.3.1.2 Heat Transport Via Conduction

The transport of heat by conduction in the laser aided thruster chamber will be treated qualitatively in this section for several reasons. One of these reasons is the uncertainty in the gas decomposition products for a complete, three dimensional, laser beam coupling to the propellant. Molmud has carried out a one dimensional calculation of decomposition species assuming steady state conditions in the coupling. As Section 8.3.2 will note, the actual 3-D, time dependent coupling of the radiation to the gas flow may involve temporal fluctuations in addition to spatial variations, with consequent time varying gas composition along the thrust chamber walls. A second major reason for a qualitative approach is uncertainty in the gas thermodynamic properties because of the very high temperatures involved in the flow.

In a qualitative approach, and using the description of heat transport given by Sutton⁽¹⁴⁾, the gas film coefficient, h_g , is given by

$$h_g = 0.026 \frac{(\rho v/g)}{D^{0.2}} c_p \mu^{0.2} Pr^{0.4} \quad (35)$$

where the units of h_g are in Btu/sec °R ft², for D, chamber diameter, in feet, c_p is specific heat of the gas in Btu/degree per pound, and μ is absolute gas viscosity in lb sec/ft². The calculated average local gas velocity, in feet per second, is v , ρ is gas density in pounds/ft³, g is the gravitational constant, and Pr is the Prandtl number, given by

$$Pr = \frac{c_p \mu g}{\kappa} \quad (36)$$

where κ is the conductivity of the gas in Btu/sec ft² °R/ft.

When representative values of the various gas parameters are used, values of h_g in the range of 5×10^{-5} Btu/sec °F in² are obtained. While these values may not apply in the present case (because of the temperature ranges involved) the use of h_g of 5×10^{-5} can provide, at least, an estimate of the heat transport across any gas film utilized in a film cooling of the thrust chamber walls. For a ΔT between the gas in the thruster and the thruster wall of 10^4 °R, the heat transport to the walls would be $\sim .5$ Btu/sec in². Using 1 Btu = 1055 Joules, and

$1 \text{ in}^2 = 6.45 \text{ cm}^2$ leads to a heat transport of $\sim 82 \text{ watts/cm}^2$. If the thruster chamber has a diameter of 30 cm and a length of 15 cm, the total wall area of this cylindrical section is $2\pi(15)(15)\text{cm}^2 = 1413 \text{ cm}^2$, and the total heat transport at 82 watts per cm^2 is ≈ 116 kilowatts. While this heat transport is not large for conditions of 10 megawatts, or even 1 megawatt, in the output thrust beam, it is clearly excessive for a condition of only 100 kilowatts in the output flow.

The qualitative calculation above which produced .5 Btu/sec in^2 is in the general range of experience of heat transport to walls (.1 to 25 Btu/sec in^2), except that larger values than .5 Btu/sec in^2 will certainly be expected to occur in the throat region. Irrespective of the precise value of this heat transport, it can be demonstrated that there is not a sufficient heat capacity in the incoming methanol to allow a regenerative cooling of the walls. For an assumed specific impulse of 800 seconds, the mass flow rate for .1, 1, and 10 megawatts of thrust beam flow energy is 3.25, 32.5, and 325 grams per second. In the temperature range of the incoming methanol liquid, the specific heat is $\sim .6 \text{ cal/gm/}^\circ\text{K}$. If the maximum allowable temperature rise in the methanol liquid is 100°K (and this is certainly a high estimate), without methanol boiling in the cooling coils, then the allowable heat transport into the incoming methanol is only 820, 8200, and 82000 watts for the three output flow conditions in the gas of 0.1, 1, and 10 megawatts. Even for the largest of liquid flows above, estimated heat transport to the walls of 116 kilowatts (for the cylindrical section only) exceeds permissible heat input to the liquid.

Two alternative modes of operation can be suggested for cooling the thrust chamber walls. The first of these would be to use the total propellant in storage as a coolant, with only a small fraction of the circulating methanol being injected into the thrust chamber. While this approach is possible for comparatively short burns, there are anticipated problems for the longer periods of thruster operation (during which the entire tankage system would attain temperatures that could impact on the operation of that system and other spacecraft systems), and near the end of operation (where the total propellant is no longer a high heat capacity element).

A second alternative to the regenerative cooling operation above, is to allow certain sections of the thrust chamber to radiatively cool. This approach also has disadvantages. One of the disadvantages is the heat loading which the radiating portions of the thruster would impose on other portions of the spacecraft (and for the thruster/mirror configuration used in Reference 12, on the mirror). A second, possible, disadvantage to radiative cooling is heat loading on the rear face thruster window. The window has extremely low absorption in wavelengths of the order of a few microns (for the alkaline earths). Longer wavelengths are, however, readily absorbed in the window. The concern for any radiative transport of heat in this laser aided thruster would be that excessive quantities of heat appear in wavelength ranges above ~ 10 microns, emphasizing again that there are only small allowable temperature rises in this material without window fracture and that the total heat capacity of the window is not large.

A final means of accommodating the heat flow from the thrust chamber gas is to utilize the heat capacity of the "downstream" elements of the thruster. If the thruster total mass is M_t and a fraction of this mass, β , can be allowed to rise in temperature, specific heat is c_{pt} , and the allowable temperature rise is ΔT_t , a total heat transport of $\beta M_t c_{pt} \Delta T_t$ can occur between the chamber gas and the walls. The time in which ΔT_t occurs will be Δt where

$$\Delta t = (\beta M_t c_{pt} \Delta T_t) / P_{gw} \quad (37)$$

where P_{gw} is the rate of heat transport from the gas to the walls. Using βM_t of 100 kilograms, a c_{pt} of 1 Joule/gram/°K, a ΔT_t of 1000°K and $P_{gw} = 10^5$ Joules/sec leads to a thruster heat up time of 10^3 seconds. This time is considerably above that required in the direct flyover with laser beam input at perigee. Other missions with longer thrusting periods are, of course, possible and if the total thrusting period exceeds the Δt above, an appeal could be made to multiple burns. A final point to emphasize here is that cooling of the thrust chamber window will be required during the overall thruster cool down period, which can be lengthy if only radiative cooling is present for the hot chamber walls and nozzle.

8.3.1.3 Heat Transport Via Radiation

Radiated energy is present in the thrust chamber because of the high temperatures of the gas, and, specifically, in view of the basic method of energy input into the propellant. This section will consider both line spectrum and black body forms of radiative energy transport.

The coupling of the laser radiation to the propellant relies heavily on the strong absorption of methanol decomposition products to incoming laser radiation. If the incoming laser radiation is from a CO laser, the CO formed in the heating of the methanol will absorb strongly with a resultant absorption distance of the order of 1 centimeter⁽¹³⁾. Reradiation from CO in the thrust chamber will also be absorbed in the gas volume. Because of the opacity of the gas in these wavelengths, significant transport of energy to the walls is not expected.

The second form of radiation to be considered here is black body radiation from the hot gas region, principally due to the level of ionization which builds up in the heated flow. Molmud⁽¹³⁾ has evaluated the absorption distance for radiation via inverse bremsstrahlung and concluded that, at the electron densities determined to exist for the referenced calculation (~ 800 kw of absorbed laser energy in the flow), the absorption coefficient is $\sim 4 \times 10^{-4} \text{ cm}^{-1}$, and is not a major contributor in absorption. Since this absorption process is of limited extent, emission will also be limited. Thus, although high temperatures are present in the chamber, the hot gas volume for the dimensions used in this thruster design, yield an optically thin emitter whose radiation to the walls will not be significant, particularly in view of the large expected values of heat transport via conduction.

8.3.1.4 Gas Injection Cooling of Thruster Chamber Walls

Section 8.3.1 has indicated that the conductive heat transport to the walls, for a gas film cooling of the wall, could be at the 100 kilowatt level for the gas temperatures involved and for the thruster dimension employed. It has also been demonstrated there that the heat capacity of the incoming methanol fluid is not sufficient to allow a regenerative cooling of the walls by methanol fluid flow through the chamber wall structure. The alternative of circulating excess methanol

(returning some to the propellant tank) presents end-of-mission problems when the remaining volume of methanol vanishes, and, in addition, allows heat transport to the walls to result in a net heat loss with a subsequent penalty to the total thruster operation (particularly at low power levels where as much energy may be lost at the walls as appears in the useful, output, gas flow). A second alternative of using the heat capacity of the thruster walls, with cutoff of thrusting when the walls pass some upper temperature limit is also unattractive since it limits the allowable burn time and also allows the heat loss to the walls to exist and to detract from overall thruster efficiency.

Another approach to the cooling of thruster walls will be considered here and will involve a form of regenerative cooling. Figure 70 illustrates this possible cooling scheme. A significant difference between wall cooling with the inlet fluid methanol and wall cooling with injected H_2 is that a much larger ΔT is allowed for the H_2 injection than for the methanol (where temperature rises in excess of $\sim 100^\circ K$ could result in a complete boiling of the incoming fluid, blocking further fluid injection). In the gas injection cooling case, it is desirable that the intervening walls be of high heat conductivity and low heat capacity for better coupling to the H_2 gas and for reduced efficiency penalties from non-recoverable heat investments.

8.3.2 Laser Radiation/Propellant Coupling Problems

8.3.2.1 Laser Beam Positional Change in Thrust Chamber

Figures 69 and 70 have illustrated a laser beam of diameter, D_b , which enters the thrust chamber along the axis of that chamber and couples to the propellant in a region centered on the thrust chamber axis. From Reference 12, however, it is apparent that there will be some wander of the laser beam position. The extent of this wander is presently difficult to describe precisely and will depend, among other things, upon the mirror and concentrator attitude control system pointing accuracy and the mirror and concentrator optical qualities, in the presence of thruster firing and spacecraft motion relative to the laser beam source. In order to prevent damage to the exterior surfaces of the thruster by laser beam motion outside the limits of the window, the

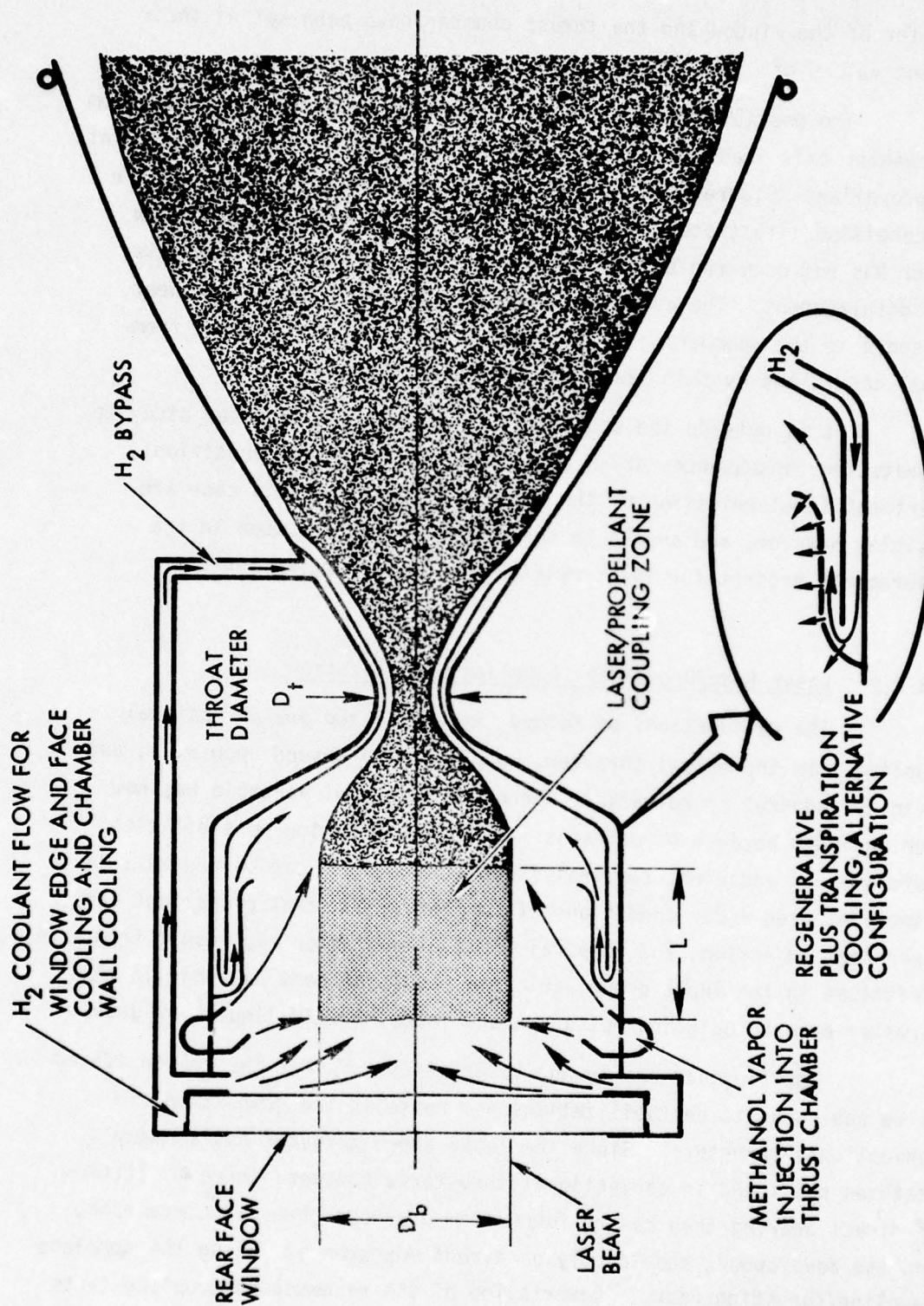


Figure 70. Laser Aided Thruster with H₂ Gas Bypass for Throat and Chamber Wall Cooling.

diameter of the window and the thrust chamber have been set at their present values of ~ 30 cm.

The possibility of a movement of laser beam position away from the chamber axis leads to possible asymmetric introduction of energy into the propellant. Figure 71 illustrates this off-axis coupling case. In the condition illustrated there, laser beam deposition on the window holder has not occurred so that no damage has resulted yet from this beam displacement. The energy introduction to the methanol and heat transport to the chamber walls must, however, be perturbed away from normal conditions by this laser beam shift of position.

It is outside the scope of this qualitative thruster study to estimate the consequences of an off-axis laser injection condition. Experimental determination of the flow conditions for this case are possible, however, and should be considered a priority item in the measurements program for the complete coupling/thrusting tests.

8.3.2.2 Laser Beam/Propellant Coupling Stabilization

The calculations of Molmud have utilized one-dimensional coupling. In the actual thruster, coupling will depend upon r , z , and θ (in cylindrical coordinates), where the azimuthal variable has now been included because of off-axis laser beam injection possibilities. There are, in addition, temporal fluctuations which can be present, in principle, even under conditions of completely constant propellant and laser beam injection, and temporal fluctuations which may result from variations in the input propellant as a result of heat exchange in the thruster between outgoing hot gases and incoming cold liquids or gases.

The fluctuations in the laser aided thruster may be considered to be analogous to destabilizations and noise in the combustion of conventional thrusters. Since the laser aided thruster has so many features not found in conventional thrusters, however, there is little of direct bearing than can be found from previous chemical combustion, and the development should rely on direct measurement, using the complete coupling/thrusting tests. Description of the recommended coupling tests is given in the Test Plan. ⁽¹⁴⁾

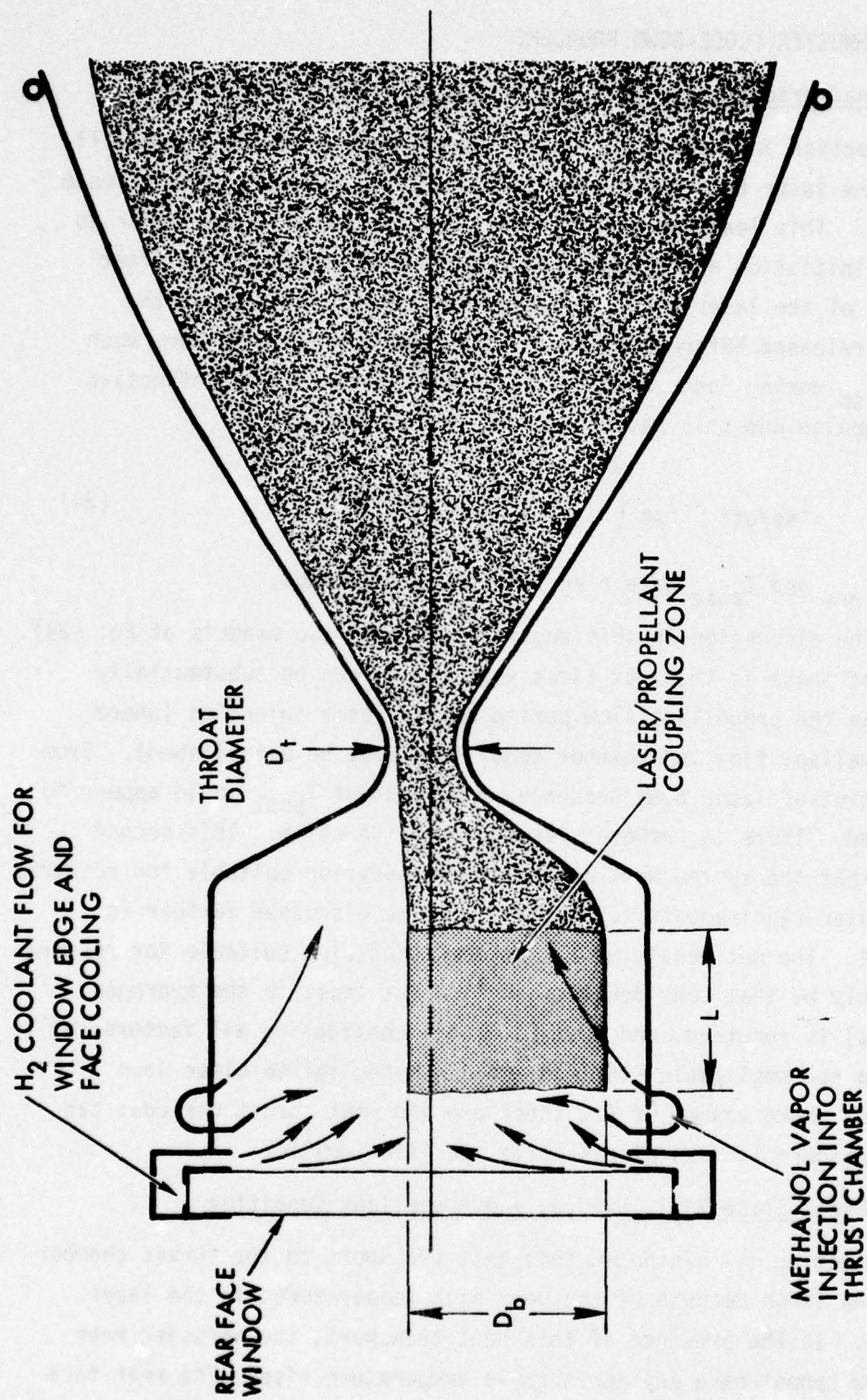


Figure 71. Asymmetric Laser Beam/Propellant Coupling Resulting from Off-Axis Laser Beam Injection into Thrust Chamber.

8.4 THRUSTER CLOSE-DOWN PROBLEMS

8.4.1 Inadvertent Laser Beam Deposition on Thruster End Walls

Section 8.2 has noted that severe damage to the thruster will result if the laser beam is present in the thrust chamber in the absence of methanol. This leads to a requirement for propellant onset prior to laser beam initiation and a period of propellant continued flow after the removal of the laser beam. Because the specific impulse of the propellant released before and after laser beam injection is very much less than I_{sp} during laser heating, there will be an overall effective specific impulse and this has been given in Eq. (34) by

$$I_{sp/eff} = I_{sp} \left(\frac{T_t}{T_t + T_{pre} + T_{post}} \right) \quad (34)$$

where T_t , T_{pre} and T_{post} have been previously described.

The discussion in this section will note two aspects of Eq. (34). The first of these is that, at first view, T_{post} can be substantially shorter than the propellant flow period before laser injection (where proper propellant flow and chamber conditions must be established). From the standpoint of laser beam presence, a neglect of T_{post} would appear to be justified. There is, however, another consideration. This second aspect is that the system must be left in a condition suitable for restart. The particular requirements for restart will be discussed further in Section 8.4. The net result of a shut-down condition suitable for restart will probably be that considerable gas flow (at least in the hydrogen gas coolant) is required, and that Eq. (34), considering all factors, will have both a non-negligible start-up and a non-negligible close-down period. For short values of T_t , these pre and post thrust periods, can cause a considerable loss of effective specific impulse.

8.4.2 Final State Wall, Window, and Propellant Condition

Section 8.4 has noted that heat transport to the thrust chamber walls may be large because of the very high temperatures in the laser heated gas. In the presence of this heat transport, the thruster rear face window cannot have any appreciable temperature rise. The rear face window also cannot have material deposition on it as a result of the

thrusting since a surface layer would probably lead to excessive absorption at the layer and consequent window damage. A final significant factor here is that the decomposition products of methanol at 750°K include substantial amounts of solid carbon. These several features, taken together, will require a continued flow of hydrogen coolant gas after the end of thrusting until two conditions have been achieved. The first of these conditions is the complete cleansing of the system of methanol vapor (to avoid solid carbon formation and deposition). The second condition is the lowering of wall temperatures to that point that there is insufficient heat content in these members to flow backward, after H₂ coolant gas cutoff, and heat the window to the fracture point.

Of the two conditions above, the easier one to satisfy is probably the methanol cleansing, since the surfaces near this propellant will be at elevated temperatures after the burn and will have no significant inventory of methanol for evaporation and carry-out. The second condition, of sufficient wall cooling, may be considerably more difficult to achieve since heat flows can be prolonged and large sections of the total thruster (particularly from the throat to the nozzle exit) will be at elevated temperatures.

8.5 SUMMARY

This section has described the laser aided thruster as a new technology item. The gas temperatures involved move into a previously unexplored regime of thruster operation. This factor is coupled with a comparatively reduced flow of liquid propellant, thus requiring any regenerative cooling of the walls by incoming fluid to function properly under a unique set of circumstances. There is, moreover, the possibility that the source of energy input (the laser beam) may wander away from the thrust chamber center line, introducing asymmetries in the laser/propellant coupling in the chamber, and compounding the problems of essentially unexplored stabilization conditions.

These several factors argue for a series of laser beam/propellant coupling tests in a laser coupling test cell in advance of any detailed thruster design.

REFERENCES

1. "NASA Baseline Space Tug Configuration Definition" - MSFC 68M00039-2, 15 July 1974.
2. Dr. Malcolm Currie, statement to the Senate, quoted in Defense Space Business Daily 9 March 1976.
3. Ed Dupnik, Johnson Space Flight Center, private communication.
4. Ball Armstrong, NASA HQ, private communication.
5. Personal communication from G. Emanuel to W. L. Davenport.
6. Yariv, Amnon; Introduction to Optical Electronics; Holt, Rinehart and Winston, Inc., New York; C 1971 (p. 158).
7. De Maria, Anthony J.; Review of CW High Power CO₂ Lasers; Proceedings of the IEE; June 1973.
8. Mirels, Harold; Chemical Lasers; presented June 20, 1974 as part of UCLA course, Lasers - Quantum Electronics - Holography.
9. Lacina, W. B. and G. L. McAllister; High Energy Scaling Generalization for CO Electric Discharge Lasers; Northrop Research and Technology Center, Hawthorne, California, 1974
10. "Performance Analysis of a Laser Propelled Interorbital Transfer Vehicle," M. A. Minovitch, Final Report, Contract NAS 3-18536, NASA CR-134966, February, 1976.
11. "Laser Receiver System Study", J. M. Sellen, Jr., see R&D Status Report 6, Contract F04611-76-C-0003.
12. "Laser Assisted Propulsion-Coupling Mechanisms", P. Molmud, see R&D Status Report 6, Contract F04611-76-C-0003.
13. Rocket Propulsion Elements, George P. Sutton, Third Edition, John Wiley and Sons, Inc., New York.
14. Laser Coupling Test Plan, submitted separately to AFRPL.

APPENDIX A DERIVATION OF ORBITAL EQUATIONS

For Changing Altitudes:

Altitude changes involve both increasing and decreasing altitude from the initial parking orbit.

Increasing altitude:

$$V_{ci} + \Delta V_p = V_p$$

$$\Delta V_p = V_p - V_{ci}$$

Where

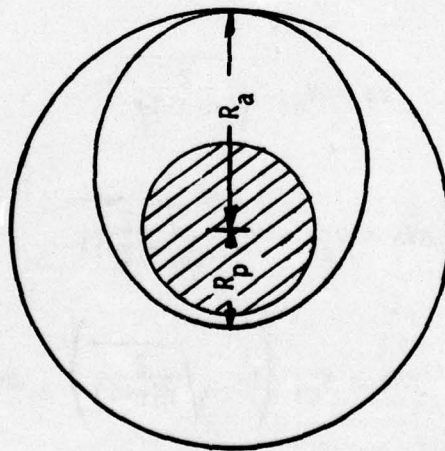
ΔV_p = vel. increment added at perigee.

V_p = vel at perigee

V_{ci} = velocity of initial circular parking orbit.

Now

$$V_p = V_{ci} \sqrt{\frac{2n}{n+1}}$$



So

$$\Delta V_p = V_{ci} \sqrt{\frac{2n}{n+1}} - V_{ci}$$

$$\Delta V_p = V_{ci} \left[\sqrt{\frac{2n}{n+1}} - 1 \right]$$

Where

$$n = R_a/R_p$$

R_a = radius from center of earth to altitude at apogee

R_p = radius from center of earth to altitude at perigee

$$R_a = h_a + r; R_p = h_p + r$$

h_a = altitude above earth at apogee

r = radius of earth (3444 NM)

h_p = altitude above earth at apogee

and ΔV_p is the velocity increment added at perigee to reach altitude h_a .

For decreasing altitudes

$$V_{ci} - \Delta V_a = V_a$$

$$\Delta V_a = V_{ci} - V_a$$

Now

$$V_a = V_{ci} \sqrt{\frac{2}{n(n+1)}}$$

So

$$\Delta V_a = V_{ci} - V_{ci} \sqrt{\frac{2}{n(n+1)}}$$

Then

$$\Delta V_a = V_{ci} \left(1 - \sqrt{\frac{2}{n(n+1)}} \right), \text{ which is the}$$

retro-velocity increment to be subtracted at apogee to get to a lower altitude or perigee

For Circularization

Circularization is required both at the increased and at the decreased orbital altitude.

Circularization at the increased altitude

$$V_a + \Delta V_a = V_{cf}$$

$$\Delta V_a = V_{cf} - V_a$$

Where

ΔV_a = velocity increment added at apogee

V_a = velocity at apogee

V_{cf} = circular velocity at final altitude.

Now

$$V_a = V_{cf} \sqrt{\frac{2}{n(n+1)}}$$

So

$$\Delta V_a = V_c - V_c \sqrt{\frac{2}{n(n+1)}}$$

$$\Delta V_a = V_{cf} \left(1 - \sqrt{\frac{2}{n(n+1)}} \right), \text{ which is the}$$

velocity increment to be added at apogee to circularize the orbit.

Circularization at the decreased altitude

$$V_{cf} = V_p - \Delta V_p$$

$$\Delta V_p = V_p - V_{cf}$$

Now

$$V_p = V_{cf} \sqrt{\frac{2n}{n+1}}$$

here V_{cf} is V_{ci} when raising altitude

$$\Delta V_p = V_{cf} \sqrt{\frac{2n}{n+1}} - V_{cf}$$

$$\Delta V_p = V_{cf} \left(\sqrt{\frac{2n}{n+1}} - 1 \right), \text{ which is the}$$

retro-velocity increment to be subtracted at perigee to circularize at the lower orbit.

where:

ΔV_p = velocity increment subtracted at perigee

V_{cf} = circular velocity at the decreased altitude orbit

V_p = velocity at perigee after falling from apogee

APPENDIX B
ECCENTRIC ORBIT VELOCITY CALCULATIONS

B-1. VELOCITY INCREMENT DETERMINATION WITHOUT PLANE
CHANGES FOR ECCENTRIC ORBITS

21,000 x 300 NM Orbit

Step 1: 100 NM Circular to 300 NM Circular

Where V_{c100} is parking orbit circular velocity at 100 NM

$$\Delta V_p = V_{c100} \left(\sqrt{\frac{2n}{n+1}} - 1 \right) \quad \text{for } \Delta V \text{ to be added at perigee}$$

to reach some altitude from a
parking orbit of 100 NM

for 300 NM final altitude:

$$n = \frac{R_a}{R_p} = \frac{r+h}{r+100} = \frac{3443.93 + 300}{3443.93 + 100} = \frac{3743.93}{3543.93} = 1.056$$

$$\frac{2n}{n+1} = 1.028 \sqrt{1.028} = 1.014$$

$$\Delta V_p = V_{c100} (0.014)$$

$$V_{c100} = \sqrt{\frac{\mu}{R_{100}}} = \sqrt{\frac{62628.22 \text{ NM}^3/\text{sec}^2}{3543.93 \text{ NM}}}$$

$$R_{100} = r + 100 = 3443.93 + 100$$

$$V_{c100} = \sqrt{17.672} = 4.2038 \text{ NM/sec}$$

$$= 25,560 \text{ ft/sec}$$

$$\Delta V_p = 25,560 \times 0.014 = 357.84 \text{ ft/sec for transfer ellipse}$$

For circularization

$$\Delta V_a = v_{c_{300}} \left(1 - \sqrt{\frac{2}{n(n+1)}} \right)$$

for circularization at 300 NM

$$n = 1.014$$

$$\frac{2}{n(n+1)} = \frac{2}{1.014(2.014)} = 0.979$$

$$\sqrt{.979} = 0.989 \quad 1 - 0.989 = 0.011$$

Now

$$v_{c_{300}} = \sqrt{\frac{\mu}{R}} = \sqrt{\frac{62628.22}{\underbrace{3443.93 + 300}_{3743.93}}} = \sqrt{16.73} = 4.09 \text{ NM/sec}$$

$$4.09 \text{ NM/sec} \times 6080.2 \text{ ft/NM} = 24,868 \text{ ft/sec}$$

$$\Delta V_a = 24,868 \times 0.011 = \underline{273.55} \text{ ft/sec for circularization at apogee}$$

Step 2: ΔV to get to 21,000 NM from 300 NM Circular

$$\Delta V_p = v_{c_{300}} \left(\sqrt{\frac{2n}{n+1}} - 1 \right)$$

$$n = \frac{R_a}{R_p} = \frac{r + 21,000}{r + 300} = \frac{3443.9 + 21,000}{3443.9 + 300} = \frac{24,443.9}{3743.9}$$

$$n = 6.53 \quad \text{so} \quad \sqrt{\frac{2n}{n+1}} = \sqrt{\frac{13.06}{7.53}} = 1.317$$

$$\Delta V_p = 24,874 (1.317 - 1)$$

$$\Delta V_p = 7885 \text{ ft/sec}$$

So total ΔV for 21,000 x 300 NM is:

$$\Delta V_p \text{ to get to 300 NM} = 357.84$$

$$\Delta V_a \text{ to circular at 300 NM} = 273.55$$

$$\Delta V_p \text{ to get to 21,000 apogee} = 7885.00$$

with 300 NM perigee

$$\text{TOTAL} = 8516.39$$

21,000 x 170 Orbit

Transfer Ellipse

$$\Delta V_p = v_{c100} \left(\sqrt{\frac{2n}{n+1}} - 1 \right)$$

$$n = \frac{R_a}{R_p} = \frac{r+170}{r+100} = \frac{3444 + 170}{3444 + 100} = \frac{3614}{3544} = 1.02$$

$$n = 1.02$$

$$\frac{2n}{n+1} = \frac{2(1.02)}{1.02 + 1} = 1.01 \quad ; \quad \sqrt{\frac{2n}{n+1}} = \sqrt{1.01} = 1.005$$

$$\Delta V_p = 25,560 (1.005 - 1)$$

$$\Delta V_p = 127.8 \text{ ft/sec for transfer ellipse to 170 NM}$$

from 100 NM parking orbit

Circularization at 170 NM

$$\Delta V_a = v_{c_{170}} \left(1 - \sqrt{\frac{2}{n(n+1)}} \right)$$

$$\frac{2}{n(n+1)} = \frac{2}{1.02 (1.02 + 1)} = \frac{2}{1.02 \times 2.02} = 0.971$$

$$\sqrt{\frac{2}{n(n+1)}} = \sqrt{0.971} = 0.985$$

Now

$$1 - \sqrt{\frac{2}{n(n+1)}} = 1 - 0.985 = 0.015$$

$$v_{c_{170}} = \sqrt{\frac{\mu}{R}} = \sqrt{\frac{62628.22}{3444 + 170}} = \sqrt{17.33} = 4.16 \text{ NM/sec}$$

3614 NM = 25,310 ft/sec

$$\Delta V_a = 25,310 (0.015) = 379.7 \text{ ft/sec}$$

Transfer to 21,000 NM from 170 NM Circular Orbit

$$\Delta V_p = v_{c_{170}} \left(\sqrt{\frac{2n}{n+1}} - 1 \right)$$

$$n = \frac{R_a}{R_p} = \frac{3444 + 21,000}{2444 + 170} = \frac{24444}{2614} = 6.764$$

$$n = 6.764$$

So

$$\sqrt{\frac{2n}{n+1}} = \sqrt{\frac{2(6.764)}{6.764 + 1}} = \sqrt{1.742} = 1.32$$

with

$$\Delta V_p = v_{c_{170}} \left(\sqrt{\frac{2n}{n+1}} - 1 \right)$$

$$\Delta V_p = 25,310 (0.32) = 8099 \text{ ft/sec}$$

So total ΔV for 21,000 x 170 NM orbits

$$\Delta V_p \text{ to get to 170 NM} = 127.8$$

$$\Delta V_a \text{ to circular at 170 NM} = 379.7$$

$$\Delta V_p \text{ to get to 21,000 apogee} \\ \text{with 170 NM perigee} = 8099.2$$

$$\text{TOTAL} = 8606.7$$

600 x 250 NM Orbit

$$\Delta V_p = v_{c_{150}} \left(\sqrt{\frac{2n}{n+1}} - 1 \right)$$

$$n = \frac{R_a}{R_p} = \frac{3444 + 250}{3440 + 100} = \frac{3694}{3540} = 1.0435$$

$$\sqrt{\frac{2n}{n+1}} = \sqrt{\frac{2(1.0435)}{1.0435 + 1}} = \sqrt{1.0213} = 1.011$$

$$\Delta V_p = 25,560 \text{ NM} (1.011 - 1) = 281.16 \text{ ft/sec for transfer} \\ \text{ellipse to 250 NM}$$

Circularization at 250 NM

$$\Delta V_a = v_{c_{250}} \left(1 - \sqrt{\frac{2}{n(n+1)}} \right)$$

$$v_{c_{250}} = \sqrt{\frac{\mu}{R}} = \sqrt{\frac{62628.22}{3444 + 250}} = \sqrt{16.95} = 4.12 \text{ NM/sec}$$
$$= 25,034.6 \text{ ft/sec}$$

$$\sqrt{\frac{2}{n(n+1)}} = \sqrt{\frac{2}{1.011 (1.011 + 1)}} = \sqrt{0.984} = 0.992$$

Now

$$1 - \sqrt{\frac{2}{n(n+1)}} = 0.008$$

$$\Delta V_a = 25,034.6 (0.008) = 200.28 \text{ ft/sec}$$

Transfer Ellipse to 600 NM

$$\Delta V_p = v_{c_{250}} \left(\sqrt{\frac{2n}{n+1}} - 1 \right)$$

$$n = \frac{R_a}{R_p} = \frac{3444 + 600}{3444 + 250} = \frac{4044}{3694} = 1.095$$

$$\sqrt{\frac{2n}{n+1}} = \sqrt{\frac{2(1.095)}{2.095}} = \sqrt{1.045} = 1.022$$

$$\Delta V_p = 25,024.6 (0.022) = 550.8$$

Total

$$\Delta V_p \text{ to get to 250 NM} = 281.2$$

$$\Delta V_a \text{ to circular at 250 NM} = 200.3$$

$$\Delta V_p \text{ to get to 600 NM} \\ \text{with 250 perigee} = \underline{550.8}$$

$$\text{TOTAL} = 1032.3$$

300 x 75 NM Orbit Decreasing Altitude from 100 NM
Parking by a Transfer Ellipse to 75 NM Perigee

$$\Delta V_a = V_{c_{100}} \left(1 - \sqrt{\frac{2}{n(n+1)}} \right) \text{ retro at 100 NM parking to} \\ \text{reduce orbital altitude at} \\ \text{perigee to 75 NM}$$

$$n = \frac{R_a}{R_p} = \frac{3444 + 100}{3444 + 75} = \frac{3544}{3519} = 1.007$$

$$\sqrt{\frac{2}{n(n+1)}} = \sqrt{\frac{2}{1.007(2.007)}} = 0.9896$$

and

$$\left(1 - \sqrt{\frac{2}{n(n+1)}} \right) = 0.0104$$

so

$$\Delta V_a = 25,560 \times 0.0104 = 266.2 \text{ ft/sec for transfer ellipse}$$

Circularizing at 75 NM

$$\Delta V_{p_c} = V_{c_{75}} \left(\sqrt{\frac{2n}{n+1}} - 1 \right)$$

$$\sqrt{\frac{2(1.007)}{2.007}} = \sqrt{1.0035} = 1.0017$$

$$\left(\sqrt{\frac{2n}{n+1}} - 1 \right) = 0.0017$$

$$V_{c_{75}} = \sqrt{\frac{\mu}{R}} = \sqrt{\frac{62628.22}{3444 + 75}} = \sqrt{17.8} = 4.219 \text{ NM/sec}$$

3519 = 25,649.5 ft/sec

$$\Delta V_{p_c} = 25,649.5 \times 0.0017 = 43.6 \text{ ft/sec}$$

Raising Altitude to an Apogee of 300 NM

$$\Delta V_p = V_{c_{75}} \left(\sqrt{\frac{2n}{n+1}} - 1 \right)$$

$$n = \frac{R_a}{R_p} = \frac{3444 + 300}{3444 + 75} = \frac{3744}{3519} = 1.064$$

$$\sqrt{\frac{2n}{n+1}} = \sqrt{1.031} = 1.0154$$

$$\Delta V_p = 25,649.5 \times 0.0154 = 395.0 \text{ ft/sec}$$

We now have an eccentric orbit of 300 x 75 NM and the total ΔV required was:

$$\Delta V_a, \text{ decreasing altitude to 75 NM} = 266.2$$

$$\Delta V_{p_c}, \text{ circularizing at 75 NM} = 43.6$$

$$\Delta V_p, \text{ raising to an apogee of 300 NM} = \underline{395.0}$$

$$\text{TOTAL} = 704.8 \text{ ft/sec}$$

B-2. VELOCITY INCREMENT DETERMINATION WITH PLANE CHANGES FOR ECCENTRIC ORBITS

21,000 x 300 NM Orbit

$$\Delta V_p = 359 \text{ ft/sec for transfer to 300 NM from 100 NM parking orbit}$$

$$\Delta V_a = 274 \text{ ft/sec to circularize at apogee for 300 NM orbit}$$

$$\Delta V_p = \underline{7885} \text{ ft/sec to raise to apogee of 21,000 NM}$$

$$\text{TOTAL} = 8516.39 \text{ ft/sec}$$

Using the average orbital speed for performing the plane change as a first approximation:

$$v_{p_{300}} = v_{c_{300}} \sqrt{\frac{2n}{n+1}} = 24,868 \times \sqrt{\frac{2(6.53)}{7.53}} = 32,750 \text{ ft/sec}$$

$$v_{a_{21,000}} = v_{c_{21,000}} \sqrt{\frac{2}{n(n+1)}}$$

$$V_{c_{21,000}} = \sqrt{\frac{u}{R}} = \sqrt{\frac{62628}{3444 + 21,000}} = \sqrt{\frac{62628}{24,444}} = \sqrt{2.562} = 1.600 \text{ NM/sec}$$

$$= 9728 \text{ ft/sec}$$

$$n = 6.53 ; \sqrt{\frac{2}{n(n+1)}} = \sqrt{\frac{2}{6.53(7.53)}} = \sqrt{0.04067} = 0.2018$$

So

$$V_{a_{21,000}} = 9728 \times 0.2018 = 1964 \text{ ft/sec}$$

$$V_{\text{aver}} = \frac{32,750 + 1964}{2} = 17,357 \text{ ft/sec}$$

From Page II-48 Space Planers Guide

<u>Plane Change, deg</u>	<u>ΔV, ft/sec</u>
20°	6,000
40°	12,000
60°	18,000

$$72.52 + 22.56 = 95.08$$

Assuming the maneuvers and plane changes are done concurrently, as a first order approximation:

	<u>Total ΔV</u>
$20^\circ - 8516.4^2 + 6,000^2 = 7252 \times 10^4 + 3,600 \times 10^4 = 10,852 \times 10^4 ; \sqrt{} = 10,400 \text{ ft/sec}$	
$40^\circ - 8516.4^2 + 12,000^2 = 7252 \times 10^4 + 14,400 \times 10^4 = 21,652 \times 10^4 ; \sqrt{} = 14,700 \text{ ft/sec}$	
$60^\circ - 8516.4^2 + 18,000^2 = 7252 \times 10^4 + 32,400 \times 10^4 = 39,652 \times 10^4 ; \sqrt{} = 19,913 \text{ ft/sec}$	

Now

21,000 x 170 Orbit

$$V_{c_{170}} = 25,310 \text{ ft/sec}$$

$$V_{c_{21,000}} = 9728$$

$$V_{p_{170}} = V_{c_{170}} \sqrt{\frac{2n}{n+1}}$$

and

$$n = 6.764 \quad ; \quad \sqrt{\frac{2n}{n+1}} = 1.32$$

so

$$V_{p_{170}} = 25,310 \times 1.32 = 33,409 \text{ ft/sec}$$

Now

$$V_{a_{21,000}} = V_{c_{21,000}} \sqrt{\frac{2}{n(n+1)}}$$

$$= 9728 \times \sqrt{\frac{2}{6.76(7.76)}} = 1899.5 \text{ ft/sec}$$

$$\text{Aver orbital transfer velocity} = \frac{33,409 + 1899.5}{2} = 17,654 \text{ ft/sec}$$

Assuming the maneuvers and plane changes are done concurrently, as a first, order approximation:

Total ΔV (Maneuvers and Plane Changes)

20°	10,500
40°	14,800
60°	20,000

600 x 250 Orbit

$$v_{c250} = 25,034.6 \text{ ft/sec}$$

$$v_{c600} = \sqrt{\frac{\mu}{R}} = \sqrt{\frac{62628}{3444 + 600}} = \sqrt{15.487} = 3.935 \text{ NM/sec}$$

$$= 23,926.7 \text{ ft/sec}$$

So

$$v_{p250} = 25,034.6 \times \sqrt{\frac{2n}{n+1}} = 25,034.6 \times 1.022 = 25,585 \text{ ft/sec}$$

$$v_{a600} = 23,927 \times \sqrt{\frac{2}{n(n+1)}} = 23,927 \times \sqrt{\frac{2}{1.095(2.095)}} = 22,341 \text{ ft/sec}$$

$$\text{aver orbital vel} = \frac{25,585 + 22,341}{2} = 23,963 \text{ ft/sec}$$

For Plane Changes:

	ΔV	
20°	8,300	From AF Planners Guide Page II-48 Figure IIC-12
40°	10,600	
60°	24,900	

Assuming plane change done concurrently with other maneuvers:

$$20^\circ 1032^2 + 8,300^2 = 106.5 \times 10^4 + 6,889 \times 10^4 = 6,995.5 ; \sqrt{} = 8,364$$

$$40^\circ 1032^2 + 16,600^2 = 106.5 \times 10^4 + 27,556 \times 10^4 = 27,662 ; \sqrt{} = 16,632$$

$$60^\circ 1032^2 + 24,900^2 = 106.5 \times 10^4 + 62,001 \times 10^4 = 62,108 ; \sqrt{} = 24,921$$

300 x 75 Orbit

$$V_{c75} = 25,649.5 \text{ ft/sec}$$

$$V_{c300} = \sqrt{\frac{\mu}{R}} = \sqrt{\frac{62628}{3444 + 300}} = 4.09 \text{ NM/sec}$$

$$\frac{3744}{\times 6080} = 24,867 \text{ ft/sec}$$

$$V_{p75} = V_{c75} \sqrt{\frac{2n}{n+1}} = 25,649.5 \times 1.064 = 27,291 \text{ ft/sec}$$

$$V_a = V_{c300} \sqrt{\frac{2}{n(n+1)}} = 24,867 \times \sqrt{\frac{2}{1.064(2.064)}} = 23,731 \text{ ft/sec}$$

aver orbital vel = 25,511 ft/sec

Figure IIC-12

	<u>ΔV</u>
20°	8,500
40°	17,000
60°	25,500

$$20^\circ \quad 705^2 + 8,500^2 = 49.7 \times 10^4 + 7,225 \times 10^4 = 7,274.7 \times 10^4 ; \sqrt{} = 8,529$$

$$60^\circ \quad 705^2 + 17,000^2 = 49.7 \times 10^4 + 28,900 \times 10^4 = 28,950 \times 10^4 ; \sqrt{} = 17,015$$

$$60^\circ \quad 705^2 + 25,500^2 = 49.7 \times 10^4 + 65,025 \times 10^4 = 65,075 \times 10^4 ; \sqrt{} = 25,510$$

The results of the ΔV calculations for the eccentric orbits are shown in Section 3.